

Sheffield Hallam University

Relationships between homogeneity, structure and mechanical properties in certain sintered iron, nickel, carbon materials.

DIXON, Harold.

Available from the Sheffield Hallam University Research Archive (SHURA) at:

<http://shura.shu.ac.uk/19563/>

A Sheffield Hallam University thesis

This thesis is protected by copyright which belongs to the author.

The content must not be changed in any way or sold commercially in any format or medium without the formal permission of the author.

When referring to this work, full bibliographic details including the author, title, awarding institution and date of the thesis must be given.

Please visit <http://shura.shu.ac.uk/19563/> and <http://shura.shu.ac.uk/information.html> for further details about copyright and re-use permissions.

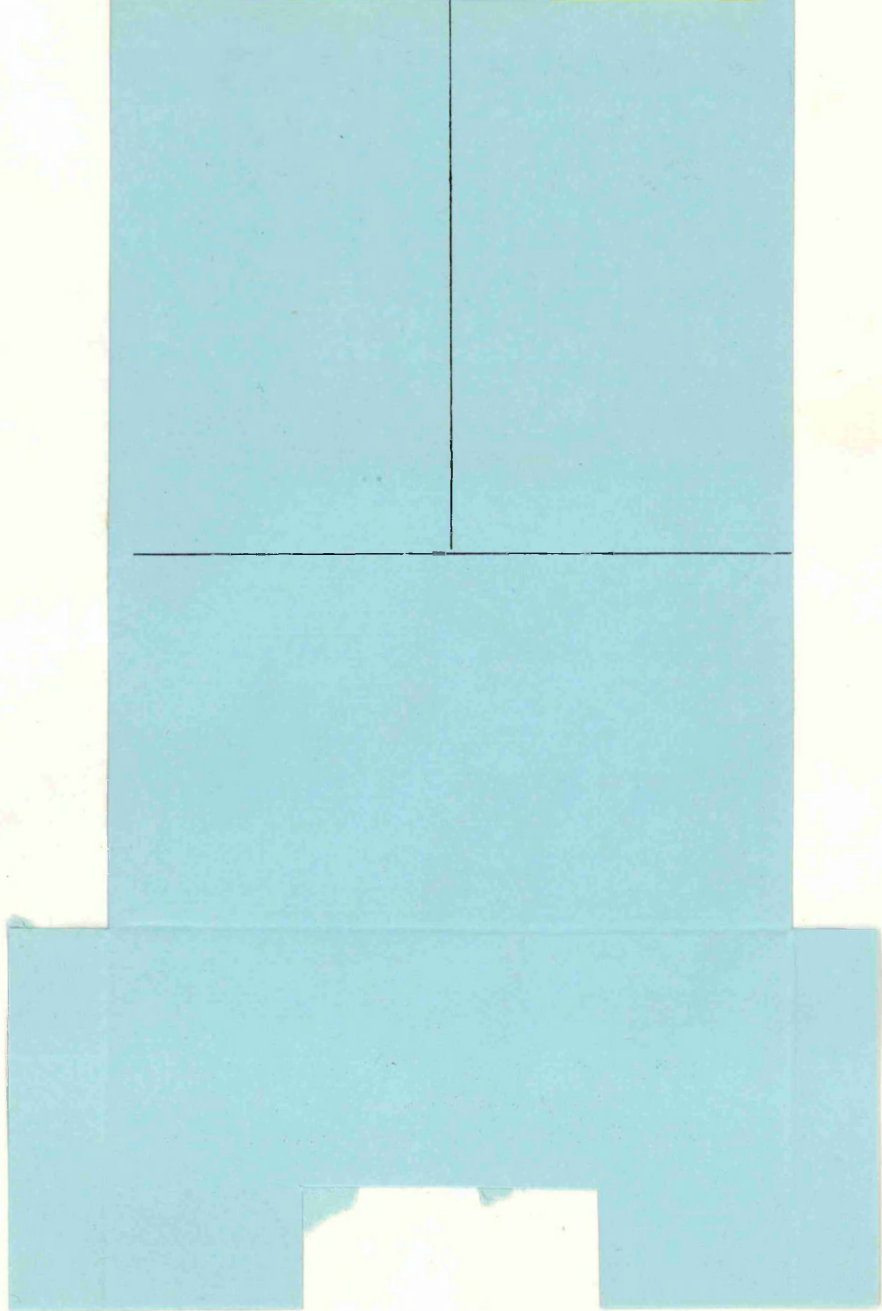
DAK CODE/NO.

101 381 307 3.

SHEFFIELD CITY
POLYTECHNIC LIBRARY
POND STREET
SHEFFIELD S1 1WB

02050.

Sheffield Hallam University
REFERENCE ONLY



ProQuest Number: 10694444

All rights reserved

INFORMATION TO ALL USERS

The quality of this reproduction is dependent upon the quality of the copy submitted.

In the unlikely event that the author did not send a complete manuscript and there are missing pages, these will be noted. Also, if material had to be removed, a note will indicate the deletion.



ProQuest 10694444

Published by ProQuest LLC (2017). Copyright of the Dissertation is held by the Author.

All rights reserved.

This work is protected against unauthorized copying under Title 17, United States Code
Microform Edition © ProQuest LLC.

ProQuest LLC.
789 East Eisenhower Parkway
P.O. Box 1346
Ann Arbor, MI 48106 – 1346

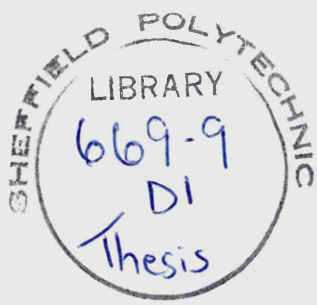
RELATIONSHIPS BETWEEN HOMOGENEITY, STRUCTURE
AND MECHANICAL PROPERTIES IN CERTAIN
SINTERED IRON:NICKEL:CARBON MATERIALS.

BY

HAROLD DIXON

A THESIS SUBMITTED TO THE COUNCIL
FOR NATIONAL ACADEMIC AWARDS FOR
THE DEGREE OF DOCTOR OF PHILOSOPHY.

Department of Metallurgy,
Sheffield City Polytechnic,
October, 1977.



77-20379 01 2

All the work reported in this thesis was carried out during the period for which the author was registered for a higher degree.

During this time, a postgraduate course of 25 lectures on Heat and Mass Transfer was attended; this was an integral part of an M.Sc. course in Metallurgical Process Management.

ACKNOWLEDGEMENTS

Grateful thanks are due especially to Dr. A.J. Fletcher and to Dr. R.T. Cundill for their continued support and encouragement over six years of part-time study.

Thanks are also due to the Technical Staff of the Department of Metallurgy but particularly those of the Sections under the leadership of Mr. B. Lewis, Mr. N. Rhodes, Mr. R. Day, Mr. P. Haywood and Mr. D. Latimer, without whose services this research would not have been possible.

Appreciation must also be expressed of several colleagues at Rotherham College of Technology, in particular Mr. J. McCullough and Mr. F. Gent for helpful advice and discussion. The continued approval of the Rotherham Borough Council Education Committee in granting a teaching concession has proved to be invaluable and sincere thanks are due to my Head of Department, Mr. L.H. Baxter, for adapting this to my greatest advantage, to my resolute colleagues for accepting this and to the Principal, Mr. D.B. Edwards, for supporting these arrangements.

The use of specialised facilities at the Sheffield Laboratories (Hoyle St.,) of the British Steel Corporation is sincerely acknowledged.

CONTENTS

	<u>Page No</u>
1. SYNOPSIS	1
2. PURPOSE OF THE INVESTIGATION	3
3. REVIEW OF PREVIOUS WORK	4
3.1 The Structures and Properties of Fully Dense Iron:Nickel:Carbon Alloys	5
3.2 The Influence of Process Parameters on the Properties, Structure and Homogeneity of Powder Compacts.	10
3.2.1 Mixtures of Elemental Powders	11
3.2.2 Mixtures of Partially and Fully Pre-alloyed Powders	18
3.2.3 Techniques for the Production of Coated Powders	20
3.2.4 The Mixing & Compaction of Powders	23
3.2.5 The Sintering and Heat Treatment of Compacted Metal Powders	26
3.3 Relationships between Properties, Structure and Homogeneity in Sintered Powder Compacts	37
3.3.1 Physical and Mechanical Property Relationships in Powder Compacts	38
3.3.2 Relation of Microstructure to Homogeneity and Properties in Powder Compacts	49
3.3.3 Models of the Homogenisation Process	58
3.3.4 Measurement of the Degree of Homogeneity	63
4. EXPERIMENTAL PROCEDURE	68
4.1 Physical Properties of Powders	68
4.2 Processing of Powders	68
4.2.1 Production of Sintered Compacts	68
4.2.2 Nickel Plating of Iron Powder	70
4.2.3 Chemical Analysis of Powder and Sintered Compacts	72
4.3 Determination of the Properties of Compacts	72
4.4 Examination of the Structures of Sintered Material	74

4.4.1	Optical Microscopy	74
4.4.2	Transmission and Scanning Electron Microscopy	75
4.4.3	X-Ray Diffractometry	76
4.5	Determination of Homogeneity by Electron Probe Micro-analysis	77
4.5.1	Point Analysis	77
4.5.2	Areal Analysis	78
5.	EXPERIMENTAL RESULTS	79
5.1	Properties of Powders used in the Investigation	79
5.2	Properties and Structure of Blended Iron: Graphite Alloys, Die-pressed	79
5.3	Properties and Structure of Blended Iron: Graphite:1% Nickel Alloys, Die-pressed	82
5.4	Properties and Structure of Blended Iron: Graphite:3% Nickel Alloys, Die-pressed	83
5.4.1	Mechanical and Physical Properties	83
5.4.2	Structure	83
5.4.3	Determination of the Degree of Homogeneity	87
5.5	Properties and Structure of Blended Iron: Graphite:3% Nickel Alloys, Isostatically Pressed	92
5.5.1	Properties of Blended, Plated and Pre- Alloyed Materials	93
5.5.2	Structure of Blended, Plated and Pre- Alloyed Materials	98
5.5.2.1	Optical and Electron Micro- scopy of Blended Materials	98
5.5.2.2	Optical and Electron Micro- scopy of Plated Materials	101
5.5.2.3	Optical and Electron Micro- scopy of Pre-alloyed Materials	103
5.5.2.4	Scanning Electron Microscopy of Fracture Surfaces	106
5.5.2.5	Quantitative Optical Microscopy	107
5.5.2.6	X-Ray Diffraction	108
5.5.3	The Homogeneity of Blended, Plated and Pre-Alloyed Materials	109

6.	DISCUSSION OF RESULTS	112
6.1	Relationships involving the Tensile Strength of Iron:Nickel:Carbon Materials	112
6.1.1	Alloys of High Homogeneity	116
6.1.1.1	The Determination and Use of Stress Concentration Factors	117
6.1.1.2	Relationship between Micro-structure and Tensile Strength	120
6.1.2	Alloys of Low Homogeneity	124
6.1.2.1	Relationship between Micro-structure and Tensile Strength	125
6.1.3	Relationship between Tensile Strength, Porosity and Homogenisation Parameter	129
6.1.4	The Effect of Temperature at Constant Time	130
6.2	Relationships involving the Tensile Ductility of Iron:Nickel:Carbon Materials	131
6.3	Relationships involving the Hardness of Iron:Nickel:Carbon Materials	132
6.4	Relationships involving the Impact Strength of Iron:Nickel:Carbon Materials	135
6.5	General Mechanical Property Relationships	137
6.6	The Mechanism of Homogenisation	139
7.	CONCLUSIONS	144
	REFERENCES	147
	TABLES	155
	FIGURES	182

1. SYNOPSIS

The commercial production of low alloy steels from blended mixtures of powders normally results in a product which is chemically heterogeneous. Although reference has often been made to the effects of heterogeneity in sintered steels, few investigations have included an assessment of homogeneity and none of these has related the quantitative measurement of homogeneity to the mechanical properties of the product.

A study was made of three classes of sintered material, each containing 3% nickel and $0.33\% \pm 0.03\%$ carbon but with different initial degrees of homogeneity. This was achieved by the use of blended elemental powders, a nickel-plated iron powder produced in a specially developed apparatus and a pre-alloyed powder. Electron probe micro-analysis was employed for the quantitative measurement of the degree of homogenisation that had occurred in each of these materials during sintering. The homogenisation parameter so determined was related to the mechanical and physical properties and microstructure of the materials after these had undergone various sintering treatments.

In each class of material, the degree of homogenisation that was developed during sintering times of up to eight hours was given by an exponential relationship which was similar to that predicted theoretically by other workers. The established equation $\sigma_s = \sigma_o (1 - F P)$, in which σ_s and σ_o are the tensile strengths of sintered and fully dense materials respectively, P is the fractional porosity and F is the

empirically determined stress concentration effect of the pores, was found to predict tensile strength more accurately than other published equations, provided that the materials concerned possessed homogenisation parameters below a certain value. Although these materials of high homogeneity consisted mainly of lath martensite, the presence in the microstructure of isolated regions of acicular martensite, bainite and ferrite was not detrimental to tensile strength provided that the above criterion was maintained. The tensile strength of alloys of low homogeneity was not predictable by the use of the above equation; the presence in the microstructure of nickel-rich austenite, especially in the form of continuous interparticle networks, was particularly deleterious in this respect. The impact fractures of all three classes of material were ductile despite the low values of impact strength which were due, not to the type of microstructure associated with material of low homogeneity, but mainly to pore shape and distribution. It was considered, on the basis of metallographic evidence, that homogenisation in the materials investigated proceeded by a complex mechanism that involved both surface and volume interdiffusion.

2. PURPOSE OF THE INVESTIGATION

The use of blended mixtures of powders to produce sintered components of low alloy steels presents certain advantages over the use of fully pre-alloyed powders. In particular, the elemental powders are cheaper and the pressure required to produce a specific density is lower than is the case with pre-alloyed powders. However, the commercial production of sintered low alloy steels does not normally result in a chemically homogeneous product, since it is desirable on economic grounds to use a short sintering treatment. The use of such heterogeneous material has a deleterious effect upon hardenability and mechanical properties.

Although reference has often been made to the effects of inhomogeneities in sintered low alloy steels, few investigations have included an assessment of the degree of homogeneity in these materials; none of these has related the degree of homogeneity to the mechanical properties of the product in a quantitative manner.

Since variations in chemical homogeneity are likely to result in variations in the microstructure of sintered and heat treated low alloy steels, a study of the relationships between the degree of homogeneity, microstructure and mechanical properties may lead to an improved understanding of the mechanism by which the microstructures of materials with different degrees of homogeneity influence mechanical properties. This in turn may lead to the development of improved combinations of properties in these materials.

3. REVIEW OF PREVIOUS WORK

In 1960, Schwarzkopf¹ presented a brief review of "modern" powder metallurgy in which he referred to the co-operation between the industry and research organisations, particularly with regard to those materials which could not be produced by other methods. However, in the field of ferrous powder metallurgy, much of the research work was confined to the iron powder producers. Since 1960, a great deal of research and development has been undertaken by both producers and academic institutions in an effort to adapt powder metallurgical products to high performance applications². The usual approach to improvements in particular properties has been via the elimination of porosity in the final product³. Despite this current trend towards the manufacture of near fully dense powder products, the principal interest in the industry still centres around those materials which differ from traditional fully-dense materials* in that they contain from 5% to 25% porosity. Powder producers are still actively engaged in research into alloying methods and their effects upon microstructure and mechanical properties of sintered low alloy steels⁴. In 1971, Dixon and Clayton⁵ stated that the bulk of sintered components were produced for low and medium strength applications, often as replacements for items formerly made from castings and stampings; furthermore they suggested that a demand existed for components with improved properties as a replacement for wrought materials. It was their opinion that it was difficult and expensive to produce

*Hitherto referred to as wrought material.

sintered parts with adequate ductility, fatigue and impact resistance for such replacements. This opinion, in conjunction with that of Lennox⁶ that the powder metallurgical industry could cope with a 40% increase in production, clearly suggests that research should be continued in an effort to improve further the mechanical properties of porous low alloy steels. The principal objectives of this literature survey are firstly to assess the influence of variations in process parameters upon homogeneity, structure and properties and, secondly, to review published relationships between these characteristics of the material. In addition, a section has been included concerning the structures and properties of wrought fully-dense materials which contain nickel as the major alloying element.

3.1 THE STRUCTURES AND PROPERTIES OF FULLY DENSE IRON-NICKEL-CARBON ALLOYS.

The mean composition of alloys examined in the current work was 0.33% carbon: 3% nickel: balance iron. Commercial fully-dense wrought alloys of similar composition contain other elements but principally manganese to the extent of approximately 0.6%⁷. The influence of manganese is similar to that of nickel in that it retards transformation to ferrite and pearlite during cooling from the austenite region⁸.

Investigations into the effects of nickel on the structure of iron-carbon alloys^{9,10,11,12} have shown that these alloys transform from austenite to martensite at relatively low cooling rates but that the solid solution strengthening effect of nickel is very slight. It follows that the principal influence of nickel in low alloy steels is to lower the

critical cooling velocity. Hall¹³ has listed critical cooling velocities for carbon steels and compared them with those of 3% nickel steels at the same carbon levels. At the 0.4% carbon level, the critical cooling velocity was reduced from 510°C/s to 34°C/s by the addition of 3% nickel. For materials above a certain section size in which a nickel composition gradient existed, local differences in critical cooling velocity would be expected to lead to local differences in microstructure. In pure iron-nickel alloys¹⁴ and iron-carbon alloys¹⁵, it is known that a transition occurs from cubic massive martensite to tetragonal lenticular martensite at approximately 28 atomic % nickel and 2.8 atomic % carbon respectively. Massive martensite has been described by Bell¹⁶ as packets of parallel plates which, after progressive polishing and etching, correspond to rectangular slabs below the surface. The alternative description of this structure as lath-type martensite seems most suitable since, unlike lenticular martensite, massive martensite forms in such a way as to fill space completely. The martensite slabs outline the {111} planes of the parent austenite and do not cross the pre-existing grain boundaries. The optical appearance of lenticular martensite is that of acicular plates embedded in retained austenite¹⁶. Since neither the laths of massive martensite nor the plates of lenticular martensite cross the austenite grain boundaries, it might be expected that a relationship exists between austenite and martensite grain size. Zackay et al¹⁷ have reported that this is the case up to austenitising temperatures of 1000°C, i.e. austenite grain size and martensite plate length were almost identical in

steels which were austenitised below this temperature. At austenitising temperatures in excess of 1100°C , although austenite grain size increased, the martensite plate length became almost constant at $175\mu\text{m}$. Consequently, for a fully hardenable steel, there may be little difference in martensitic structure between specimens which were austenitised at different temperatures above 1100°C or for different times at those temperatures. Differences in austenite grain size were not considered by Kelly and Nutting¹⁸ to be a significant factor towards the yield stress of martensite possessing a high carbon content.

Steven and Haynes¹⁹ have given empirical formulae for the estimation of the starts of the martensite and bainite transformations in low alloy steels:

$$M_s = 561 - 474C - 33Mn - 17Ni - 17Cr - 21Mo \quad (^{\circ}\text{C})$$

and
$$B_s = 830 - 270C - 90Mn - 37Ni - 70Cr - 83Mo \quad (^{\circ}\text{C})$$

For an alloy of composition 3% nickel: 0.4% carbon: balance iron, these formulae provide estimates of 611°C and 321°C for B_s and M_s respectively. A TTT diagram for a wrought steel of similar composition²⁰ shows a typical pearlite-bainite transformation curve, with a minimum incubation period of 10 seconds at 500°C , and an M_s temperature of 310°C . Although it is not possible to assess the accuracy of the calculated B_s temperature, the good agreement of M_s and the correlation provided by the authors' own data provide sufficient justification to consider that mixtures of upper and lower bainite might result if such an alloy did not fully transform to martensite on quenching. Pickering²¹ has shown that the temperature above which upper bainite might form and below

which lower bainite might form is a function of carbon content. According to his results, steels containing 0.33% carbon might be expected to form upper bainite at transformation temperatures above 525°C but to form lower bainite below this temperature. The calculated B_s temperature of 611°C clearly suggests that upper bainite may be formed in such steels under certain conditions. Bain and Paxton²² referred to upper and lower bainite under the optical microscope as the subtle difference between a feathery and an acicular microstructure respectively. These fine distinctions do not facilitate positive identification of the phases. Pickering²¹ has studied the mechanism of the bainite reaction and the following is a summary of the relevant findings with respect to morphological differences between the two products. In upper bainite, morphology is dependent upon carbon content. At low carbon contents, bainitic ferrite forms as sheaves of parallel laths, between which the austenite becomes progressively enriched in carbon. When the solubility of carbon in austenite is exceeded, the precipitation of cementite occurs directly from the austenite. Ferrite laths become narrower at lower transformation temperatures because of the decreasing rate of carbon diffusion in front of the ferrite-austenite interface. At higher carbon contents or at lower transformation temperatures, a lamellar appearance may be produced as the cementite films between ferrite laths become more continuous. In lower bainite, morphology is relatively independent of carbon content. Initially, the ferrite laths are very thin, due to the low diffusion rate of carbon at the lower temperatures of formation of this phase. Thickening of

the ferrite laths can only be accomplished by the precipitation of cementite within the ferrite. The carbide precipitates appear to be small rods or plates at an angle of about 55° to the long axes of the ferrite plates. Once the carbon content of the ferrite has been lowered sufficiently by this precipitation, further bainitic growth occurs; the process continues until impingement of neighbouring plates. Although the morphology of bainite would appear to be well established, some doubt has been expressed concerning the mechanism of the lower bainite reaction. In a study of the crystallography of the transformation in a 0.69% carbon steel, Ohmori²³ suggested that cementite may form directly at the ferrite-austenite interface rather than from the ferrite. In further work on low alloy steels, Ohmori et al²⁴ distinguished between three types of bainite according to morphology and transformation temperature; the lowest temperature form was similar in appearance to the lower bainite as described above²¹ in that the cementite plates formed on specific ferrite planes. It was suggested by Ohmori et al that, since all three variants possessed the same lath-like morphology, it was reasonable that they be classified as upper bainite.

Distinguishing features between upper bainite and proeutectoid ferrite were studied by Oblak and Hehemann²⁵ in several medium carbon steels containing from 0% to 8.8% nickel. The B_s temperature of a steel containing 3.34% nickel was taken to be approximately 550°C from previous work by Troiano²⁶; substantial agreement with this figure was provided in a written discussion of the work by Kinsman and Aaronson²⁷. Structural distinctions were made by means of

isothermal transformations above and below B_s : Widmanstätten ferrite formed as single crystals with a low dislocation density whereas upper bainite formed as ferrite laths containing sub-structural units with a high dislocation density. Proeutectoid ferrite exhibited both Widmanstätten and grain boundary morphologies in a plain carbon steel but grain boundary precipitation only was observed in a 3.34% nickel steel. It was concluded that Widmanstätten ferrite and upper bainite do not form a continuous series of decomposition products.

Table I shows typical mechanical properties which have been obtained in 3% nickel steels. Quenched and tempered sections of less than 50mm may be expected to exceed 800MN/m^2 tensile strength, 20% elongation and 100J Izod impact strength. The effect of tempering temperature on the mechanical properties of 3.5% nickel: 0.4% carbon steel has been shown to be clearly predictable¹³: in steels tempered at 600°C , a variation in carbon content from 0.3% to 0.4% affected tensile strength by only 48MN/m^2 . Tensile strength correction factors could thus be applied to these steels from a knowledge of carbon content. The major function of alloy content other than carbon is to permit the development of uniform structure by increasing the hardenability of components^{29,30}.

3.2 THE INFLUENCE OF PROCESS PARAMETERS ON THE PROPERTIES, STRUCTURE AND HOMOGENEITY OF POWDER COMPACTS.

Arbstedt⁴ has recently (1976) summarised the various processing routes for the manufacture of sintered steel components. These were divided into the following four groups:

- (i) mixtures of elemental and possibly master alloy powders,
- (ii) mixtures as (i) plus partially pre-alloyed powders,
- (iii) coated iron powders and
- (iv) fully pre-alloyed atomised powders.

Group (i) was shown to represent the most popular and flexible method of alloying in powder metallurgy although certain disadvantages arose with this choice of production. These were, according to Arbstedt, segregation of alloying elements during processing, variations in properties of the finished components and lack of hardenability. The use of partially pre-alloyed powders minimised segregation. The use of iron powder particles coated with the desired alloying element was very briefly mentioned by Arbstedt because the method was seldom applied in powder metallurgy. Arbstedt attributed this to the prohibitive cost of the coating operation. Fully pre-alloyed powders were virtually all made by water atomisation of liquid steel of the required composition, so that each particle possessed this composition. Arbstedt stated that fully pre-alloyed powders had had little use in conventional ferrous powder metallurgy but that such powders were being produced on a large scale for use in the powder forging process. A few examples of the introduction of alloying elements after compaction were given, e.g. copper infiltration and gas carburising.

3.2.1 Mixtures of elemental powders.

Commercial iron powders are produced by various methods and consequently exhibit differing chemical and physical properties. Krishnamoorthy³¹ investigated the influence of the type of iron powder on the properties of sintered iron.

The highest chemical purity and best compressibility were obtained by atomised and electrolytic powders. In all the three production schedules employed by Krishnamoorthy, these two powders produced the highest densities and consequently the highest ductility and impact strength after pressing and sintering. However, due to their high purity, they generally possessed low tensile strength at a given density. Hulthen³² has referred to the custom of specifying iron powders according to compressibility as being very misleading. As an example of this, he introduced scanning electron micrographs of four iron powders with different specific surfaces. The powder with the lowest specific surface was the most compressible but the green strengths of compacts produced from this powder were very low. The strengths of sintered low alloy steel compacts were shown to increase as the specific surface of the base iron powder increased.

Esper et al³³ have studied the relationship between process conditions and the properties of sintered iron for three plain iron powders, viz., sponge iron, atomised and electrolytic iron. The stimulus for their work was that commercial iron powders had improved during recent years (1975) and that few quantitative correlations had been made between mechanical properties and sintered pore structure. The powders had different specific surfaces due to their different shapes. The results indicated that variations in specific surface and impurity levels had a pronounced effect upon the sintering behaviour of the three powders. The electrolytic powder had the lowest oxygen content and the highest specific surface and was observed to form metallic

contacts in compacts sintered at low temperatures. The atomised powder had a relatively high oxygen content which was rapidly removed from particle surfaces at about 400°C . Esper et al. suggested that this reduction left active iron atoms on the particle surfaces and in grain boundaries, which promoted sintering and maximum shrinkage. The sponge iron powder exhibited a low rate of sintering, presumably due to its low specific surface and the lower surface activity caused by the small amount of oxide. In the opinion of the authors, pronounced differences in sintering behaviour were revealed by the study, but the variations in properties reported for the normal range of sintering temperatures were relatively small.

Carbonyl and atomised iron powders were examined by Lenel et al.³⁴ for the purpose of comparing the sintering behaviour of these materials. The rate of sintering of compacts made from atomised powder was much the slower, although a major reason for this was probably the larger size of the atomised powder particles. A further reason was that the atomised particle surfaces were contaminated with small calcium manganese silicate particles introduced from the basic slag used in the steelmaking process. Compacts which had been sintered for one hour at 1100°C were fractured by impact at -196°C : the fractures in carbonyl material were predominantly transgranular whilst those in atomised material were intergranular. The presence of slag particles on the fracture faces of atomised material suggested an association between these particles and the fracture path. The stability of the inclusions, after sintering the compacts in hydrogen,

was indicated particularly by the manganese and oxygen contents which were little affected by the sintering treatment. In contrast, the much higher oxygen content of the carbonyl powder was significantly reduced by the sintering treatment. The reduction in iron oxide on the surface by hydrogen at normal sintering temperatures is of interest in the current work, although it has been shown³⁵ that small non-metallic inclusions do not seriously affect the properties of sintered steels until porosity has been reduced to below 5%. Despite the influence of specific surface upon the subsequent mechanical properties of sintered iron compacts, there appears to be little doubt that the high chemical purity of electrolytic iron powders allows high densities to be achieved. Zapf³⁶, in pointing out that impurity elements reduce the compressibility of iron powders, has reported that 90% density was possible in electrolytic iron compacts pressed at about 600MN/m^2 ; the best tensile strengths and ductilities obtainable after specific sintering programmes, involved the use of this material.

Iron powder alone is rarely used for engineering components unless appreciable tensile ductility is required. The low strength of iron compacts may be improved at the expense of ductility by the addition of graphite. Such additions also aid the reduction of oxides during sintering³⁷. This feature, according to Gummeson³⁷, in conjunction with the high ash content of natural graphites, makes it necessary to add more graphite than would be indicated by the required final analysis. Although Gummeson stated that it was not possible to determine what properties of a particular graphite

made it suitable for adding to iron powder, his data suggest that fine natural graphites of low ash content are preferable to synthetic graphites. However, these conclusions were based upon high carbon steels for high strength applications and no reference was made of tensile ductility. Dautzenberg³⁸ investigated the effects of six grades of natural graphite on the tensile strengths of sintered steels; the graphites differed both in purity and particle size. The over-riding factor in the selection of graphite appeared to be high purity. Synthetic graphites have the advantage of guaranteed purity plus the benefits of low ash content and fine particle size to aid diffusion. Chadwick and Broadfield³⁹ found that, in iron-graphite alloys, the solution of graphite was complete after one hour of treatment at 1000°C and after only 15 minutes at 1125°C. Carbon loss, in both 1% and 2% graphite alloys, was approximately 22% after sintering in a cracked ammonia atmosphere. Cundill et al⁴⁰ found that blended low alloy steels with either synthetic or natural graphite additions suffered carbon losses of between 15% and 20% after sintering in hydrogen for one hour at 1150°C. Other similar carbon losses have been reported for medium carbon steels after similar sintering treatments^{38,41,42}. Judd⁴³ reported that synthetic graphites attained equilibrium distribution very quickly; this was due to their high reactivity relative to natural graphites, which required longer sintering times to achieve the equilibrium condition. Graphite particle size^{38,44} and the use of nickel coated graphite⁴⁴ appear to exert little influence upon the properties of the final product. Although there seems to be doubt as to whether

natural or synthetic graphites are preferable, the former still dominate the alloy steel province.

The difficulties of alloying practice in powder metallurgy was the subject of an investigation by Lindskog and Skoglund⁵⁰, in which they emphasized the problems of dimensional changes due to diffusion during sintering and the risk of partly or completely oxidising alloying elements in the process. The large surface area associated with a powder compact makes it very susceptible to oxidation, so that not only is the effective alloying content reduced but the presence of residual oxides after sintering may have a deleterious effect upon mechanical properties. Oxidation therefore limits the number of alloying elements which can be used in conjunction with iron powders. Arbstedt⁴ has referred to the ease with which compacts could be prepared from elemental powder blends and also mentioned the advantage of nickel additions because of that element's low affinity for oxygen. The disadvantages of using particles of nickel were that, due to the low rate of diffusion of nickel in iron, very fine particle sizes were required (thus creating segregation problems in mixing) together with long sintering times at high sintering temperatures. Nevertheless, the element most used for its beneficial effect upon hardenability was still nickel (1976), often together with molybdenum. Jones⁵¹ considered a major advantage of adding nickel to sintered steels was that both strength and toughness could be obtained by a reduction in carbon content. This argument was well illustrated by Kravic and Gloor⁴⁶ in results which showed that a 5% nickel; 0.2% carbon steel had equivalent strength but much improved

ductility and toughness compared to a 0.5% carbon steel similarly treated and of the same density. Some published mechanical properties of sintered low alloy steels which contain nickel as the major alloying element are given in Table 2. The values of ductility figures should be regarded with caution as it was not usually clear upon what basis the figures had been calculated. Although there are differences in density, there is evidence that both increases of nickel content and the degree of sintering give rise to increases in tensile strength. Further additions of manganese and/or molybdenum increase tensile strength at the expense of tensile ductility. It may be argued, from the sintering times and treatments shown in Table 2, that full advantage of the nickel addition is not obtained in cases where insufficient homogenisation occurs, i.e. improved mechanical properties may be obtained after treatments involving increased sintering times. This view has been expressed by Burr and Krishnamoorthy⁴⁴ who recommended high temperature sintering followed by heat treatment specifically designed for sintered materials. It is of interest to note that these authors found that molybdenum could be added as a cost-saving ferro-alloy without detriment to final properties but that ferro-nickel was inferior to elemental additions. Cundill et al⁴⁰ have reported on the structures and properties of both pre-alloyed and blended nickel steels, which had been sinter forged to near full density. The significant lack of hardenability in blended alloys was attributed to the segregation of alloying elements. This was associated with the non-attainment of fully martensitic structures after heat treatment. Steels with chromium as the major alloying element, rather than nickel, were found

to possess similar tensile strengths but inferior tensile ductilities, due to the more severe segregation exhibited by these alloys. The adverse effects of shrinkage in nickel-containing steels may be counteracted by copper additions^{46,52}.

3.2.2 Mixtures of partially and fully pre-alloyed powders.

These powders are designed to minimise segregation. It has been shown⁴ that the effect of partial pre-alloying on the compressibility of water atomised iron with nickel, copper and molybdenum is practically negligible. Arbstedt⁴ considered it unlikely that completely pre-alloyed powders would find many applications in which high compressibility was essential; a further factor was the adverse influence of these powders on tool wear. The partial pre-alloying process involves the heat treatment of a mixture of iron powder and alloying elements in a reducing atmosphere. The appearance of pre-alloyed particles by scanning electron metallography was examined by Wastenson⁴¹: nickel could be detected as small particles adhering to iron particle surfaces. The most commonly used powder of this type (according to Wastenson) consists of 1.75% nickel; 1.5% copper; 0.5% molybdenum; balance iron. Sintered compacts of this powder were compared with compacts of similar analysis prepared from elemental powders: the former were found to be superior in tensile strength, ductility and constancy of dimensions. Nickel contents in excess of 1.75% were found to increase the amount of retained austenite in the microstructure after cooling from the sintering temperature. Consequently, it was suggested that increases in nickel content should only be carried out with simultaneous reductions in carbon content;

this procedure would then allow nickel-rich areas to transform to martensite on cooling. A further aspect of the work was that impact strength and tensile ductility were linked only with the sintered density of the test pieces; nickel content, type of iron powder or time at sintering temperature did not affect this correlation.

The principal advantage of fully pre-alloyed compacts over blended and partially pre-alloyed compacts is in increased hardenability^{53,54}. With respect to fully pre-alloyed powders, Lindskog⁵⁴ stated that the improvement in hardenability must be balanced against the loss in compressibility caused by the introduction of the alloying element. It has been reported that fully pre-alloyed iron-carbon powders may possess compressibility approaching that of the pure iron powder³⁸. This report, due to Dautzenberg, showed that this was made possible by an annealing treatment. The bulk of fully pre-alloyed powders is made by atomisation⁴. The shape of the atomised particles is apparently extremely variable depending on the particular material involved, changing from angular through irregular to near spherical shapes⁵⁵. Although it has often been stated^{55,56,57,58} that atomised powders are contaminated by oxide films, oxygen contents are not often given in reports of powder characteristics. Davy-Loewy have given typical figures for low alloy steel powders as 0.3% oxygen. Kapustin et al⁵⁸ have reported that the oxygen in sponge iron powders was present as both FeO and Fe₃O₄. It was the opinion of these authors that the form of the oxide contamination was important from the point of view of effective reduction annealing. An

alternative method of producing homogenous powders has been developed at the Institute of Materials Science in the Ukraine^{59,60}. Mixtures of elemental powders such as iron and titanium⁶⁰, iron and manganese or nickel and manganese⁵⁹ were placed in active media with halides of the respective metals and heated to allow "thermal diffusion impregnation" to occur. This process depends upon the composition of the gaseous phase, the rate of surface reactions and the diffusion rate of the elements into the solid particles. Several hours of treatment at 1100°C were reported to be necessary in order to obtain an acceptable degree of homogenisation, which was determined by means of an electron probe micro-analyser.

3.2.3 Techniques for the production of coated powders.

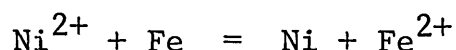
Arbstedt⁴ considered the technique of coating metal powders as one which resulted in extremely good starting conditions for diffusion during sintering. However, he dismissed the method on the grounds of prohibitive cost. In a review of the production of metal powders and coatings by precipitation, Burkin⁶¹ referred to the lack of data in this recently established technology. Two coating techniques were discussed by Burkin, which he described as reduction by hydrogen and electroless plating. In both methods, reduction of the solution in which solids are suspended takes place but electroless plating employs reducing agents other than hydrogen, e.g. hypophosphites. Other techniques have been described in the literature but the one of greatest commercial significance must be that of hydrogen reduction as developed by Sherritt Gordon Mines Ltd.⁶². This method was developed from the method used by the Company to manufacture metal

powders by gaseous reduction of aqueous solutions⁶³. The process of nickel coating utilises the reduction of ammoniacal solutions of nickel sulphate by hydrogen at 200-350 psi. at a temperature of 150-200°C. The reduction of nickel ions to metal is a heterogeneous reaction, i.e. it proceeds at a useful rate only on some solid catalytic surface. In normal powder production, this surface is provided by nickel seed powder, which is replaced in the coating process by the core material. Due to the tendency of nickel to deposit preferentially on freshly deposited nickel and so produce non-uniform coatings, it is the practice to activate the surface of the core material by the addition of anthraquinone. By this means, nickel has been deposited on iron, copper, aluminium, alumina, tungsten carbide, graphite, glass, phosphorus etc.^{62,64}. However, Burkin⁶¹ has pointed out that, if the proportion by weight of nickel is less than about 20%, the coating is discontinuous in almost every case.

Electroless nickel plating of conventional materials is well documented and the theory and practice of the method has been given by Brenner⁶⁵. He defines the process as chemical plating not involving chemical reaction with the basis metal, which is associated with the deposition of metal only on catalytic surfaces. The composition of a plating bath for nickel typically consists of nickel chloride, hypophosphite ion as a reducing agent and an organic acid which acts as a complexing agent as well as, together with other additions, a buffer. Both acid and ammoniacal baths have been found to be usable at temperatures approaching 100°C. The role played by the complexing agent is critical if the

formation of insoluble salts is to be prevented and the metal stabilised against homogenous reaction, i.e. reaction resulting in the formation of metal powder rather than metal plating. Rao et al⁶⁶ experimented in the electroless nickel plating of iron powder; the plating was considered to be uniform and studies of sintering characteristics were reported to be in progress.

An unpublished report of a nickel coating process has been made by Rigg⁶⁷. A simple cementation reaction was shown to be possible for coating iron powder by its addition to nickel chloride solution:



Provided that the pH and the temperature of the solution were carefully controlled, it was claimed that the process was suitable for the preparation of products containing up to 50% of nickel. An interesting feature of the report was that the efficiency of nickel recovery was greatest for low nickel contents but no report of coating continuity was given.

Pinner et al⁶⁸ have presented a detailed account of the conventional methods of the electroplating of nickel. The standard Watts bath of nickel sulphate, nickel chloride and boric acid was considered to be adequate, provided that strict control of temperature and pH was maintained. For the barrel plating of small parts in bulk, nickel chloride was replaced by ammonium chloride; this solution has been found to be capable of depositing very thin coatings at room temperature and at low current density. A method of electrodepositing iron or nickel on to stainless steel powder has

been described by Salt⁶⁹. This was developed in order to replace the persistent oxide film on steel particles in a plating solution (Fig. 1). At a solution flow rate slightly above that required for fluidisation, the particles were in a constant state of agitation and thus were able to make frequent electrical contact with one another. Using the apparatus shown in Fig. 1, 60g of stainless steel powder were fluidised in ferrous chloride at controlled pH and temperature. The passage of 3A at a potential of 18V for 5 minutes was sufficient to indicate that most of the particles had received a coating of iron. This treatment resulted in the deposition of 0.32% of iron by weight. A larger prototype was also described briefly by Salt, in which 1.5kg of powder received an iron coating equivalent to 1.3% by weight, after a plating time of one hour. A simple but apparently effective method of powder recovery was the reversal of the pumping direction, which left the plated powder on the sintered glass disc.

3.2.4 The mixing and compaction of powders.

A review of the production of powder metallurgy parts by Marshall⁷⁰ referred to the various types of industrial mixers which were designed to produce uniform mixtures in short mixing times. He pointed out that the reasons for this were not only economic but that powder characteristics could be altered by long mixing times and that there existed a distinct possibility of unmixing of the constituents. At that time, Marshall was of the opinion that little was known about the fundamentals of mixing (1968). It was envisaged that, generally, the efficiency of mixing could be neglected⁷⁰.

Incorrect mixing offsets the benefits of deliberately using fine alloy powders to reduce diffusion distances and promote rapid homogenisation during sintering. Examples are to be found^{71,72} which support the view expressed by Dixon and Clayton⁷³ that consistent performance in pressing and sintering cannot be maintained unless consistently uniform mixtures of powders are made available.

In almost all cases involving the manufacture of iron-base parts, a lubricant is mixed in with the constituent powders before pressing, in order to reduce die wall friction⁷⁰. Geijer and Jamison⁷⁴ found that, whilst zinc stearate and stearic acid both slightly reduced the sintered strength of parts (relative to the strength of parts pressed without admixed lubricant), the greater compressibility of the mixtures enabled higher densities to be obtained at specific pressures. Work by Yarnton and Davies⁷⁵ suggested that additions of lubricant just sufficient for the production of a monomolecular layer over each particle would give a consistent product. Excessive lubricant addition was shown to retard the close packing of irregular particles. Further work by these authors⁷⁶, on the effects of lubricating the die wall, showed that this method was superior to that of admixed lubrication. This conclusion was also reached by Leopold and Nelson⁷⁷. Although it would be clearly inconvenient in the rapid production of powder compacts, the use of die wall lubrication would eliminate the low temperature de-waxing treatment commonly given to compacts prior to sintering. In addition, the use of die wall lubrication appears to produce more uniform compaction and thus a greater consistency in the

final product.

In the die pressing of soft electrolytic iron, Goetzel⁷⁸ stated that a compaction pressure of almost 700MN/m^2 was necessary to obtain 90% of the theoretical density. This figure is some 15% higher than that given by Zapf³⁶ and indicates that densities after pressing depend largely upon specific pressing conditions. In an investigation into the properties of low alloy nickel steels, Munro⁷⁹ pressed compacts at 540MN/m^2 as this was considered to be typical of current (1972) commercial practice. Unckel⁸⁰ showed that the lack of uniformity in die-pressed compacts of iron could give rise to density differences of up to 30%.

The mechanical properties of sintered compacts formed by isostatic pressing have been reported as superior to those of compacts formed by die compaction⁸¹. Van Buren and Hirsch regarded this improvement as a characteristic feature of isostatically pressed material. Jackson⁸² has referred to the production of uniform components by isostatic pressing and gave the attainment of uniform strength in all directions as a major advantage of the technique. Jackson was of the opinion that angular particles, as typified by electrolytic powder, produced the strongest and most dense compacts. There appears to be some conflict as to whether de-airing of powder is beneficial^{81,82,85}. In a review of the isostatic pressing of metal powders, Morgan and Sands⁸³ reported that it was generally accepted for compacts produced by this process to possess more uniform densities than those produced by die compaction. This was believed to be due to the absence of die wall friction. Both James⁸⁴ and Sellors⁸⁵ have provided

pressure-density relationships for several types of iron powder. It can be concluded from their data that, whereas 80% density is normally achieved at pressures of about 300MN/m^2 the attainment of 90% density would require pressures in excess of 650MN/m^2 .

3.2.5 The sintering and heat treatment of compacted metal powders.

The most important variable to influence the structure, homogeneity and properties of powder compacts is the sintering process. Despite the extensive amount of information⁸⁶ available on the theory of sintering, no single definition of the sintering process has been universally accepted. To some degree, this signifies the complexity of the problem. However, it is generally agreed^{86,87,88,89} that the process may be divided into three stages as follows:

- (a) interparticle neck growth,
 - (b) densification and grain growth
- and
- (c) pore spheroidisation and slow densification.

There appears to be little doubt^{90,91} that the parameter most usually considered to provide direct evidence for the initiation and continuation of sintering is densification. The industrial powder metallurgist is unlikely to equate sintering with densification but would probably take the view⁸⁸ that powders should be simply consolidated into components with controlled structures, properties and dimensions. The criterion of the rate of neck growth, used by Kuczynski⁹² to differentiate between the several mass transport mechanisms considered to be possible in sintering, has been criticised by Rhines^{90,93}. This author pointed out that the only

geometric change necessary in densification was the approach of particle centres, i.e. there was no direct relationship between densification and neck growth since the latter could occur without any change in the relative positions of particle centres. Rhines was of the opinion that neck growth measurements could not be used to identify the transport mechanism that was responsible for densification. The topological model of sintering proposed by Rhines⁹³ was developed subsequently^{87,90} and a brief summary of how this relates to the mechanistic approach is given below. The model is concerned with the geometrical changes which occur during sintering and which may be observed by cutting a series of sections (serial sections) through the powder compact. Of prime importance to this model is the genus of the powder compact, which Rhines defined as follows:

$$G = C - P + 1$$

in which G = genus of the aggregate,

C = number of particle contacts

and P = number of particles.

The genus of a compact has been found to be independent of the relative size and shape of the particles in the compact and, together with other topological properties, to change as follows.

(a) During interparticle neck growth, the genus remains almost constant along with grain size. Pore surface irregularities are smoothed whilst the pore surface area and mean curvature decrease.

(b) The dominant geometric change to occur during the second

stage of sintering is that of constriction and closure of interconnected pore networks. The genus decreases rapidly towards zero. Pore surface area decreases linearly with the volume fraction of porosity. Dehoff and Aigeltinger⁸⁷ have suggested that this indicates the establishment of a balance between those transport mechanisms which produce surface rounding and those which promote densification. The mean pore intercept and the mean grain intercept remain essentially constant during this stage.

(c) The coarsening of isolated pores is accompanied by a non-linear decrease in pore surface area and the mean pore curvature decreases. The mean pore intercept increases as coarsening continues and the mean grain intercept suddenly increases sharply.

Dehoff and Aigeltinger⁸⁷ stated that, because the above geometrical changes could only be effected by different processes, the kinetics of sintering could not be described in terms of a single mechanism. Although it is well established that there are four possible mechanisms by which the phenomena observed in sintering may occur^{88,94}, viz. viscous or plastic flow, evaporation-condensation, surface and grain boundary diffusion and volume diffusion, there has been a continuous debate as to which mechanisms predominate at each stage. The complex nature of the process has led to the use of wire models rather than powder compacts in attempts to distinguish between the different mechanisms of material transport. This approach has, in its turn, been criticised⁹⁵ as inadequate because the assumed simplicity departed substantially from conditions which existed in practice.

Kuczynski⁹⁴ considered that the most important mechanisms involved in neck formation, were volume diffusion, which produced densification, and surface diffusion, which produced shape changes but not densification. By the use of copper wire models, Alexander and Baluffi⁹⁶ were able to show that pores ceased to shrink once they became detached from grain boundaries, which illustrates the role of boundaries as vacancy sinks. The technique of Alexander and Baluffi⁹⁶ was employed by Pranatis and Seigle⁹⁸ in an investigation into the sintering behaviour of iron and nickel. In iron sintered at temperatures within the alpha range, the observed lack of void shrinkage was ascribed to the predominance of surface diffusion over volume diffusion at the low sintering temperature. The rate of neck growth in nickel was in agreement with Kuczynski's theoretical prediction for a volume diffusion mechanism; void shrinkage in nickel was noticeably inhibited in samples from which grain boundaries had been deliberately eliminated. Kuczynski and Stablein⁹⁷ found that, in iron-nickel wire models, surface diffusion of nickel occurred around the iron and was followed by grain boundary diffusion during the early stages of neck formation. These authors concluded that:

- (a) the volume changes produced during sintering were mainly associated with diffusion processes,
- (b) that interdiffusion between different elements hindered sintering by the creation of porosity, and
- (c) that surface diffusion was probably predominant at low temperatures.

The above works, though here but briefly surveyed, are

representative of the convincing evidence of the major role played by diffusional processes in the sintering of industrially important metals. However, it is clearly not true to say that the sintering of any material occurs solely by diffusional processes. Thummler and Thomma⁸⁶ and Moon^{88,89} have referred to work other than on metals in which evaporation-condensation and plastic flow were found to be the dominating influences in sintering. With reference to the early stages of sintering, upon which the bulk of research has been concentrated, Lenel^{99,100} has persistently argued in favour of a plastic flow mechanism and has suggested that the generally accepted rate law for neck growth by plastic flow (due to Kuczynski⁹²) is incorrect. Lenel has drawn a parallel between sintering and creep. He postulates that dislocation motion predominates while the stresses due to surface tension forces are high (as in creep at high stresses): when the necks between particles grow and pores begin to spheroidise, surface tension forces relax and material transport by diffusion becomes the dominant mechanism (as in diffusion controlled creep at low stresses).

In a discussion of multi-component systems in which there was mutual solubility, Thummler and Thomma⁸⁶ differentiated between the following:

- (a) sintering of homogenous solid solutions,
- (b) sintering with simultaneous homogenisation, and
- (c) sintering with the decomposition of solid solutions.

The sintering of pre-alloyed iron-nickel powders is an example of the sintering of a homogenous solid solution. Changes in the homogeneity of such a material could arise due to the

different rates at which iron and nickel diffuse to the interparticle neck regions. It is known^{88,89} that the diffusion of iron into nickel is greater than that of nickel into iron so that the neck regions may become initially rich in iron. An example of similar behaviour was reported by Kuczynski et al¹⁰¹, in the sintering of an initially homogenous copper-indium solid solution; the precipitation of an indium-rich intermetallic compound was observed at the neck surfaces. This effect was considered to be due to the greater diffusivity of the indium. The sintering of blended iron-nickel powders is an example of sintering with simultaneous homogenisation. Thummler and Thomma⁸⁶ considered that the inhibition or promotion of sintering, due to the presence of the second component, was decided, not by the solid solution formation, but by the partial diffusion coefficients of the components. As a consequence of the variable rates of diffusion throughout homogenisation, new lattice vacancies would be formed which would promote sintering by the resultant increase in atom mobility. On the other hand, sintering would be inhibited by the coagulation of vacancies to form Kirkendall porosity. Both sintering and homogenisation appear to be controlled by diffusion processes but the rates of these processes may be quite different for reasons discussed above. Thummler and Thomma⁸⁶ made the point that homogenisation should not be equated with sintering. It is clear that changes in density could result from either or both of these processes. It was stated earlier that densification was often taken as evidence for the progress of sintering; in the copper-nickel system¹⁰², it was found that sintering (as indicated by densification) was inhibited by the process of homogenisation.

Fisher and Rudman¹⁰² related the observed initial expansion of copper-nickel powder mixtures to the degree of interdiffusion of these elements. Beyond a certain degree of interdiffusion, expansion ceased and further treatment resulted in shrinkage of the material. Homogenisation can therefore occur irrespective of densification and, if the latter is controlled mainly by volume diffusion and grain boundary diffusion^{88,89,94,96,98}, then this is some support for the view^{97,102,103,104} that a significant contribution towards homogenisation is made by surface diffusion.

The choice of sintering temperature depends upon the objectives of the sintering process. A compromise is normally taken between the economic factors in production and desirable attributes of the sintered material^{88,89}. If densification and its associated benefits are the main aims, then the lowest practicable temperature should be employed to inhibit grain growth. Most iron-base materials are sintered at 1000°C-1150°C⁵ but, if higher strengths and some degree of ductility and toughness are required, sintering may be performed at 1300°C-1350°C. In a report of industrial developments, B.S.A.¹⁰⁵ have stated that, for the bulk of the steels they produced (about one third of the British market in 1970), the sintering temperature range was 1120°C-1140°C; high strength alloys were sintered at temperatures up to 1300°C. Harrison and Dixon¹⁰⁶ were able to show that, in nickel-containing steels, the sintering temperature of 1300°C could be reduced to 1150°C without substantially affecting properties, provided pre-alloyed powders were used rather than blended powders. In an investigation of the properties of

nickel-molybdenum steels, Munro⁷⁹ selected a sintering temperature of 1300°C in the belief that the corresponding diffusion rates would produce optimum properties in compacts made from blended powders. The above data indicate that sintering temperatures within the range 1000°C-1350°C are feasible for low alloy steels but that, depending upon the nature of the powders and the properties required in the compacts, optimum results may be obtained by sintering at approximately 1150°C or 1300°C.

Sintering is inhibited by non-reducible oxide layers^{86, 95,107}; hence sintering in reducing gases prevents the formation of such barriers to diffusion. Heath and Evans¹⁰⁷ studied the effects of sintering atmosphere on the fracture characteristics of copper; sintering in nitrogen was associated with tensile fracture necks which possessed central ductile regions surrounded by annular brittle regions, whereas sintering in hydrogen was associated with ductile failure only. In the latter case, fracture dimples were found to contain discrete oxide particles rather than the continuous oxide films observed in compacts sintered in nitrogen. The sintering atmosphere performs the function, not only of oxidation control, but also of carbon control^{108,109}. Coult and Munro¹⁰⁸ considered that, in the sintering of steels, changes in carbon content were due to reactions between the admixed graphite and surface oxides or furnace gases. Their view of the unwise application of equilibrium data, in the absence of information about the kinetics of the reactions, was shared by Kaufman¹⁰⁹. This author maintained that few, if any, production facilities were capable of achieving uniform and

constant carbon concentrations in steel compacts during normal sintering cycles (1973). Kaufman's data indicated that the use of atmosphere control to regulate carbon content throughout the compacts was unlikely to be of practical value. He suggested that, in those cases of sintering with admixed graphite at 1122°C , the interior carbon content of compacts would be governed completely by the reaction of graphite with adsorbed water vapour and residual oxides. Furthermore, the exterior regions of compacts would suffer decarburisation at a rate dependent upon the composition and flow rate of the control atmosphere and upon the amount of adsorbed gases on iron particle surfaces. Carbon control was shown to be best performed after the completion of high temperature sintering by means of a hydrocarbon atmosphere at temperatures as low as 760°C . The cylinder gases used by Kaufman were carbon monoxide, methane, nitrogen and hydrogen, each of which was subjected to purification and some of which were used to form mixtures. Residual oxygen was removed from hydrogen by passing it through a platinised asbestos catalytic purifier, after which the resultant water vapour was removed in magnesium perchlorate drying towers. These reagents have also been recommended for the treatment of atmospheres for experimental purposes¹¹⁰.

Marshall⁷⁰ has reported that sintered steels may be heated in a neutral atmosphere after sintering and then quenched to produce a hard martensitic component in a similar way to that applied to solid steel parts. Reference was made to the problems associated with the production of case hardened parts in compacts of measurable permeability, but no

mention was made of quenching media for sintered steels. The quenching of sintered iron-graphite compacts was investigated by Chadwick and Broadfield³⁹, who found that oil was effective with porous specimens, that water only was effective with dense specimens but that water quenching of very porous specimens was associated with the formation of surface cracks. They concluded that these results could be explained by the effect of permeability on the quenching rate. Kravic and Gloor⁴⁶ reported that sintered nickel steels responded well to the conventional processes of heat treatment; compacts were quenched in oil and tempered at temperatures up to 650°C. Although reports on the properties of sintered and heat treated steels have become more numerous^{42,44,79,111}, little work into heat treatment conditions has been carried out. Burr and Krishnamoorthy⁴⁴ referred to the lack of information concerning the heat treatment of sintered steels and suggested that improved properties might be obtained by selecting treatments specifically for these materials. These authors hardened blended compacts of a nickel-molybdenum steel by oil quenching from customary austenitising temperatures and followed this by tempering over a wide range of temperature. It was concluded that tempering at the relatively high temperature of 650°C - 675°C was necessary in order to produce an optimum combination of tensile strength, ductility and impact strength. In view of the cost consciousness of the powder metallurgical industry¹¹², it is surprising to the present author that few investigations have been performed in which heat treatment was combined with the sintering operation. Munro⁷⁹ has pointed out that the role of carbon in sintered steels has been underrated, since these materials are

normally cooled from the sintering temperature at a rate which is insufficient to allow the martensite reaction to occur. Fischer⁴² approved of the use of heat treatment of steels subsequent to sintering but commented on the drawbacks of such operations. These were considered to be the increased cost of manufacture, quench cracking or distortion, problems of atmosphere control and the need for additional processing steps such as degreasing and surface cleaning. Fischer found that, in low alloy steels subjected to controlled cooling of between 10°C and 38°C per minute after sintering, increased amounts of nickel resulted in improved tensile strength and hardness. Fischer also mentioned the possibility of developing air hardening steels. Fedorov et al¹¹³ investigated the effects of similar rates of cooling as those employed by Fischer, but on iron-copper-graphite material; he found that increased tensile strength could be obtained by an increase in the cooling rate after sintering. In both of the above investigations^{42,113}, the increase in tensile strength was associated with the establishment of non-uniform microstructures.

Table 3 shows typical mechanical properties of sintered and heat treated low alloy steels of medium carbon content. Certain points concerning this data should be noted.

(a) Sintering temperatures prior to heat treatment were at the upper limit of the range often quoted for steels^{5,105}, i.e. around 1300°C. This high sintering temperature was clearly selected in order to make full use of alloying additions in the subsequent heat treatment.

(b) A comparison of Tables 2 and 3 shows that quenching and

tempering normally increased the tensile strength at each composition but that tensile ductility could be reduced. The values of ductility were often given without any reference to the standard employed, i.e. the relationship between the gauge length and cross sectional area of the test pieces was not usually given. It is likely that the quoted values, certainly in the case of data due to Munro⁷⁹, would be lower by some 20% were the current British Standard relationship applied¹¹⁶.

3.3 RELATIONSHIPS BETWEEN PROPERTIES, STRUCTURE AND HOMOGENEITY IN SINTERED POWDER COMPACTS.

A relationship of major interest to the powder metallurgical industry is that between the density and mechanical properties of the product, since the prediction of mechanical properties from a knowledge of density is of considerable practical importance. In instances where iron compacts have been employed to investigate this relationship, complications due to variable microstructure have been eliminated. In the case of steels, the microstructure is markedly affected by the overall composition of the material and by local variations of composition within the compact. Thus the homogeneity of steels is likely to exert a major influence on the relationship between mechanical properties and density. The contribution of homogeneity has normally been considered qualitatively by reference to non-uniform microstructure and not to measurements of the distribution of alloying elements. The degree of homogenisation has been measured and compared to that predicted by model behaviour, usually in attempts to identify the mechanisms responsible for homogenisation. There have been few reports relating properties, structure and homogeneity

in sintered materials and, so far as this author is aware, none of these have attempted to quantify the relationships over a range of density.

3.3.1 Physical and mechanical property relationships in powder compacts.

Krishnamoorthy³¹ studied the properties of iron compacts sintered to within the range of 86%-100% of the theoretical density. Tensile ductility was much more adversely affected by porosity than was tensile strength. Impact strength was so low that the influence of density did not become apparent until compacts exceeded 94% of theoretical density. Wastenson⁴¹ performed a similar set of experiments but for a series of low alloy steels which contained nickel, molybdenum and copper. Tensile strength and hardness were each found to exhibit linear relationships with density, which differed according to whether compacts had been single or double pressed. Tensile ductility and impact strength were not sensitive to preparation conditions but varied only with sintered density. The above reports indicate that tensile strength is more likely to show a correlation with density than other mechanical properties over a wide range of density.

McAdam¹¹⁷ plotted his own experimental data together with that of earlier workers^{43,118,119} on a graph of elastic modulus against porosity for iron-base alloys; the graph indicated that, despite differences in alloy constitution and sintering treatments, tensile properties depended largely upon density. He expressed the relationship in the form of an equation, viz.,

$$E_n = 29 (1 - P)^{3.4} \times 10^6 \text{ p.s.i.}$$

in which E_n = nominal elasticity and

P = fractional porosity.

This was modified to a dimensionless equation, viz.,

$$\frac{E_n}{E} = \left(\frac{\Delta S}{\Delta T} \right)^{3.4}$$

in which E = modulus of elasticity,

ΔS = sintered density and

ΔT = theoretical density.

In a review of the methods available for obtaining high density, Eudier¹²⁰ reported that sintered steels were rarely produced above 90% of theoretical density, on account of the low compressibility of iron powders, the necessity of avoiding shrinkage if dimensional control was to be obtained and difficulties of re-pressing solid parts after sintering. It was suggested, for a given density, the tensile strength of a powder compact was proportional to the corresponding strength of a fully-dense alloy. However, this relationship only applied if the latter possessed adequate tensile ductility; this property could be improved in relatively dense compacts by phosphorus additions. This beneficial effect of phosphorus additions has been confirmed by Wastenson⁴¹. Eudier¹²⁰ considered that, for a specific sintering time and temperature, the principal factors affecting densification were pore dimensions, oxide content, grain size, sintering atmosphere and the Kirkendall effect. The influence of pore geometry on the mechanical properties of sintered irons and steels was investigated by Gessinger et al¹²¹, who derived an empirical exponential relationship to correlate tensile strength with

porosity content and mean pore size. That porosity exerts the major effect upon mechanical properties was also shown by the equation put forward by Pines and Suchinin¹²², viz.,

$$\sigma = \sigma_0 (1 - \mu P)$$

in which σ_0 = strength of pore-free material and

μ = fraction of unsintered particle contacts.

This equation was very similar in form to that proposed by Eudier¹²⁰, viz., $\sigma = \sigma_0 (1 - K P^{\frac{2}{3}})$ in which K fluctuated between 0.98 and 2.26 according to the type of powder.

Haynes^{123,124} considered that the good correlation given by Eudier's equation was purely fortuitous and advanced his own theory to account for the variation in tensile strength with porosity, again in the form of an equation, viz.,

$$\sigma_{rel} = \frac{\sigma_{TS}}{\sigma_0^{TS}} = \frac{1 - P}{1 + a (F - 1) P} = \frac{1 - P}{1 + b P}$$

in which

σ_{rel} = relative strength of porous material,

σ_{TS} = tensile strength of porous material,

σ_0^{TS} = tensile strength of pore-free material,

P = fractional porosity,

F = theoretical stress concentration factor
of the pores,

a = arbitrary constant,

and $b = a (F - 1) = a$ constant, which was shown to be 2 for many ductile materials. By taking into account the stress concentrating effect of the pores, the theory of Haynes predicted the upper and lower limits of porous materials. The stress concentration factor, values for which Haynes obtained from previous workers, was considered to be relatively constant

at 2.5 for sintered materials with well rounded pores. The choice of a suitable multiplying factor "a" was apparently governed by the ductility of the matrix and was higher for materials with little matrix ductility. Haynes developed his theory further¹²⁴ in an evaluation of the strengths of sintered and heat treated plain carbon and low alloy steels. The basis for this work, as it was for that of Eudier¹²⁰, was that sintered steels for engineering applications must possess a limited amount of ductility. Eudier¹²⁵ had earlier shown that, in sintered steels of 86% of theoretical density, tensile strength could be predicted as 70% of that of the fully dense steel, provided that the latter possessed a minimum ductility of 20% elongation. If this was not the case, the sintered steel was brittle and exhibited a lower tensile strength than that predicted. According to Haynes, the minimum acceptable ductility was obtained when the ratio

$$\frac{\text{Yield strength}}{\text{Tensile strength}} = \frac{1}{1 + b P}$$

For pure iron, Haynes considered this ratio to be approximately 0.5 so that sintered pure iron with well rounded pores ($b = 2$) should have acceptable ductility up to approximately 50% porosity. This was believed to be the case.

The introduction of a factor to express the stress concentration effect of the pores was a logical development from the expression which simply related tensile strength to sintered density,^{120,123,129} i.e.

$$\sigma_s = \sigma_o (1 - P)$$

in which σ_s = tensile strength of sintered material,

σ_o = tensile strength of fully dense material
and P = fractional porosity.

Unfortunately, the relationships given in the literature, which relate to work on irons and steels and which incorporate such factors, have not usually included experimentally determined values of these factors. The usual approach has been to either incorporate the factors into constants or to employ theoretical factors based upon elasticity theory. It is generally accepted^{117,123,126,127,128} that, for similarly shaped pores, the elastic modulus varies approximately linearly with changes in porosity level of up to 30%. Values of stress concentration factor have thus been calculated by means of this linear dependence. In an attempt to verify theoretical predictions of the effects of pore properties, Nazare and Ondracek¹²⁷ performed some experimental work on cermets in which the dispersed phase was either spherical or oblate. It was suggested that the value of Young's modulus was given by

$$E_{\text{porous}} = E_{\text{solid}} (1 - F P)$$

in which F = stress concentration factor
and P = fractional porosity.

Agreement between the experimental and theoretical values was considered to be good. For porosity or dispersed phase contents of up to 30%, oblate shaped particles were shown to reduce the modulus more than did spherical particles. Values of "F" were given as 2 and 3.8 for spherical and oblate particles respectively. Comparisons of their own data with that from other published work showed that a wide variety of materials, from iron to uranium dioxide, possessed values of

elastic modulus which fitted the above relationship. Deviations from the theoretical prediction, especially in the range of high porosity, were ascribed to the effect of pore shape. The equation given by Nazare and Ondracek¹²⁷ was identical to that suggested by Pohl¹³⁰, who found that "F" varied between 2.6 and 3.4 in sintered irons and steels, but between 2.6 and 3.8 in sintered bronzes. The work of MacKenzie¹²⁶ suggested that the lower limit of "F" for spherical pores was approximately 2.

Gallina and Mannone¹²⁸ studied the effect of porosity on the tensile strength of sintered iron to ascertain whether the effect was similar to that found in a previous investigation¹³¹, which was concerned with elastic properties. This was in fact found to be the case and the following relationship was proposed to predict the strengths of sintered iron compacts:

$$\sigma_s = \sigma_o (1 - 3.6P) (1 - P)^{\frac{2}{3}}$$

in which σ_s = tensile strength of sintered iron,

σ_o = tensile strength of fully dense material,

and P = fractional porosity.

With increasing porosity content of up to 30%, the experimental results increasingly departed from those given by the above equation. This departure was shown to be due to the increasingly adverse influence of coarse particle size.

In view of the versatility¹³² of exponential equations, it is not surprising that several of the published empirical relationships between mechanical properties and compact variables are of this type. The values of tensile strength and ductility of compacts produced from ferritic and austen-

itic stainless steel powders were fitted by Napara-Volgina et al¹³³ to the exponential equation given below,

$$\sigma_s = \sigma_o \exp (- B P)$$

in which B = a coefficient determined by experiment.

The equation was found to predict the above properties equally well over a porosity range from 0% to 28%. The high level of ductility in these materials may well have accounted for the accurate predicted relationships, as suggested by other workers^{123,124,125}. Other Russian investigators^{134,135} have also expressed experimental data in terms of exponential equations. Shcherban¹³⁴ considered that tensile strength and ductility, bend strength, impact strength and elastic modulus all showed a similar dependence upon sintered density, viz.,

$$\sigma_{is} = \sigma_{io} (1 - P^2)^2 \exp (- B P)$$

in which

σ_{is} = i-th mechanical property of the sintered material,

σ_{io} = i-th mechanical property of the fully dense material,

P = fractional porosity

and B = a coefficient determined by the mechanical property and the preparation conditions of the sintered material.

The above relationship predicted deviations from experimental data in cases for which porosity was greater than about 30%. Shcherban stated that, in order to study the effects of any factor upon mechanical properties, it was only necessary to determine the effect of the factor upon the magnitudes of " σ_{io} " and "B". Although no practical examples were provided in the report, a uniform distribution of small pores was con-

sidered to reduce stress concentration, reduce the value of "B" and hence improve the mechanical properties. Other beneficial effects upon properties were said to be increased sintering time and temperature, the use of pre-alloyed powders rather than blended powders and the use of fine powder particles. An interesting point made by Shcherban was that ductile materials usually exhibited lower values of "B", which recalls Haynes' equation in which the value of "b" changed according to whether or not the minimum acceptable level of ductility was obtained. The dependence of "B" on sintering temperature was illustrated in a plot of σ_{is}/σ_{io} against sintering temperature/melting temperature; the result was an S-shaped curve in which a rapid change occurred in the value of σ_{is}/σ_{io} over the range of 0.6-0.8 of sintering temperature/melting temperature. This transition region would appear to correspond to the well known Tamman temperature used as an index of significant lattice mobility⁹⁵. A difficulty in the use of Shcherban's equation must be that, although the mechanical property value of the fully dense material is incorporated, the value of the coefficient "B" must also be changed by a factor appropriate to the mechanical property under consideration. Methods of testing which promoted rapid crack initiation and propagation were characterised by high values of the coefficient; for iron compacts sintered at 1200°C for two hours, data in the report indicated that the upper limit of the coefficient changed from 5.8 for impact testing to 4.8 and 3.3 for tensile ductility and strength respectively. The report indicated that the above test methods, if applied to different materials, brought about

significant changes in the value of the coefficient. It would appear that the all-embracing nature of the equation, whilst attempting to allow for any variable, could not easily be applied to the influence of any one variable. Salak et al¹³⁵ reviewed many of the published relationships between porosity and mechanical properties, in order to compare these with computed equations which best fitted a considerable wealth of data from many sources. It was noted that, although the previous work involved different factors such as pore shape, size, distribution, grain size and stress concentration factors but not all of these, several of the equations predicted similar curves. The strength of sintered iron was best expressed by the following equation:

$$\sigma_s = 344 \exp(-0.043 P) \text{ MN/m}^2 \text{ in which}$$

$$\sigma_s = \text{tensile strength of sintered iron,}$$

$$344 = \text{tensile strength of solid iron (MN/m}^2\text{),}$$

$$P = \text{fractional porosity}$$

and $0.043 = \text{an empirical constant.}$

The curve corresponding to this equation and those of several other workers were plotted on a graph of porosity versus tensile strength, which included 834 data points. The equation put forward by Haynes¹²³ gave a good fit for the tensile strengths of compacts with less than 20% porosity. The value of "b" in Haynes' equation was taken as 3 by Salak et al, which can be shown to be detrimental to that authors case. A value of 5 for "b" predicts strengths which lie close to those predicted by the equation of Salak et al. The considerable scatter band of the data was thought to be due to the shape, size and distribution of the pores in different

compacts. Reference was made to Modry¹³⁶ who found, by mercury porosimetry, that changes in pore shape occurred more rapidly in compacts with low porosity. This behaviour permits further reference to the "b" coefficient in Haynes' equation¹²³. For constant sintering conditions, the stress concentration factor in compacts of low porosity (with more rounded pores) would be expected to be less than that in compacts of high porosity (with less rounded pores). Thus the value of the Haynes coefficient, which incorporates a stress concentration factor ($b = a(F-1)$), would be expected to change gradually from a high to a low figure in compacts of decreasing initial porosity. It was stated earlier that the value for the theoretical stress concentration factor assumed by Haynes was 2.5 so that, for the case in which "b" is equal to 3, "a" is equal to 2. Using this latter value of "a" together with the limits of stress concentration factor, as determined by Nazare and Ondracek¹²⁷, the "b" coefficient in the Haynes equation can be made to change from 2 at near zero porosity (for ductile material with spherical porosity) to 5.6 at 30% porosity, (for similar material with oblate porosity). This modification of the Haynes relationship fitted the data in the report of Salak et al almost as well as that computed by those authors. However, neither of the equations could predict the strengths of compacts which deviated significantly from the mean values. Salak et al¹³⁵ also computed similar equations to predict the tensile ductility and hardness of sintered iron compacts; in both these cases, the inability of the computed relationship to accurately predict the measured values was ascribed to the greater sensitivity of

these properties to pore structure. The correlation between pore structure and mechanical properties has been discussed by Esper et al¹³⁷ with respect to different types of iron powder. These authors had earlier shown¹²¹ that strength was an exponential function of porosity only in compacts of comparable pore structure. By measurements of the correlation coefficient, these authors were able to show that the mean linear pore size exerted some influence upon strength as shown below:

$$K = A L \exp \left(- B P^{\frac{2}{3}} \right)$$

in which

K = radial crushing strength,

L = mean linear pore size,

P = fractional porosity

and A and B = constants which varied according to the iron powder type.

Neglecting the influence of pore structure, the correlation coefficient was reduced from 0.95 to below 0.90; lower values of the coefficient were also obtained by the use of the equations derived by Eudier¹²⁰ and Haynes¹²³. Reference was made to the equations due to Salak et al¹³⁵ in which no allowance was made for pore structure; the good correlation obtained was believed to be due to that between porosity and pore structure in compacts sintered under industrial conditions. An interesting illustration of the effect of pore structure on strength was provided in an investigation by Brockelman¹³⁸, in which the relationship between sonic velocity in iron compacts and the tensile strength of the compacts was much closer than that between this property and

sintered density.

Talmage¹³⁹ found that a linear relationship existed between the hardness and tensile strength of sintered materials and that this was similar to that for solid materials. His results indicated that this relationship was valid provided that the material was sufficiently uniform in both microstructure and pore structure. Buckle¹⁴⁰ has shown that pores exert a significant influence upon the apparent hardness of sintered products. He recommended that the characteristic hardness-load curves be established for heterogeneous and porous structures. In distinguishing between micro-indentation, low load and macro hardness tests, his work showed that there was a transition in measured hardness between high and low loads and that the critical field of medium loads gave unreliable results.

The overall picture concerning the influence of density on properties appears to be one in which

- (a) empirical relationships may be established with tensile strength,
- (b) relationships with other properties are confused by the increased sensitivity of these properties to pore structure, and
- (c) the existing relationships do not allow sufficiently for such variables as differences in pore structure and differences in microstructure.

3.3.2 Relation of microstructure to homogeneity and properties in powder compacts.

A survey of ferrous materials made by powder metallurgy over 40 years ago¹⁴¹ enumerated some of the difficulties which

hindered the development of these materials. Prominent amongst these were the attainment of metallurgical structures and grain sizes typical of conventional wrought products. Stern¹⁴² compared the mechanical properties of sintered steels made from different iron powders and attributed the superiority of electrolytic iron powders to the improved microstructures in the sintered steels. Work on similar material, to which nickel was added, was performed by Delisle and Knopp⁴⁵; these authors found that diffusion of nickel in a 3.5% nickel alloy was incomplete after six hours treatment at 1280°C. Compacts which were quenched and tempered possessed microstructures of nickel-rich martensite areas in a pearlite matrix: increased nickel contents produced continuous networks of the martensite regions and were responsible for reduced tensile ductility. The authors were convinced that further improvement in mechanical properties would result from the more uniform distribution of the martensite areas, a condition only considered to be possible by improved mixing and/or controlled homogenisation. Because of the slow rate of homogenisation in certain alloys, recourse has sometimes been made to changes in composition^{143,156} in efforts to improve mechanical properties.

The rate of homogenisation in copper-nickel alloys was measured by Rhines and Colton¹⁴⁴, with the aim of establishing optimum heat treatment conditions from a more detailed knowledge of the homogenisation process. Extension of this work by Rhines and Meussner¹⁴⁵ showed that the hardness and strength of a 70% copper; 30% nickel alloy attained maximum values short of complete homogenisation due to the creation of

a continuous network of 50% copper; 50% nickel. This phenomenon demonstrated the possibility of achieving, by suitable heat treatment, a combination of mechanical properties superior to those of the homogenous alloy. Heck¹⁴⁶ has also suggested that intentional heterogeneity could be used as a method by which improved mechanical properties may be obtained. Heck found that, in low alloy steels containing nickel, pre-alloyed powder compacts offered strength advantages over blended compacts in the sintered condition. However, in the quenched and tempered condition, compacts made from blended powders were better than homogenous compacts. The mechanical test results given by Heck showed that tensile ductility was only of the order of 1% elongation in any of the alloys. The speculation that less heterogeneity might result in improved ductility was refuted by the microstructures of the pre-alloyed compacts, which were apparently uniform. In a further detailed study of similar alloys, Heck collaborated with Fischer¹⁴⁷ in a programme which involved electron probe micro-analysis. Blended material exhibited very wide scatter in alloy distribution after compacts had been sintered for 15 minutes at 1120°C, viz., 0 - 11% nickel in alloys which contained 2% of this element. Variation in pre-alloyed compacts was less than 0.3% nickel. No details of the measurement technique were provided in this report. Heat treatment and further examination of blended compacts showed that three main features were distinguishable in the microstructures. The first of these was a light etching ferrite which contained 0- 1.5% nickel and possessed a hardness of HRB 74 (calculated from microhardness data). The second

feature was mainly a dark etching acicular, but occasionally lamellar, product which contained 1 - 3% nickel and was characterised by a hardness of HRB 90. A light etching constituent was the third feature containing 3-11% nickel and with a hardness which ranged from HRC 30 at the edges to HRC 60 at the centres of the areas. These latter areas were described as martensitic at the centres and bainitic at the edges. Martensite content was observed to be greater in compacts that had been sintered at higher temperatures.

Lindskog and Skoglund⁴⁸ suggested that a certain degree of heterogeneity may increase the strength of alloys of the type investigated by Fischer and Heck¹⁴⁷, i.e. 2% nickel; 0.5% molybdenum; 0.5% carbon. Partially pre-alloyed compacts which had been sintered for 15 minutes at 1120°C possessed a heterogeneous microstructure of the following phases: martensite (8-31% nickel), upper bainite (0.8-4% nickel), fine pearlite (0.1-0.8% nickel) and coarse pearlite and ferrite (0.1-0.2% nickel). Fully pre-alloyed compacts exhibited uniform structures of upper bainite after all sintering treatments. Pre-alloyed compacts which were fully dense before sintering showed little increase in tensile strength with sintering time, whereas the tensile strengths of partially pre-alloyed compacts increased rapidly until they reached and maintained the values attained by fully pre-alloyed compacts. In compacts of 96% density, the rate of increase in the tensile strength of partially pre-alloyed compacts was again rapid up to a sintering time of one hour, before and after which these alloys maintained a strength advantage over the fully pre-alloyed compacts. The authors attributed the

behaviour of the fully dense material to the attainment, by the partially pre-alloyed compacts, of a degree of homogeneity which was equivalent to that of the fully pre-alloyed compacts. The superiority of the partially pre-alloyed material, in compacts of 96% density, was explained by differences in pore structure due to the adverse effects of pre-alloying on the rate of sintering. Unfortunately, no details of tensile ductility or other properties were provided in this work, although it was contended that hardenability was much more sensitive to heterogeneity than were the properties of non-uniform microstructures.

The attainment of adequate hardenability in sintered low alloy preforms was considered by Eloff and Kaufman⁵³, who showed that blended compacts exhibited extensive non-uniformity in microstructure after sintering and heat treatment. The low hardenability of these materials was associated with the retention in the microstructure of nickel-depleted regions which did not transform to martensite on quenching. Lindskog⁵⁴ considered the factors that affected hardenability in blended and pre-alloyed steels. The well known effect of grain size²² on hardenability was thought to indicate poor hardenability in sintered steels since these were generally known to possess smaller grain sizes than most wrought fully-dense steels. For steels containing 2% nickel; 0.5% molybdenum; 0.9% carbon which were sintered to 90% density at 1120°C for one hour, the critical cooling rates (50% martensite basis) of blended and pre-alloyed compacts were determined as 19°C/s and 2.25°C/s respectively. Thus the heterogeneity of blended compacts was shown to adversely influence hardenability. The existence of voids was considered to make difficult both

hardness testing and the control of carbon content at the surface of the material. Therefore, the Jominy test was rejected as inadequate for the testing of sintered steels. The size and distribution of the pores themselves were not independently considered by Lindskog⁵⁴. Research into the insulating properties of ceramic materials^{148,149} has shown that, in similar materials of similar porosity, those specimens which contained the larger pores possessed the higher thermal conductivity. It may follow that, for similar steels sintered under similar conditions, those which contained the larger pores would exhibit the better hardenability.

The problem of whether uniform or non-uniform structures provide better properties was considered by Holcomb and Lovenduski¹¹¹ in 1974; these authors suggested that irrefutable evidence to support one view or the other did not exist at that time. Some criticism was made of the work of Heck¹⁴⁶ in that, although he found that a degree of non-uniformity in structure was desirable in blended alloys, the composition chosen by that author was not typical of commercial practice. The results of Holcomb and Lovenduski¹¹¹ on nickel-molybdenum steels were contrary to those of Heck. However, it was admitted by the former authors that, when a comparison was made on the basis of constant compaction pressure and composition, the superior compressibility of blended compacts was sufficient to produce equivalent strength but significantly greater ductility than in pre-alloyed compacts. The microstructures which gave rise to these properties were described as martensite in the pre-alloyed compacts and as mixtures of ferrite, pearlite and martensite in the blended compacts.

Fischer⁴² subjected nickel-manganese-molybdenum steels to controlled cooling from the sintering temperature in an effort to achieve high strengths without conventional heat treatment. The optical microstructures consisted of ferrite, pearlite, bainite and an amount of martensite which increased with increased nickel content. X-ray diffraction results indicated that the increased amounts of martensite were also associated with increased amounts of retained austenite. The dual effect of nickel upon the microstructure of these blended alloys was considered to prevent any great improvement in mechanical properties. Svensson⁴⁷ also concluded that the strengthening effect of nickel could be limited by austenite retention and suggested ways in which the problem could be overcome:

- (a) a ferrite stabilising element such as molybdenum could be added,
- (b) nickel could be incorporated in the form of partially pre-alloyed powders,
- (c) an increase in nickel content should be accompanied by a decrease in carbon content, and
- (d) the degree of homogeneity should be increased.

An increase in the degree of interdiffusion associated with an increase in the sintering temperature may not be entirely predictable. Although interdiffusion data for iron and nickel are available^{150,151,152,153}, it has been shown that the interdiffusion coefficient is concentration dependent at certain temperatures^{150,153} but not at others¹⁵³. Nevertheless, Wastenson⁴¹ was able to produce a linear relationship between tensile strength and the product of diffusion coefficient and sintering time, i.e. he predicted tensile

strengths by the use of diffusion coefficients which were assumed to be constant at particular sintering temperatures. This relationship depended upon the formation of regions of nickel-rich martensite, so that, when the degree of homogeneity reached a certain value after long sintering times, it was stated that the relationship would no longer apply. Similar nickel-rich areas of martensite were reported by Burr and Krishnamoorthy⁴⁴ to be present in blended compacts of a 5% nickel; 0.5% molybdenum; 0.5% carbon steel. These compacts had been sintered at 1300°C, re-austenitised at 870°C and then quenched in oil. Due to the difficulty of identifying the microstructural constituents, micro-hardness measurements were also utilised, from which it was concluded that the remaining dark etching areas were also martensite. Tempering treatments were performed over a wide temperature range in order to select conditions which were most suitable for sintered steels of the above composition. Tempering of the structure at 650°C or 675°C made it difficult to distinguish the original areas and it was suggested that the presence of these areas in the quenched compacts had little influence upon the mechanical properties of the tempered compacts. Some indication was given in the work that sintered steels leaner in nickel might be characterised by the presence in the structure of non-martensitic transformation products. It was also found that deliberately inefficient mixing of the component powders resulted in microstructures that contained intermediate transformation products, together with light etching regions of austenite which were surrounded by nickel-rich martensite. This structure possessed a similar morphology to that

described by Terchek and Hirschhorn¹⁵⁴ for a steel of similar composition but with only 0.25% carbon; increased amounts of ferrite islands were observed in the microstructure as the austenitising temperature was reduced. Despite the presence of soft ductile regions in both structures, a noticeable difference between the two materials was that the compacts produced by Terchek and Hirschhorn¹⁵⁴, unlike those of Burr and Krishnamoorthy⁴⁴, gave improved tensile ductility. The latter authors were interested in the possibility of achieving a reasonable level of properties without the necessity of post-sintering heat treatment. To this end, they allowed some compacts to "cold zone" cool after these had been sintered and re-austenitised at 870°C; the microstructures consisted of light and dark etching martensite and approximately 50% upper bainite. The tempered compacts possessed very similar mechanical properties to those which had been quenched and tempered; no compacts were "cold zone" cooled directly from the sintering temperature.

In later work, Terchek and Hirschhorn¹⁵⁵ studied the microstructure and mechanical properties of age hardening alloys made from elemental powders including nickel. Tensile test pieces, in which ferrite was dispersed in the nickel-depleted regions of age hardened martensite, were shown to possess combinations of properties, especially high tensile ductility, which could not be obtained in quenched and tempered test pieces. Clearly, the question of whether uniform or non-uniform microstructures are preferable is one which can only be answered with regard to specific alloys intended for specific applications. The following points may be made

concerning the relationship of microstructure to homogeneity and mechanical properties.

- (a) High levels of homogeneity and uniform microstructures are normally associated with optimum mechanical properties.
- (b) The inherent high degree of homogeneity in pre-alloyed compacts allows the attainment of uniform microstructures provided that the material possesses sufficient hardenability.
- (c) The high level of homogeneity required to produce uniform microstructures in blended compacts is best achieved by a combination of efficient mixing and high temperature sintering.
- (d) In certain compositions, or by the application of certain heat treatments, it is possible to produce a degree of low homogeneity in blended compacts which results in unusual microstructures and mechanical properties.
- (e) It may be possible to eliminate conventional heat treatment after sintering and attain improved mechanical properties by the use of certain cooling rates from sintering temperature.

3.3.3 Models of the homogenisation process

A chemically inhomogenous solid solution may become increasingly homogenous by diffusion^{22,88,89,157,158}. For an inhomogenous solid metal, Shewmon¹⁵⁸ considered that concentration would vary in an approximately periodic manner along any given straight line. The initial concentration at a point along the x axis could be described by the equation:

$$c(x) = c_o + c_m \cos(\pi x/l)$$

in which

c_o = final concentration,

c_m = maximum variation of concentration from the final concentration,

l = distance along the x-axis.

The flow of solute atoms from regions of high concentration to those of low concentration would result in a relaxation towards a constant value, i.e. towards a state of homogeneity. For the case in which diffusivity was assumed to be constant, Shewmon gave a solution to Fick's second law as follows:

$$c(x,t) = c_o + c_m \cos(\pi x/l) \exp(-\pi^2 Dt/l^2)$$

in which

$c(x,t)$ = concentration at a point along the x-axis after time t ,

D = diffusion coefficient.

In the above equation, $\cos(\pi x/l)$ represents the assumed sinusoidal variation of concentration. If this function is set to unity, then the controlling factor in homogenisation is $\exp(-\pi^2 Dt/l^2)$ or $\exp(-t/\tau)$ in which $\tau = l^2/\pi^2 D$ = relaxation time.

Despite the mathematical complexity admitted by Shewmon in this determination of the rate of homogenisation, it was considered that useful information about this rate could be obtained by the determination of the effect of various factors upon the relaxation time. It may be seen that the major influences on relaxation time are provided by those factors which alter the values of l and D . The above equations describe homogenisation in terms of periodic wavelength and relaxation time; in the real situation, concentration

distribution would be described by the superimposition of many sine waves of different wavelengths and relaxation times. In this case, the attainment of homogeneity would ultimately depend upon the longest wavelength in the system.

An example of the use of the above analysis was provided by Lavender and Jones¹⁵⁹ in a study of banding in wrought steels. Manganese concentration was assumed to vary sinusoidally through the steel and the band wavelength was determined by micro-radiography. The amplitude of the bands was considered to be a fraction $1/f$ of the original amplitude when

$$\exp(-\pi^2 Dt/l^2) = 1/f$$

It was estimated that banding would not be observed when it was reduced to one tenth of its original amplitude. Results of micro-radiography on banded steels, which had been subjected to high temperature treatment, were compared with calculations of the time and temperature required to effectively remove banding. The good agreement between practical and theoretical results which was obtained in these experiments provides confirmation of the above analysis of homogenisation. Moon^{88, 89} has described the homogenisation process in the same terms as Shewmon¹⁵⁸ but with reference to sintered products. In addition to simultaneous densification during sintering, this author mentioned the process of inter-diffusion in iron-nickel compacts in which the volume diffusion rate of iron into nickel was the greater. The problem of predicting the degree of inter-diffusion in this system is more difficult than suggested by this behaviour. Thus Kuczynski and Stablein⁹⁷, by the use of wire models, showed that the rapid diffusion of

nickel occurred both around and into iron particles by surface and grain boundary diffusion respectively. Such phenomena add weight to Moon's contention that quantitative predictions about the rate of inter-diffusion in multi-component systems could not be made at that time (1971).

Homogenisation studies have often been concerned with simple non-ferrous systems such as that of the isomorphous copper-nickel alloys^{102,103,144,145,160,161,162}. The alloying process in such systems has been described by Schwarzkopf¹⁶³ as one in which the major component envelopes the minor component particles; homogenisation is thus more rapid when the minor component particles have the smaller size. This behaviour has clearly given rise to the concentric sphere model which has been used to describe homogenisation^{103,161,162}. This model is based upon a particular geometry, in which each minor component particle is embedded in a matrix shell such that the mean composition of the composite is equal to that of the whole compact. In the case of a single minor constituent particle, this geometry approximates well to the real compact but, even on the assumption of ideal mixing, it does not take into account the effect of particle size variation. The assumed geometry is thus one of adjacent composites of equal size, which reflects the sinusoidal variation of composition discussed by Shewmon¹⁵⁸ and Moon^{88,89}. It may be considered that an adequate prediction of homogeneity, after long treatment times, would need to include the many concentration sine waves provided by different sized composites.

Following the introduction of the concentric sphere model by Fisher and Rudman¹⁰³, Heckel¹⁶¹ applied experimental

data from X-ray diffraction line broadening and electron probe micro-analysis to the homogenisation process in the copper-nickel system. The data was in the form of the degree of interdiffusion and the range of composition that existed in each compact after different sintering treatments. Heckel considered that, although the model prediction was in reasonable agreement with the degree of interdiffusion obtained in practice, a wide departure from the predicted behaviour was obtained with respect to the range of composition. The later stages of homogenisation persisted to much longer times than was predicted by the concentric sphere model. This behaviour is not surprising in view of the situation discussed earlier, in which homogenisation depended upon the longest wavelength in the concentration distribution. The deficiency of the model in this respect was appreciated by Heckel, who introduced a concept of "effective particle size" to account for the effect of particle aggregates. This parameter was defined as the ratio of effective/actual particle size and, for a degree of interdiffusion of 0.95 in the later stages of homogenisation, the "effective particle size" was found to be approximately five times the actual particle size. A major conclusion of Heckel's work was that, as the temperature dependence of homogenisation was similar to that found for bulk diffusion couples, the homogenisation process was also controlled by volume diffusion. This conclusion was at variance with that of Fisher and Rudman¹⁰³ who found that surface diffusion was rate controlling at temperatures up to 950°C and that volume diffusion was rate controlling above this temperature. In later work, Heckel et al¹⁶² considered

the usefulness of work on the homogenisation process to be fourfold, viz:-

- (a) a basis for systematic consideration of homogenisation,
- (b) a prediction of homogeneity after a specific sintering treatment,
- (c) predictions of changes in homogeneity when processing conditions were altered, and
- (d) a basis for the comparison of experimental data.

However, the authors admitted that the application of model behaviour to multiphase multicomponent systems appeared to be a formidable task. The analysis has been subsequently applied to the homogenisation of nickel in an age-hardening 5% nickel steel which was sintered to 95% of theoretical density.

Terchek and Hirschhorn¹⁵⁵ found that, when a mean nickel particle size of $5\mu\text{m}$ was employed, the "effective particle size" required to correct the predicted behaviour was almost $13\mu\text{m}$. An unsintered compact was examined by quantitative optical metallography which showed that the mean nickel particle agglomerate size was $7.5\mu\text{m}$ and that the interparticle distance was $133\mu\text{m}$. It was concluded that variables not incorporated into the model, such as minor variations in particle shape and distribution and porosity, must also retard the homogenisation process.

3.3.4 Measurement of the degree of homogeneity.

In a review of the techniques available for the study of homogenisation, Heckel et al¹⁶² stated that little attention had been paid to the prediction or determination of homogeneity in sintered materials. They were of the opinion that X-ray diffraction, quantitative microscopy and electron probe micro-

analysis were most useful in this respect. Techniques other than these have been used and these include dilatometry^{102, 143,164}, electrical resistivity^{144,145} and differential thermal analysis¹⁶⁴. X-ray diffraction techniques^{101,102,103, 161,162,165,166,167} are limited to those alloy systems in which line broadening and peak shift measurements may be made by virtue of the atomic dimensions and mutual solubility of the components. With regard to optical microscopy, Wolff¹⁶⁸ asserted that normal etching procedures were unsuitable for the assessment of homogeneity due to their low sensitivity to small changes in alloy composition. Smith and Hehemann¹⁰⁴, however, were able to investigate the homogenisation kinetics in tungsten-rhenium compacts by quantitative optical microscopy. This partially miscible alloy system did not lend itself to analysis by the concentric sphere model. By measurement of the formation and dissolution of an intermediate phase, these authors, in a reference to the controversy surrounding the roles of surface and grain boundary diffusion during the homogenisation process, showed that a major contribution had been made in their experiments by grain boundary diffusion. The early stages of homogenisation in particular may be followed by quantitative microscopy. DeHoff and Aigeltinger⁸⁷ have outlined the principles and applications of this technique in relation to sintered compacts. In order to reduce the likelihood of subjective counting errors and to ensure that the sample is representative, they recommend that it is better to sample the structure many times than to count extensively on a small number of areas. As ideally packed compacts would be periodic both in pore structure and microstructure, it was considered essential that non-uniform jumps between measure-

ments were taken. DeHoff and Aigeltinger stressed the importance of a decision governing the number of measurements to be made in order to establish a particular level of accuracy, although the statistical treatment employed was quite general and may be found in works such as that by Spiegel¹⁶⁹. The three stages of sintering, as described by Rhines⁹³ and characterised by pore structure, were shown to be clearly distinguishable by quantitative microscopy. DeHoff¹⁷⁰ had previously discussed the statistical background of quantitative microscopy from which it was clear that he considered the standard deviation to be the best measure of the dispersion of values about the mean value; in addition, he preferred the use of the standard error and confidence limits of the population mean as estimates of reliability. The application of statistical theory is thus well established in quantitative metallography. The techniques of point counting, lineal analysis and areal analysis have been described and compared by Hilliard¹⁷¹, Modin and Modin¹⁷² and more recently by Pickering¹⁷³. Whilst visual measurements have been used in diffusion studies, these are not suitable for a detailed analysis of the distribution of alloying elements. The application of probe analysis to diffusion investigations was considered by Ranzetta and Scott¹⁷⁴. The preferred method of sampling given by these authors involved the movement of the specimen in short steps under a stationary probe, so that the X-ray intensities of one or more elements could be counted at each step. The analogy of this procedure to point counting is self evident. By such means, concentration plots across diffusion couples could be

obtained. Prolonged counting at one point was not recommended, on account of probe instability and specimen contamination. With reference to quantitative work, Ranzetta and Scott¹⁷⁴ stated that the most usual method of analysis was to align the spectrometer to give maximum counts on a peak and then to perform background counts on both sides of the peak. In this way, a peak/background ratio was obtained for comparison with data from a standard of known purity. Poole and Martin^{175,176} have reviewed the instrumental and experimental aspects of micro-analysis; they emphasized that very careful attention must be paid to operation of the instrument if reproducible and accurate results are to be obtained.

Lindskog and Skoglund⁵⁰ employed electron probe micro-analysis to study the influence of heterogeneity on the tensile strength of a sintered 2% nickel; 0.5% molybdenum; 0.5% carbon steel. Fully and partially pre-alloyed powders were used, which had been screened to between 100 and 220 B.S. mesh sieve size. Compacts of 95% and 99% of theoretical density were sintered at 1120°C for times of between 15 minutes and 16 hours. The nickel concentrations at 100 randomly distributed points, in cross sections of the compacts, were determined and the coefficient of variation was taken as a quantitative measure of the heterogeneity in the compacts. Points which were coincident with porosity were disregarded. The degree of homogeneity in the 99% dense partially pre-alloyed material was shown to approach that of the fully pre-alloyed material after 16 hours of sintering: that of the less dense material appeared to approach a level of homogeneity somewhat below this value. In the early stages of homogenisation (up to one hour), tensile

strength was observed to increase rapidly but thereafter slowly approached a peak value. It was concluded by Lindskog and Skoglund⁵⁰ that the tensile strength of this sintered low alloy steel was related to the degree of homogeneity in the compacts, but it was not clear what contribution, if any, was made by the pore structure.

4. EXPERIMENTAL PROCEDURE

4.1 Physical Properties of Powders

The initial work was concerned with the mechanics of handling powders and the production of compacts in various conditions. In order to establish a reproducible production technique, preliminary work was carried out on compacts prepared from -240 B.S. mesh electrolytic iron with admixed natural or synthetic graphite powders. Subsequently, compacted mixtures of elemental powders incorporated -200 B.S. mesh electrolytic iron, fine grade carbonyl nickel and synthetic graphite. This latter grade of iron was also used as the raw material for the production of a composite powder, each particle of which consisted of an iron core with a coating of electrolytically deposited nickel. Pre-alloyed powder of 3% nickel: 97% iron was produced by water atomisation; sieve fractions of greater than 100 B.S. mesh sieve size were discarded. Sieve analyses of the raw materials were carried out on batches of 200g for a time of 2 hours. Mean particle sizes were determined by an air permeability method, namely the Fisher sub-sieve sizer.

4.2 Processing of Powders

4.2.1 Production of Sintered Compacts

Mixing

Initial batches of powder of 200g and 300g were mixed in a horizontal rotary drum for a period of 2 hours. After the first reproducibility trials, larger powder batches were needed, particularly for isostatic pressing. Powder batches of up to 2.5kg were mixed for times of up to 1 hour in a

turbolator mixer.

Pressing

A single acting hydraulic press of 500kN capacity was used to compact mixtures of powders at a pressure of 460 MN/m^2 . The compacts so produced weighed approximately 25g with dimensions of 16.3mm diameter and 17.3mm length. A dwell time of 2 seconds was allowed at maximum pressure and the compacts were ejected by placing a suitable ring below the die and continuing the top stroke. Those parts of the die which were in contact with the powders were coated with a lubricant to minimise frictional effects.

Large compacts of up to 2.5kg were produced by means of a Somers isostatic press, which incorporated wet bag tooling. A flexible silicone rubber bag was lined with polythene sheet and the required amount of powder was placed inside the bag. The bag was sealed with a polythene lid and rubber stopper and this assembly was placed in a cylindrical perforated steel support. An additional rubber stopper was positioned underneath the bag, but inside the steel support, to complete the assembly. The whole of this unit was suspended in oil inside the pressure vessel, which was then sealed to enable the maximum hydraulic pressure of 345 MN/m^2 to be applied by means of an intensifier. The removal of the compact was a direct reversal of the above procedure.

Sintering

All compacts were sintered by being placed directly into the hot zone of a tube furnace at temperatures between 1000°C and 1300°C . Furnace temperatures were maintained within 10°C

of the stated sintering temperature. Both before and during the insertion of each compact into the furnace, a purging gas of 10% hydrogen: 90% nitrogen was passed through the tube. The flow of this gas was maintained for not less than 3 minutes after the insertion of the compact into the furnace. The purging gas was replaced by hydrogen as the sintering atmosphere for the greater part of the treatment; gas flow was constant during this period at 0.8 litre/minute. It should be noted that oxygen was removed by passing the hydrogen through a catalytic purifier and that moisture was taken up by either activated alumina or magnesium perchlorate according to the availability of these reagents. Prior to the finish of each sintering treatment, purging gas was employed to facilitate the removal of compacts from the furnace. Directly after the completion of sintering, compacts were removed from the hot zone and immediately quenched in cold water with vigorous agitation.

Heat Treatment

As given above, the first stage of heat treatment was performed by quenching compacts directly from the sintering temperature. Specimens for metallographic examination and hardness tests were cut from the quenched compacts. The major portion of each compact was then coated in a proprietary compound (Berkotekt) in order to prevent decarburisation during the subsequent tempering treatment. This was performed in an air recirculation furnace for a period of 1 hour at 600°C, after which compacts were allowed to cool in air.

4.2.2 Nickel Plating of Iron Powder

Fig. 2 diagrammatically illustrates the apparatus which

was specifically made for the purpose of plating -200 B.S. mesh electrolytic iron powder particles with nickel. Before the electrodes were placed in position, nitrogen was passed through the sintered disc and 200cc of electrolyte were added to the inner container. The electrolyte employed was a standard barrel plating solution (composition given in Table 4). Stability of the liquid/gas mixture was controlled by the nitrogen gas pressure and undue frothing by a minute addition of a silicone anti-foam emulsion. A few minutes were generally allowed to ensure that stability had been achieved. The outer container was then filled with electrolyte and iron powder was added slowly to the inner cell in order to maintain stable fluidising conditions. After the electrodes had been placed in position, 15A were passed through the circuit at a potential of up to 10V. The random motion of the iron particles brought them periodically into contact with the cathode rods during which time plating of the powder with nickel was produced. During the process, plating tended to deplete the catholyte of nickel ions, which resulted in increased electrical resistance and a reduction in current density. This inability of the apparatus to provide a sufficient continuous supply of nickel ions from the outer to the inner compartment was indicated by the increasing pH of the inner cell. (The use of an alternative porous membrane has recently overcome this problem). As the purpose of the apparatus was simply to provide a product which was not otherwise obtainable, further development work was not undertaken by this author. The problem of inadequate ion supply was circumvented by running the equipment for periods of approximately 20 minutes during which time the pH of the catholyte increased from about 4.6 to 7; the solution

in the inner cell was decanted and replaced with fresh electrolyte. Three such runs were found to be required in order to produce a nickel coating to the extent of 3% by weight. The wet product was thoroughly washed with water, rinsed in industrial alcohol and allowed to dry in a warm atmosphere.

4.2.3 Chemical Analysis of Powders and Sintered Compacts

Carbon analysis was performed by the method of non-aqueous titration. Combustion of the sample in excess oxygen produced carbon dioxide from the carbon in the sample. The subsequent absorption of carbon dioxide allowed a titration to be carried out, the results of which were related directly to the carbon content of the sample.

Nickel determinations were made by the colorimetric method. This involved the dissolution of the sample and the formation of a coloured complex due to the presence of nickel. The absorption of monochromatic light by the solution was related directly to the nickel concentration of the sample.

Coulometric analysis was used to determine the combined amount of oxygen in oxides and in solution in the metal. The sample was heated and oxygen was converted firstly to carbon monoxide and secondly to carbon dioxide; the carbon dioxide was passed to a cell of known pH: this property changed according to the amount of carbon dioxide admitted. An automatic titration device restored the pH to its original value and the amount of electricity consumed in electrolysis was proportional to the oxygen content of the sample.

4.3 Determination of the Properties of the Compacts

Density The uniformity in the shape of die-pressed compacts

facilitated the determination of density from measurements of mass and dimensions. Isostatically pressed compacts were cut from larger cylindrical compacts and were thus irregular in shape. The volumes of these irregular compacts were measured by means of mercury displacement in a mercury balance. Since the masses of these compacts could be determined by conventional means, density measurements were simplified.

Tensile Properties

Sintered and tempered compacts were machined to Hounsfield metric 'B' dimensions, i.e. 20mm^2 cross sectional area and 25.25mm gauge length, which conforms to current British Standards¹¹⁶. A constant rate of loading was obtained by the use of a Hounsfield motor-driven machine. Test piece diameters were measured with a micrometer both before and after testing. Reduction of area values were so slight in those cases for which it could possibly be detected that these values have not been reported. Elongation values were calculated directly from the test curves on the assumption that the limit of proportionality and the elastic limit were coincidental. Measurement errors were minimised by the use of the maximum magnification of extension that was available on the machine (16x).

Hardness

In view of the reported difficulties^{54,139,140} involved in the production of reliable hardness data for sintered materials and the necessity of avoiding the critical range of loads which can give unreliable results¹⁴⁰, Vickers diamond hardness values were determined for certain compacts by the use of a wide range of loads. Micro-indentation hardness was

performed on a Reichert projection microscope with this facility. Test loads of from 5g to 200g permitted Meyer analysis type plots to be made of the results. Macro-hardness tests were made on a standard Vickers hardness testing machine and test loads ranged from 1kg to 30kg. Almost all the hardness data in this investigation has been reported as plateau hardness data (\overline{HD}), which was determined from these macro-hardness tests. Reasonably consistent results from tests performed under a range of loads were considered to give a reasonable representation of the macro-hardness of the compacts. The mean value of such combined data has been described by this author as the plateau hardness, as an indication of its lack of dependence upon test conditions and thus its dependence upon the condition of the compacts.

Impact Strength

Test pieces were machined from sintered and heat treated compacts. Unnotched test pieces of 45mm in length and 8mm in diameter were tested on a Hounsfield balanced impact machine.

4.4 Examination of the Structures of Sintered Material

4.4.1 Optical Microscopy

Specimens of approximately 10mm square cross section were cut from sintered and quenched compacts and then mounted in cold setting resin prior to conventional wet grinding. The primary polishing stage was conducted on napless laps which were impregnated with diamond abrasive pastes. Final polishing was carried out on a slowly rotating vibratory polishing machine, which incorporated $\frac{1}{4}\mu\text{m}$ grade gamma alumina. All

sections for micro-examination in the etched condition were etched in 1% nital. Photomicrographs were taken from the central regions of the compacts since these represented those portions of the compact from which mechanical test pieces were machined; these areas, unlike those of the outer regions of the compacts, were free from decarburisation.

The equipments employed for photomicrography were a Reichert projection microscope for 35mm work and a Zeiss Ultraphot microscope for plate work.

Quantitative optical microscopy was undertaken by means of a Union SMS 2-1038 microscope. This instrument was equipped with a specimen stage which could be moved through increments of 0.005mm in two directions at right angles to each other. It was possible to estimate 0.001mm provided that the stage movement was confined to one direction. If the latter proviso was not observed, backlash in the graduated micrometer barrel mechanism gave rise to errors in measurement.

4.4.2 Transmission and Scanning Electron Microscopy

Transmission electron microscopy was conducted on Philips EM100B and Jeol JEM 6AS instruments. As the purpose of electron microscopy was to ascertain the finer structural details of the quenched compacts in order to supplement and confirm optical microscopy, use was made of replica techniques. Direct carbon replicas were not successful as these tended to break up almost completely, an effect probably associated with the residual porosity in the compacts. Better results were achieved by the use of two-stage replicas. Specimens were initially prepared as for optical microscopy, after which

cellulose acetate sheet, moistened in acetone, was draped over the specimen surface. When dry, the sheet was stripped from the specimen surface and secured firmly to a glass microscope slide. In order to attain some degree of shadow contrast, the slide was mounted at an angle to a carbon evaporation source in a vacuum coating unit. A thin layer of carbon was evaporated onto the surface replica, after which the excess plastic was removed from around the replica area. Immersion of small squares of the composite in acetone dissolved the cellulose acetate backing thereby leaving squares of carbon replica in the acetone. Each square was then washed by immersion in methanol and transferred to a bath of distilled water. Squares were then caught on electron microscope grids and allowed to dry thoroughly before these were examined in the electron microscope.

Scanning electron microscopy was conducted on a Philips PSEM 500. Fractured test pieces were mounted on aluminium studs with colloidal silver adhesive in order to maintain good electrical contact between the specimen and the stud. In addition to the preparation of photomicrographs of typical areas of the fracture surfaces, use was made of the energy dispersive qualitative analysis system attached to the instrument.

4.4.3 X-Ray Diffractometry

Both unsintered and sintered compacts were examined by X-ray diffraction by means of a Philips 1010 1kW X-ray diffractometer. Cobalt K_{α} radiation was employed for this purpose. The goniometer was aligned by the use of a pure silicon standard; this was then replaced by a compact and

the pulse height analyser was set for optimum conditions with respect to the BCC {110} reflection. All scans included the major reflections from martensite, austenite and/or nickel. Line broadening measurements were made at the position of half peak height above background level.

4.5 Determination of Homogeneity by Electron-Probe Micro-Analysis.

The instrument employed for this work was a Cambridge Microscan Mk. IIA, a single channel instrument which required the use of specimens of less than 6mm in diameter. Probe voltage and beam current were kept constant at 25kV and 0.15 A respectively.

4.5.1 Point Analysis

Sections were cut from fractured tensile test pieces so that mechanical properties could be directly compared with the level of homogeneity that existed in each test piece. Specimens were polished to $\frac{1}{4}\mu\text{m}$ finish and areas examined under the electron-probe with the lithium fluoride crystal spectrometer set to receive nickel $K\alpha$ radiation. The spectrometer setting was checked by the establishment of the position at which the maximum count rate was obtained for a pure nickel standard. A line trace was then made across the specimen surface and the nickel distribution plotted on a chart recorder. Magnifications of 600x and 1200x corresponded to line trace lengths of $166\mu\text{m}$ and $83\mu\text{m}$ respectively. Nickel concentrations were determined at equi-distant points along each line trace by means of a corrected intensity ratio with reference to a pure nickel standard. The result of this procedure was a series of line traces each calibrated directly in nickel concentration.

4.5.2 Areal Analysis

The initial setting up of the spectrometer was accomplished in a similar manner to that described above. The specimen was so aligned that the electron beam struck the specimen just off-centre; the specimen rotation mechanism thus facilitated the traverse of the specimen surface in an ever increasing spiral. A large number of short movements permitted a great part of the specimen surface to be sampled. At no time were the electron or X-ray images of the specimen surface used to select specimen areas. At each step, the maximum area possible was scanned by the electron beam, as determined by the magnification in use. Nickel concentration was calculated for each area by the method given above. The result of this procedure was a series of nickel concentrations, each of which was the mean nickel content of a small area of the specimen surface.

5. EXPERIMENTAL RESULTS

Although most of the results used in the subsequent discussion were obtained from isostatically pressed* material the results of the earlier work on die-pressed** compacts have also been reported in detail, since the techniques used in the latter part of the investigation were developed using these materials.

5.1 Properties of Powders used in the Investigation

The mean particle sizes and chemical analyses of the powders employed are given in Table 5. Natural graphite was found to be of lower purity than the synthetic material. The pre-alloyed atomised powder possessed the highest oxygen content, although the plating of the electrolytic powder was associated with an increase in oxygen content. Sieve analyses of the electrolytic and atomised powders (Table 6) showed that both were largely comprised of particles well below the minimum sieve size, although the atomised material contained the larger fraction of coarse particles.

5.2 Properties and Structure of blended*** iron: graphite alloys, die-pressed.

In order to eliminate any effects of lubricant within the powder compacts, lubricant was only applied to the wall of the mould cavity. Table 7 shows the results of an examination of the suitability of various lubricants; a suspension of zinc

-
- * Isostatically pressed:- formed by isostatic pressure upon a flexible mould.
 - ** Die-pressed:- pressed in a one-piece die by movement of the top punch only.
 - *** Blended alloys:- alloys produced from a mechanical mixture of elemental powders.

stearate in acetone sprayed onto the die wall produced the greatest density* in the resultant compacts. This lubricant was thus selected for future use.

The densities of compacts that contained 1% natural graphite and 0.5% synthetic graphite were compared before and after sintering for 2 hours at 1300°C. (Due to the differences in purity of the graphites and on the assumption of a 20% carbon loss^{38,39,40,41,42}, during sintering, both materials were expected to finally contain just under 0.4% carbon). The density changes are given in Tables 8 and 9; these were found to be slight in the alloys which contained synthetic graphite whereas changes in the natural graphite materials were of the order of 2.5%. The level of green density in the synthetic graphite materials was some 4% higher than in those which contained natural graphite. Therefore synthetic graphite was selected for use during the experimental programme.

Hardness tests were carried out on sintered compacts using a wide range of loads, in order to assess the reliability of this test for porous materials. The results are shown in Table 10, from which it may be seen that natural graphite materials gave almost constant hardness data when loads between 30kg and 0.1kg (inclusive) were employed. In contrast, the synthetic graphite materials exhibited an apparent increase in hardness when tested at loads below 1kg. This latter behaviour is illustrated further in Fig. 3; the two linear parts of the Meyer line are clearly associated with load independent data and load dependent data for high and low

* Density:- the ratio of measured density to the density of the fully dense material expressed as a percentage.

loads respectively. At intermediate loads, there existed a band of unreliable data which was associated with the change in slope of the Meyer line. Inspection of Table 10 reveals that the natural graphite materials showed a similar relationship between load and hardness but also indicates that the slope of the Meyer line and thus the hardness line at low test loads were quite different to those exhibited by the synthetic graphite materials. Thus, in order to obtain satisfactory hardness data in the present work, certain rules were followed. These were:

- (a) the region of unreliable data at intermediate loads should be avoided,
- (b) due to the change in slope of the Meyer line (and hardness line) at low loads, the hardness of compacts should not be obtained by the use of loads within that range,
- (c) low load testing should be reserved for the assessment of hardness variations within a compact,
- (d) hardness tests should involve the use of the hardness plateau which is specific to each compact; this procedure should provide a more reliable measure of intrinsic hardness than single load tests.

The mean hardness value along such plateaux will be referred to as plateau hardness (\overline{HD}): all hardness data in this work, except where specified, correspond to this measurement.

The microstructures of the sintered alloys are shown in Figs. 4 and 5. Natural graphite alloys appeared to consist of martensite, a dark etching product and ferrite with the latter sometimes present as Widmanstätten plates. Synthetic

graphite alloys exhibited an apparently lighter etching martensite, nodular pearlite and some grain boundary ferrite.

5.3 Properties and Structure of blended iron: graphite: 1% nickel alloys, die-pressed.

Two compacts were made of this mixture which incorporated 0.5% of synthetic graphite. The density of the compacts increased from 88.5% in the green condition to 89.1% in the sintered condition, an effect opposite to that shown by nickel-free compacts.

Hardness tests were performed as described previously and the results are shown in Table 11. It can be seen that, despite similar processing conditions and similar densities, the compacts exhibited different hardness plateaux. The actual hardness values along the plateaux were similar but, in compact number 1, test loads below 5kg gave unreliable results whilst, in the case of compact number 2, the plateau extended to below 1kg. The greatest discrepancy was shown at intermediate loads. In these two cases, the plateau hardnesses (\overline{HD}) would be reported as the mean value of the relatively constant data indicated in Table 11, i.e. as 343 \overline{HD} and 353 \overline{HD} for compacts 1 and 2 respectively.

The microstructures of these alloys, after these had been quenched from the sintering temperature, were similar to those of the nickel-free alloys which also contained 0.5% of synthetic graphite. Martensite appeared to be the major phase in association with a smaller quantity of the dark etching intermediate product than was present in the nickel-free alloys; some grain boundary ferrite was again in evidence (Fig. 6).

5.4 Properties and Structure of blended iron; graphite: 3% nickel alloys, die-pressed.

The principal objective of this section of the work was to establish a reproducible means of quantitatively assessing chemical homogeneity within sintered compacts (Section 5.4.3). If this could be achieved, then a further objective was to determine whether sintering conditions influenced the degree of homogeneity attained during sintering.

5.4.1 Mechanical and Physical Properties

As in the case of the 1% nickel alloys, densification occurred during the sintering treatment. Table 12 shows that the plateau hardness increased with sintering time and that higher hardness values could be obtained by sintering at 1300°C rather than at 1150°C for the same time.

5.4.2 Structure

Optical microscopy was found to be useful at low magnification for the qualitative assessment of the progress of both sintering and homogenisation. The topographical stages of sintering, as discussed by Rhines⁹³ and DeHoff and Aigeltinger⁸⁷, may be followed by the measurement of the volume, shape and distribution of pores in polished sections of compacts. It was found in the current work that a magnification of 160x was sufficiently high to reveal individual pore curvature and sufficiently low to show a realistic distribution of the total porosity. The early stages of homogenisation were characterised by the presence (in the microstructure of sintered and quenched compacts) of light etching nickel-rich areas. Low magnification facilitated a visual assessment of the distribution of these areas but higher magnification

was required to assess the smaller scale heterogeneities which resulted in non-uniformity of the phases present after quenching. In view of the similarity of certain features, which were revealed at high magnification in these alloys, to those in isostatically pressed alloys, consideration of finer structural details will be presented later (Section 5.5.2).

Fig. 7 shows the heterogeneous nature of compacts sintered for 15 minutes at 1150°C . The high proportion of interconnected porosity and the low degree of interdiffusion between iron and nickel resulted in low hardenability, as shown by the mixture of equilibrium and non-equilibrium products in the structure. Fig. 8 shows the structure obtained after sintering the material for one hour at 1150°C ; although the centres of the original nickel particles were still clearly visible, some degree of interdiffusion between nickel and iron had occurred, as indicated on the photomicrograph. It would appear that preferential diffusion had occurred along the iron particle boundaries. The associated improvement in the hardenability of the material resulted in a structure which consisted mainly of non-equilibrium products with no evidence of pearlite areas. Six hours treatment at 1150°C produced the more uniform microstructure shown in Fig. 9; sufficient diffusion had occurred to cause the smaller areas of high nickel concentration to disappear. Consequently, the mean distance between nickel particles was much greater than in compacts sintered for one hour (see Fig. 8). Some interparticle porosity was still present but, generally, the pores were becoming coarse and isolated, so that it was not possible to distinguish clearly the original powder particles.

Compacts sintered at 1300°C exhibited similar features to those sintered at 1150°C, but both microstructural and sintering changes occurred more rapidly. Fig. 10 shows the structure of a compact sintered for 15 minutes, which is rather similar to that of a compact sintered for one hour at 1150°C (see Fig. 8), except that in the former case the light etching areas were already becoming diffuse and the network of this constituent was not so evident. Six hours treatment followed by quenching again produced a more uniform microstructure, as shown in Fig. 11, although the residues of the largest nickel agglomerates* were still visible. Variations in the morphology of the quench products were very noticeable. It appeared at low magnification that the lighter etching areas were acicular whereas the darker etching areas were lath martensite. Sintering had progressed appreciably so that the amount of concave shaped porosity was at least equalled by the amount of convex shaped porosity; in fact, a large number of the pores were enclosed by near convex surfaces, i.e. were almost spherical.

Fig. 12 shows a diffractometer recording for the pressed but unsintered material. The principal nickel reflection, namely the $\{111\}$, was completely overlapped by the iron $\{110\}$ reflection. Fig. 13 shows the chart record for a compact sintered for 15 minutes at 1150°C, in which there is a clear distinction between the BCC $\{110\}$ peak and the adjacent FCC $\{111\}$ peak, which indicates the formation of a nickel-iron solid solution during sintering and its retention after the quenching

* Agglomerate:- a volume comprised of several nickel particles.

of the material to room temperature. The FCC interplanar spacings for the iron-nickel solid solutions (listed in Table 13), together with the shift of the $\{200\}$ reflection, suggest that elemental nickel had already been substantially consumed by interdiffusion of nickel and iron; the data indicates a mean value of about 60% nickel: 40% iron for this retained austenite. The line broadening of the BCC $\{110\}$ reflection was probably due to both the presence of martensite and to an increased range of lattice parameters associated with the solid solution of nickel in iron. The BCC line broadening illustrated in Fig. 14 for a compact sintered for 30 minutes at 1150°C was considered to be due mainly to this latter phenomenon. Inspection of the low angle side of the BCC $\{110\}$ reflection in Fig. 14 reveals the presence of the austenite $\{111\}$ reflection; this has been partly overlapped by the considerable line broadening of the BCC reflection. Line broadening persisted in compacts sintered for longer times at 1150°C and the austenite $\{200\}$ reflection was reduced to near background level in material sintered for $2\frac{1}{2}$ hours. This behaviour is consistent with the view that, although interdiffusion of nickel and iron had occurred to a significant degree (such that no nickel-rich austenite was detectable in compacts sintered for 6 hours at 1150°C), local differences in nickel concentration resulted in transformation products with a range of lattice dimensions in all compacts sintered at 1150°C . Compacts which were sintered at 1300°C showed similar behaviour to those sintered at 1150°C as shown in Fig. 15, but detectable amounts of austenite were not found in compacts sintered for longer than 15 minutes.

5.4.3 Determination of the Degree of Homogeneity.

A series of point analyses were made across the surfaces of certain compacts as described in Section 4.5.1. Fig. 16 shows a microprobe trace from a compact expected to possess a high degree of chemical homogeneity, since it had been sintered for 6 hours at 1150°C. Magnification of the specimen surface was 1200x and nickel concentration was determined at steps of 4.15 μm along the trace. This increment was close to the mean size of the nickel particles (3.7 μm). From 21 probe analyses, the mean nickel concentration was found to be 2.60% and the coefficient of variation 42%, the latter providing an estimate of heterogeneity. A compact sintered for 5 minutes at the same temperature was then examined as a comparison; 5 separate traces were recorded and found to vary greatly, as shown in Fig. 17. Analytical data obtained from these traces indicated that the mean nickel concentrations were within the range of 2.53% to 19.52% and the coefficients of variation fell in the range from 99% to 260%. Clearly, in order that a sample be properly representative of a population, the sample mean should approximate to the population mean. Thus, each trace in itself could not be regarded as a complete sampling distribution. Many such traces would be needed to fulfil this requirement. Reduction of the surface magnification to the minimum available would increase the length of trace from 83 μm to 400 μm but this would reduce the sensitivity of the technique. Despite the problems associated with the use of line traces to indicate heterogeneity quantitatively, point analyses along each trace would allow the limits of nickel concentration that existed within a compact to be determined.

The technique of areal analysis in optical microscopy is not popular, due to difficulties in the measurement of areas of non-uniform shape and the long time required to carry out these determinations. The electron probe micro-analyser however, has the facility for scanning surface areas in conjunction with chemical analysis of the areas. The mean nickel concentration of one such area represents the summation of the concentrations obtained from a whole set of percentage nickel vs. distance curves in that area. As homogenisation proceeds, the range of nickel concentration in such an area will become narrower and the mean nickel content of that area will approach the mean nickel content of the compact. If a representative sampling technique is employed for a large population, then, according to the central limit theorem of statistics¹⁶⁹, the sample means will be normally distributed with a mean value equal to the mean of the population. For the powder compacts under consideration, the true mean nickel concentration was known to be 3%, so that for any sampling technique to be valid the sample means should give an overall mean near to this figure.

Compacts sintered at 1150°C were subjected to areal analysis and the population variance for each compact was determined from the results of 10 specimen areas of 500 μ m square at a probe magnification of 250x. Each graphical point in Fig. 18 thus represents an analysis over a total specimen surface area of 2.5mm². Fig. 19 shows one of the 500 μ m square areas in a compact sintered for 15 minutes. A result was considered to be representative when the sample mean was within the 99% confidence limits of the true mean, after making a

porosity correction. It may be seen from Fig. 18 that the dispersion about the mean nickel content, measured by population variance, decreased rapidly in the early stages of sintering and became almost steady in compacts sintered for times in excess of one hour. The same batch of specimens was then re-examined at a probe magnification of 1200x. Twenty areas of $83\mu\text{m}$ square were analysed for each graphical point. Although this corresponded to a total of only 0.14mm^2 per point, the mean nickel concentrations were closer to the true mean than the results given above. This confirms the view put forward by DeHoff and Aigeltinger⁸⁷ (albeit in relation to optical microscopy), that, for sampling to be representative, the structure should be sampled many times rather than be counted extensively on a smaller number of areas. Fig. 20 shows the graphical result from which it may be observed that a low level of heterogeneity was indicated in compacts which were sintered for more than $2\frac{1}{2}$ hours. Fig. 21 shows the distribution of nickel in one area of a compact sintered for 15 minutes.

At this stage of the work, a turbolator mixer became available so that larger powder batches could be handled. An analysis check of the uniformity of mixing was carried out, after which further batches of powder were mixed for a time of one hour. A set of compacts was pressed and sintered in a similar manner to the compacts described above: areal analysis was performed at 1200x probe magnification. Fig. 22 shows the results of this analysis. Comparison of Figs. 20 and 22 illustrates that reproducible results were obtained, thus suggesting that errors due to specimen variations (such as

surface preparation, local density differences and non-uniform mixing) were minimal.

Compacts sintered at 1300°C were subjected to areal analysis at 1200x probe magnification. The results, given in Fig. 23, showed little evidence that a low level of heterogeneity was achieved in shorter times at 1300°C than at 1150°C. In view of the known temperature dependence of diffusional processes, these results were assumed to be due to the insensitivity of the technique at the probe magnification employed. In order to assess the influence of probe magnification, a single compact was employed for a series of areal analyses over a range of magnification: an area was selected which had a mean nickel content, at low magnification, near to the true nickel content for the compact after taking porosity into account. Fig. 24 shows the effect of increasing the probe magnification to the maximum of 4800x; the mean nickel concentration of each area is indicated beneath each illustration. Areal analyses were then undertaken at different magnifications on the same specimen, using 20 areas at each magnification. The results are given in Table 14, from which it may be seen that the variance of the nickel concentrations increased with increased magnification, i.e. there was an increase in sensitivity. The foregoing data indicate that the area scanning technique requires high magnification of the specimen surface in order to reveal heterogeneity remaining in compacts sintered for long times. The maximum probe magnification of 4800x was therefore selected as the norm for subsequent areal analyses; this corresponded to areas of 20 μ m square and was thus still large enough to contain several

original nickel particles.

The compacts for which results have been presented above were re-examined by areal analysis at the maximum magnification of 4800x. It is well known that the statistical accuracy of sampling is increased by the use of many small samples rather than by using fewer large samples. Consequently the counting time of 10 seconds, employed previously for the analysis of each area, was retained but the number of areas analysed was increased to 40 for each graphical point. This represented a total area of 0.016mm^2 per point. The time taken for the collection of microprobe data from each specimen was of the order of one hour. In order to reduce the standard error by 50%, it would have been necessary to analyse 160 areas for each graphical point. This degree of increased accuracy was not considered to be sufficient justification for the longer experimental time and the associated problems of probe stability. Fig. 25 shows the results for compacts sintered at 1150°C with 99% confidence limits included. Attempts were made to fit several types of curve to the experimental data but the most convincing was the exponential relationship given below:-

$$H_t = 26.44 \exp(-2.303 \times 10^{-2} t) + H_r$$

in which

H_t = variance after time t ,

t = time in minutes

and $H_r = 1.78$ = residual variance at infinite time.

The residual variance may be shown to be due to two factors, the foremost of which is the nature of the specimen itself, i.e.

variation in porosity and surface flatness between specimen areas. A second factor is that of instrument stability leading to slight changes in probe current during measurement. The above equation (which is plotted in Fig. 25) was obtained by a process of best fit until the value of the residual variance was such that the correlation coefficient between the experimental and computed values was at a maximum (0.975 in this case). Fig. 25 indicates that homogenisation was initially rapid but became almost steady in compacts sintered for times of $2\frac{1}{2}$ hours or more at 1150°C .

Compacts sintered at 1300°C also homogenised rapidly in the early stages of sintering but these reached a similar low value of variance (2.5) in only about 70 minutes compared to $2\frac{1}{2}$ hours in compacts sintered at 1150°C . The equation of the curve shown in Fig. 26 is given below:

$$H_t = 11.48 \exp(- 2.594 \times 10^{-2} t) + 0.55$$

in which

H_t = variance after time t , hereafter referred to as the homogenisation parameter H .

The best fit between the experimental and the computed values was obtained at a correlation coefficient of 0.999. It is noticeable that the predicted values of the homogenisation parameter at zero and infinite time were less than those predicted by the equation for compacts sintered at 1150°C .

5.5 Properties and Structure of blended iron: graphite: 3% nickel alloys, isostatically pressed.

In order to compare the properties, structures and homogeneity of these alloys, a large number of similar sized compacts were required. The uniformity of isostatically

pressed material allowed large compacts to be made which were then cut into smaller sections. A 2kg compact of low density, produced for a pressure v. density trial, was used to check the variation of chemical analysis and density that might be expected throughout such a section. Hardness data and nickel analyses are given in Fig. 27 and Table 15. The ranges of these properties in this low density compact were considered to be acceptable. The carbon contents of all the sintered materials, for which results have been given in this section, were within the range of $0.33\% \pm 0.03\%$.

5.5.1 Properties of blended, plated and pre-alloyed materials

(a) Blended materials

The properties of blended compacts sintered at 1150°C are shown in Table 16. Tensile strength, impact strength and density increased steadily as sintering time increased from 15 minutes to 8 hours. The maximum tensile strength was 460 MN/m^2 for a compact density of 90.5%. Tensile ductility was observed to be variable, although the trend was towards an increase in ductility as sintering time was increased. The hardness of sintered and quenched compacts increased up to a sintering time of one hour, after which there was little change in this property. Comparison of this hardness data with that given earlier for die-pressed alloys (see Table 12) shows that the latter results were consistently higher over a similar range of sintering time. The reason for this behaviour is not clear since the range of density was very similar in both sets of compacts. In tempered compacts, hardness increased progressively with sintering time; a broadly similar relationship was observed between hardness and tensile strength

as that shown in wrought low alloy steels^{13,29}.

Blended compacts sintered at 1300°C exhibited a higher level of mechanical properties than those sintered at 1150°C, as may be seen from Table 17. The maximum tensile strength was 560MN/m² for a compact density of 90.9%, which was an increase of 100MN/m² over that of the compact sintered for the same time of 8 hours at the lower temperature (compact density of 90.5%). Tensile ductility was more consistent and reached 5.2% in the compact sintered for 8 hours. Quenched compacts possessed greater hardness and were much closer in value to the die-pressed alloys than was the case for compacts sintered at 1150°C. The hardness of tempered compacts increased steadily with increased sintering time.

In order to investigate the effects of sintering temperature upon the properties of compacts, a series of blended compacts were sintered for one hour at temperatures between 1000°C and 1300°C. The results are shown in Table 18, from which it may be seen that density and tensile strength increased in an approximately linear manner with sintering temperature. Tensile ductility and hardness data varied erratically as the sintering temperature increased.

(b) Plated materials*

The nickel plated electrolytic iron powder, which was prepared from five separate batches, was mixed with synthetic graphite to provide the 2kg of material required by a single isostatic pressing. The analysis of this compact was 2.99%

* Plated materials:- materials produced from a mechanical mixture of nickel-plated iron powder and elemental graphite.

nickel: 0.48% graphite: 96.51% iron. Table 19 shows the details of each of the component powder batches which made up the compact.

The properties of plated materials sintered at 1150°C are shown in Table 20. Tensile strength increased rapidly over the full sintering range to such an extent that, although values were initially lower than for corresponding blended alloys, the strength of compacts sintered for two or more hours exceeded that of blended alloys (446MN/m² cf 390MN/m²) after sintering for 2 hours). This result is noteworthy because, even though density increased by only a similar amount to that of blended alloys, densities over the whole sintering range were overall some 4% lower than in blended alloys. In contrast, the increased porosity clearly had a deleterious effect upon impact strength. Tensile ductility was little different to that observed in blended materials. Hardness values increased as the time of sintering was increased with the exception of the results obtained from specimens treated for 8 hours. A fixed load of 20g was considered to be low enough to produce data that distinguished between the microhardness of small scale non-uniformities in the microstructure of compacts sintered for 15 minutes at 1150°C: the results are given in Fig. 28. Under these conditions, the range of hardness values extended from 264 to 356 MHD. It is of interest to note that certain areas which were dissimilar in appearance gave similar hardness results (impressions 3,4 and 5 in Fig. 28). It was not considered possible to correlate the above microhardness results with those of the plateau hardness data in Table 20.

The relationships between the mechanical properties of plated alloys and sintering time at 1300°C were very different to those obtained after sintering at 1150°C (Table 21). Tensile strength increased from 462MN/m² to 550MN/m² when the sintering time increased from 15 minutes to 8 hours at 1300°C whereas, in the case of alloys sintered at 1150°C, this property increased from 251MN/m² to 483MN/m² after the same increase in sintering time. This latter increase was associated with a density change of from 84.2% to 86.4%, in contrast to the much greater change of from 85.2% to 90% observed in those alloys sintered at 1300°C. Of particular interest is a comparison of this data with the corresponding data for blended alloys which, after sintering treatments at 1300°C, gave a very similar range of tensile strength associated with a much narrower density range of from 89.2% to 90.9%. Tensile ductility was also similar to that obtained in blended alloys but hardness was variable.

Table 22 shows that the density and mechanical properties of plated compacts treated for one hour improved with increased sintering temperature. The approximately linear relationships of both density and tensile strength with sintering temperature were similar to those obtained from blended alloys.

(c) Pre-alloyed materials*

The atomisation of a 3% nickel:iron powder was carried out at the Sheffield Laboratories (Hoyle St.) of the British Steel Corporation. 0.5% of synthetic graphite was added and

*Pre-alloyed materials:- materials produced from a mechanical mixture of 3% nickel:iron atomised powder and elemental graphite.

mixed with the atomised powder before a 2kg batch was isostatically pressed. The compressibility of this material was lower than that of the other two materials previously considered; thus the mean green density of these compacts was some 2% less than that of the plated material and some 6% less than that of the blended material. The properties of pre-alloyed compacts sintered at 1150°C are shown in Table 23. The tensile strength range was very similar to that of the blended alloys which were similarly treated, despite the 6% difference in initial density. Comparison of Tables 16 and 23 shows that tensile ductility and impact strengths were also similar in these two types of material. The hardness of pre-alloyed material was surprisingly high throughout the range of sintering times, since these were the least dense alloys produced.

The density of pre-alloyed compacts sintered for 8 hours at 1300°C increased from 82.2% to 86.5% during sintering, whilst the tensile strength of the same material subjected to the same treatment increased from 401MN/m² to 491MN/m² (Table 24). This effect was similar to that observed in plated materials, i.e. a relatively small improvement in tensile strength was associated with a relatively large increase in density. Although tensile ductility was variable, it was noticeable that positive measurements of this property were obtained in all the compacts tested. As in the compacts sintered at 1150°C, hardness values were relatively high in view of the low density of the material.

Table 25 shows the effect of an increase in sintering temperature on the properties of compacts that had been

sintered for one hour. The range of tensile strengths ($357\text{MN}/\text{m}^2$ to $419\text{MN}/\text{m}^2$) over the sintering range of 1000°C to 1300°C was less than that reported for the blended and plated materials sintered for the same time ($273\text{MN}/\text{m}^2$ to $498\text{MN}/\text{m}^2$ and $96\text{MN}/\text{m}^2$ to $460\text{MN}/\text{m}^2$ respectively). In addition, some measure of tensile ductility was produced in each compact, a feature that was not observed in the more dense plated alloys.

5.5.2 Structure of blended, plated and pre-alloyed materials.

5.5.2.1 Optical and electron microscopy of blended materials.

The microstructure of blended compacts sintered for 15 minutes at 1150°C was very heterogeneous, as may be seen in Fig. 29. However, the distribution of the light-etching nickel-rich areas was rather more uniform than that observed in die-pressed alloys (see Fig. 7). In addition, there was evidence of diffusion between iron and nickel around the surfaces of the iron particles. Such diffusion paths did not appear in die-pressed alloys until after 30 minutes of sintering at this temperature. It is of interest that the amount of light-etching material was considerably greater than that of the nickel particles originally mixed with the iron.

The dark-etching areas were more clearly revealed at higher magnification. The areas remote from the nickel-rich regions contained pearlite and some ferrite (Figs. 30 and 31), although most of the material appeared to possess a martensitic structure. Fig. 30 also shows a coring effect within the light-etching areas, in which the original positions of the nickel particles are probably indicated by the lightest

portions. The association of diffusion with the particle boundaries is clearly shown in Fig. 31.

The structures of compacts sintered for times greater than 15 minutes at 1150°C developed in a similar manner to those of the die-pressed alloys. The particle structures became less distinct as sintering continued and after 2 hours the light-etching areas had become isolated. However, these light-etching areas persisted up to the longest times investigated (8 hours). Fig. 32 shows these areas together with an apparently martensitic structure which showed a variable morphology. It is evident from Fig. 33 that both lath and acicular martensites were present in material that had been sintered for 8 hours at 1150°C . No ferrite or pearlite was found by optical microscopy in specimens sintered for more than 2 hours. However, the examination of surface replicas by electron microscopy showed that certain amounts of both ferrite and bainite were present in all compacts sintered at 1150°C irrespective of sintering time; the morphology of these phases was similar to that described below for compacts sintered at 1300°C .

Fig. 34 is typical of the microstructure of material sintered for 15 minutes at 1300°C , which consisted of light-etching regions and areas of transformation products with a relatively uniform morphology. Higher magnification clearly indicates that the product formed on quenching was lath martensite (Fig. 35). Reference to Fig. 10 shows that the interparticle diffusion paths previously discussed with reference to the die-pressed material were similar to those shown in Fig. 34. It is convenient at this point to show the

100.

tempered structure of a compact sintered for 15 minutes at 1300°C (Fig. 36). The distribution of nickel-rich areas did not appear to be affected by the tempering treatment, but some carbide precipitation was observed in all but the most lightly etched regions.

Transmission electron microscopy of two-stage surface replicas was used to examine those parts of the structure that could not be clearly identified by optical microscopy. Although compacts sintered at 1300°C were more uniform than those sintered at 1150°C, isothermal decomposition products were still present in all members of the former group. Thus, Fig. 37 shows ferrite at a prior austenite grain boundary together with some upper bainite, while other areas exhibited ferrite precipitation within the original grains (Fig. 38). Fig. 39 shows the presence of upper and lower bainite adjacent to grain boundary ferrite, while Fig. 40 shows more clearly the general morphology of lower bainite with the presence of structural sub-units.

The presence of ferrite and bainite was still detected in the compacts that had been sintered for 8 hours at 1300°C (Figs. 41 and 42) although it is emphasized that this material, like all those sintered at this temperature, contained mostly martensite (Fig. 43). It was difficult to determine whether the quantity of these non-martensitic decomposition products was reduced by an increase in sintering time to 8 hours.

As sintering continued, the mean distance between the visible nickel-rich areas increased although Fig. 44 shows the presence of these light-etching regions even after sinter-

ing for 8 hours at 1300°C. However, only a small number of the largest agglomerates of nickel particles were still visible after this time. After 8 hours of treatment, the high degree of convex-shaped porosity indicated that the final stage of sintering had been reached (Fig. 44).

5.5.2.2 Optical and electron microscopy of plated materials

The microstructure of plated material sintered for 15 minutes at 1150°C indicated that the nickel-plating operation had resulted in a nickel-rich network around the iron particles, as shown in Fig. 45. Occasionally, the nickel was present in the form of particles, probably from material that had broken off the electrodes. The network was still clearly visible in the tempered structure (Fig. 46); this micrograph also shows the interconnected porosity very clearly. There were similarities between the above structure (Fig. 45) and that of die-pressed material sintered for one hour at the same temperature (see Fig. 8) but the network in the plated material was thin and continuous whereas that produced by interparticle diffusion in the die-pressed material was coarse and irregular. Comparison of these microstructures clearly shows a significantly greater homogeneity in the plated alloys during the early stages of sintering. However, the largely martensitic structure of the original iron particles (Fig. 45) was shown by electron microscopy to be associated with other transformation products. The network around the iron particles was essentially featureless, as had been indicated by optical microscopy, but certain areas of the microstructure contained bainite. Fig. 47 shows an area of lower bainite-martensite aggregate with an area of upper bainite on the opposite side

of a boundary. The lamellar appearance of the latter is due to the nearly continuous carbide filaments alongside the bainitic ferrite laths. A further example of this is shown in Fig. 48.

The structure of plated alloys sintered for one hour at 1150°C represented the point at which the interparticle network was no longer discernible (Fig. 49), although some nickel-rich areas could be distinguished. At higher magnification (Fig. 50), the microstructure was seen to be essentially composed of lath martensite; some isolated pores had been formed with convex geometry but substantial amounts of interconnected porosity suggested that sintering was still in the early stages. After all sintering times at 1150°C, bainitic areas similar to those described above were still detected by electron microscopy. In material sintered for 8 hours, the microstructure was still mainly lath martensite (Fig. 51); some degree of interconnected porosity persisted up to this time.

Plated material sintered for 15 minutes at 1300°C showed no trace of an austenite network in the microstructure; thus the structure was similar to that of material sintered for one hour at 1150°C (compare Figs. 52 and 49). At higher magnification, this structure appeared little different to that of material sintered for as long as 8 hours at 1150°C (compare Figs. 51 and 53), i.e. it was largely composed of lath martensite. However, non-martensitic decomposition products were found by electron microscopy. Fig. 54 shows an unusual form of upper bainite (although similar structures have been reported by Pickering²¹), in which the carbide

filaments typical of this product may be clearly distinguished. Lower bainite and ferrite were also found in plated material sintered for 15 minutes at 1300°C (Figs. 55 and 56 respectively).

Changes in the microstructure which were produced during sintering for times in excess of 15 minutes were slight; this indicated that microstructural uniformity was achieved in very short times at 1300°C. Fig. 57 is typical of the structure of material sintered for 8 hours at 1300°C; this micrograph clearly shows the isolation and rounding of pores that occurred during this extended sintering treatment. Although the structures of all these materials were for the most part martensitic (Fig. 58), areas of bainite were found even in material which had been sintered for the maximum time of 8 hours at 1300°C. It should be noted that the structure of blended material sintered for 8 hours at 1300°C (Fig. 44) was similar to that of the plated material sintered under similar conditions (Fig. 57), except that the former still retained evidence of nickel-rich areas.

5.5.2.3 Optical and electron microscopy of pre-alloyed materials.

The sintering of pre-alloyed materials for times of up to 8 hours at 1150°C produced little change in the microstructure. All the structures examined under the optical microscope appeared to be predominantly martensite. In compacts sintered for one hour or less, isolated light-etching areas were found which did not appear to contain any martensite; these were free from distinguishable features. Figs. 59 to

62 show the gradual disappearance of these light-etching areas and the lack of change in the morphology of the martensite as the time of sintering increased to 2 hours. Fig. 63 (a) shows that the light-etching areas contained a significant quantity of chromium and nickel, while the martensite areas (Fig. 63(b)) contained no chromium and significantly less nickel. It must be assumed that the powder provided by the manufacturers was contaminated with a small quantity of stainless steel powder ($<1\%$). Examination of these structures at higher magnification showed that the martensite possessed a lath morphology throughout the greater part of the material although certain areas contained an acicular form of martensite (Figs. 64 and 65). Electron microscopy showed the difference in morphology more clearly; Fig. 66 shows an area of a compact sintered for 8 hours at 1150°C , in which certain lens-shaped units are more akin to acicular martensite than to lath martensite. The band of narrow laths in this micrograph is considered to be a region of lath martensite.

The principal changes which could be distinguished in these alloys were those of pore shape, from which the different stages of sintering could be ascertained. Pre-alloyed compacts possessed the lowest density of all those employed in this work so that the changes in pore structure which occurred during densification could be more clearly observed in these than in the other types of material. Figs. 67 to 69 show the progress of sintering in terms of pore structure, from which it may be seen that the individual particles could

still be identified after prolonged sintering times. Fine, concave-shaped, interparticle porosity was gradually replaced by coarse, convex-shaped pores. Fig. 67 is considered to represent stage I sintering^{86,87,88,89} as new interparticle necks were clearly about to form (as indicated on the micrograph). Fig. 68 represents an intermediate stage in which neck growth was still occurring although a considerable amount of convex-shaped porosity was present. Fig. 69 illustrates the situation at the change from stage II to III where some concave-shaped porosity still remained but pores were becoming isolated and coarse.

Pre-alloyed compacts sintered at 1300°C showed similar microstructures to those sintered at 1150°C. Fig. 70 shows the structure of material sintered for 15 minutes at the higher temperature, in which the features are virtually indistinguishable from those described above. The light-etching areas were not visible in compacts sintered for times in excess of 15 minutes. Thus the microstructure shown in Fig. 71, for a compact sintered for 15 minutes, is typical of that for compacts which were sintered for up to 8 hours at 1300°C, viz., lath martensite in intimate association with a small amount of acicular martensite. No evidence was found of the presence of ferrite or bainite in any of these pre-alloyed materials.

An examination of the pore structure showed that the rate of sintering at 1300°C was considerably greater than that at 1150°C (see Figs. 72 to 74). The irregular porosity in Fig. 72 shows a high pore surface area in relation to the total pore volume; this structure is very similar to that of

material sintered for one hour at 1150°C (Fig. 68). After 8 hours treatment at 1300°C, stage III sintering was clearly in progress as indicated by the coarse nature of the isolated pores (Fig. 74).

5.5.2.4 Scanning electron microscopy of fracture surfaces

Sections from tensile test pieces which had been sintered for 15 minutes at 1150°C were fractured by impact and the freshly exposed surfaces were examined by scanning electron microscopy. Fig. 75 shows the fracture face of the blended material, which retained a particulate nature after this treatment. A considerable range of particle size was visible and many of the smaller units were evidently the original nickel particles. All fracture surfaces were invariably of the ductile type. Thus, Fig. 76 shows the dimples which are characteristic of ductile fracture surfaces.

Apart from the lack of very small particles, the nature of the fracture surface of the plated compact was similar to that of the blended compact (see Fig. 77). Large smooth areas of unsintered particle surfaces clearly indicate the interparticle character of the porosity. Parts of the surface which had actually undergone failure again showed evidence of ductile fracture (Fig. 78).

Fig. 79 shows that the pre-alloyed powder particles were noticeably more spherical than the electrolytic powder particles, from which the other materials had been prepared. Both the rounded surfaces and the ductile nature of the fracture face may be clearly seen in Fig. 80.

5.5.2.5 Quantitative Optical Microscopy

This technique was applied to unsintered sections of materials which contained regions of pure nickel, i.e. blended and plated compacts.

A distance of 40mm was traversed across the surface of the blended compact to provide the lineal analysis data given in Table 26. The distance traversed across nickel particle agglomerates was separately recorded in order to determine the mean intercept length of "effective" nickel particles. Segregation of several such particles produced an intercept length frequently considerably greater than the individual particle size ($3.7\mu\text{m}$). The mean intercept length was converted to a more realistic effective particle diameter by use of the following equation¹⁷³:

$$\bar{r} = \pi / 4\bar{m} \quad \text{in which}$$

\bar{r} = the mean radius of non-uniform, non-spherical particles

and \bar{m} = the mean reciprocal diameter of intersection.

The effective nickel particle diameter calculated by this method was $12.2\mu\text{m}$ and the mean distance between effective nickel particles was $295\mu\text{m}$. In this determination, the volume fraction of nickel was found to be 2.6%.

Lineal analysis data for plated material are given in Table 27. Although the nickel coating could be observed while measurements were being made, errors due to lack of resolution and fine mechanical movements precluded the precise determination of plating thickness. The structure was treated as though a grain size determination was to be performed in which the grain boundaries were thicker than

normal. Thus, grain size measurements were equal to the mean distance between nickel-rich areas. The mean linear intercept was converted to the more realistic mean distance between nickel centres by the following relationship¹⁷³:

$$\bar{D} \cong 1.75 \bar{d} \quad \text{in which}$$

\bar{D} = the mean grain diameter

and \bar{d} = the mean linear intercept.

The mean distance between nickel-rich centres was $30.3\mu\text{m}$, a value somewhat larger than the mean particle size of $18\mu\text{m}$ that was determined by use of the Fisher sub-sieve sizer.

5.5.2.6 X-ray Diffraction

The results for blended compacts examined by X-ray diffractometry are given in Table 13. Line broadening data and line shift measurements showed that the range of nickel concentration in the BCC phase in the isostatically pressed material was less than that in the die-pressed material after similar sintering treatments.

In plated compacts sintered for 15 minutes at 1150°C , very little line broadening of the BCC phase was observed, whilst only the strong $\{111\}$ reflection could be positively identified to show the presence of the FCC phase (Fig. 81). Specimens sintered for more than 15 minutes at 1150°C did not apparently contain any austenite.

Pre-alloyed compacts showed no evidence of retained austenite by X-ray diffraction, irrespective of the sintering time employed.

5.5.3 The Homogeneity of blended, plated and pre-alloyed materials.

Results obtained with the electron probe micro-analyser from blended compacts sintered at 1150°C are shown in Fig. 82 with 99% confidence limits included. The homogenisation parameter (H) was lower in specimens of this material than in the die-pressed specimens sintered for the same time (Section 5.4.3). This indicates that a higher level of homogeneity existed in the isostatically pressed compacts after any particular sintering time. The equation of the curve in Fig. 82 is given below:

$$H = 9.84 \exp (-7.864 \times 10^{-3}t) + 1.29$$

in which

$$H = \text{the homogenisation parameter after time } t \text{ (in minutes).}$$

The fit between the experimental and the computed values corresponded to a correlation coefficient of 0.996. Compacts sintered at 1300°C exhibited lower values of the homogenisation parameter over the whole sintering range than those sintered at the lower temperature (compare Figs. 82 and 83). The equation of the curve in Fig. 83, for which the correlation coefficient was 0.993, is given below:

$$H = 4.97 \exp (-1.118 \times 10^{-2}t) + 0.02$$

The values of the homogenisation parameter predicted by this equation for zero and infinite times were less than those given by the equation for compacts sintered at 1150°C.

Fig. 84 shows the micro-analysis results for plated material sintered at 1150°C. The value of the homogenisation parameter for material sintered for 15 minutes was an order

of magnitude less than that obtained from blended material, which indicates a much higher level of homogeneity within compacts produced from nickel-plated powder. Despite this, the homogeneity of compacts sintered at 1150°C continued to increase up to the maximum sintering time of 8 hours. At a maximum correlation coefficient of 0.982, the equation of the curve in Fig. 84 was found to be:

$$H = 0.66 \exp (- 8.407 \times 10^{-3} t) + 0.09$$

The material which was sintered for 8 hours at 1150°C possessed a homogenisation parameter of 0.10; this degree of homogeneity was not reached in blended and isostatically pressed material until after a sintering time of approximately 6 hours at 1300°C. Blended and die-pressed material did not attain this degree of homogeneity after any treatment. Fig. 85 shows the homogenisation parameter of plated material sintered at 1300°C, for which the maximum correlation coefficient of 0.994 between the experimental and computed values gave the following relationship:

$$H = 0.34 \exp (- 1.456 \times 10^{-2} t) + 0.01$$

A homogenisation parameter of 0.10 was attained in this material after a sintering time of approximately 90 minutes; this compares to the sintering time of 8 hours that was required for the attainment of the same high level of homogeneity in similar material at the lower temperature. Sintering for 8 hours at the higher temperature resulted in a range of 2.73%± 0.23% in the mean nickel concentration over different areas of the probe specimen.

Micro-analysis results for pre-alloyed material are

given in Table 28. It is of interest to note that a sintering treatment of 15 minutes at 1150°C was sufficient to produce a level of homogeneity ($H=0.10$) equal to that attained in plated material which had been sintered for 8 hours at the same temperature. Despite the high state of homogeneity that existed in pre-alloyed material before the commencement of sintering, a small increase in homogeneity was produced during sintering at 1150°C . The value of $H = 0.02$, which was attained after a sintering time of 4 hours, indicates that the same high degree of homogeneity was present as that in plated material sintered for the same time but at the higher temperature of 1300°C . The range of mean nickel concentration in pre-alloyed material which corresponded to the above value of $H = 0.02$ was $2.53\% \pm 0.36\%$. The lower mean value for pre-alloyed material may be explained by the lower density of this material. Sintering treatment at 1300°C produced very little increase in homogeneity, as shown in Table 28. The homogenisation parameter of 0.02, which was attained after sintering for 4 hours, corresponded to a range of mean nickel concentration of $2.50\% \pm 0.28\%$.

6. DISCUSSION OF RESULTS

6.1 Relationships involving the Tensile Strength of Iron: Nickel:Carbon Materials

The relationship between porosity and tensile strength in the materials under consideration during the present investigation is shown in Fig. 86. It should be noted that all compacts were isostatically pressed under the same compaction pressure. Thus the greater compressibility of the blended material resulted in compacts whose densities were approximately 4% greater than those of the plated material and approximately 6% greater than those of the pre-alloyed material. The greater density of the blended material was maintained after all sintering treatments at 1150°C but, in the case of compacts sintered at 1300°C, the rates of densification in the plated and pre-alloyed materials were greater than that in the blended material. Thus the density advantage of the latter was reduced to approximately 1% and 4.5% over plated and pre-alloyed compacts respectively after a sintering treatment of 8 hours at 1300°C. For those cases in which tensile strength is a function of the amount of porosity, these differences in density could be of practical importance, since poor compressibility becomes a great disadvantage commercially.

An increase in density did not always produce a significant increase in tensile strength. Thus, the results obtained from compacts that had been sintered for one hour at 1150°C (Fig. 86) clearly show that the range of porosity varied from 11.1% in blended compacts to 17.3% in pre-alloyed material, while the corresponding tensile strengths showed a difference

of only 20MN/m^2 . The published relationships between strength and porosity suggest that this variation in tensile strength should be about 100MN/m^2 . It will be shown that this lack of correlation with previous work can be related to variations in the degree of homogeneity and associated changes in microstructure that are produced during sintering and subsequent heat treatment.

Any discussion of the mathematical relationships between tensile strength and the amount of porosity requires a knowledge of the tensile strength of the fully dense material. From published information^{7,13,28} on the mechanical properties of wrought steels of the appropriate size and composition, it is reasonable to assume that a fully dense alloy similar to that used in this investigation would possess a tensile strength of 800MN/m^2 after hardening and tempering for one hour at 600°C , (Table 1). The most simple relationship between tensile strength and porosity is

$$\sigma_s = \sigma_o (1-P)$$

in which

σ_s = the tensile strength of sintered material,

σ_o = the tensile strength of fully dense material

and

P = fractional porosity.

However it should be noted that this equation ignores the stress concentration factors associated with the pores. Furthermore, this relationship does not appear to apply to compacts which contain more than approximately 30% porosity^{127, 130}. This has led to its modification by several workers^{117,}

120,122,123,127,128,130 while others have produced empirical exponential equations^{133,134,135,137}. The present author has used the equation due to Haynes¹²³ to predict the tensile strengths of the materials under consideration. This equation states that

$$\sigma_s = \sigma_o \left(\frac{1-P}{1+bP} \right)$$

in which

$$b = a (F-1)$$

a = an arbitrary constant,

F = stress concentration factor

and σ_o = the tensile strength of fully dense material, which has been taken to be 800MN/m² in the present work.

These predicted relationships between tensile strength and porosity are shown as a set of curves, each with a constant level of "b", in Figs. 87 to 89. Fig. 87 also shows the experimental values for blended compacts (taken from Tables 16 and 17) which may thus be compared to those given by the Haynes' equation.

It is evident from Fig. 87 that:-

- (a) The experimental results can only be predicted from the Haynes' equation by the use of variable values of "b", the magnitudes of which range between 11 and 3.5.
- (b) The values of "b" required to predict the results obtained from compacts sintered at 1150°C and 1300°C are quite different.
- (c) The required values of "b" decrease as the sintering time increases.

Fig. 88 suggests a similar range of "b" values in the case

of plated materials sintered at 1150°C , although the magnitude of the same coefficient appropriate to the sintering of the same material at 1300°C falls within the range of 2.8 to 3.9. In contrast, the "b" values associated with the pre-alloyed material are relatively constant and most fall within the same range as those associated with plated material sintered at 1300°C (compare Figs. 88 and 89).

The reduction of "b" values within the range of about 3 to 4.5 can be explained by the change in stress concentration factors associated with the change in pore shape that accompanies the sintering process, since $b=a(F-1)$ in which F =a stress concentration factor associated with particular pore shapes and "a" = a constant. Values of "b" that lie in the range of 2.8 to 4.5 can be associated with acceptable values of the stress concentration factor. However, the present work suggests that some results require "b" values far in excess of 4.5, which give stress concentration factors far greater than those that can be associated with the known geometry of the pores in sintered compacts^{126,127,130}.

Thus it is evident that the present tensile strength results fall into two distinct groups. The first includes results that can be explained from a consideration of the theory associated with the Haynes' equation coupled with the theory that relates stress concentration factors to pore shape ("b" values of 2.8 to 4.5). However, there are also a large number of results that cannot be explained by this means, viz., the tensile strength results obtained from most of the blended materials and also those plated materials that had been sintered at 1150°C for less than 2 hours, ("b"

values of 4.5 to 11). It will be shown that the former are associated with a high degree of homogenisation while the latter possess considerable heterogeneity, the degree of which increases as the value of "b" increases.

Fig. 90 shows the relationship between the homogenisation parameter (H) and the tensile strength of all the compacts that were sintered at either 1150°C or 1300°C. The curves related to the blended and plated alloys show an abrupt change in slope at an H value of 0.45. Virtually all the materials that correspond to values of H below this value are also included within the group which is associated with acceptable variations in the value of "b", and the few exceptions lie only just outside the acceptable range. It has been found convenient to discuss the relationship between the level of porosity and the tensile strength of this group of homogeneous materials first, before considering this relationship in compacts where H exceeds 0.45.

6.1.1 Alloys of High Homogeneity

Alloys within this group are associated with a homogenisation parameter below 0.45, as shown in Fig. 90. Since the increase in the degree of homogenisation that occurs during the sintering of such materials is small, it would be expected that this group of compacts would show relationships that most closely approximate to the previously published equations involving tensile strength and the amount of porosity. In such equations the stress concentration factor (F) appears either directly, as in the equation $\sigma_s = \sigma_o / (1 - F P)^{127,130}$, or by means of a related constant, as in the previously discussed Haynes' equation¹²³. Therefore the

discussion must begin with an examination of the stress concentration factors associated with the materials under consideration.

6.1.1.1 The Determination and Use of Stress Concentration Factors.

The difficulty involved in empirical determinations of stress concentration factors, e.g. by quantitative metallography^{121,137}, has led to the use of theoretical factors based on elasticity theory^{126,127,130}. Pohl's¹³⁰ calculations suggest that stress concentration factors (F) for sintered irons and steels are of the order of 2.6 to 3.4, a range similar to the generally applicable factors of 2.0 to 3.8 given by Nazare and Ondracek¹²⁷. The theoretical lower limit given by the latter authors was also found by Mackenzie¹²⁶ to be associated with spherical porosity.

In order to determine the values of F associated with the present tensile strength results the theoretical strength values obtained by the use of the equation $\sigma_s = \sigma_o(1-F P)$ with appropriate values of F have been compared with the experimental results obtained during this investigation. In Fig. 91, this relationship has been plotted for different values of 'F' on the assumption that the fully dense material would possess a tensile strength of 800MN/m^2 . The experimental results shown relate to pre-alloyed compacts sintered at 1300°C ; it may be seen that a mean value of $F = 2.8$ could be taken for this data but this suggests that the stress concentration factor does not change during the sintering process. That the pore structure does indeed change is shown most clearly by reference to Figs. 72 to 74. The angular pores and

interconnected porosity in compacts sintered for 15 minutes (Fig. 72) are replaced by larger rounded pores with little interconnected porosity in compacts sintered for 8 hours (Fig. 74). Therefore a change in stress concentration factor would be expected. In Fig. 91, the experimentally determined plot of tensile strength against porosity is shown to depart slightly from the line that corresponds to $F = 2.8$, so that F may increase from 2.7 to 3.0 as the sintering time increases from 15 minutes to 8 hours. A similar analysis yields values of 2.75 to 3.45 for pre-alloyed compacts sintered at 1150°C for 15 minutes to 8 hours respectively (Table 29). Figs. 67 to 69 show the development of the pore structure corresponding to the stress concentration factors in Table 29; sintering is clearly less advanced in these compacts than in those sintered for similar times at 1300°C . Comparison of Figs. 67 and 68 shows that new interparticle necks were still forming after a sintering treatment of one hour. The replacement of fine interconnected porosity of concave shape by coarse pores of convex shape is significantly slower than in compacts sintered at 1300°C . The rounding of angular pores in the vicinity of interparticle necks is a particular feature which may be distinguished in compacts sintered for one hour at 1150°C (Fig. 68); this structure is very similar to that of compacts sintered for only 15 minutes at 1300°C (Fig. 72) whereas compacts sintered for 15 minutes at 1150°C (Fig. 67) show considerable pore angularity. The stress concentration factor associated with the pore structure in Fig. 67 is 3.45 in contrast to the values of 3.00 and 3.05 for the pore structures shown in Figs. 72 and 68 respectively.

The values of F given in Table 29, which have been determined by the use of the equation $\sigma_s = \sigma_o (1 - F P)$, give rise to several conclusions as stated below.

- (a) All the empirically determined values fall within the limits given in the literature ($F = 2.0$ to 3.8).
- (b) The full range of these empirical values ($F = 2.7$ to 3.45) is very close to that given in the literature for irons and steels ($F = 2.6$ to 3.4).
- (c) The range of values for compacts sintered at 1150°C ($F = 2.75$ to 3.45) is greater than that for compacts sintered at 1300°C ($F = 2.7$ to 3.0).
- (d) The theoretical lower limit of the stress concentration factor, i.e. $F = 2$, was not approached in any of the compacts. This would be expected in view of the condition that spherical pores are necessary for such a low value of F . Such a pore structure was not observed in any compact, although Fig. 74 shows that material sintered for 8 hours at 1300°C contained pores with a high proportion of convex shaped surfaces. Thus the lower calculated limit of $F = 2.7$ is considered to be not unreasonable in the present investigation.
- (e) The fact that only results from compacts of high homogeneity were used to calculate stress concentration factors reduced to a minimum the influence of compositional and structural changes during sintering.

The Use of Stress Concentration Factors in the Prediction of Tensile Strength.

Fig. 92 shows the relationship between tensile strength and porosity in those compacts whose homogenisation parameter falls below 0.45 . The predicted data in Fig. 92 have been

obtained by the use of the equation $\sigma_s = 800 (1 - F P)$, in which the stress concentration factors have been those given in Table 29. This assumes that the stress concentration factor (F) is a function of sintering time and temperature and not of powder type or the level of porosity. Since F is associated with the shapes of the pores, which are affected mainly by the sintering process, this would appear to be a reasonable assumption. The justification for the use of this equation to predict tensile strength in material of high homogeneity, in preference to others reported in the literature^{120,123,135}, is provided by the results in Table 30.

These results show that the mean departure of the predicted tensile strengths from the actual tensile strengths is least for the case in which the above equation is employed. It is of interest to note that a change in the values of the variables from those used by Salak et al¹³⁵ (in a comparison of existing equations) to those indicated thus (*), produces predictions which are improved but which do not show such good general agreement as those provided by the equation $\sigma_s = 800 (1 - F P)$. Consequently this equation has been used exclusively in the subsequent discussion.

6.1.1.2 Relationship between Microstructure and Tensile Strength.

Although the degree of homogeneity of pre-alloyed material was greater than that of the other two classes of material (Fig. 90), the tensile strengths of the pre-alloyed compacts were generally lower than those obtained in either of the other sets of alloys. However, pre-alloyed materials suffer a density disadvantage relative to the other materials which reduces the tensile strength of the former in comparison

with the latter. Thus it is preferable to compare the microstructures of these materials with the tensile strengths that have been adjusted to values associated with a constant level of porosity. This may be achieved by the adjustment of all tensile strength values to the levels predicted at 10% porosity by the use of the relationship $\sigma_s = \sigma_o (1 - F P)^*$. Fig. 93 shows these corrected values for all the results pertaining to compacts which were sintered at either 1150°C or 1300°C: only those associated with homogenisation parameters below 0.45 are to be discussed in this section.

These materials of high homogeneity may be divided into two distinct groups. The larger group is comprised of specimens which possessed tensile strengths within the range of 558MN/m² to 583MN/m² and these results are contained within the narrow band shown in Fig. 93. Specimens within the smaller group include some which possessed significantly lower tensile strengths than those materials in the larger group.

The microstructures of compacts belonging to the larger group may be summarised as follows.

(a) Plated alloys

All the members of this class of material, except for those compacts sintered for one hour or less at 1150°C, belonged to the larger group. The microstructures of all these compacts were similar and, as illustrated by Fig. 52, the main constituent was lath martensite. The similarity between the structure illustrated in this figure and that of

*This involved the use of "smoothed" data from Figure 86.

compacts sintered for 15 minutes at 1300°C (Fig. 53) was very marked. Electron microscopy of compacts sintered at both 1150°C and 1300°C revealed that the high degree of homogeneity in these alloys was not sufficient to allow fully martensitic structures to be obtained by quenching the compacts from the sintering temperature. Grain boundary ferrite (Fig. 56), upper bainite (Figs. 54 and 56) and lower bainite (Fig. 55) were present in the microstructures of all these alloys. Although no light-etching nickel-rich areas were distinguishable, certain areas were characterised by acicular martensite (Fig. 58).

(b) Pre-alloyed material

Again, all the members of this class of material, except for those compacts sintered for one hour or less at 1150°C, belonged to the larger group. There was little variation in the microstructures of these alloys, which consisted entirely of martensite. The morphology of this phase was predominantly of the lath type (Fig. 65). However, in Fig. 66, an area of acicular martensite is seen to be adjacent to a lath region.

Thus the main structural difference between the plated and pre-alloyed materials in this group of compacts is the presence of non-martensitic decomposition products in the former. It is rather surprising, in view of the presence of ferrite and upper bainite in the plated alloys, that there is no significant difference in the mean tensile strengths of these two classes of material.

The compacts belonging to the smaller group in Fig. 93 also fall into two categories.

(a) Blended alloys sintered for 4 hours or more at 1300°C.

The microstructure shown at low magnification (Fig. 44) consisted mainly of lath martensite, although optical examination at higher magnification also revealed the presence of acicular martensite, mainly in the vicinity of nickel-rich areas (Fig. 43). In this Figure, blocks of lath martensite occur adjacent to lens shaped units of acicular martensite. Electron microscopy showed the presence of ferrite and bainite in all compacts of this group. Thus Fig. 39 shows grain boundary ferrite in an upper bainite-lower bainite aggregate, while Fig. 40 shows only lower bainite in the same compact, which had been sintered for 4 hours at 1300°C. Similar structures were present in compacts sintered for 8 hours at 1300°C (Figs. 41 and 42). Isolated areas of austenite persisted even in specimens in the most homogeneous condition.

(b) Pre-alloyed material sintered for one hour or less at 1150°C.

The microstructures of compacts in this group were similar to those of pre-alloyed materials which had been sintered for longer times at the same temperature; they consisted predominantly of lath martensite with a limited quantity of acicular martensite. However, in addition, these materials also contained light-etching areas which did not appear to contain any martensite. Figs. 59 to 61 show the gradual disappearance of this constituent, which was not present in compacts sintered for times greater than one hour. As indicated in Fig. 63, this constituent was rich in chromium and nickel.

As has already been shown in the discussion of the plated material, bainite and ferrite in isolated regions within the general microstructure do not appear to have a detrimental effect upon the tensile strength of materials of high homogeneity. Therefore the relatively poor strength of the smaller group of compacts is probably associated with the light-etching regions of austenite. However, the austenitic regions in the pre-alloyed material should not be considered typical of a homogeneous alloy of this composition even in the earliest stages of sintering, since the presence of this phase is due to the slight contamination of the powder during manufacture.

6.1.2. Alloys of Low Homogeneity.

Alloys within this group are those which possess a homogenisation parameter above 0.45, as shown in Fig. 90. It was shown in Section 6.1 that the tensile strengths of these materials did not conform to any of the equations that have been developed to predict the relationship between tensile strength and porosity. This lack of correlation between these properties is probably due to the structural changes that occur during sintering and homogenisation. In order to separate the effect of porosity from the effects of these other variables on tensile strength, the equation relating porosity to tensile strength in alloys of high homogeneity ($\sigma_s = \sigma_o (1 - F P)$) may be used; this procedure eliminates the effect of porosity on tensile strength in materials which undergo significant structural changes during sintering.

Thus Fig. 93 indicates that, in cases where the homogenisation parameter exceeds 0.45, there is a separate relation-

ship between tensile strength and homogenisation parameter in each of the three series of compacts. Furthermore, in each case, the tensile strengths of these materials are lower than those obtained in the alloys of high homogeneity. An explanation for this must be sought in the effect of the homogenisation process on the microstructures of the materials under consideration.

6.1.2.1 Relationship between Microstructure and Tensile Strength

The significant features of the microstructures of alloys of low homogeneity are given below.

(a) Blended alloys sintered for up to 2 hours at 1150°C

The bulk of the microstructures in these materials consisted of martensite with small quantities of ferrite: however, coarse nickel-rich networks of light-etching material surrounded the original iron particles (Fig. 29). Fig. 30 shows that, although iron and nickel interdiffusion had occurred after 15 minutes sintering, this was still confined to the vicinity of the original sites of the nickel particles. The hardenability within each compact was thus extremely variable; Fig. 30 shows localised regions of pearlite in the interior of some of the original iron particles, which remain depleted in nickel until a late stage in the homogenisation process. Fig. 31 shows a mainly martensite structure in an area containing a greater initial concentration of nickel particles. The indication provided by these microstructures of the existence of a wide range of nickel concentration was confirmed by X-ray diffraction, (Table 13). Quantitative optical microscopy data (Table 26) from unsintered material shows that, although the mean nickel particle intercept distance was only $7.76 \mu\text{m}$ (equivalent to a particle diameter of $12.2 \mu\text{m}$), the range of nickel

particle intercepts varied from $1\mu\text{m}$ to $55\mu\text{m}$.

The resultant fluctuations in composition and therefore microstructure are believed to contribute significantly to the low tensile strength of blended compacts sintered for up to 2 hours at 1150°C .

(b) Blended alloys sintered for 4 hours or more at 1150°C .

The microstructures of these alloys did not contain a clearly defined nickel-rich network but rather separate nickel-rich areas which persisted after sintering for 8 hours (Fig. 32). This figure exhibits a variation in the morphology of the martensite which is best observed at higher magnification (Fig. 33); acicular martensite has apparently formed in those areas sufficiently rich in nickel for this product to form but which are also insufficiently rich in this element to depress M_s below room temperature. The remaining areas are largely comprised of lath martensite but minor amounts of ferrite and bainite were also detected by electron microscopy.

(c) Blended alloys sintered for up to 2 hours at 1300°C .

These alloys contained separate nickel-rich areas in the microstructure, the remainder of which was predominantly lath martensite (Fig. 34). Separate regions of acicular martensite were not detected and the martensite was more uniform in appearance (Fig. 35) than that described in (b) above (Fig. 33). Electron microscopy revealed that ferrite (Fig. 38) and bainite (Fig. 37) were present in those specimens that had been sintered for 2 hours at 1300°C prior to quenching.

(d) Plated alloys sintered for one hour or less at 1150°C .

The principal microstructural feature of this material

was clearly the nickel-rich network around the original iron particles, which was a consequence of the plating operation (Fig. 45). Despite the presence of this network, X-ray diffraction measurements (Table 13) showed that less line broadening occurred in the BCC structure of plated compacts than that in blended compacts which were sintered under similar conditions and which were characterised by a coarse austenitic network, i.e. there was evidence of more extensive nickel solution in plated compacts. This behaviour might be expected in view of the great difference in the mean distance between effective nickel centres, viz., $30.3\mu\text{m}$ and $295\mu\text{m}$ in unsintered plated and blended compacts respectively. After sintering for 30 minutes, plated compacts possessed only a faintly visible network, which disappeared completely after a sintering treatment of one hour (Fig. 49). Optical microscopy at higher magnification showed that lath martensite was the major phase present (Fig. 50) although electron microscopy revealed the presence of a certain amount of ferrite and bainite.

The poor tensile strengths of blended compacts sintered at 1150°C are probably due to the presence of a considerable amount of austenite. In those compacts sintered for up to 2 hours, the very low strengths can be explained by the distribution of this phase, i.e. broad networks around the original iron particles. In these alloys the production of some pearlite on subsequent cooling from the sintering temperature is probably detrimental: however, the presence of the different types of martensite and the upper and lower bainite

is unlikely to be detrimental since similar structures were produced in compacts which possessed considerably higher tensile strengths, viz., those materials of high homogeneity. The presence of austenite in the blended material that had been sintered for 4 hours or more at 1150°C and for up to 2 hours at 1300°C is also probably responsible for the relatively poor tensile strength of these compacts. However, the austenite is in this case present in the form of isolated patches rather than as a continuous network; this may account for the higher tensile strength of this group of materials in comparison with the plated material that contained a network of austenite.

The tensile strength of the plated material sintered at 1150°C for 15 minutes is rather lower than might be expected from one with a comparatively high degree of homogeneity. This is associated with the presence in the microstructure of a thin continuous network of austenite around the original iron particles. Thus, although the contribution made by the compositional fluctuations associated with this network to the magnitude of the homogenisation parameter is comparatively small, the presence of this type of microstructure appears to be very detrimental to tensile strength. The disappearance of this network in plated compacts sintered for longer times at 1150°C and the development of a lath martensite microstructure with minor amounts of ferrite, bainite and acicular martensite is associated with a much higher level of tensile strength.

It may be concluded that, in all the materials examined, the presence of austenite, especially in the form of a thin

network around the original iron particles, is particularly detrimental to tensile strength.

6.1.3 Relationship between Tensile Strength, Porosity and Homogenisation Parameter.

It has been shown that the equations relating tensile strength and the level of porosity break down when the homogeneity of the material falls below a certain value. Although a quantitative assessment of the homogeneity of iron-nickel-carbon materials has been made by the use of the homogenisation parameter (H), the method by which this parameter was measured indicates that the values obtained have no fundamental significance. Therefore it is not surprising that there is no single equation that may be used to relate H to the tensile strength and porosity of all the materials under investigation.

The following general relationship has been found to be applicable:

$$\sigma_s = \sigma_o (1 - F P) (1 - (k H P + c))$$

in which

σ_s = the tensile strength of the sintered material,

σ_o = the tensile strength of the fully dense material
= 800MN/m²

F = the stress concentration factor (Table 29),

P = fractional porosity (Tables 16,17,20,21,23,24),

H = homogenisation parameter (Tables 31 and 32)

and

k and c = empirical constants (Table 33)

In this equation, the empirical constants k and c depend upon the type of material and the sintering temperature. Thus the value of the homogenisation parameter in the prediction

of tensile strength is small. Nevertheless, it has proved to be extremely useful in the present investigation as a means of expressing, in a quantitative way, the degree of homogeneity in alloys of complex microstructure. The predicted tensile strengths of all materials sintered at 1150°C & 1300°C have been plotted against the actual tensile strengths in Fig. 94; the degree of correlation is considered to be acceptable.

The homogenisation parameter is really of importance only as far as it is related to the production of particular microstructural constituents, which affect the mechanical properties of the material. Since the microstructures of the alloys under consideration are very complex, it is difficult to assess the relative importance of each constituent. However, the analysis carried out during the present investigation emphasises the importance of the removal of austenite from the microstructure.

6.1.4 The Effect of Temperature at Constant Time.

The experimentally determined tensile strengths of compacts which had been sintered for one hour at temperatures in the range 1000°C to 1300°C are compared in Table 34 with the strengths predicted by the use of the equation $\sigma_s = 800(1 - F P)$. In the case of materials sintered at temperatures below 1150°C, F has been assumed to be constant at 3.1. For higher temperatures the appropriate values in Table 29 have been used. Again the best correlation between actual and predicted values is obtained from pre-alloyed material.

The results from blended and plated material sintered

for one hour at temperatures below 1150°C are probably adversely affected by the lack of homogeneity in these compacts. This is clearly shown in Figure 95 which gives the relationship between porosity and tensile strength for all the materials subjected to a sintering treatment of one hour. It is evident that equations of the type $\sigma_s = 800 (1 - F P)$ where $F \approx 3$ are unable to predict the relationship between tensile strength and porosity in the blended and plated materials i.e. in those compacts that are most heterogeneous. These results are consistent with those discussed in Sections 6.1.1 and 6.1.2; i.e. results from materials sintered for various times at 1150°C and 1300°C.

Figure 96, which shows graphically the experimental data given in Table 34 suggests that if sintering times are limited to about one hour, as is usually the case in commercial practice, the blended and plated materials require a sintering temperature of at least 1150°C. The strength of the pre-alloyed material, on the other hand, is insensitive to variations in sintering temperature within the range investigated.

6.2 Relationships involving the Tensile Ductility of Iron: Nickel:Carbon Materials.

There was considerable scatter in the data for those compacts sintered at 1150°C and 1300°C. Whilst the tensile ductility showed a slight tendency to increase with increase in sintering time in the case of blended and plated compacts (Tables 16,17,20 and 21), no such trend was observed in pre-alloyed compacts (Tables 23 and 24). Salak et al¹³⁵ have shown that the tensile ductility of sintered iron is sensitive

to preparation conditions; from the considerable amount of data provided in their report, it may be seen that the percentage elongation varied from 6% to 20% in compacts that contained 10% porosity after sintering. It was concluded by these authors that the scatter in the relationship between the percentage elongation and porosity was due to the great sensitivity of the former property to the pore structure. In the present work, there is no significant relationship either between the percentage elongation and porosity or between the percentage elongation and the homogenisation parameter, as may be seen from Table 35. In the latter case however, it is worth noting that some measure of ductility was observed in all the pre-alloyed compacts; this behaviour was not observed in all blended and plated compacts, even though these were of lower initial porosity content. Furthermore, the tensile ductility in pre-alloyed materials showed a tendency to remain constant irrespective of the sintering time and temperature. Despite these observations, there is no convincing evidence to suggest that homogeneity had any specific influence upon tensile ductility in the present investigation.

6.3 Relationships involving the Hardness of Iron:Nickel:Carbon Materials.

The hardness testing of porous materials presents special problems because, unlike fully dense materials, the choice of test load may be extremely critical¹⁴⁰. Each hardness result specified in this work refers to the mean value determined along a load independent hardness plateau on the hardness/load graph.

In those sintered steels that originally contained nickel particles, the extent of iron and nickel interdiffusion did not significantly affect the hardness, provided that martensite was produced on quenching from the sintering temperature. Kelly and Nutting¹⁸ have remarked that the addition of nickel to martensitic carbon steels is likely to produce only a very small effect on hardness. In support of the above remarks, Fig. 28 shows that similar microhardness results were obtained in areas with different etching characteristics (due to differences in nickel concentration). Thus it follows that, in cases where martensitic structures of constant carbon content are produced throughout the compact, variations in hardness will be due mainly to variations in the amount and nature of the porosity.

Fig. 97 shows the relationship between hardness and the quantity of porosity in compacts which were quenched in water directly from the sintering temperature. The scatter within the band containing the results from the most homogeneous alloys ($H < 0.45$) is typical of that reported in the literature. Salak et al¹³⁵ found a variation from approximately 60HB to 90HB in plain iron compacts which had been sintered to a porosity level of 10%; in such material, variations in hardness could only be due to variations in the pore structure. Thus it may be assumed that those results in Fig. 97, which do not lie between the two dotted lines, are affected by factors other than the level of porosity. Since these results were obtained without exception from material that was not highly homogeneous ($H > 0.45$), it is probable that the homogenisation factor influenced the hardness values.

This effect is probably associated with the effect of the degree of homogeneity on the microstructure of the material. Those compacts which gave hardness results inside the band indicated in Fig. 97 possessed microstructures which were mainly lath martensite (Section 6.1.1.2). In contrast, the microstructures of compacts associated with results outside the marked band in Fig. 97 were distinguished for the most part by substantial amounts of austenite; the greatest departure from the band was provided by those materials which showed the presence of nickel-rich austenite in the form of a continuous network. With regard to the three results just outside the band in Fig. 97, the microstructure of the blended compact contained fewer isolated patches of austenite than the other blended materials outside the band, while the microstructures of the two plated compacts represented the final stages of the disappearance of the thin continuous austenite network. Thus, it would appear that the hardness of the materials under consideration is influenced both by pore structure and microstructure; the degree to which the latter is influential is indicated to some extent by the degree of homogeneity existing within the material.

Fig. 98 shows the relationship between hardness and tensile strength for all compacts which had been tempered at 600°C after quenching from the sintering temperature. The relationship found by Talmage¹³⁹ for a variety of sintered products is shown for comparison. The departure of the data from a convincing linear relationship suggests that it would be difficult to predict one property from a knowledge of the other, although this can often be accomplished in wrought low

alloy steels which have been similarly treated^{13,29}. It was not possible to distinguish different relationships between hardness and tensile strength in alloys of differing homogeneity.

6.4 Relationships involving the Impact Strength of Iron: Nickel:Carbon Materials.

One of the chief criticisms levelled against sintered steels is that their toughness is generally much inferior to that of wrought steels. This deficiency is so well recognised that it has become the practice to employ unnotched impact test pieces; the results of this investigation certainly illustrate that this practice is necessary in order to make sufficient distinction between the toughness of different sintered steels. It should be noted that the impact strengths reported in the present work refer to a cross-sectional area of approximately 50mm^2 whereas much of the data in the literature refers to a cross-sectional area of 100mm^2 , i.e. square section Izod test pieces.

The impact strengths of material sintered at 1150°C have been plotted against porosity content in Fig. 99. In each type of alloy, i.e. blended, plated and pre-alloyed, impact strength is a linear function of porosity and, in any one group of alloys, large increases in impact strength are associated with small reductions in porosity content. In Fig. 99 it may be observed that the porosity content of the plated compact which had been sintered for 15 minutes is almost the same as that of the pre-alloyed compact which had been sintered for 8 hours. It is improbable that this difference in impact strength can be due to the small difference in porosity (0.2%). Thus it must be

concluded that this difference in impact strength is due to differences in either pore structure (Figs. 46 and 69) or homogenisation parameter (0.68 and 0.01 for the plated and pre-alloyed compacts respectively). The quoted differences in homogenisation parameter have previously (Sections 6.1.2 and 6.1.1.2) been shown to be associated with differences in microstructure. The most significant difference in the microstructure of these two compacts was the nickel-rich network in the plated material, as shown in Fig. 45. In addition to the absence of such a network, the pre-alloyed material possessed the convex-shaped pores associated with a material that had been sintered for 8 hours. The plated material, on the other hand, possessed much fine interconnected concave-shaped porosity. The most important feature of the fracture of plated material sintered for 15 minutes (Figs. 77 and 78) was clear evidence of ductility and yet the impact strength of the same material was extremely low. This suggests that it was the pore shape and distribution rather than the austenite network in the microstructure that was responsible for the low impact strength of the plated material. Thus the improvement in the impact strength of all three series of alloys, which was obtained by an increase in sintering time, (Fig. 99), may be associated with the change in pore shape and distribution that accompanies the sintering process.

This conclusion is supported by Fig. 100, which shows the relationship between impact strength and the homogenisation parameter in all three materials. It is evident that a correlation between these properties only occurs when a single type of material is considered; this is due to the fact that

changes in pore shape and distribution occur simultaneously with a decrease in homogenisation parameter, the former changes taking place as sintering time increases.

The relationship between impact strength and sintering time is shown more clearly in Fig. 101. As would be expected, the improvements in impact strength obtained with the plated and pre-alloyed materials are reasonably similar although the blended material is significantly better than either of the other materials. Evidently, the magnitude of the results from the blended material may not be explained by the effect of sintering time on the pore structure alone. The situation here is complex and further work will be required to clarify it.

6.5 General Mechanical Property Relationships

The dependence of many mechanical properties upon porosity is borne out by the work of Salak et al¹³⁵, who computed exponential equations that relate the porosity of iron compacts with tensile strength, percentage elongation and hardness. In view of the similarity of these equations, it is hardly surprising that an all-embracing equation has been proposed by Shcherban¹³⁴, viz.,

$$\sigma_{is} = \sigma_{io} (1 - P^2)^2 \exp(-BP)$$

in which

σ_{is} = i-th mechanical property of the sintered material,

σ_{io} = i-th mechanical property of the fully dense material,

P = fractional porosity

and B = a coefficient determined by the mechanical

property and the preparation conditions of the sintered material.

The properties considered by Shcherban to conform to this relationship included all those which have been determined in the present investigation. The interdependent variables which were considered to influence the value of the coefficient 'B' must make the cumulative errors involved in calculations quite considerable. Nevertheless, certain of Shcherban's conclusions are of especial interest; in particular, he gave ranges of 'B' for various materials. The maximum values for iron compacts were 5.8 for impact strength, 4.8 for tensile ductility, 4.0 for hardness and 3.3 for tensile strength. The order of these values generally agrees with certain of the conclusions made in the present work, which are summarised below.

(a) Impact strength (B = 5.8)

This property was considered to be mainly dependent upon pore structure.

(b) Tensile ductility. (B = 4.8)

There was no convincing evidence that homogeneity and thus microstructure exerted any influence upon this property.

(c) Hardness. (B = 4.0)

The amount of porosity and the pore structure were considered to be the main influences upon this property: there was evidence that gross irregularities in the microstructure also exerted some influence.

(d) Tensile strength. (B = 3.3)

The amount of porosity, the pore structure and the homogenisation parameter (which is related to the microstructure)

were all shown to be significant factors in the determination of the level of tensile strength in blended, plated and pre-alloyed materials.

Thus it may be seen that those properties with high values of 'B' in Shcherban's work are those associated primarily with the amount and nature of porosity in the current work whereas those properties with lower values of 'B' are influenced also by other factors, such as the microstructure and the degree of homogenisation.

6.6 The Mechanism of Homogenisation.

Reference has been made to the controversy that surrounds the relative contributions of surface and volume diffusion towards the homogenisation process (Section 3.3.3). In the present work, the progress of homogenisation has been followed in compacts with differing degrees of initial homogeneity. It was observed that, in the early stages of the sintering treatment in the least homogeneous alloys, i.e. blended materials, surface diffusion made a significant contribution to the homogenisation process. Nickel rapidly diffused over the surfaces of the iron particles, which became enveloped in a nickel-rich light etching phase (Figs. 8 and 29 for die-pressed and isostatically-pressed materials respectively). These early stages in the homogenisation process were associated with a rapid change in the value of the homogenisation parameter. The later stages were associated with an increase in the distance between nickel-rich centres as the smaller nickel-rich regions disappeared. However, some of these regions persisted after sintering for 8 hours at 1300°C. At this

stage, homogenisation appeared to be controlled by volume and grain boundary diffusion.

It was observed that the nickel-plating of iron particles produced a nickel-rich network in the microstructure which was similar in some ways to that obtained in blended material by diffusional processes. However, the network in the latter material was of a coarse and irregular nature. The creation and subsequent breakdown of the irregular network and the disappearance of isolated nickel-rich areas in the microstructure required a much longer homogenisation time in blended than in plated material. Thus it would appear that, in material which originally contained nickel particles, surface and grain boundary diffusion were an important first stage of the homogenisation process. In plated material, volume interdiffusion of iron and nickel could occur at all the iron particle surfaces as soon as the sintering treatment was begun: this resulted in rapid homogenisation and the uniform disappearance of the nickel-rich network. Thus, in plated material, surface diffusion may have contributed little towards the homogenisation process.

In the current work, it is considered that a principal function of the initial surface diffusion in compacts containing nickel as an elemental addition, is the creation of a much larger iron-nickel contact area than is provided by the original distribution of particles. This occurs at both 1150°C and 1300°C and provides the starting point for extensive volume diffusion throughout the compacts. Significant improvements in mechanical properties, especially tensile strength, are not observed until volume diffusion has proceeded to such

an extent that nickel-rich networks are no longer present and the microstructure appears to be uniform under the optical microscope.

Homogenisation has been considered^{89,158,159} to be governed by the equation,

$$c(x,t) = c_o + c_m \cos (\pi x/l) \exp (-\pi^2 Dt/l^2) \quad \text{in which}$$

$c(x,t)$ = concentration at a point along the x axis after time t ,

c_o = final concentration,

c_m = maximum variation of concentration from the final concentration,

l = distance along the x axis

and D = a constant diffusion coefficient.

From this equation, the controlling factor in homogenisation is $\exp (-\pi^2 Dt/l^2)$ or $\exp (-t/\tau)$ in which $\tau = l^2 / \pi^2 D$ = the relaxation time.

The empirical equations governing the progress of homogenisation in the current work are of the form

$$H_t = A \exp (-kt) + H_r \quad \text{in which}$$

H_t = the degree of homogenisation after time t
(in minutes)

H_r = the residual heterogeneity after infinite time

and A and k = empirical constants.

In die-pressed and isostatically-pressed blended materials and in plated materials, the ratios of the values of "k" for compacts sintered at 1300°C to those for compacts sintered at 1150°C were 1.13, 1.42 and 1.73 respectively. If homogenisation is considered to be due to a single diffusion mechanism and the interdiffusion coefficient is assumed to remain constant

at each sintering temperature (as in the theoretical equation above), the relaxation time at 1300°C would be approximately nine times that at 1150°C. Since the above ratios of "k" are all less than 2, it would appear that homogenisation in these materials is more complex than could be accounted for by a simple diffusion model which incorporates a single diffusion mechanism. The present metallographic observations of a complex mechanism that involves both surface and volume diffusion support this view.

Nevertheless, Heckel¹⁶¹ treated the process in copper-nickel compacts as one which could be best represented by the concentric sphere model¹⁰³; this model is based upon the assumption that uniform spherical particles of the minor component are embedded in the major component to form a three-dimensional grid with a uniform interparticle distance. The model ignores the effect of porosity and involves a constant interdiffusion coefficient. This model predicted considerably greater rates of homogenisation than were observed experimentally during the later stages of the process. A major reason for this anomaly was given as an increase in the effective diffusion distance as sintering continued; since the smaller and more closely spaced solute-rich areas were consumed early in the homogenisation process, the later stages were governed by the increasing distance between the remaining larger agglomerates. Since the model did not take the effect of porosity into account, any effects in the experimental compacts due to surface diffusion are ignored in the theoretical treatment. In fact, the rate of homogenisation decreased as the amount of porosity in the unsintered compacts increased. This

departure of experimental behaviour from that predicted by the concentric sphere model was also reported by Terchek and Hirschhorn¹⁵⁵; these authors found that the nickel agglomerate size needed to correct the predicted behaviour was much greater than that actually measured in a 5% nickel steel. Thus, it is clear that current models are unable to fully account for the progress of homogenisation which is observed in real compacts.

7. CONCLUSIONS

1. Certain of the experimental techniques employed in this work may prove to be of use in future investigations; the major points concerning these techniques are given below.

(a) By means of an electron probe micro-analyser, a technique has been introduced by which the degree of heterogeneity may be quantitatively measured in sintered compacts.

(b) A technique has been developed whereby each particle in a batch of iron powder may be uniformly plated in nickel. This process is potentially capable of much greater development and work by other investigators is currently in progress with this objective.

(c) The insensitivity of these porous materials to the stresses imposed by quenching has allowed compacts to be quenched directly from the sintering temperature into cold water. Since the sintering treatment did not promote excessive grain growth and the subsequent quenching treatment did not induce cracking in the compacts, the conventional hardening treatment was not used during the present work. Further work would be required to determine the general feasibility of this procedure in commercial practice.

2. Over the limited range of porosity examined (8.7% to 18%), the equation $\sigma_s = \sigma_o (1 - F P)$ has been found to predict tensile strength more accurately than other published equations, provided that the alloys concerned possessed homogenisation parameters (H) below 0.45. The values of the stress concentration factor (F) in this equation were determined empirically and were found to be dependent upon sintering time and

temperature rather than powder type or the level of porosity. The most homogeneous materials consisted, after quenching, of a fully martensitic structure of the lath type. However, some of the materials that were slightly less homogeneous contained isolated regions of acicular martensite, bainite and ferrite. Provided that the associated values of the homogenisation parameter were less than 0.45, the presence of these constituents was not detrimental to tensile strength.

3. In alloys of low homogeneity ($H > 0.45$), the actual tensile strengths were invariably significantly lower than the values predicted by the above equation. These poor tensile strength values were mainly associated with the presence of austenite in the microstructure. The distribution of this phase is very significant since an inter particle network, especially one that is thin and continuous as in plated alloys, is particularly detrimental to tensile strength.

4. The tensile strength of pre-alloyed material was found to be insensitive to variations in sintering temperature in compacts sintered for one hour within the range of 1000°C to 1300°C . This behaviour, which was not characteristic of plated and blended materials, was evidently associated with the inherently high degree of homogeneity of this material and the resultant uniformity in microstructure.

5. The impact fractures of blended, plated and pre-alloyed materials were clearly ductile in nature despite the associated low values of impact strength. This investigation indicates that the changes in pore shape and distribution that accompany the sintering process are mainly responsible

for improvements in this property rather than the micro-structural changes which result from the process of homogenisation.

6. An approximately linear relationship exists between hardness and porosity provided that the material possesses a homogenisation parameter below 0.45. No relationship between these properties could be detected in the more heterogeneous materials.

7. It has been suggested that theoretical models proposed in the literature do not fully account for the progress of the homogenisation process which is observed in real compacts. The following conclusions are based upon the present metallographic observations which support the view that homogenisation in the iron:nickel:carbon materials investigated takes place by a complex mechanism that involves both surface and volume interdiffusion.

(a) In blended material, surface diffusion made a significant contribution to the early stages of the homogenisation process. The later stages of the process were considered to be controlled by volume and grain boundary diffusion.

(b) The nickel-plating operation produced material in which extensive volume interdiffusion of iron and nickel could occur at the start of the sintering treatment; this resulted in rapid homogenisation and the rapid development of a microstructure that was beneficial to mechanical properties.

REFERENCES

1. Schwarzkopf, P., Powder Met., 1961, 1, Ed. Leszynski, W. Interscience.
2. P.M. for High Performance Applications, 1972, Ed. Burke, J.J. & Weiss, V., Syracuse Univ. Press.
3. Lawley, *ibid*, 3.
4. Arbstedt, P.G., Metals Technology, May-June, 1976, 214.
5. Dixon, R.H.T. & Clayton, A. Powder Met. for Engineers, 1971, 53, Machinery.
6. Lennox, J.W., News from the B.M.S.A., No. 9981/B, 27/4/72
7. Nickel Alloy Steels, Mond Nickel Co. Ltd.,
8. Duckworth, W.E., Metals & Materials, Met. Review 128, Nov. 1968, 145.
9. Gilbert, A. & Owen, W.S., Acta Met., Jan. 1962, 10, 45.
10. Winchell, P.G. & Cohen, M., Trans. ASM, 1962, 55, 347.
11. Pickering, F.B. & Gladman, T., I.S.I. Special Report 81, 1963, 10.
12. Owen, W.S., Proc. 2nd Int. Symp. on Materials, Univ. of Calif., June 1964.
13. Hall, A.M., Nickel in Iron and Steel, 1954, 89, J. Wiley & Sons.
14. Swanson, W.D. & Parr, J.G., J.I.S.I., Feb. 1964, 202, 104.
15. Marder, A.R. & Krauss, G., Trans. A.S.M., 1969, 62, 957.
16. Bell, T., Martensite, 1970, 65, Ed. Petty, E.R., Longman.
17. Zackay, V.F., Justusson, M.W. & Schmatz, D.J., Strengthening Mechanisms in Solids, A.S.M., 1960, 179.
18. Kelly, P.M. & Nutting, J., I.S.I. Special Report 93, 1965, 166.
19. Steven, W. & Haynes, A., J.I.S.I., 1956, 183, 349.
20. Atlas of I.T. Diagrams, I.S.I. Special Report 40, 1949, 33.
21. Pickering, F.B., Transformation & Hardenability in Steels, Feb. 1967, 109, Climax Molybdenum.
22. Bain, E.C. & Paxton, H.W., Alloying Elements in Steel, A.S.M., 1961.

23. Ohmori, Y., Trans. I.S.I. Japan, 1971, 11, 95.
24. Ohmori, Y., Ohtani, H. & Kunitake, T., *ibid*, 1971, 11, 250.
25. Oblak, J.M. & Hehemann, R.F., Ref. 21, 15.
26. Troiano, A.R., Trans. A.S.M., 1949, 41, 1093.
27. Kinsman, K.R. & Aaronson, H.I., Written discussion of Ref. 25, 33.
28. B.S.C. Data Sheets on General Engineering Alloy Steels, River Don Works, Sheffield.
29. Janitsky, E.J. & Baeyertz, M., Metals Handbook, A.S.M., 1939, 515.
30. Irvine, K.J., J.I.S.I., June 1969, 207, 6, 837.
31. Krishnamoorthy, G.M., Powder Met., 1971, 14, 27, 164.
32. Hulthen, S.I., Powder Met., 1970, 13, 26, 234.
33. Esper, F.J., Exner, H.E. & Metzler, H., Powder Met., 1975, 18, 35, 107.
34. Lenel, F.V., Ansell, G.S. & Strife, J.R., Mod. Dev. in P.M., 1974, 6, 275, Plenum Press.
35. Lindskog, P., Hulthen, S., 2nd Eur. P.M. Symp. 1968, 17.
36. Zapf, G., Powder Met., 1970, 13, 26, 130.
37. Gummeson, P.U., Perspectives in Powder Met., 1968, 3, 304, Plenum Press.
38. Dautzenberg, N. Powder Met. Int., May, 1971, 3, 2, 67.
39. Chadwick, R., Broadfield, E.R., I.S.I. Special Report 38, 1947, 123.
40. Cundill, R.T., Marsh, E. & Ridal, K.A., Powder Met., 1970, 13, 26, 165.
41. Wastenson, G., Powder Met. 1975, 18, 35, 124.
42. Fischer, J.J., Mod. Dev. in Powder Met., (Ed. Hausner, H.H.), 1974, Vol. 8, 75, Plenum Press.
43. Judd, J.A., Ref. 39, 117.
44. Burr, D.J., & Krishnamoorthy, G.M., Tech. Pub. P.B.L. 173, Int. Nickel, Ltd.,
45. Delisle, L. & Knopp, W.V., Am. Inst. Min. Met. Engrs. Tech. Pub. 2340, 1948.

46. Kravic, A.F., & Gloor, A.B., Powder Met., 1966, 9, 18, 185.
47. Svensson, L.E., Powder Met., 1974, 17, 34, 271.
48. Smart, R.F., Developments in Powder Met. 1973, Mills and Boon Ltd.,
49. Wilsden, S.C., Ridout, P.J., I.S.I. Special Report 58, 1956.
50. Lindskog, P., & Skoglund, G., 3rd Eur. P.M. Symp., Nov. 1971, Conf. Suppl. Pt. 1, 375.
51. Jones, W.D., Fund. Prin. of Powder Met., 1960, 428, W. Clowes & Sons.
52. Adler, A. Materials Engineering, March, 1968, 32.
53. Eloff, P.C. & Kaufman, S.M., Powder Met. Int., May, 1971, 3, 2, 71.
54. Lindskog, P., Powder Met., 1970, 13, 26, 280.
55. Davy-Loewy Ltd., Pub. No. DL/9/575.
56. Watkinson, J.F., Powder Met., 1958, 1/2, 13.
57. Fishman, B.D., Silaev, A.F., Tolstogusov, N.V. & Valov, M.E., Sov. Met. and Metal Ceramics, June 1974, 13, 6, 138, 439.
58. Kapustin, E.A., Maslov, V.A., Kulakov, A.M., Yurenko, A.S. & Sadovskii, G.M., Sov. Met. & Metal Ceramics, June 1974, 13, 6, 138, 447.
59. Martyukhin, I.D., Protective Coatings of Metals, 1971, 3, 117.
60. Dovzhenko, L.D., Borisov, V.T., Radomyselskii, I.D., Protective Coatings of Metals, 1973, 5, 48.
61. Burkin, A.R., Metallurgical Review 111, 1967, 12, 1.
62. Meddings, B., Lund, J.A., Mackiw, V.N., Canadian Min. & Met. Bull, July 1963, 525.
63. R. & D. Division, Sherritt-Gordon Mines Ltd., Fort. Sask. Alberta, Canada. Powder Met., 1958, 1/2, 40.
64. Meddings, B., Kunda, W., Mackiw, V.N., Ref. 1, 775.
65. Brenner, A., Modern Electroplating (Ed. Lowenheim F.A.) 1963, 698, J. Wiley & Sons.
66. Rao, B.V., Rao, Y.V., Saha, R.L., Acharyulu, S.L.N., Menon, U.G.K., Tamhankar, R.V., Trans. Indian Inst. Metals, Feb. 1973, 26, 1.

67. Rigg, T. Unpublished report, 11/11/75.
68. Pinner, W.L., Knapp, B.B., & Diggin, M.B., Modern Electroplating (Ed. Lowenheim, F.A.), 1963, 260, John Wiley & Sons.
69. Salt, F.W., Chem. Eng. in I. & S. Industry, Symposium, March, 1968, 169.
70. Marshall, P.R., Metals & Materials, Met. Review 123, June 1968, 53.
71. Tracey, V.A. Powder Met. 1966, 9, 17, 54.
72. Walker E.V., Worn, D.K. & Walters, R.E.S., Symposium on Powder Met., 1954, I.S.I. Special Report 58, 1956, 204.
73. Dixon, R.H.T., & Clayton, A., Ref. 5, 10.
74. Geijer, E., Jamison, R.S., Ref. 1, 585.
75. Yarnton, D., & Davies, T.J., Metallurgia, Oct. 1962, 153.
76. Yarnton, D., & Davies, T.J., Powder Met., 1963, 11, 1.
77. Leopold, P.M., & Nelson, R.C., International J. Powder Met., 1965, 1, 3, 37.
78. Goetzel, C.G., Treatise on Powder Met., 1949, Vol. 1, Chap. VIII.
79. Munro, P.M., Powder Met. Int., Feb. 1972, 4, 1, 20.
80. Unckel, H., Ref. 78, 280.
81. Van Buren, C.E. & Hirsch, H.H., Persp. in Powder Met., 1967, Vol. 1, Chap. 3, Plenum Press.
82. Jackson, H.C., ibid., Chap. 2.
83. Morgan, W.R. & Sands, R.L., Metals & Materials, Met. Review 134, May, 1969, 85.
84. James, P.J., Production Engineer, Dec. 1971, 515.
85. Sellors, R.G.R., Powder Met., 1970, 13, 26, 85.
86. Thummler, F. & Thomma, W., Metals & Materials, Met. Review 115, June 1967, 69.
87. DeHoff, R.T. & Aigeltinger, E.H., Persp. in Powder Met. (Ed. Roll, K.H. & Hausner, H.H.), 1970, Vol. 5, 81.
88. Moon, J.R., Powder Met. Int. 1971, 3, 3, 147.
89. Moon, J.R., ibid., 3, 4, 194.

90. DeHoff, R.T., Rummel, R.A., Rhines, F.T., & Long, A.H.
Ref. 1., 31.
91. Kuczynski, G.C., Ref. 2, 101.
92. Kuczynski, G.C., Trans. A.I.M.E., 1949, 185, 169.
93. Rhines, F.N., Proc. Metal Powder Ass. 1958, 91.
94. Kuczynski, G.C., Ref. 1, 11.
95. Stone, H.E.N., Metallurgia, Oct. 1966, 151.
96. Alexander, B.H., Baluffi, R.W., Acta Met., 1957, 5, 666.
97. Stablein, P. & Kuczynski, G.C., Acta Met., 1963, 11, 1327.
98. Pranatis, A.L., & Seigle, L., Ref. 1, 53.
99. Lenel, F.V., Fundamental Phenomena in the Materials
Sciences, (Ed. Bonis, L.J. & Hausner, H.H.), 1964,
Vol. 1, 3, Plenum Press.
100. Lenel, F.V., Ref. 2, 119.
101. Kuczynski, G.C., Matsumura, G. & Cullity, B.D., Acta Met.
1960, 8, 209.
102. Fisher, B., & Rudman, P.S., Acta Met., 1962, 10, 37.
103. Fisher, B., & Rudman, P.S., J. Appl. Physics, Aug. 1961,
32, 8, 1604.
104. Smith, D.W. & Hehemann, R.F., Trans. Met. Soc. A.I.M.E.,
1966, 236, 506.
105. B.S.A., Iron and Steel, Apr. 1970, 43, 2, 90.
106. Harrison, L., Dixon, R.H.T., Powder Met., 1962, 9, 247.
107. Heath, P.J. & Evans, P.E., J. Mat. Sci. Dec. 1964., 9,
12, 1955.
108. Coult, I.M. & Munro, A.J.E., Powder Met., 1970, 13, 26,
295.
109. Kaufman, S.M., Powder Met. Int., Feb. 1973, 5, 1, 11.
110. Yarnton, D. & Argyle, M., Practical Course in Powder Met.
1962, 18, Cassell.
111. Holcomb, R.T. & Lovenduski, J., Mod. Dev. in Powder Met.
(Ed. Hausner, H.H.), 1974, Vol. 8, 85, Plenum Press.
112. Brown, G.T., Powder Met., 1974, 17, 33, 103.
113. Fedorov, R.I., Tsyarkin, A.T., Samoilov, V.A. & Nosenko,
A.S., Sov. Powder Met. & Metal Ceramics, Aug. 1972
11, 8, 651.

114. Dixon, R.H.T. & Clayton, A. Ref. 5, 65.
115. P/M Nickel Steels Data Book, Aug. 1966, Int. Nickel Ltd.
116. B.S. 18, British Standards Institution, 1971, Part 2.
117. McAdam, G.D., J.I.S.I., 1958, 168, 4, 346.
118. Goetzel, C.G., Wire and Wire Products, 1943, 18.
119. Squire, A. Trans. A.I.M.E., Tech. Pub., No. 2165, 1947.
120. Eudier, M.A., Powder Met. 1962, 9, 278.
121. Gessinger, G.H., Metzler, H., Esper, F., & Exner, H.E.
3rd Eur. Powder Met. Symp. 1971, 289.
122. Pines, B.J., & Suchinin, H.I., Zhur Tekhn. Fiziki, 1956,
2076.
123. Haynes, R. Powder Met., 1971, 14, 27, 64.
124. Haynes, R. *ibid.*, 14, 27, 71.
125. Eudier, M.A., Ref. 1, 137.
126. MacKenzie, J.K., Proc. Phys. Soc., 1950, B. 1, 63, 2.
127. Nazare, S., & Ondracek, G. Powder Met. Int., Feb. 1974.
6, 1, 8.
128. Gallina, V. & Mannone, G., Powder Met., 1968, 11, 21, 73.
129. Green, R.J., Int. J. Mech. Sci. 1972, 14, 225.
130. Pohl, D. Europ. Symp. uber Pulvermetallurgie, Stuttgart
1968, Band 11, Bericht Nr. 6, 7 und Arch. Eisen-
huttw., demnachst.
131. Artusio, G., Gallina, V, Mannone, G., Sgambetterra, E.
Powder Met., 1966, 9, 17, 89.
132. Gent, F., Private discussion.
133. Napara-Volgina, S.G., Radomyselskii, I.D. & Gorb, M.L.
Sov. Powder Met., & Metal Ceramics, Dec. 1973,
12, 12, 960.
134. Shcherban, N.I., Sov. Powder Met. & Metal Ceramics,
Oct. 1973, 12, 10, 834.
135. Salak, A., Miskovic, V., Dudrova, E., & Rudnayova, E.,
Powder Met. Int., Aug. 1974, 6, 3, 128.
136. Modry, S., *ibid.*, ref. 36.
137. Esper, F.J., Exner, H.E. & Metzler, H., Powder Met., 1975,
18, 35, 107.

138. Brockelman, R.H., Persp. in Powder Met. (Ed. Hirschhorn, J.S., & Roll, K.H.), 1970, 201, Plenum Press.
139. Talmage, R., Proc. 17th Meeting of Metal Powder Ind. Fed. 1961, Cleveland, 168,
140. Buckle, H., Ref. 1, 221.
141. Hardy, C., Steel, 1934, 95, 21, 52.
142. Stern, G. A.I.M.E., Tech. Pub. No. 2045, 1946.
143. Fraser, R.W. & Evans, D.J.I., Powder Met., 1968, 11, 358.
144. Rhines, F.N. & Colton, Powder Met. (Ed. Wulff, J.), 1942, A.S.M., Chap. 6, 67.
145. Rhines, F.N. & Meussner, R.A., Symp. of Powder Met., 1943, A.S.T.M. 25.
146. Heck, F.W., Mod. Dev. in Powder Met. (Ed. Hausner, H.H.) 1971, Vol. 5, Plenum Press.
147. Fischer, J.J. & Heck, F.W., Mod. Dev. in Powder Met., (Ed. Hausner, H.H.), 1971, Vol. 5, 478.
148. Grimshaw, R.W., The Chem. & Phys. of Clays & other Ceramic Materials, 1971, Chap. XIV, Ernest Benn Ltd.
149. Clements, J.F., Trans. Brit. Ceramic Soc., Aug. 1966, 65, 479.
150. Birchenall, C.E., Atom Movements, 1951, A.S.M. Cleveland, 122.
151. Shewmon, P.G., Transformations in Metals, 1969, 37, McGraw-Hill.
152. Guy, A.G., Elements of Physical Metallurgy, 1959, Addison-Wesley Pub. Co.
153. Marchukova, I.D., Diffusion Processes in Metals (Ed. Svechnikov, V.N.), 1970, 49, Israel Program for Scientific Translations.
154. Terchek, R.L. & Hirschhorn, J.S., 3rd Eur. Powder Met. Symp. 1971, 9.
155. Terchek, R.L. & Hirschhorn, J.S., Mod. Dev. in Powder Met., 1974, 8, 109.
156. Badia, F.A., Heck, F.W. & Tundermann, J.H., *ibid.*, 7, 255.
157. Shewmon, P.G., Diffusion in Solids, 1963, McGraw-Hill.
158. Shewmon, P.G., Physical Metallurgy, Ed. Cahn, R.W., 1970, 383, North Holland Pub. Co.

159. Lavender, J.D. & Jones, F.W., J.I.S.I., 1950, 163, 1, 14.
160. Rudman, P.S., Acta Cryst. 13, 1960, 905.
161. Heckel, R.W., Trans. A.S.M., 1964, 57, 443.
162. Heckel, R.W., Lanam, R.D. & Tanzilli, R.A., Persp. in Powder Met., 1970, Vol. 5, 139.
163. Schwarzkopf, P., Powder Metallurgy, 1947, MacMillan.
164. Howatt, D.D., Craik, R.L. & Cranston, J.P., J.I.M., 1951-52, 80, 353.
165. Leber, S., & Hehemann, R.F., Trans. Met. Soc. A.I.M.E., 1964, 230, 100.
166. Duckett, R. & Robins, D.A., Metallurgia, Oct. 1966, 163.
167. Itin, V.I., Kozlov, I.U., Bykonya, A.F., Pugina, L.I., Yurchenko, A.G., Savitskii, K.V., & Fedorchenko, I.M. Sov. Powder Met. & Metal Ceramics, Nov. 1971, 10, 11, 862.
168. Wolff, U.E., Trans. A.S.M., 1962, 55, 363.
169. Spiegel, M.R., Statistics, 1972, McGraw-Hill.
170. DeHoff, R.T., Quantitative Microscopy, Ed. DeHoff, R.T. & Rhines, F.N., 1968, 11, McGraw-Hill.
171. Hilliard, J.E., *ibid.*, 45.
172. Modin, H. & Modin, S. Metallurgical Microscopy, 1973. Butterworths.
173. Pickering, F.B., The Basis of Quantitative Metallography, 1976, Inst. of Met. Tech. Monograph, No. 1.
174. Ranzetta, G.V.T. & Scott, V.D., Physical and Fabrication Metallurgy (Ed. Jones, M.J.), 1970, Inst. of Min. & Met. London.
175. Poole, D.M. & Martin, P.M., Metals & Materials, Met. Review 133, Apr. 1969, 61.
176. Martin, P.M. & Poole, D.M., Metals & Materials, Met. Review 150, Mar. 1971, 19.

TABLE 1

MECHANICAL PROPERTIES OF WROUGHT STEELS

%C	%Mn	%Ni	Quench Temp. °C	Temp- ering Temp. °C	Sec- tion Size mm	UTS MN/ m ²	%E1	%RA	Izod J	H _B	Ref.
0.32	0.60	3.15	820 OQ	---	28.5	1670	9	22	13	480	7
0.33	0.57	3.18	830 OQ	600	28.5	838	19	65	107	250	"
0.31	0.50	3.00	830 OQ	640	38.1	756	17.5	--	110	266	"
0.34	0.60	3.32	850 OQ	580	28.5	871	16	63	82	---	"
0.41	0.70	3.36	775 WQ	640	50	758	19	62	--	230	13
0.30	0.58	2.92	850 OQ	610	13	809	20	65	119	---	28
0.28	0.60	2.96	850 OQ	600	54	741	20	59	99	---	"
0.32	0.59	3.06	850 OQ	640	25	812	18.5	64	116	---	"

TABLE 2.

MECHANICAL PROPERTIES OF SINTERED STEELS (BLENDED)

%C	%Mn	%Ni	%Mo	Sin- ter- ing Temp °C	Sin- ter- ing Time Hours	% Theor. Density	UTS MN/ m ²	%E1	Un- not- ched Charpy J	Ref.
0.38	-	-	-	1100	1.5	90.7	400	5.7	-	45
0.5	-	2	-	1320	1	87	405	9	22	46
0.3	-	3	-	1120	1	89	370	4	-	47
0.46	-	3.5	-	1100	1.5	90.1	572	4.1	-	45
0.5	-	5	-	N.G.	N.G.	86.4	420	5	-	48
0.5	-	5	-	1320	1	87	466	7	26	46
0.4	1	3	1	1122	0.5	88	653	2.5	-	42
0.2	0.5	5	-	1300	1	88	450	9	-	49
0.5	-	5	0.5	1300	1	90	660	2.8	34	44

N.G. = not given

TABLE 3.

MECHANICAL PROPERTIES OF SINTERED AND HEAT
TREATED STEELS (BLENDED).

%C	%Ni	%Mo	Sint. Temp. °C	Quench. Temp. °C	Temp- ering Temp. °C	% Theo ret. Den- sity	U.T.S. MN/ m ²	%E1	Unnot- ched Charpy J	Ref.
0.4	-	-	N.G.	870	300	88.9	448	1	13	114
0.4	2	-	N.G.	870	300	88.9	695	1	24	114
0.4	1	-	1300	870	600	89	392	3.9	-	79
0.4	3	-	1300	870	600	89	442	2.8	-	79
0.4	5	-	1300	870	600	89	503	5.6	-	79
0.44	4	-	N.G.	870	650	88.9	386	4	24	115
0.5	5	-	1320	875	600	86.4	633	8	27	46
0.49	5	0.5	1300	870	650	90.2	740	3.6	55	44

N.G. = not given.

TABLE 4.

COMPOSITION OF ELECTROLYTE

Constituent		Weight g/litre
Nickel Sulphate.	$\text{NiSO}_4 \cdot 7\text{H}_2\text{O}$	150
Ammonium Chloride.	NH_4Cl	30
Boric Acid.	H_3BO_3	30

TABLE 5.

MEAN PARTICLE SIZES AND CHEMICAL ANALYSES OF RAW MATERIALS

Material	Size μm	Carbon %	Nickel %	Oxygen %
Natural graphite	2.9	46.0	-	-
Synthetic graphite	3.8	95.5	-	-
Carbonyl nickel	3.7	-	98.30	-
Electrolytic iron (-200 mesh)	18.0	-	-	-
Nickel plated iron	-	-	2.99	-
Atomised nickel-iron (-100 mesh)	-	-	2.99	-
Blended powder compact	-	-	-	0.195
Plated powder compact	-	-	-	0.225
Atomised powder compact	-	-	-	0.243

TABLE 6.

SIEVE ANALYSES OF -200 MESH ELECTROLYTIC IRON AND -100 MESH
ATOMISED 3% NICKEL-97%IRON POWDERS

Particle Size		Electrolytic Powder		Atomised Powder	
B.S. Mesh	Aperture μm	Fraction %	Cumul- ative %	Fraction %	Cumul- ative %
+100	+152	0.00	0.00	0.04	0.04
+150	+104	0.07	0.07	10.96	11.00
+200	+ 76	7.40	7.47	19.05	30.05
+240	+ 66	12.90	20.37	2.19	32.24
+300	+ 53	24.10	44.47	14.88	47.12
-300	- 53	55.30	99.77	52.78	99.90

TABLE 7.

EFFECT OF LUBRICANT ON SINTERED DENSITY

Material	Lubricant	% Theoretical Density
-240 mesh iron only	None	82.6
-240 mesh iron only + 1% nat. graphite	0.5% zinc stearate admixed	87.3
" " "	Stearic acid to die wall	86.1
" " "	Zinc stearate to die wall	86.5
-200 mesh iron + 0.5% syn. graphite.	Zinc stearate/ ether to die wall	88.5
" " "	Zinc stearate/ acetone to die wall	88.5

TABLE 8.

DENSITY CHANGES IN IRON-1% NATURAL GRAPHITE
ALLOYS

Green Density % Theoretical	Sintered Density % Theoretical	Actual Increase	% Increase
84.0	85.9	1.9	2.3
83.0	85.3	2.3	2.7
83.5	85.5	2.0	2.4
84.1	86.5	2.4	2.8

TABLE 9.

DENSITY CHANGES IN IRON-0.5% SYNTHETIC
GRAPHITE ALLOYS

Green Density % Theoretical	Sintered Density % Theoretical	Actual Change	% Change
88.8	88.7	-0.1	-0.1
88.9	88.3	-0.6	-0.7
88.8	88.7	-0.1	-0.1
88.7	88.7	0	0
88.0	88.0	0	0
88.3	88.5	+0.2	+0.2

TABLE 10.

HARDNESS OF IRON-0.5% GRAPHITE ALLOYS

Graphite type	30kg	5kg	1kg	0.20kg	0.10kg	0.02kg	0.01kg
Natural	163	166	167	166	170	257	290
Synthetic	278	280	293	441	530	614	736

TABLE 11.

HARDNESS OF IRON-1%NICKEL - 0.5% SYNTHETIC
GRAPHITE ALLOYS.

Compact Number	30kg	5kg	1kg	0.20kg	0.10kg	0.02kg	0.01kg
1	339	348	427	473	573	580	613
2	348	356	354	457	483	540	613

TABLE 12.

PROPERTIES OF 3% NICKEL ALLOYS, DIE PRESSED.

Sintering Temperature °C	Sintering Time (hours)	Mean Green Density %	Sintered Density %	\overline{HD}
1150	0.1	87.7	87.7	73
"	0.5	"	87.6	279
"	1	"	88.4	311
"	2.5	"	89.3	344
"	6	"	89.9	373
1300	0.25	88.2	88.1	277
"	0.5	"	88.3	336
"	1	"	88.8	346
"	2.5	"	89.5	373
"	6	"	90.1	420

TABLE 13

X-RAY DIFFRACTION DATA

Material	Sintering Conditions		FCC {111}		FCC {200}		BCC {110}		
	Temp °C	Time mins	2θ°	dÅ	2θ°	dÅ	2θ°	dA°	Relative Width
Nickel			52.21	2.034	61.05	1.762			
89.6%Ni:Fe			51.99	2.042	60.82	1.768			
79.4%Ni:Fe			51.80	2.049	60.60	1.774			
69%Ni:Fe			51.61	2.056	60.33	1.781			
58.8%Ni:Fe			51.40	2.064	60.07	1.788			
48.2%Ni:Fe			51.24	2.070	59.89	1.793			
39.2%Ni:Fe			51.08	2.076	59.70	1.798			
24.8%Ni:Fe			51.42	2.063	60.15	1.786			
Austenite			50.98	2.080	59.64	1.800			
Ferrite							52.42	2.027	
Blended and Die-pressed	-	-	Over-lap	-	61.10	1.761	52.40	2.027	1.00
"	1150	15	51.50	2.060	59.80/ 60.30	1.782/ 1.796	52.50	2.023	1.68
"	1150	30	Over-lap	-	60.00	1.790	52.40	2.027	2.25
"	1300	15	51.35	2.066	60.00	1.790	52.40	2.027	1.68
Blended and iso-statically pressed	1150	15	51.15	2.073	59.75	1.797	52.35	2.029	1.36
"	1300	15	Over-lap	-	59.70	1.798	52.45	2.025	1.31
Plated	1150	15	51.60	2.057	N.D.	-	52.60	2.020	1.05

N.D. = NOT DETECTABLE.

NOTE: Data in the top section is taken from the Powder Diffraction file of the ASTM.

TABLE 14.AREAL ANALYSIS DATA

Function	Magnification		
	1200x	2400x	4800x
Mean % Nickel \bar{X}	3.80	4.09	4.20
Variance σ^2	2.84	5.43	7.61
Standard error σ/\sqrt{N}	0.38	0.52	0.62
Min. % Nickel	1.53	0.94	0.86
Max. % Nickel	8.11	10.75	13.14

TABLE 15.

DATA PERTAINING TO FIG. 27.

Position	HD 5kg	% Nickel	Position	HD 5kg	% Nickel
1	64	2.48	14	49	2.91
2	59		15	54	
3	63		16	54	
4	60	2.86	17	55	3.34
5	63		18	58	
6	59		19	55	
7	72	3.38	20	62	
8	66		21	72	
9	69		22	76	3.30
10	64	2.71	23	84	
11	59		24	84	
12	43		25	60	3.24
13	47	2.49			

TABLE 16.

PROPERTIES OF 3% NICKEL BLENDED AND ISOSTATICALLY
PRESSED COMPACTS SINTERED AT 1150°C.

Treat- ment	Sint- ering Time Hours	% Theor- etical Density	% Porosity	UTS MN/ m ²	%E1	Un- notched Impact Strength J	\overline{HD}
WQ	0.25	88.2	11.8				164
T				310	0.9	3	109
WQ	0.50	88.4	11.6				183
T				330	2.0	6	115
WQ	1	88.9	11.1				255
T				380	0.9	10	127
WQ	2	88.7	11.3				250
T				390	2.0	16	129
WQ	4	89.7	10.3				252
T				425	4.1	14	132
WQ	8	90.5	9.5				227
T				460	3.9	17	162

WQ = Water quenched

T = Tempered

TABLE 17.

PROPERTIES OF 3% NICKEL BLENDED AND ISOSTATICALLY
PRESSED COMPACTS SINTERED AT 1300°C.

Treat- ment	Sint- ering Time Hours	% Theor- etical Density	% Porosity	UTS MN/ m ²	%E1	\overline{HD}
WQ	0.25	89.2	10.8			215
T				465	0.0	127
WQ	0.50	89.8	10.2			207
T				445	1.0	143
WQ	1	89.6	10.4			262
T				498	4.2	139
WQ	2	90.3	9.7			332
T				470	1.0	166
WQ	4	91.3	8.7			357
T				540	4.5	169
WQ	8	90.9	9.1			380
T				560	5.2	171

WQ = Water quenched

T = Tempered

TABLE 18.

PROPERTIES OF 3% NICKEL BLENDED AND ISOSTATICALLY
PRESSED COMPACTS SINTERED FOR ONE HOUR.

Treat- ment	Sint- ering Temp. °C	% Theor- etical Density	% Porosity	UTS MN/ m ²	%E1	\bar{HD}
WQ	1000	88.1	11.9			318
T				273	1.2	96
WQ	1075	88.6	11.4			312
T				320	3.8	127
WQ	1150	88.9	11.1			255
T				380	0.9	127
WQ	1225	89.0	11.0			327
T				394	0.4	117
WQ	1300	89.6	10.4			262
T				498	4.2	139

WQ = Water quenched

T = Tempered

TABLE 19.

DETAILS OF NICKEL PLATED COMPACT.

Mass of Powder kg	Nickel %	Carbon %	Iron %
0.424	2.84%	-	97.16%
0.385	3.12%	-	96.88%
0.439	2.78%	-	97.22%
0.384	2.78%	-	97.22%
0.358	3.59%	-	96.41%
0.010	-	95.5%	-
2	2.99%	0.48%	96.51%

TABLE 20.

PROPERTIES OF 3% NICKEL PLATED AND ISOSTATICALLY
PRESSED COMPACTS SINTERED AT 1150°C.

Treat- ment	Sint- ering Time Hours	% Theor- etical Density	% Porosity	UTS MN/ m ²	%E1	Un- notched Impact Strength J	\overline{HD}
WQ	0.25	84.2	15.8				196
T				251	0	2.2	115
WQ	0.50	84.9	15.1				268
T				287	0.9	5.0	110
WQ	1	85.2	14.8				261
T				370	0	3.9	125
WQ	2	85.8	14.2				290
T				446	1.9	7.5	131
WQ	4	86.2	13.8				305
T				470	2.7	8.7	135
WQ	8	86.4	13.6				304
T				483	2.3	8.7	132

WQ = Water quenched

T = Tempered

TABLE 21.

PROPERTIES OF 3% NICKEL PLATED AND ISOSTATICALLY
PRESSED COMPACTS SINTERED AT 1300°C.

Treat- ment	Sint- ering Time Hours	% Theor- etical Density	% Porosity	UTS MN/ m ²	%E1	\overline{HD}
WQ	0.25	85.2	14.8			286
T				462	0.7	126
WQ	0.50	85.8	14.2			334
T				480	0.9	122
WQ	1	87.0	13.0			310
T				460	3.8	135
WQ	2	86.8	13.2			338
T				500	2.2	136
WQ	4	87.9	12.1			309
T				528	3.9	124
WQ	8	90.0	10.0			345
T				550	6.1	144

WQ = Water quenched

T = Tempered

TABLE 22.

PROPERTIES OF 3% NICKEL PLATED AND ISOSTATICALLY
PRESSED COMPACTS SINTERED FOR ONE HOUR.

Treat- ment	Sint- ering Temp. °C	% Theor- etical Density	% Porosity	UTS MN/ m ²	%E1	HD
WQ	1000	84.2	15.8			181
T				96	0	110
WQ	1075	84.5	15.5			254
T				285	0	124
WQ	1150	85.2	14.8			261
T				370	0	125
WQ	1225	86.4	13.6			299
T				400	0.9	128
WQ	1300	87.0	13.0			310
T				460	3.8	135

WQ = Water quenched

T = Tempered

TABLE 23.

PROPERTIES OF PRE-ALLOYED AND ISOSTATICALLY
PRESSED COMPACTS SINTERED AT 1150°C.

Treat- ment	Sint- ering Time Hours	% Theor- etical Density	% Porosity	UTS MN/ m ²	%E1	Un- notched Impact Strength J	HD
WQ	0.25	82.0	18.0				239
T				337	2.4	3.1	104
WQ	0.5	82.4	17.6				264
T				349	1.5	4.5	109
WQ	1	82.7	17.3				290
T				360	2.4	6.3	106
WQ	2	82.9	17.1				283
T				399	2.2	7.5	124
WQ	4	83.6	16.4				294
T				433	3.7	5.8	129
WQ	8	84.4	15.6				300
T				464	2.9	11.4	127

WQ = Water quenched

T = Tempered

TABLE 24.

PROPERTIES OF PRE-ALLOYED AND ISOSTATICALLY
PRESSED COMPACTS SINTERED AT 1300°C.

Treat- ment	Sint- ering Time Hours	% Theor- etical Density	% Porosity	UTS MN/ m ²	%E1	\overline{HD}
WQ	0.25	82.2	17.8			265
T				401	4.3	111
WQ	0.50	83.1	16.9			277
T				399	2.5	113
WQ	1	83.6	16.4			306
T				419	1.6	125
WQ	2	85.0	15.0			332
T				465	3.0	125
WQ	4	85.8	14.2			352
T				484	2.7	138
WQ	8	86.5	13.5			340
T				491	3.5	136

WQ = Water quenched

T = Tempered

TABLE 25.

PROPERTIES OF PRE-ALLOYED AND ISOSTATICALLY
PRESSED COMPACTS SINTERED FOR ONE HOUR.

Treat- ment	Sint- ering Temp. °C	% Theor- etical Density	% Porosity	UTS MN/ m ²	%E1	\overline{HD}
WQ	1000	81.9	18.1			245
T				357	1.1	103
WQ	1075	82.2	17.8			252
T				363	1.0	102
WQ	1150	82.7	17.3			290
T				360	2.4	106
WQ	1225	83.2	16.8			286
T				389	2.0	114
WQ	1300	83.6	16.4			306
T				419	1.6	128

WQ = Water quenched

T = Tempered.

TABLE 26.

QUANTITATIVE METALLOGRAPHY DATA FOR 3% NICKEL
BLENDED MATERIAL.

Length of Traverse μm	Nickel particle traverse μm	Mean % Nickel	Number of effective Nickel particles	Mean Nickel particle intercept μm	Mean Nickel centre distance μm	Range of Nickel Particle intercepts μm
5000	138	2.76	19	7.26	241	1-19
5000	167	3.34	18	9.28	272	1-22
5000	112	2.24	16	7.00	287	1-32
5000	94	1.88	15	6.27	320	1-26
10000	184	1.84	24	7.67	392	1-20
10000	299	2.99	36	8.30	263	1-55
40000	994	2.49	128	7.76	295	1-55

TABLE 27.

QUANTITATIVE METALLOGRAPHY DATA FOR 3% NICKEL
PLATED MATERIAL.

Length of Traverse μm	Number of Grains Traversed	Mean Grain intercept μm	Range of Grain intercepts μm
498	26	19.15	2-75
492	27	18.22	1-56
509	26	19.58	4-52
526	38	13.84	2-44
2025	117	17.31	1-75

TABLE 28.

MICRO-ANALYSIS DATA FOR 3% NICKEL PRE-ALLOYED MATERIAL.

Sintering Temp. °C	Sintering Time Hours	Homogenisation Parameter H.
1150	0.25	0.11
"	0.50	0.04
"	1	0.03E
"	2	0.025E
"	4	0.02
"	8	0.01
1300	0.25	0.03
"	0.50	0.028E
"	1	0.027E
"	2	0.025
"	4	0.02
"	8	0.01

E = estimated by interpolation.

ESTIMATED TIME FOR THE PREPARATION OF THE REPORT

Homograph and Form	Time in Hours	Time in Days
0.11	0.25	1.00
0.08	0.20	"
0.07	1	"
0.06	2	"
0.05	4	"
0.04	8	"
0.03	0.25	1.00
0.028E	0.20	"
0.027E	1	"
0.025	2	"
0.02	4	"
0.01	8	"

E = estimated by interpolation.

TABLE 29.

EMPIRICAL STRESS CONCENTRATION FACTORS

Sintering Time Hours	F at 1150°C	F at 1300°C
0.25	3.45	3.00
0.50	3.20	2.95
1	3.05	2.90
2	3.00	2.80
4	2.80	2.75
8	2.75	2.70

TABLE 30.

COMPARISON OF THE MEAN DEVIATIONS OF PREDICTED TENSILE STRENGTH

Equation	Variable	Mean Deviation MN/m ²
$\sigma_s = 800 (1-FP)$	F(Table 29)	17.3
$\sigma_s = 800 (1-P/1+bP)$	b = 3	25.9
"	*b = 3.5	22.2
$\sigma_s = 800 (1-kP^{\frac{2}{3}})$	k = 1.21	74.4
"	*k = 1.6	23.4
$\sigma_s = 800 \exp (-kP)$	k = 0.043	31.0
"	*k = 0.039	20.3

* = improved predictions as described on p.120.

TABLE 31.

COMPARISON OF ACTUAL & PREDICTED TENSILE
STRENGTHS IN ALLOYS OF HIGH
HOMOGENEITY.

Compact Type	Sintering Temp. °C	Sintering Time Hours	σ_a MN/m ²	σ_p MN/m ²	σ_a/σ_p	H
Blended	1300	4	552	609	0.91	0.36
"	"	8	548	603	0.91	0.04
Plated	1150	2	445	459	0.97	0.33
"	"	4	470	491	0.96	0.18
"	"	8	483	501	0.96	0.10
"	1300	0.25	456	445	1.02	0.285
"	"	0.50	470	465	1.01	0.231
"	"	1	496	498	1.00	0.153
"	"	2	492	504	0.98	0.069
"	"	4	518	534	0.97	0.02
"	"	8	569	584	0.97	0.01
Pre-alloyed	1150	0.25	303	303	1.00	0.11
"	"	0.50	349	349	"	0.04
"	"	1	378	378	"	0.03
"	"	2	390	390	"	0.025
"	"	4	433	433	"	0.02
"	"	8	457	457	"	0.01
"	1300	0.25	373	373	"	0.03
"	"	0.50	401	401	"	0.028
"	"	1	420	420	"	0.027
"	"	2	464	464	"	0.025
"	"	4	488	488	"	0.02
"	"	8	508	508	"	0.01

KEY: σ_a = actual tensile strength from Figs. 87,88 and 89.

σ_p = predicted tensile strength using stress concentration factors in Table 29.

H = homogenisation parameter.

TABLE 32.

COMPARISON OF ACTUAL & PREDICTED TENSILE STRENGTHS IN ALLOYS OF LOW HOMOGENEITY.

Compact Type	Sintering Temp. °C	Sintering Time Hours	σ_a MN/m ²	σ_p MN/m ²	σ_a/σ_p	H
Blended	1150	0.25	310	474	0.65	10.03
"	"	0.5	340	503	0.68	9.06
"	"	1	385	529	0.73	7.43
"	"	2	370	529	0.70	5.12
"	"	4	430	569	0.76	2.78
"	"	8	460	591	0.78	1.52
"	1300	0.25	430	541	0.79	4.23
"	"	0.5	480	559	0.86	3.58
"	"	1	463	559	0.83	2.57
"	"	2	513	583	0.88	1.32
Plated	1150	0.25	220	364	0.60	0.68
"	"	0.5	330	413	0.80	0.61
"	"	1	370	439	0.84	0.49

KEY: As per Table 31.

TABLE 33.

EMPIRICAL CONSTANTS RELATING TO BLENDED
AND PLATED COMPACTS.

Material	Sintering Temperature °C	k	c
Blended	1150	0.125	0.20
"	1300	0.23	0.085
Plated	1150	3.40	-0.03
"	1300	1.25	-0.031

TABLE 34.

COMPARISON OF ACTUAL TENSILE STRENGTHS WITH
PREDICTED TENSILE STRENGTHS IN ALLOYS SINTERED
FOR ONE HOUR

Sintering Temperature °C	BLENDED		PLATED		PRE-ALLOYED	
	σ_a MN/m ²	σ_p MN/m ²	σ_a MN/m ²	σ_p MN/m ²	σ_a MN/m ²	σ_p MN/m ²
1000	273	505	96	408	357	351
1075	320	517	285	416	363	359
1150	380	529	370	439	360	378
1225	394	538	400	476	389	400
1300	498	559	460	498	419	420

KEY: σ_a = actual tensile strength
 σ_p = predicted tensile strength according to $\sigma_s = 800 (1-FP)$.

TABLE 35.

RELATIONSHIPS BETWEEN TENSILE DUCTILITY,
POROSITY AND HOMOGENISATION PARAMETER IN
ALLOYS SINTERED AT 1150°C and 1300°C.

Sintering Temp. °C	Sintering Time Hours	BLENDED			PLATED			PRE-ALLOYED		
		%El	% Porosity	H	%El	% Porosity	H	%El	% Porosity	H
1150	0.25	0.9	11.8	10.03	0.0	15.8	0.68	2.4	18.0	0.11
"	0.50	2.0	11.6	9.06	0.9	15.1	0.61	1.5	17.6	0.04
"	1	0.9	11.1	7.43	0.0	14.8	0.49	2.4	17.3	0.03
"	2	2.0	11.3	5.12	1.9	14.2	0.33	2.2	17.1	0.025
"	4	4.1	10.3	2.78	2.7	13.8	0.18	3.7	16.4	0.02
"	8	3.9	9.5	1.52	2.3	13.6	0.10	2.9	15.6	0.01
1300	0.25	0.0	10.8	4.23	0.7	14.8	0.285	4.3	17.8	0.03
"	0.50	1.0	10.2	3.58	0.9	14.2	0.231	2.5	16.9	0.028
"	1	4.2	10.4	2.57	3.8	13.0	0.153	1.6	16.4	0.027
"	2	1.0	9.7	1.32	2.2	13.2	0.069	3.0	15.0	0.025
"	4	4.5	8.7	0.36	3.9	12.1	0.020	2.7	14.2	0.02
"	8	5.2	9.1	0.04	6.1	10.0	0.010	3.5	13.5	0.01

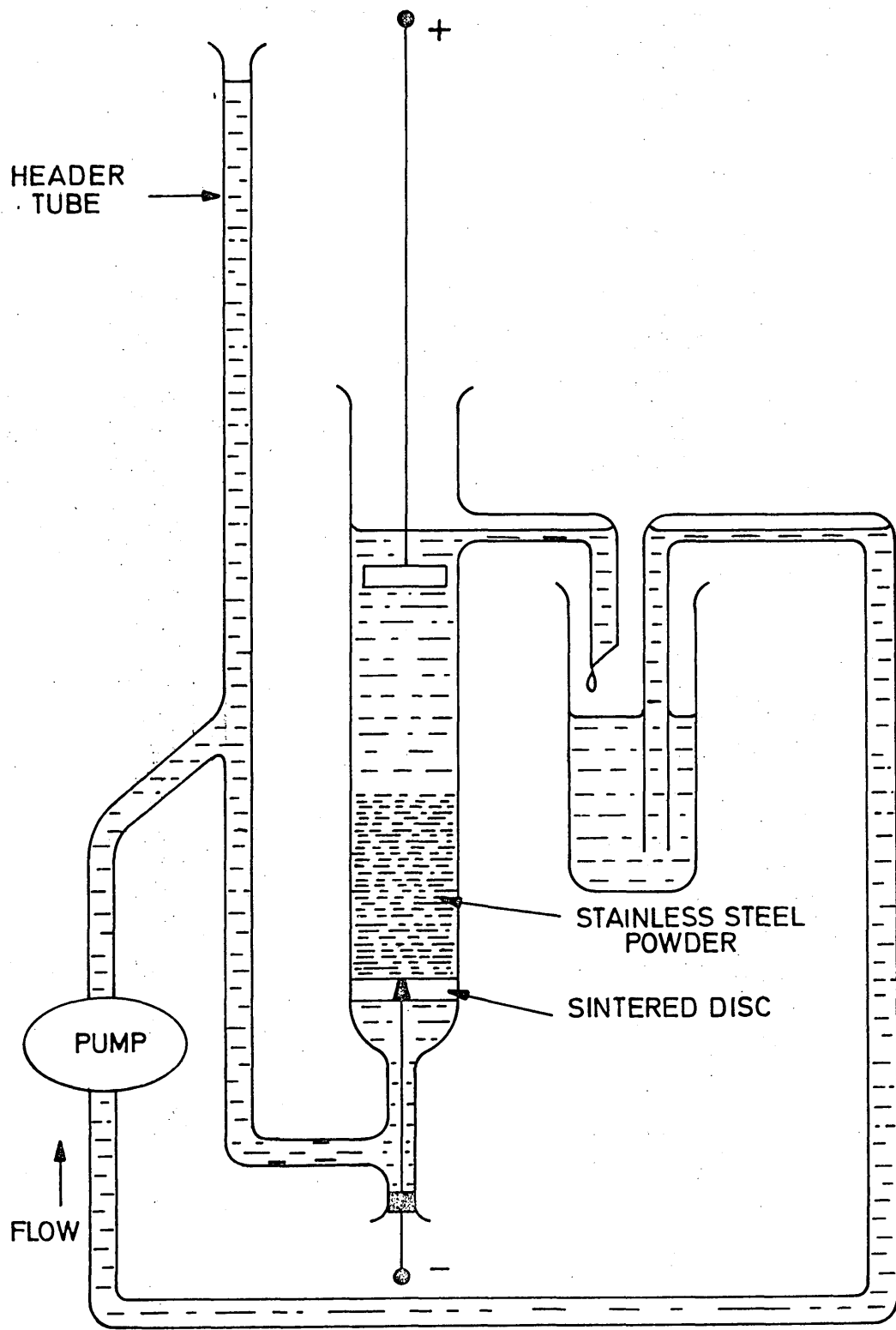


FIG. 1 APPARATUS FOR PLATING A FLUIDISED BED OF POWDER

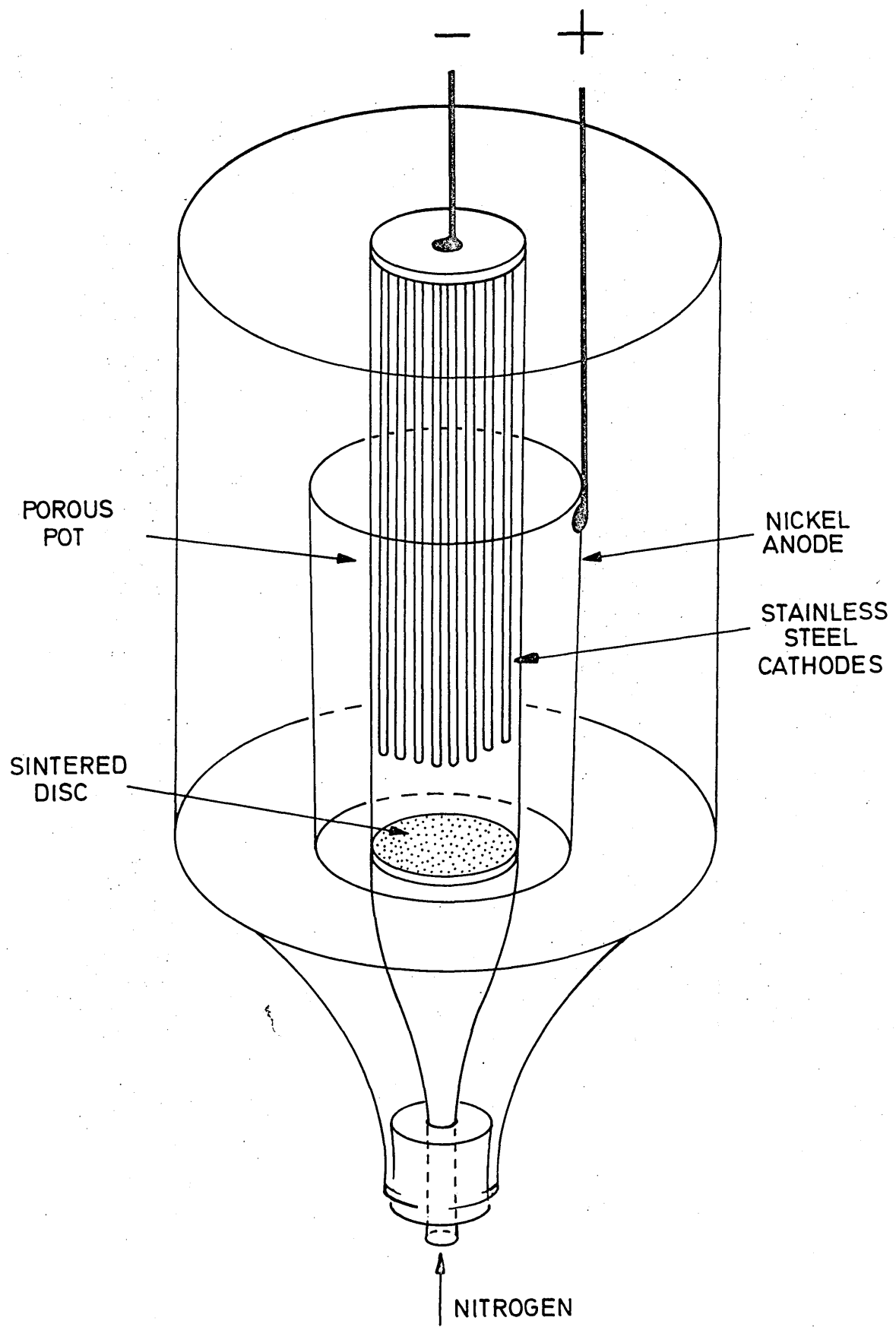


FIG. 2

NICKEL PLATING APPARATUS

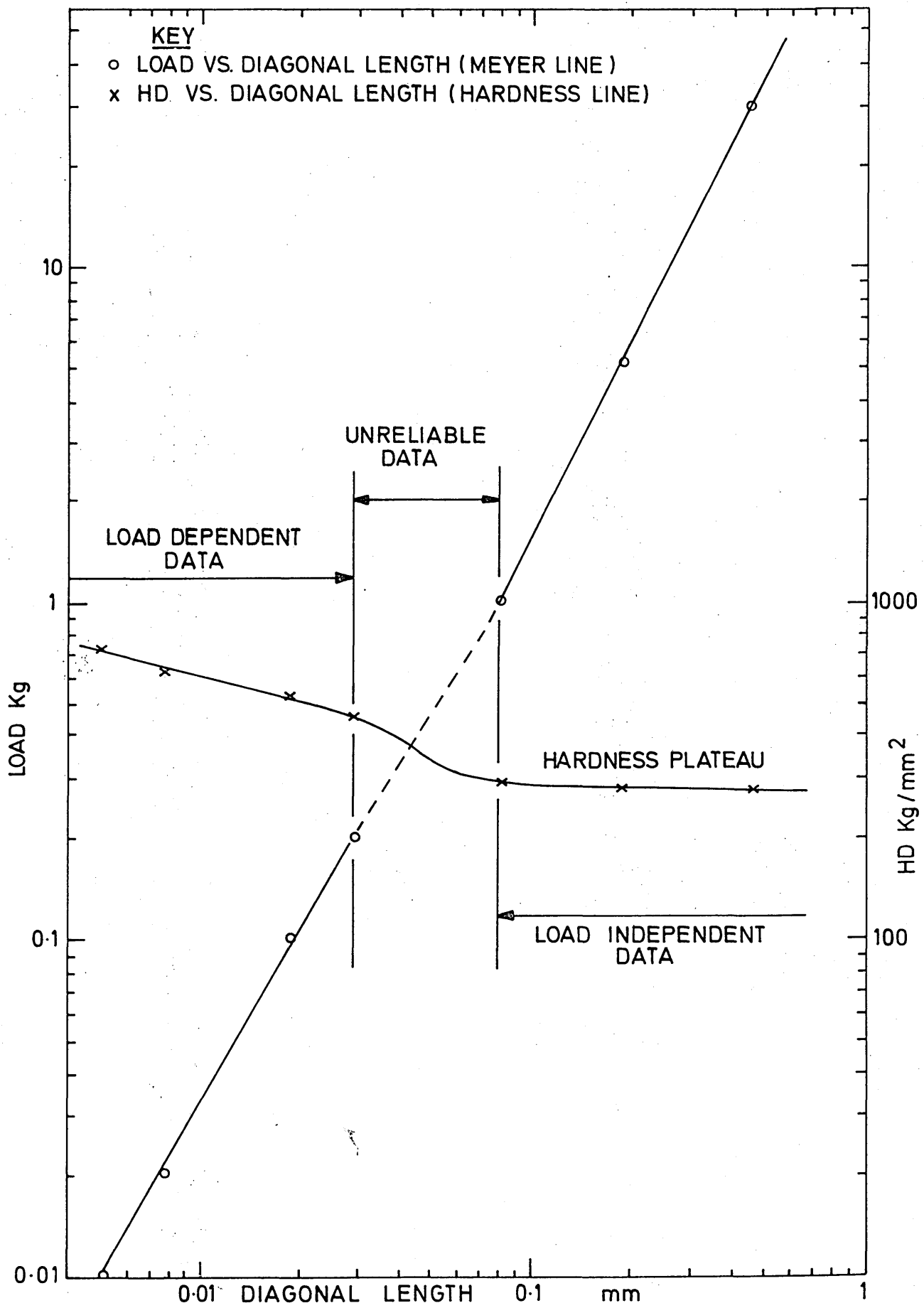


FIG. 3 HARDNESS OF IRON: SYNTHETIC GRAPHITE ALLOYS

FIG. 4.

Iron:1% Natural Graphite. Sintered for 2 hours at 1300°C.

M = martensite

DE = dark-etching product

F = ferrite

350 X

FIG. 5.

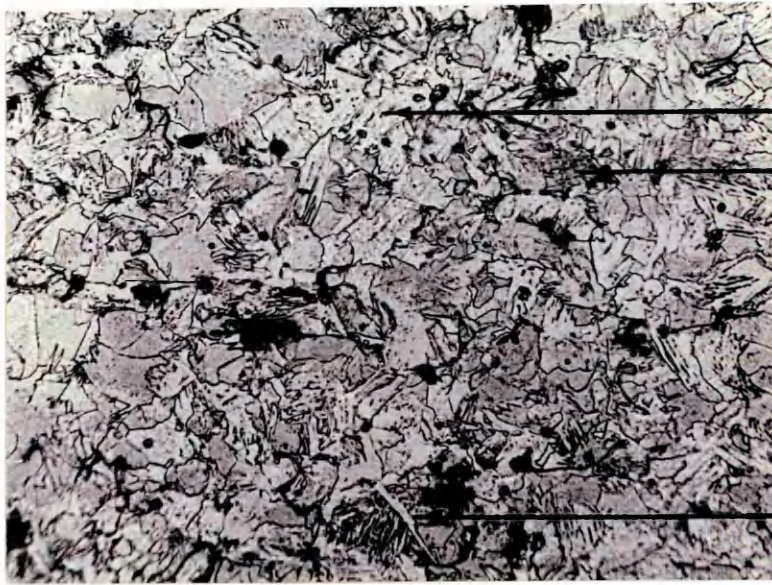
Iron:0.5% Synthetic Graphite. Sintered for 2 hours at 1300°C.

M = martensite

P = nodular pearlite

F = ferrite

350 X



M

DE

F

M

P

F

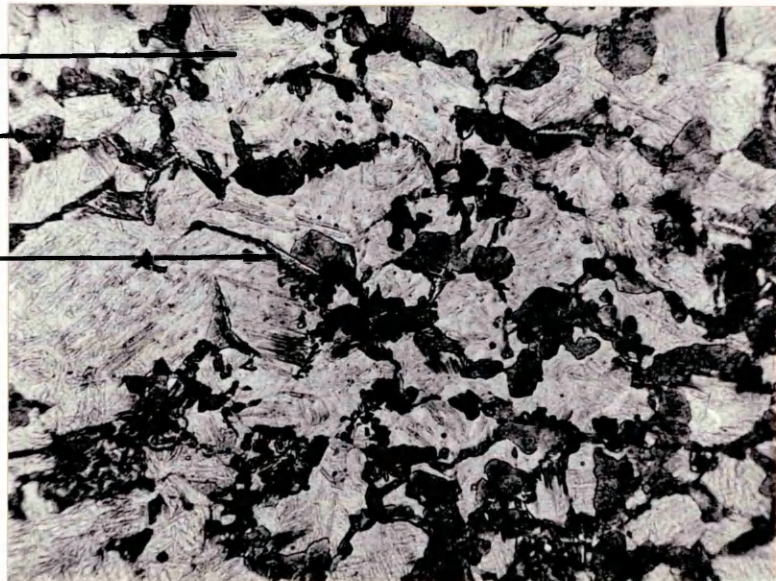


FIG. 6.

Iron:1% Nickel:0.5% Synthetic Graphite.
Sintered for 2 hours at 1300°C.

M = martensite
DE = dark-etching product
F = ferrite

350 X

FIG. 7.

3% Nickel Alloy, die-pressed. Sintered for 15 minutes
at 1150°C.

IP = interconnected porosity
NP = nickel particle agglomerates
P = nodular pearlite

160 X

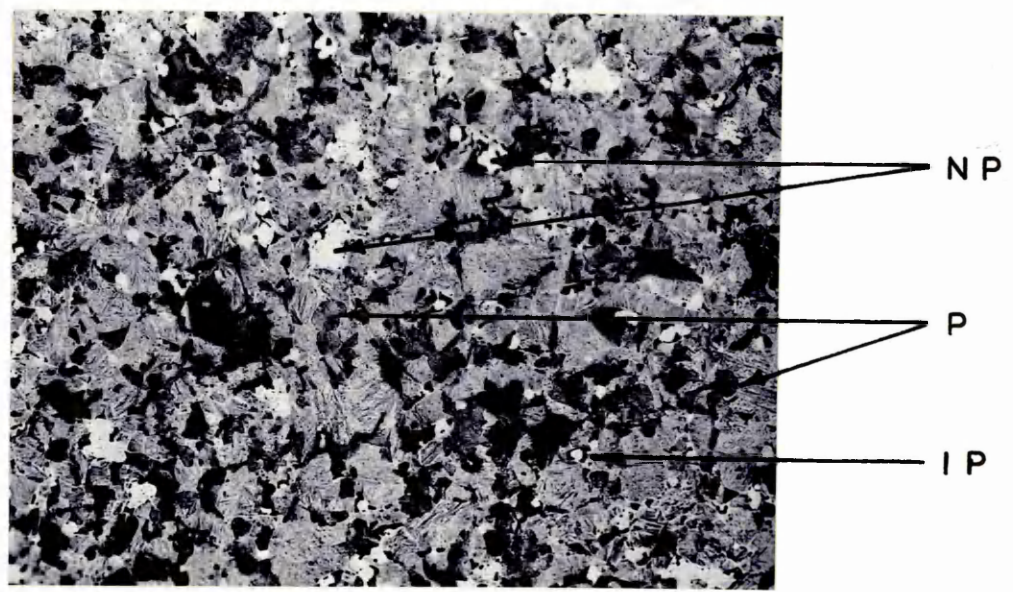
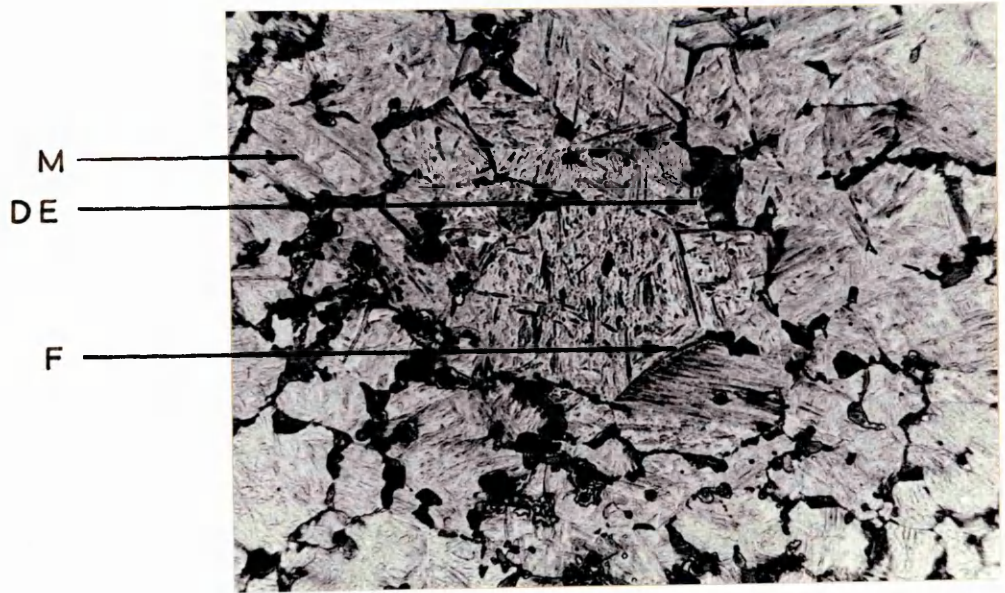


FIG. 8.

3% Nickel Alloy, die-pressed. Sintered for 1 hour at 1150°C.

IP = interconnected porosity
ID = interparticle diffusion paths
NP = nickel particle agglomerates.

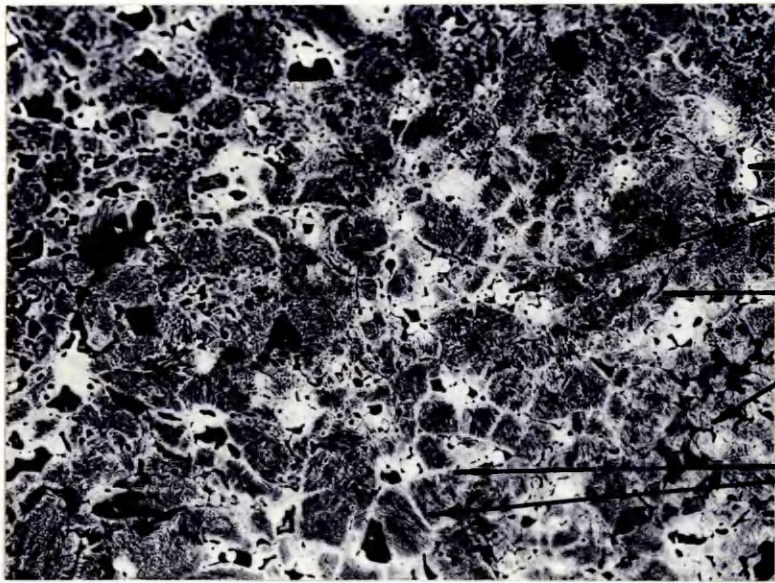
160 X

FIG. 9.

3% Nickel Alloy, die-pressed. Sintered for 6 hours at 1150°C.

CP = coarsening and isolation of porosity.
IP = interparticle porosity
NP = original nickel particle agglomerates

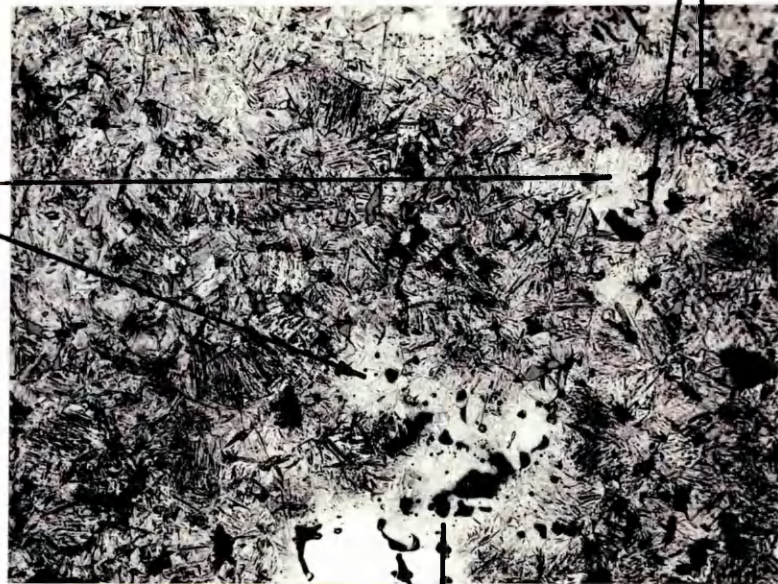
160 X



NP

IP

ID



IP

NP

CP

FIG. 10.

3% Nickel Alloy, die-pressed. Sintered for 15 minutes at 1300°C.

IP = interconnected porosity
ID = interparticle diffusion paths
NP = nickel particle agglomerates

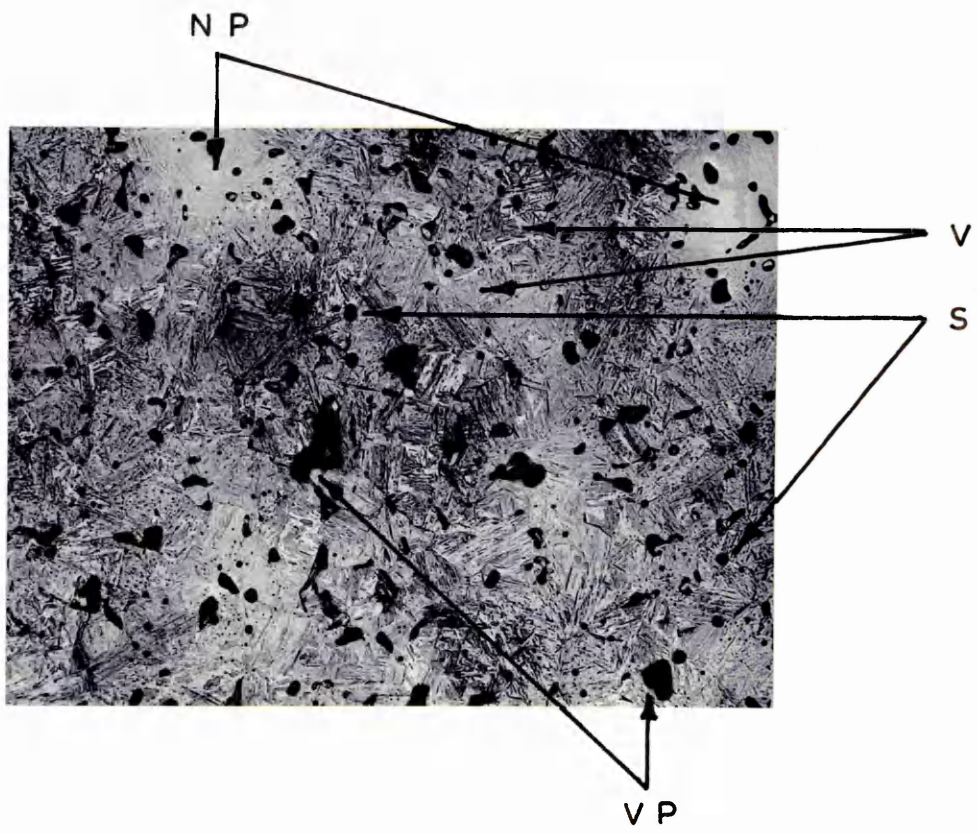
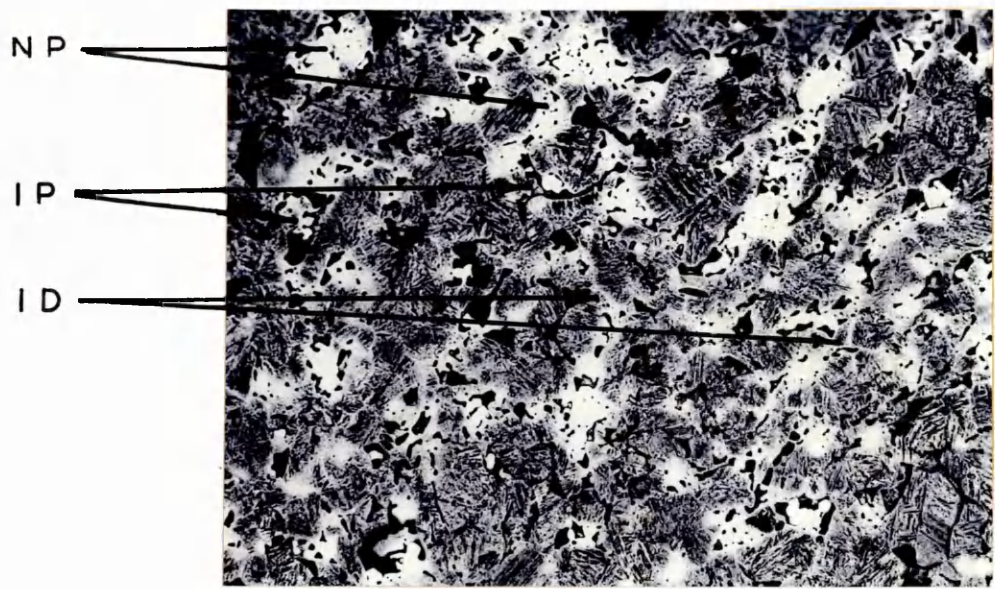
160 X

FIG. 11.

3% Nickel Alloy, die-pressed. Sintered for 6 hours at 1300°C.

NP = original nickel particle agglomerates
VP = concave pore surfaces
V = variation in morphology
S = spherical pores

160 X



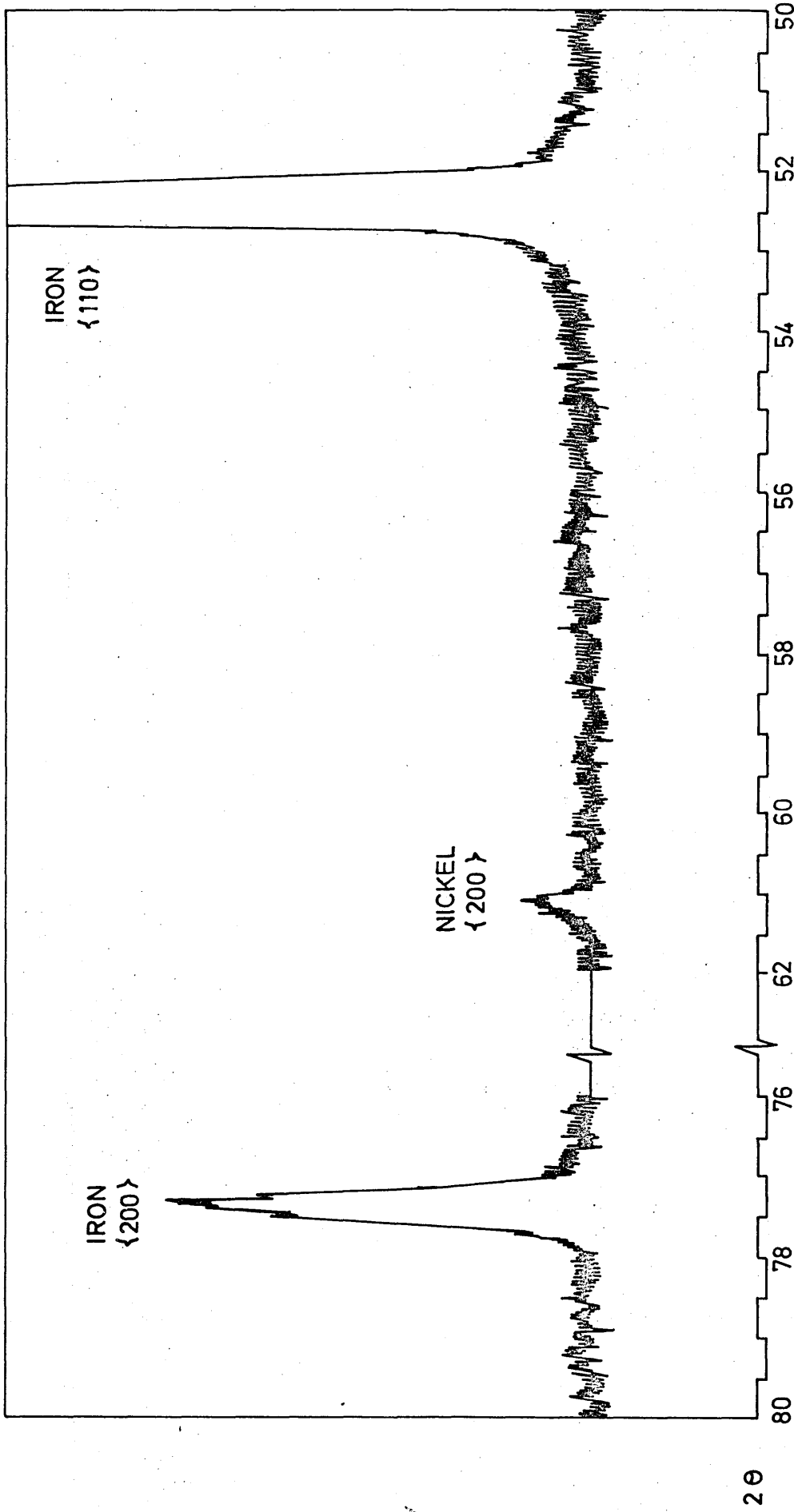


FIG. 12 X-RAY DIFFRACTOMETER CHART RECORD FOR UNSINTERED 3% NICKEL COMPACT.(DIE - PRESSED)

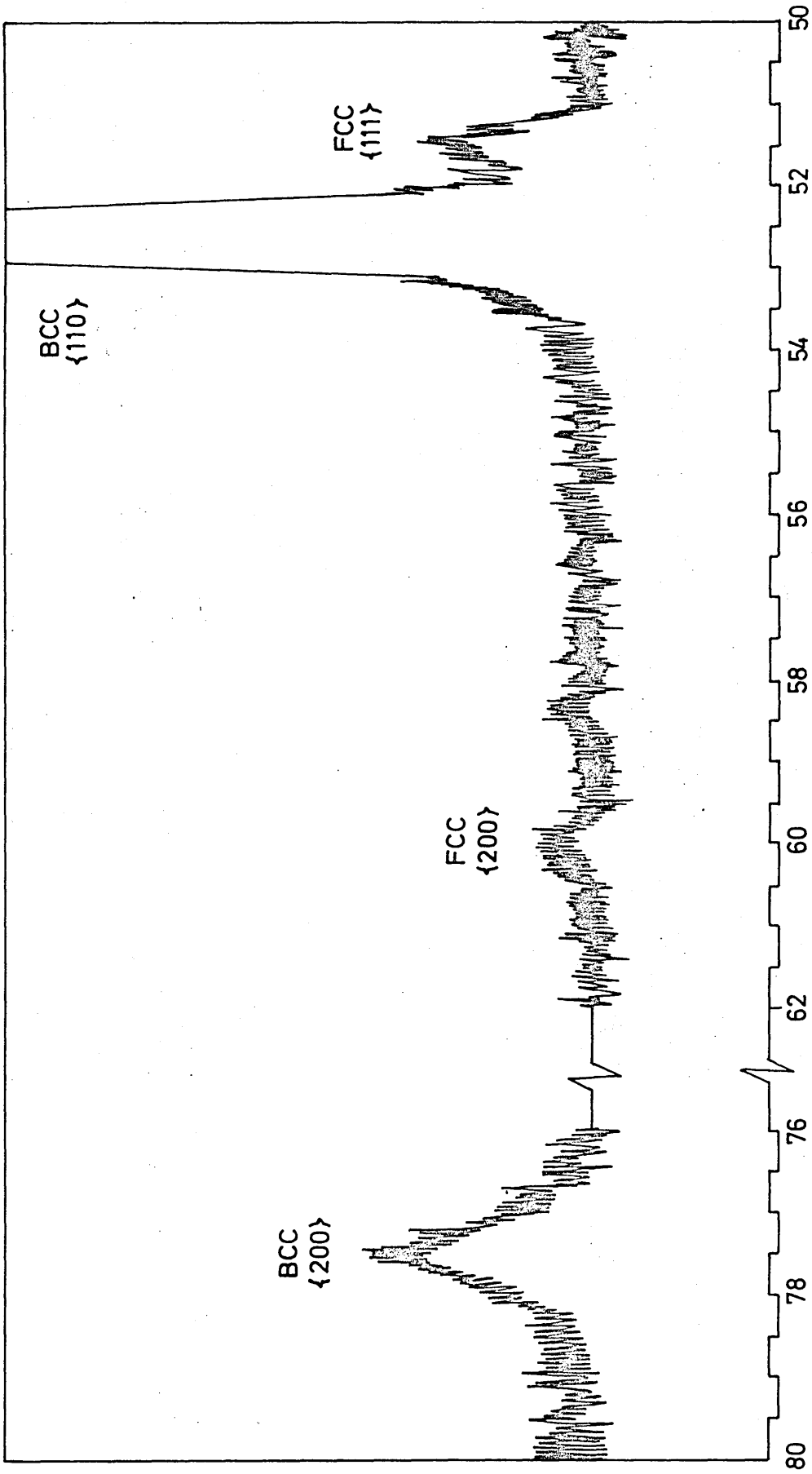


FIG. 13 X - RAY DIFFRACTOMETER CHART RECORD FOR BLENDED 3% NICKEL ALLOY (DIE - PRESSED)
SINTERED FOR 15 MINUTES AT 1150°C

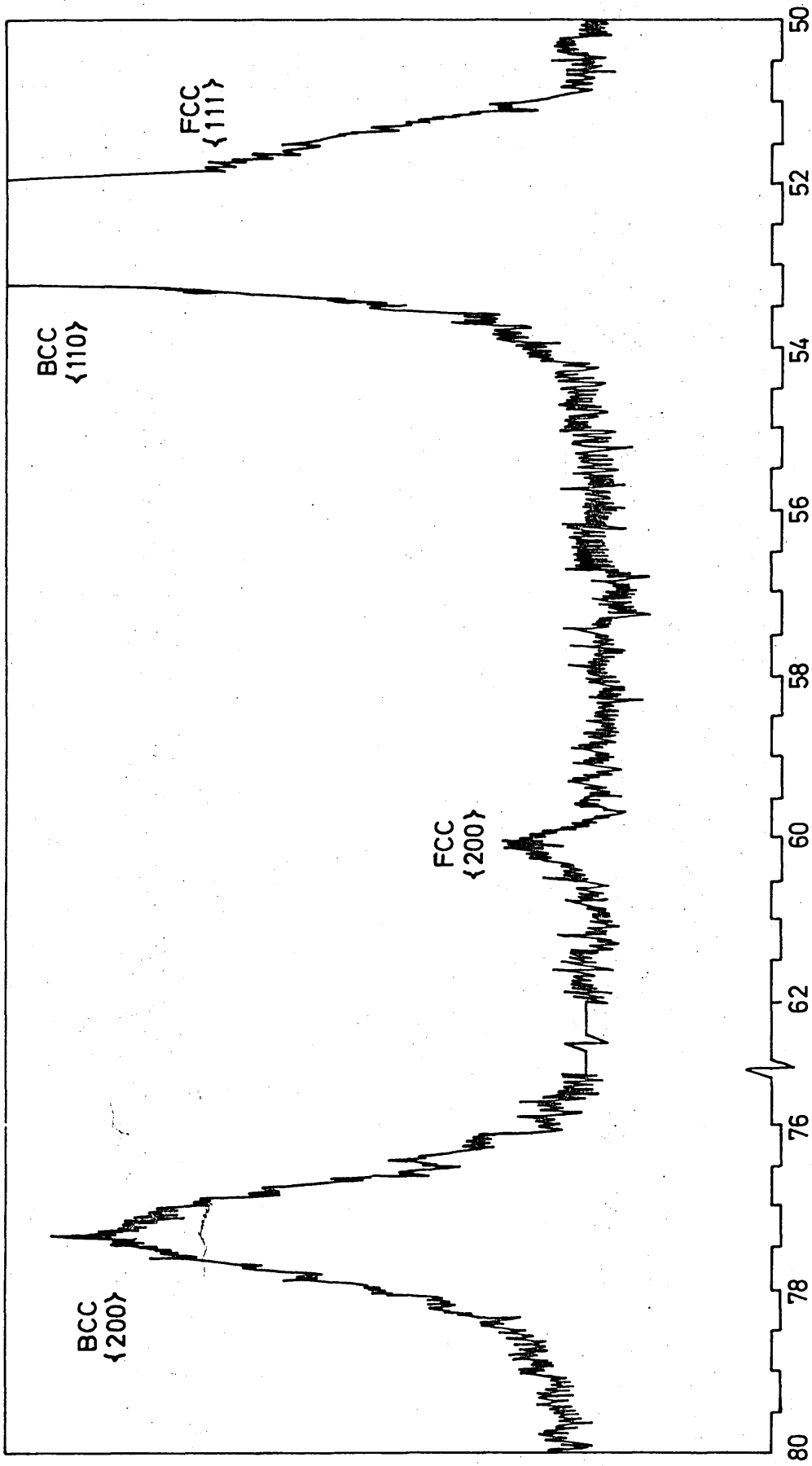


FIG. 14 X-RAY DIFFRACTOMETER CHART RECORD FOR BLENDED 3% NICKEL ALLOY (DIE-PRESSED) SINTERED FOR 30 MINUTES AT 1150°C

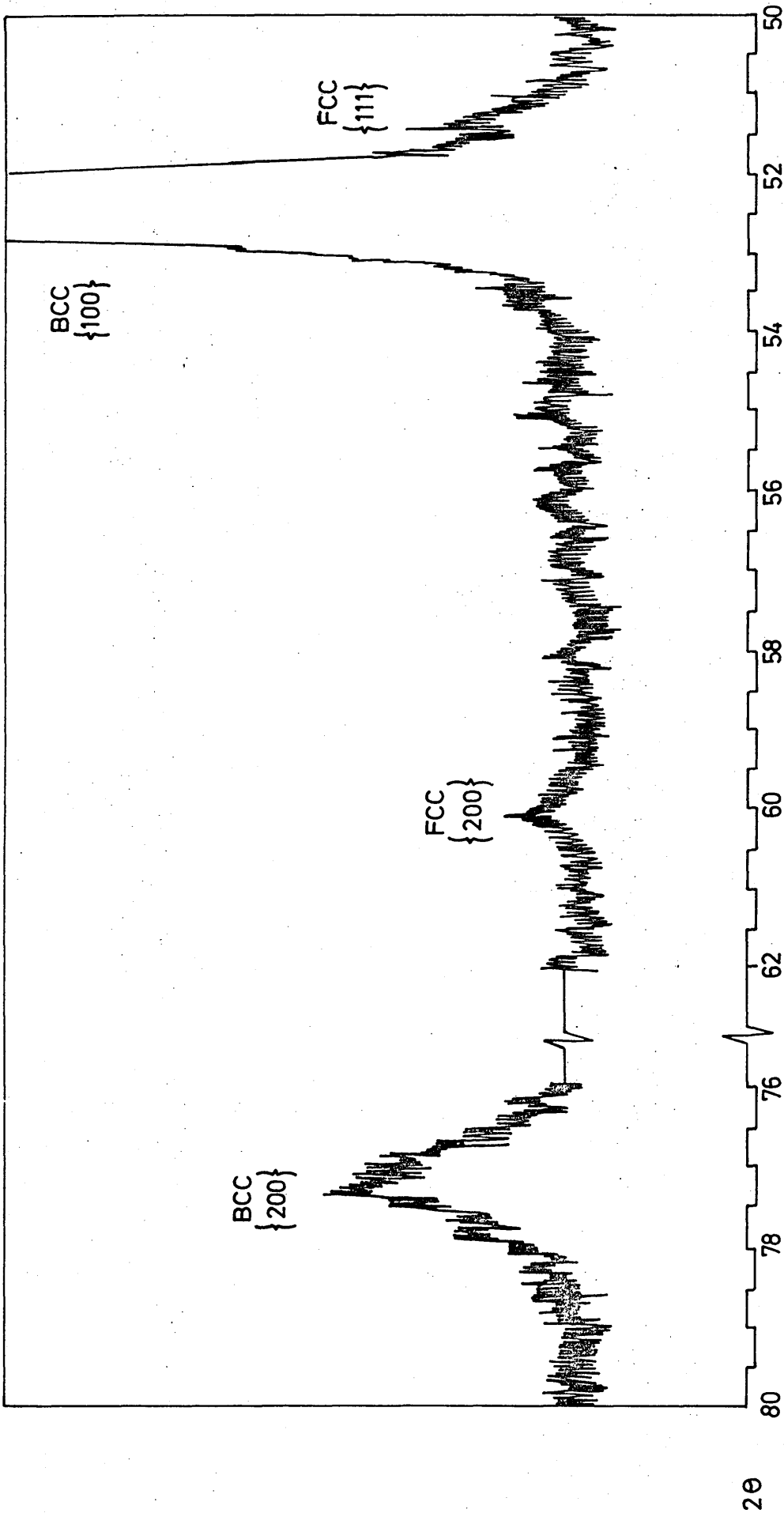


FIG. 15 X-RAY DIFFRACTOMETER CHART RECORD FOR BLENDED 3% NICKEL ALLOY (DIE - PRESSED) SINTERED FOR 15 MINUTES AT 1300 °C

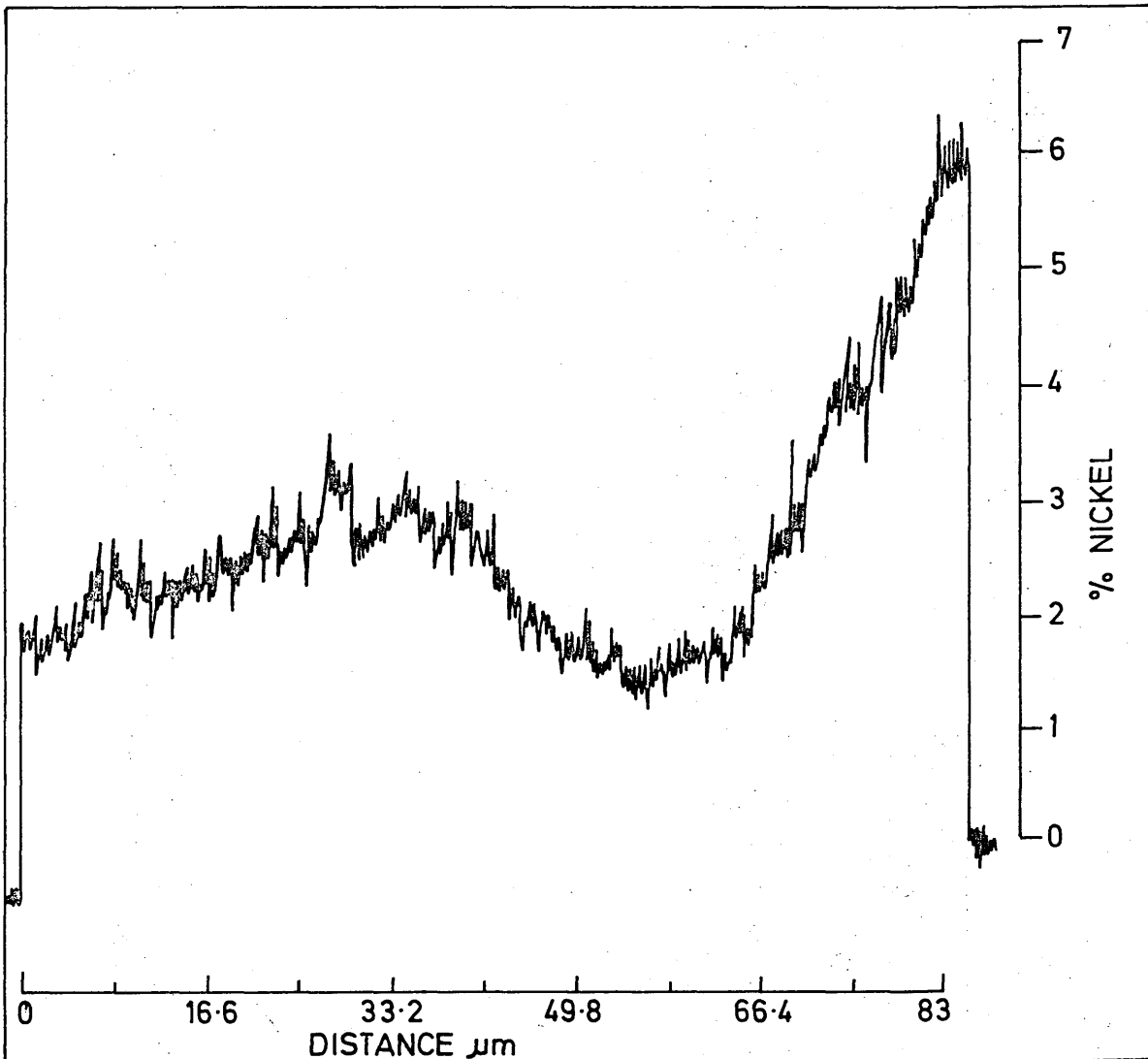


FIG. 16 LINE SCAN OF NICKEL CONCENTRATION FOR A 3% NICKEL ALLOY (DIE-PRESSED) SINTERED FOR 6 HOURS AT 1150°C

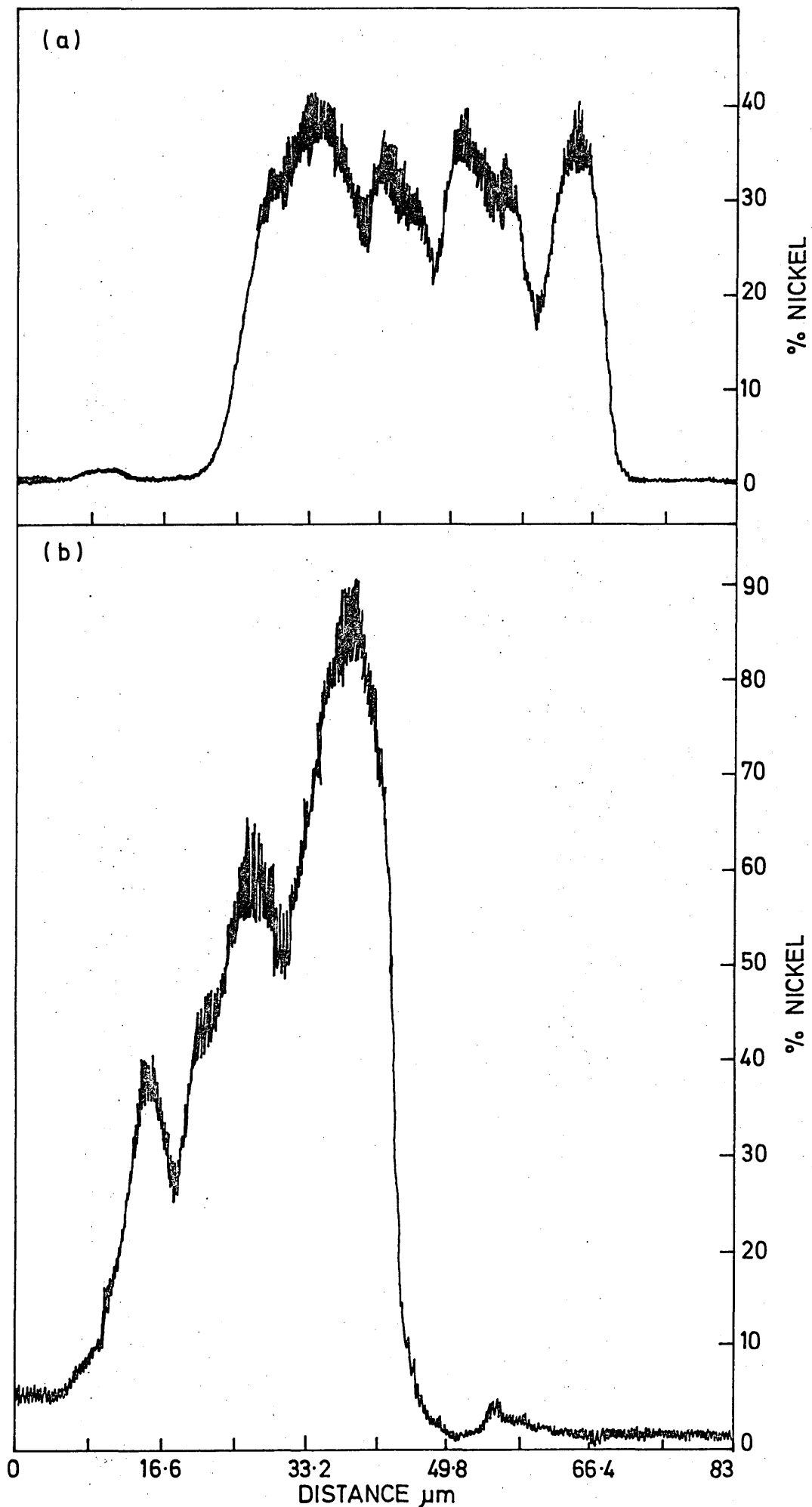


FIG. 17 LINE SCANS OF NICKEL CONCENTRATION FOR A 3% NICKEL ALLOY (DIE-PRESSED) SINTERED FOR 5 MINUTES AT 1150°C

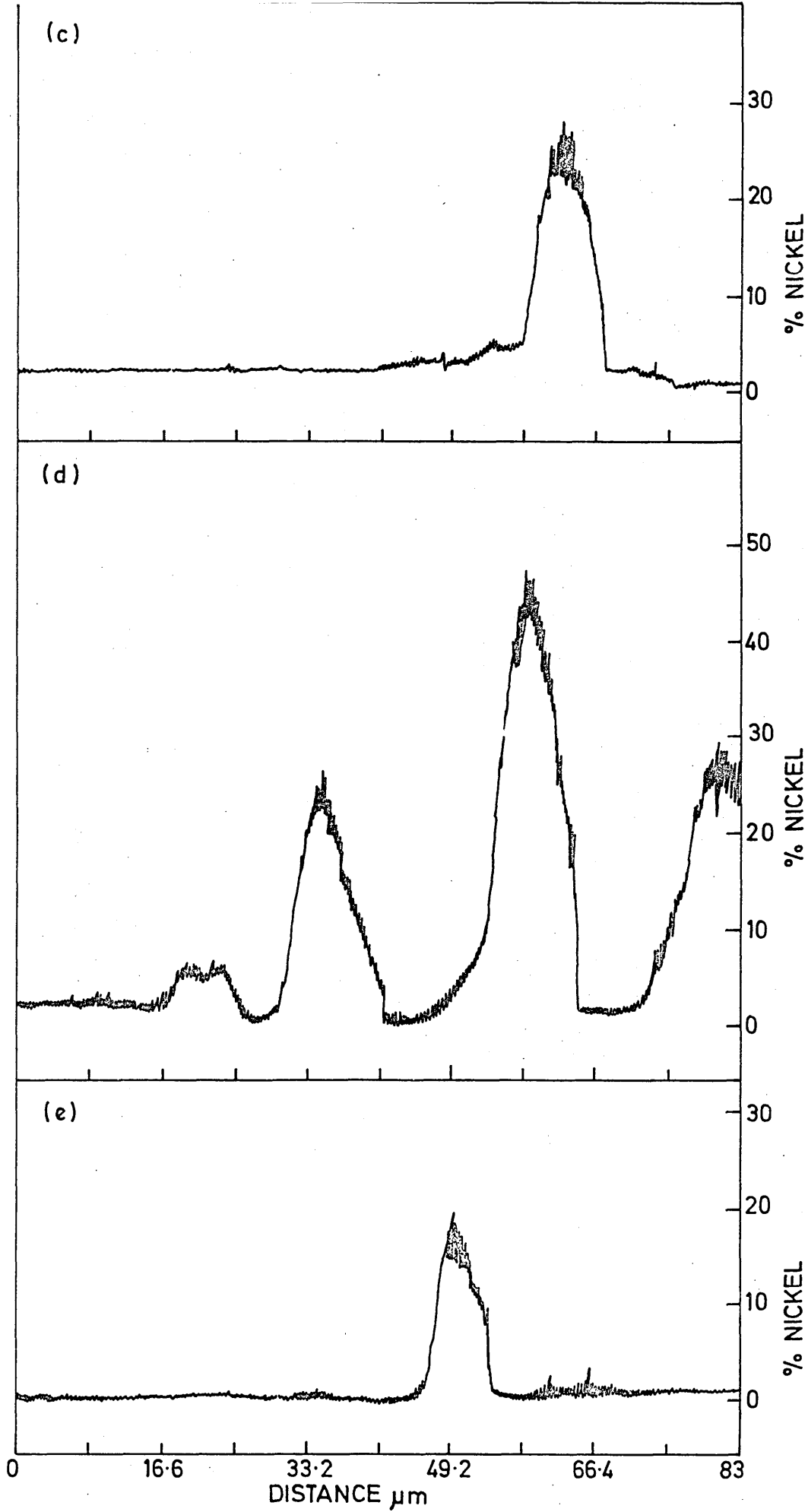


FIG. 17 LINE SCANS OF NICKEL CONCENTRATION FOR A 3% NICKEL ALLOY (DIE-PRESSED) SINTERED FOR 5 MINUTES AT 1150°C

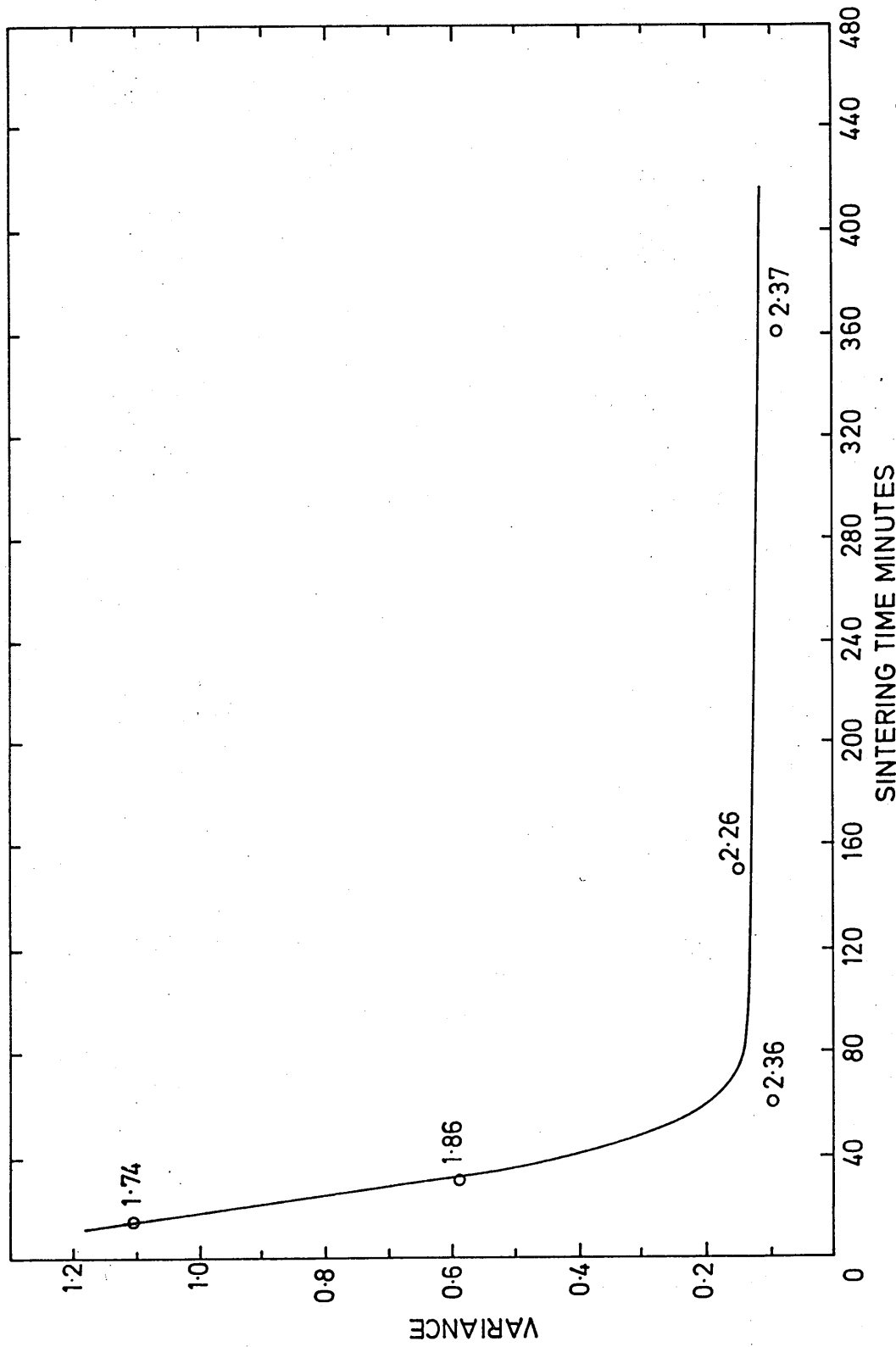


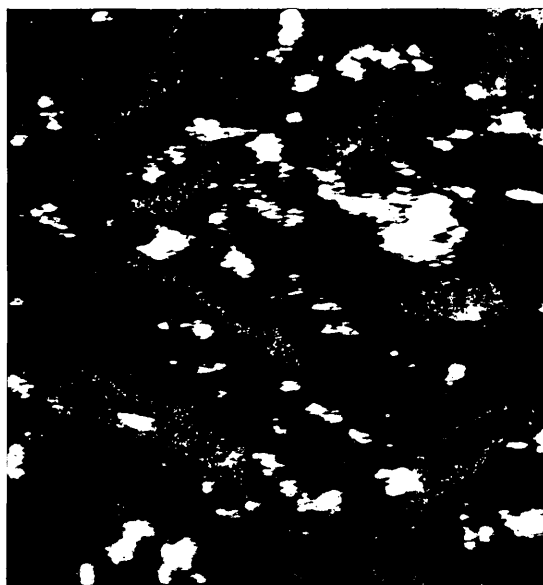
FIG. 18 AREAL ANALYSIS OF IRON: 3% NICKEL ALLOYS (DIE-PRESSED) SINTERED AT 1150°C
 PROBE MAGNIFICATION 250x SINTERING TIME MINUTES FIGURES REFER TO MEAN % NICKEL CONTENT

FIG. 19.

Nickel distribution in a 3% Nickel Alloy, die pressed.
Sintered for 15 minutes at 1150°C.

500 μm square area.

250 X



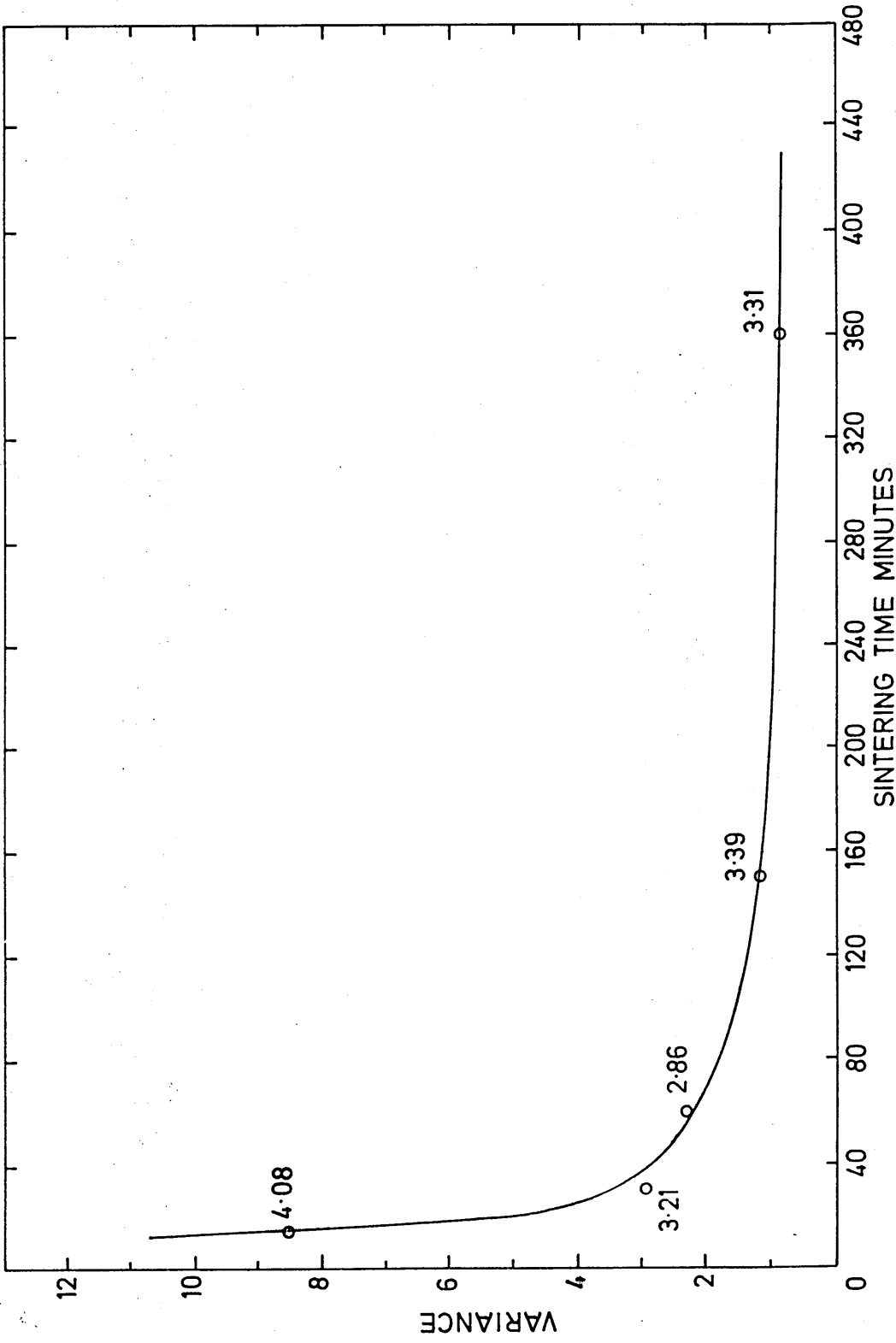


FIG. 20 AREAL ANALYSIS OF IRON: 3% NICKEL ALLOYS (DIE-PRESSED) SINTERED AT 1150°C
 PROBE MAGNIFICATION 1200x

FIGURES REFER TO MEAN % NICKEL CONTENT

FIG. 21.

Nickel distribution in a 3% Nickel Alloy, die-pressed.
Sintered for 15 minutes at 1150°C.

83 μ m square area.

1200 X

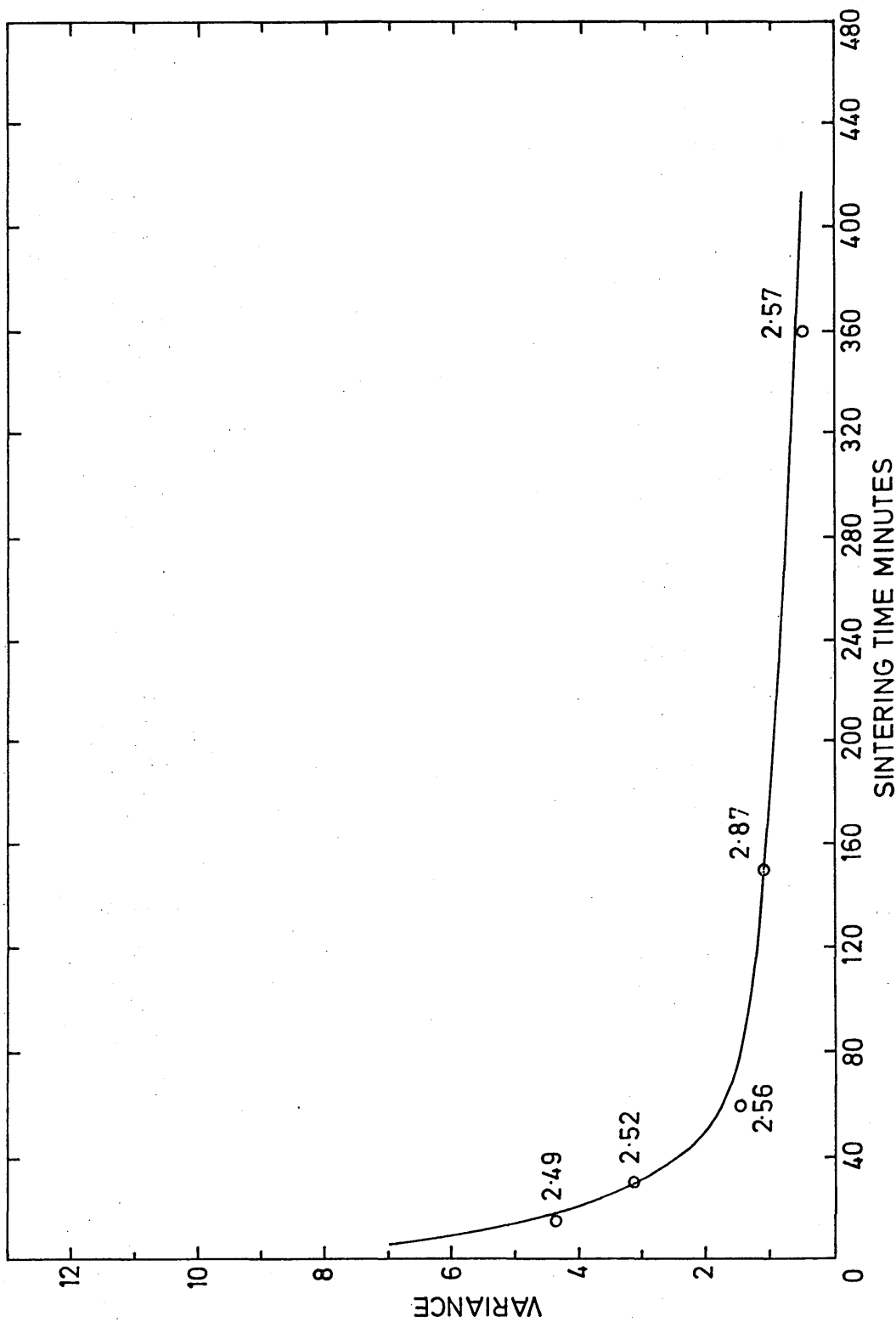


FIG. 22 AREAL ANALYSIS OF IRON : 3% NICKEL ALLOYS (DIE-PRESSED) SINTERED AT 1150°C
 PROBE MAGNIFICATION 1200x TURBOLATOR BLEND.

FIGURES REFER TO MEAN % NICKEL CONTENT

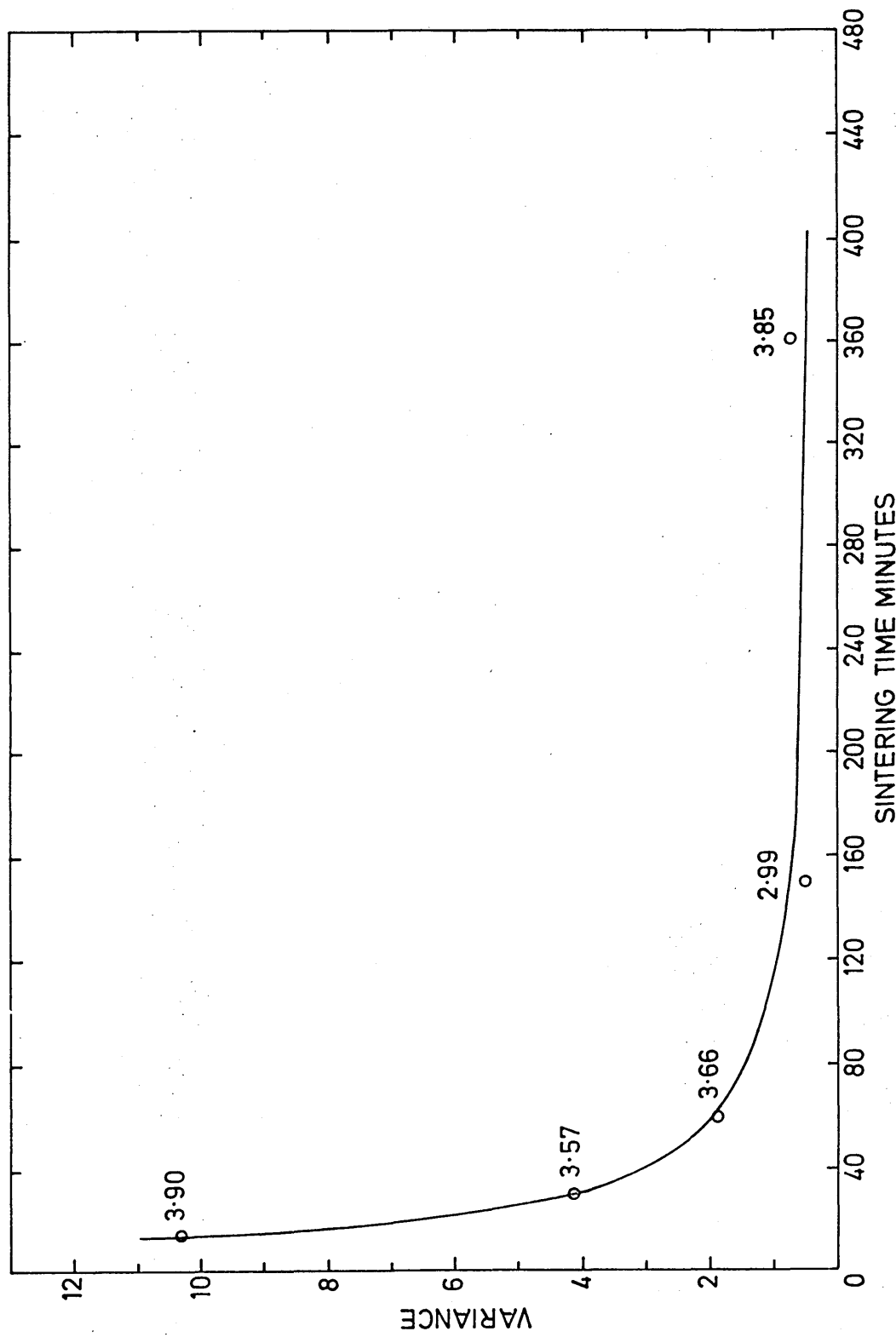
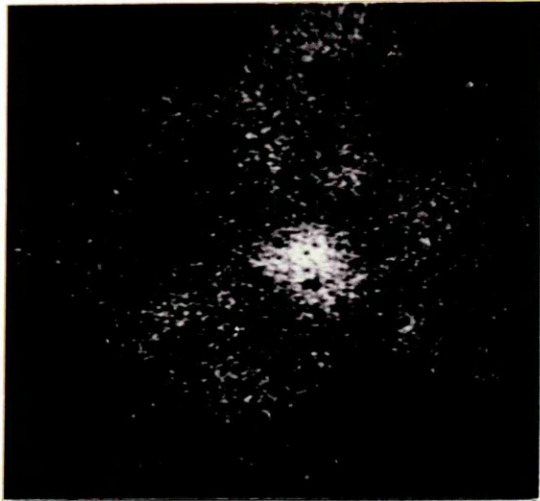


FIG. 23 AREAL ANALYSIS OF IRON: 3% NICKEL ALLOYS (DIE-PRESSED) SINTERED AT 1300°C
 PROBE MAGNIFICATION 1200x

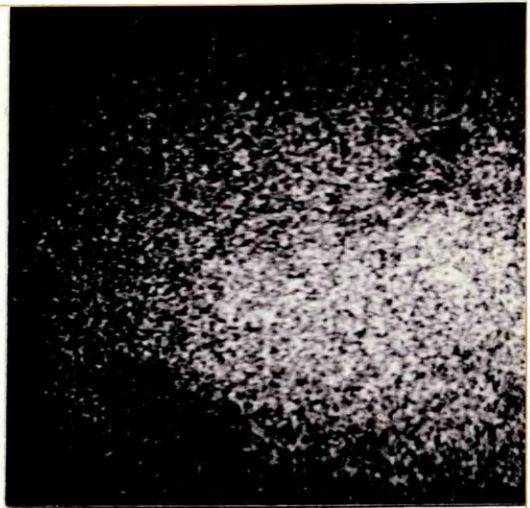
FIGURES REFER TO MEAN % NICKEL CONTENT

FIG. 24.

Nickel distribution in a 3% Nickel Alloy, die-pressed.
Sintered for 1 hour at 1300°C.



(a) 250x 2.46% Nickel



(b) 1200x 7.77% Nickel



(c) 2400x 10.80% Nickel



(d) 4800x 11.43% Nickel

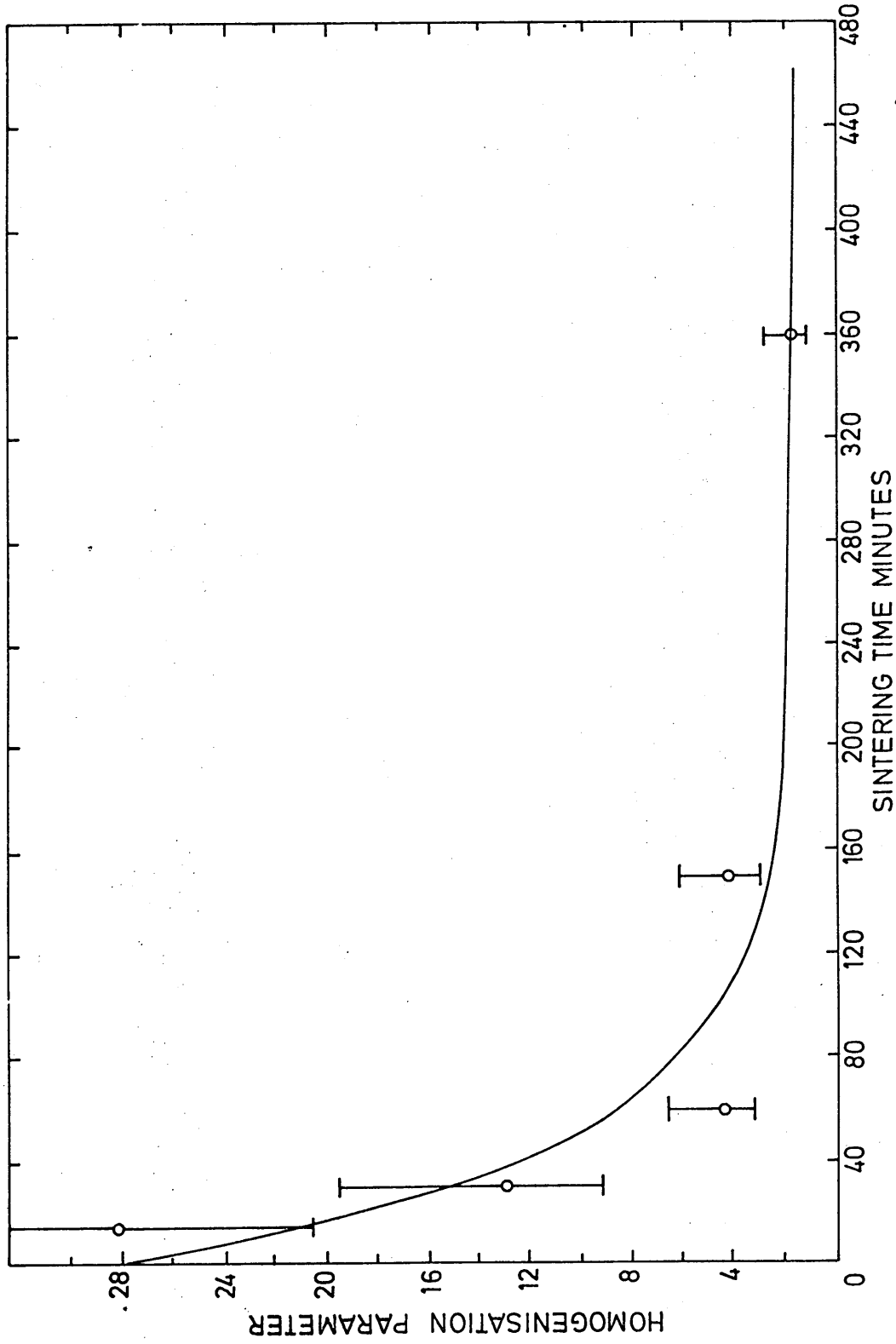


FIG. 25 AREAL ANALYSIS OF IRON: 3% NICKEL ALLOYS (DIE-PRESSED) SINTERED AT 1150°C
 PROBE MAGNIFICATION 4800 X

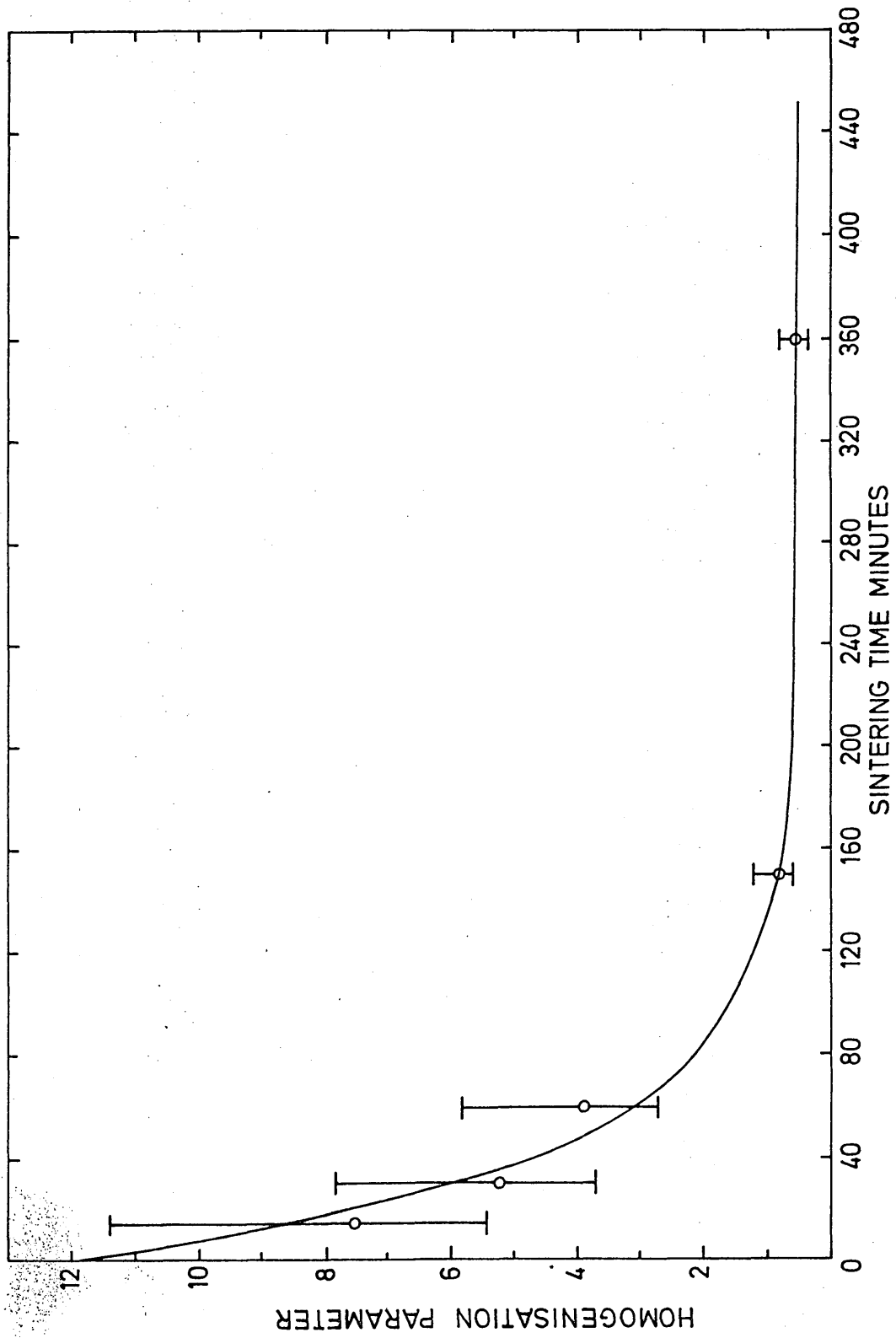


FIG. 26 AREAL ANALYSIS OF IRON: 3% NICKEL ALLOYS (DIE-PRESSED) SINTERED AT 1300°C
 PROBE MAGNIFICATION 4800x

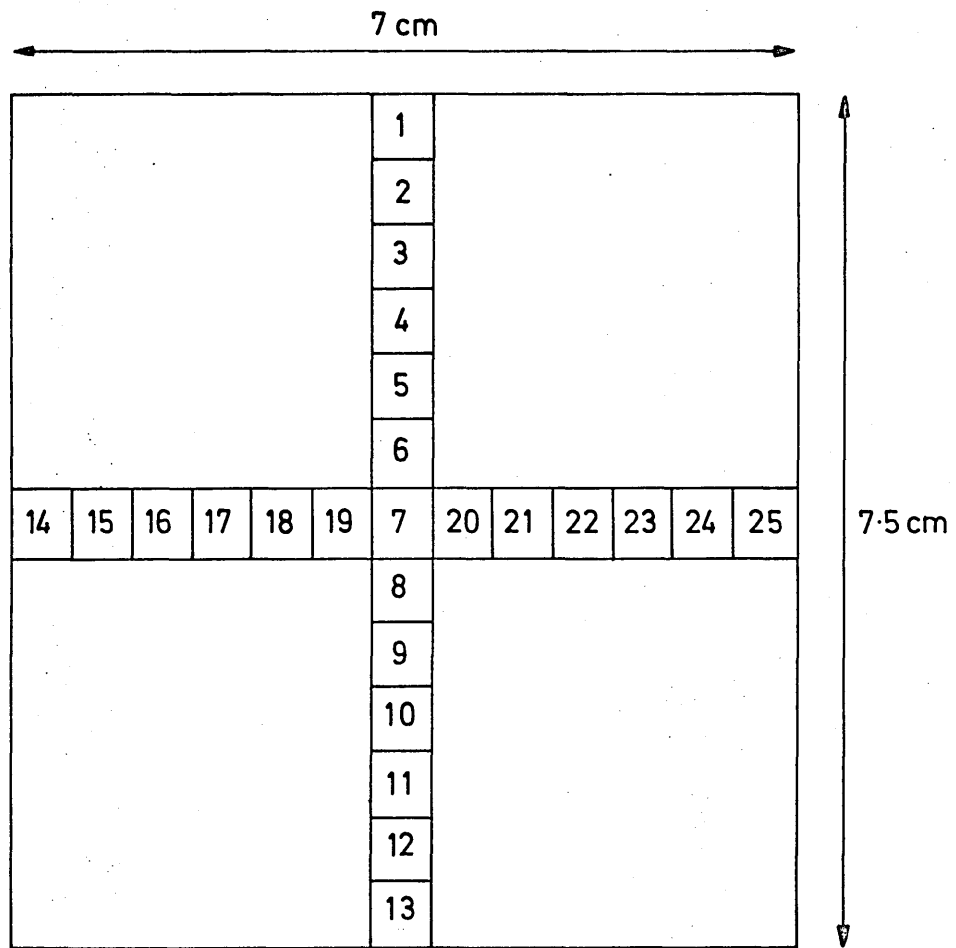


FIG. 27 CROSS - SECTION OF ISOSTATICALLY PRESSED
2 kg COMPACT

FIG. 28.

Microhardness of areas with different etching characteristics in a 3% Nickel Plated Alloy. Sintered for 15 minutes at 1150°C.

<u>Indentation</u>	<u>MHD</u>
1	264
2	273
3	356
4	334
5	334

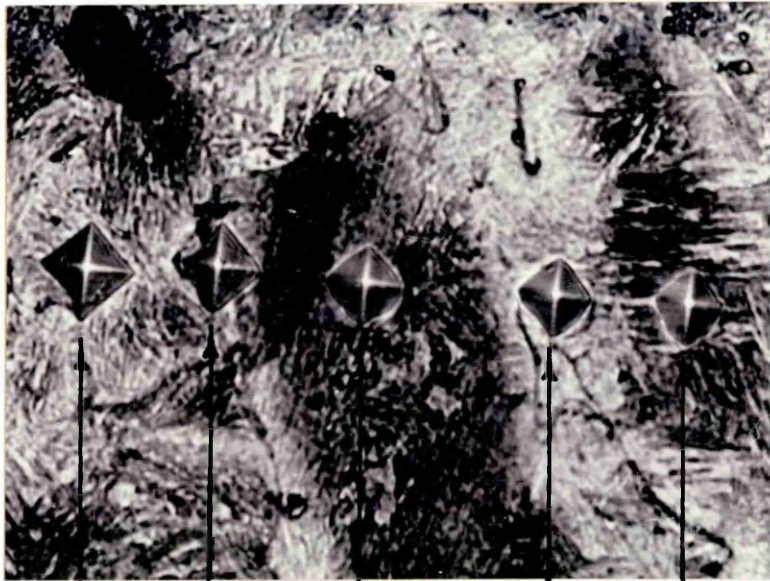
960 X

FIG. 29.

3% Nickel Blended compact. Sintered for 15 minutes at 1150°C.

DE = dark-etching product
IP = interconnected porosity
ID = interparticle diffusion paths.

160 X



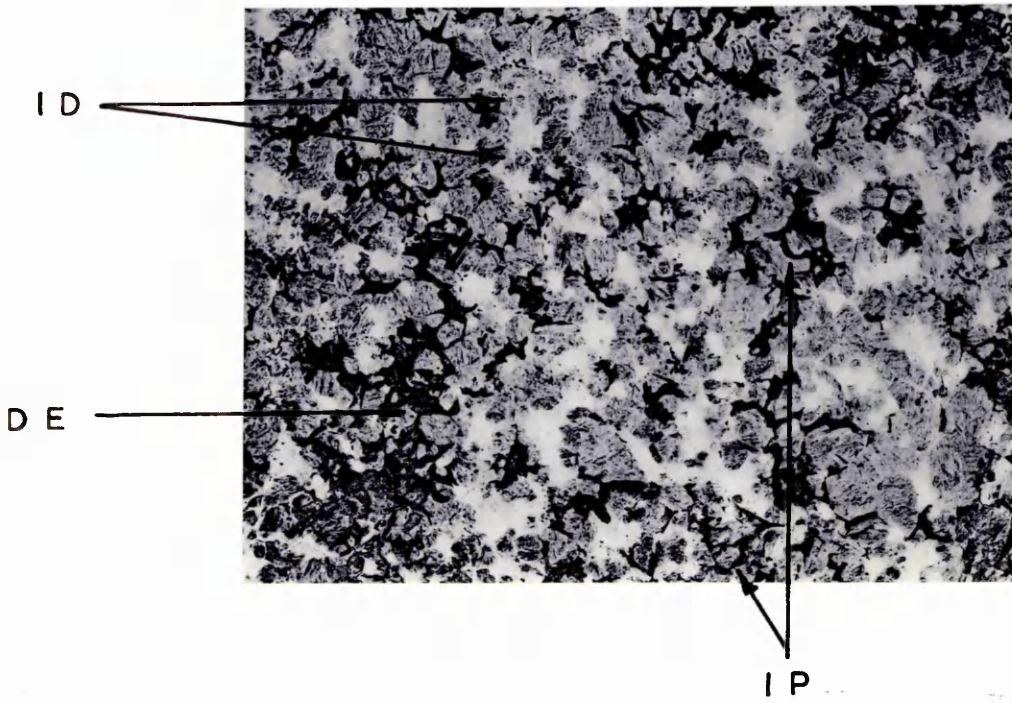
1

2

3

4

5



ID

DE

IP

FIG. 30.

3% Nickel Blended compact. Sintered for 15 minutes at 1150°C.

ID = interparticle diffusion paths
NP = original centres of nickel particles
I = original centres of iron particles
P = local regions of pearlite

1000 X

FIG. 31.

3% Nickel Blended compact. Sintered for 15 minutes at 1150°C.

F = ferrite
ID = interparticle diffusion paths
IP = interconnected porosity
D = diffusion alloy layers around iron particles.

1000 X

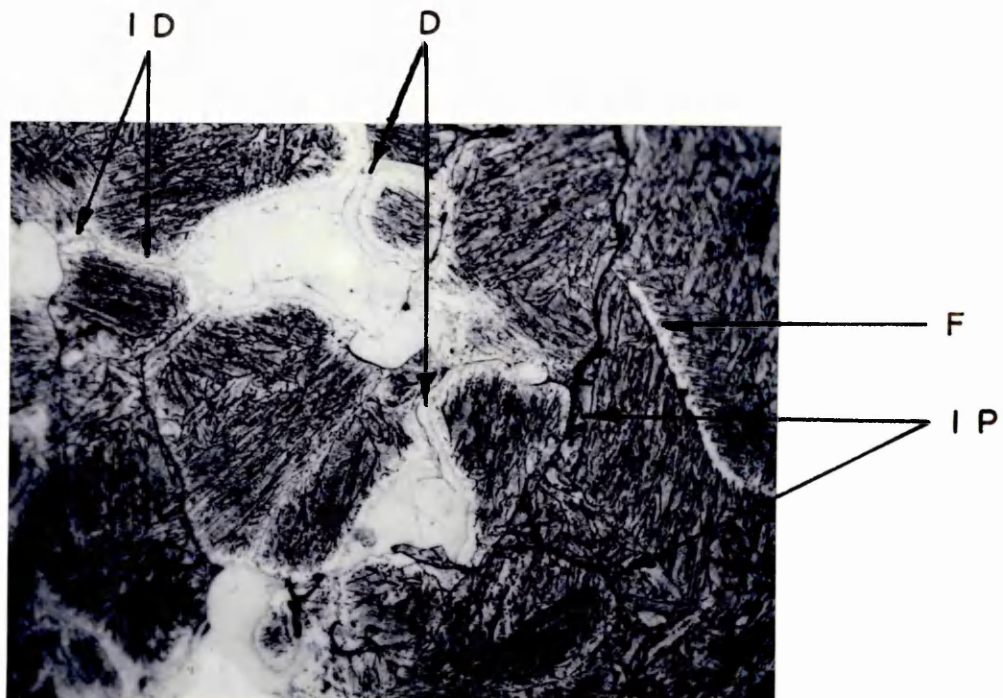
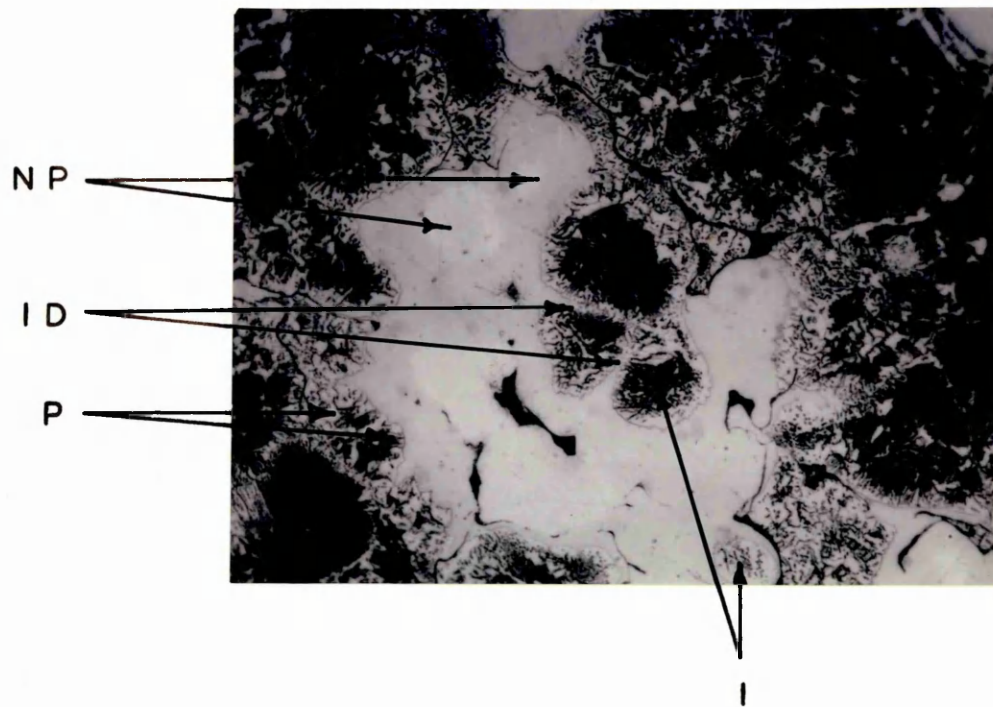


FIG. 32.

3% Nickel Blended compact. Sintered for 8 hours at 1150°C.

NP = original nickel particle agglomerates
V = variation in morphology

160 X

FIG. 33.

3% Nickel Blended compact. Sintered for 8 hours at 1150°C.

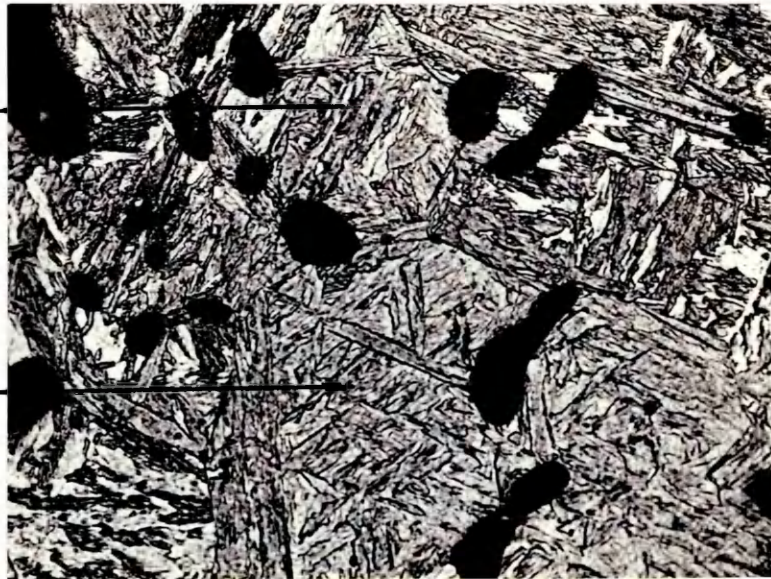
L = lath martensite
A = acicular martensite

1000 X



NP

V



L

A

FIG. 34.

3% Nickel Blended compact. Sintered for 15 minutes at 1300°C.

ID = interparticle diffusion paths
N = nickel-rich areas
U = uniform morphology

160 X

FIG. 35.

3% Nickel Blended compact. Sintered for 15 minutes at 1300°C.

NP = original nickel particle
L = lath martensite

1000 X

FIG. 36.

3% Nickel Blended compact. Sintered for 15 minutes at 1300°C and Tempered for 1 hour at 600°C.

C = carbide precipitates
N = nickel-rich areas

160 X

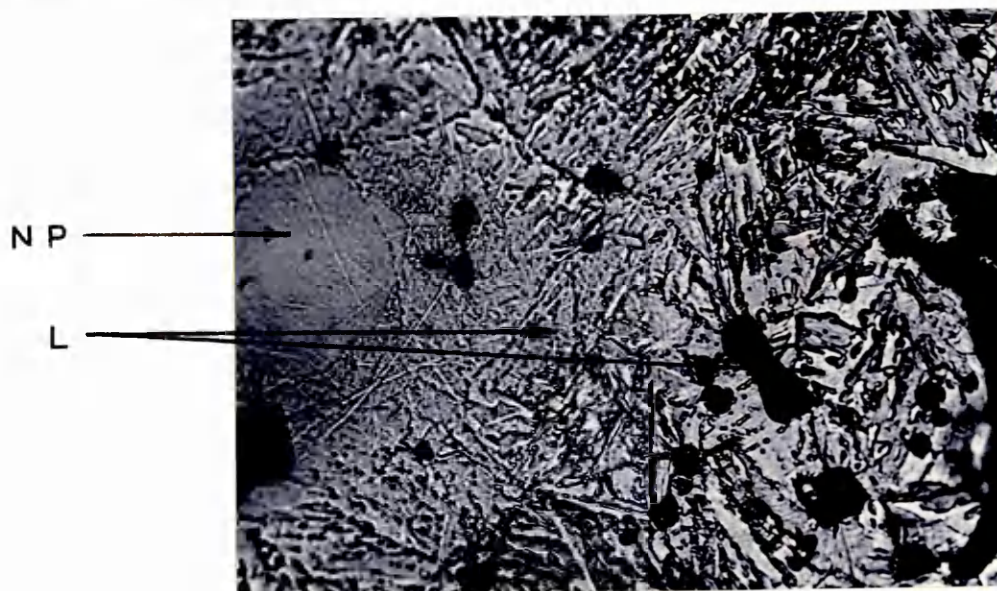
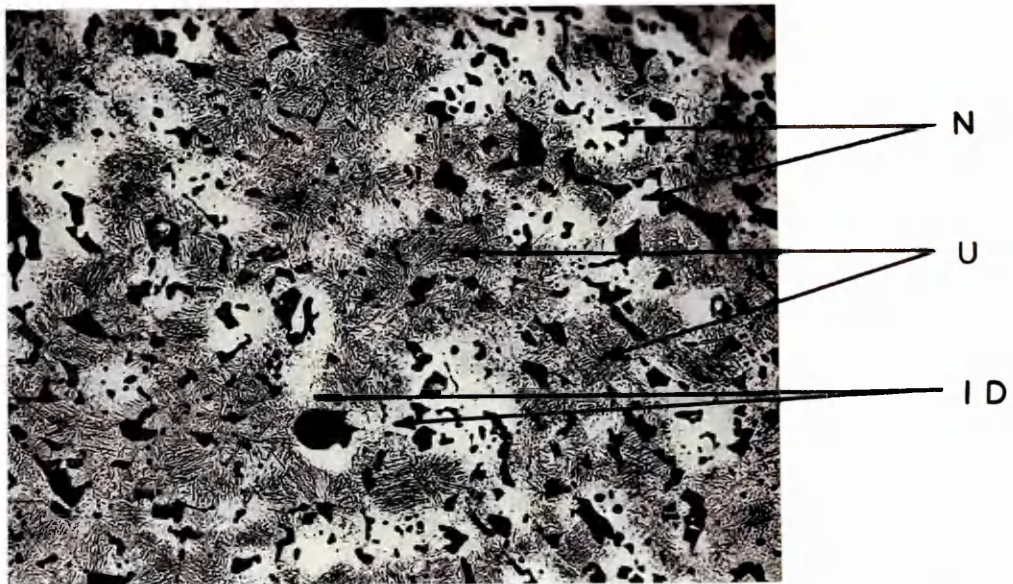


FIG. 37.

3% Nickel Blended compact. Sintered for 2 hours at 1300°C.

F = grain boundary ferrite
UB = upper bainite

10 000 X

FIG. 38.

3% Nickel Blended compact. Sintered for 2 hours at 1300°C.

F = ferrite plates

10 000 X

U B

F

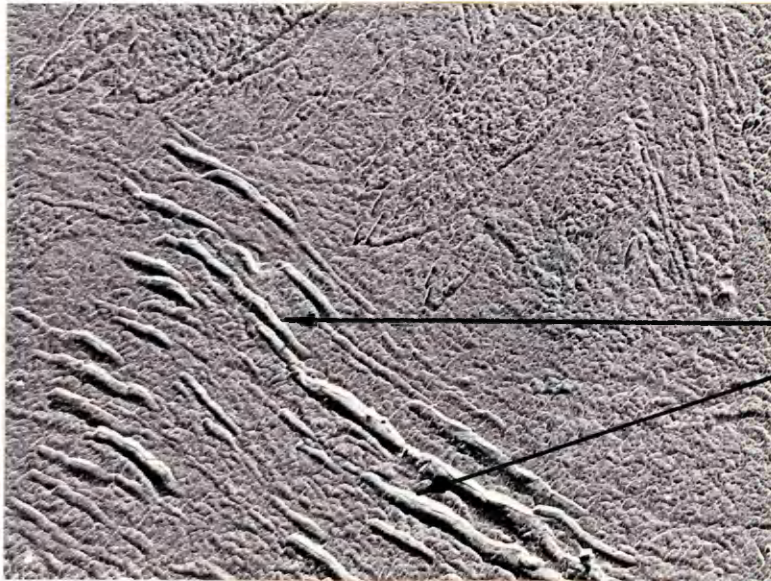
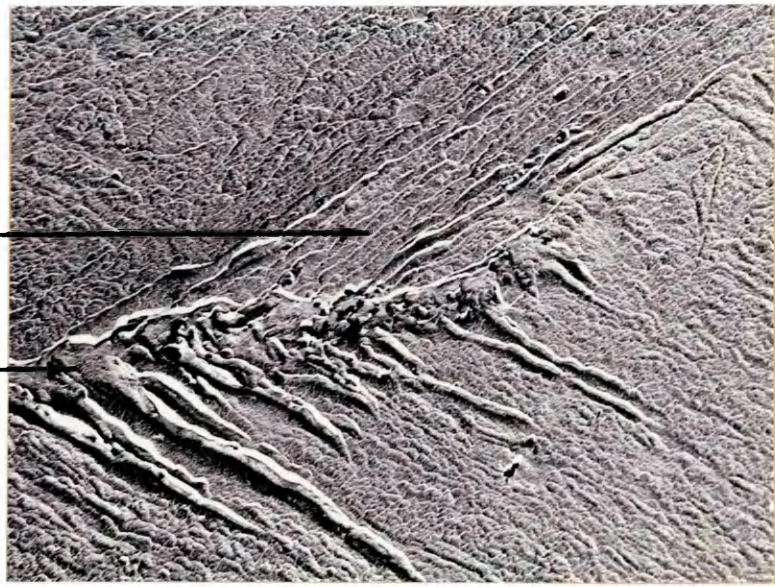


FIG. 39.

3% Nickel Blended compact. Sintered for 4 hours at 1300°C.

F = grain boundary ferrite
LB = lower bainite
UB = upper bainite

10 000 X

FIG. 40.

3% Nickel Blended compact. Sintered for 4 hours at 1300°C.

LB = lower bainite sub-units.

10 000 X

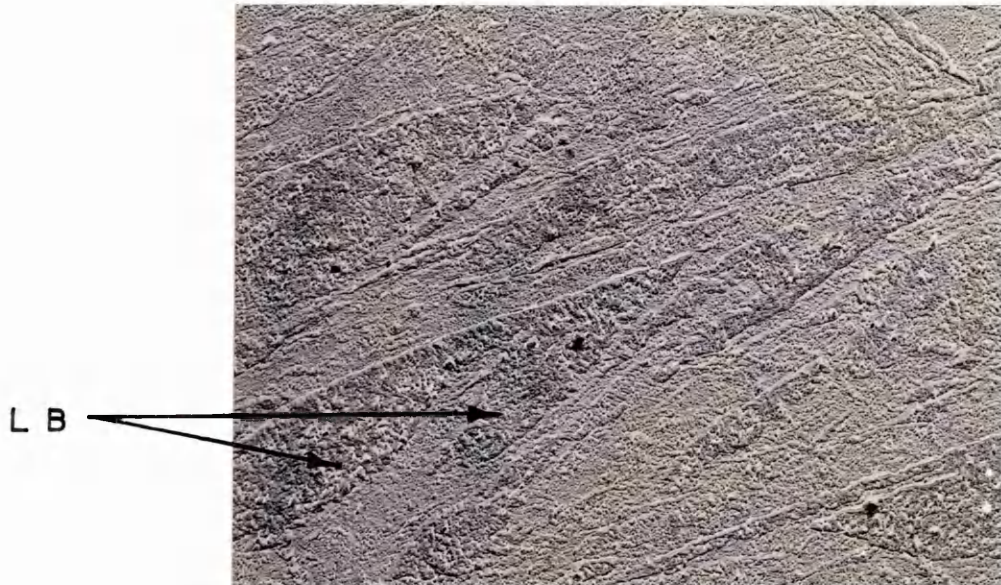
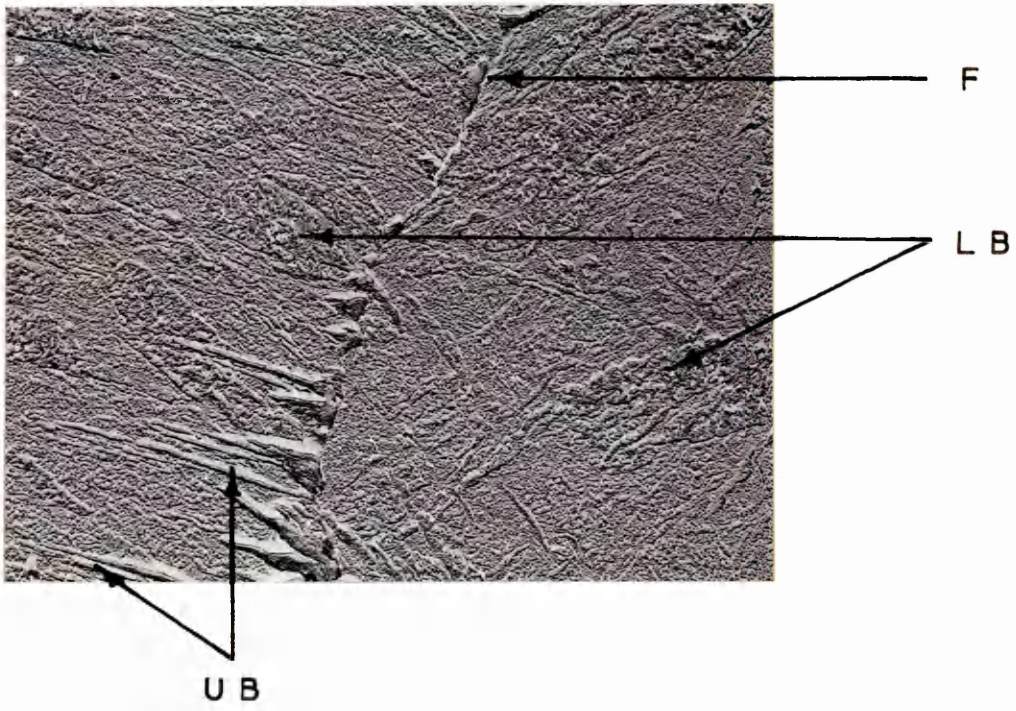


FIG. 41.

3% Nickel Blended compact. Sintered for 8 hours at
1300°C.

10 000 X

FIG. 42.

3% Nickel Blended compact. Sintered for 8 hours at
1300°C.

10 000 X



FIG. 43.

3% Nickel Blended compact. Sintered for 8 hours at 1300°C.

L = lath martensite
A = acicular martensite

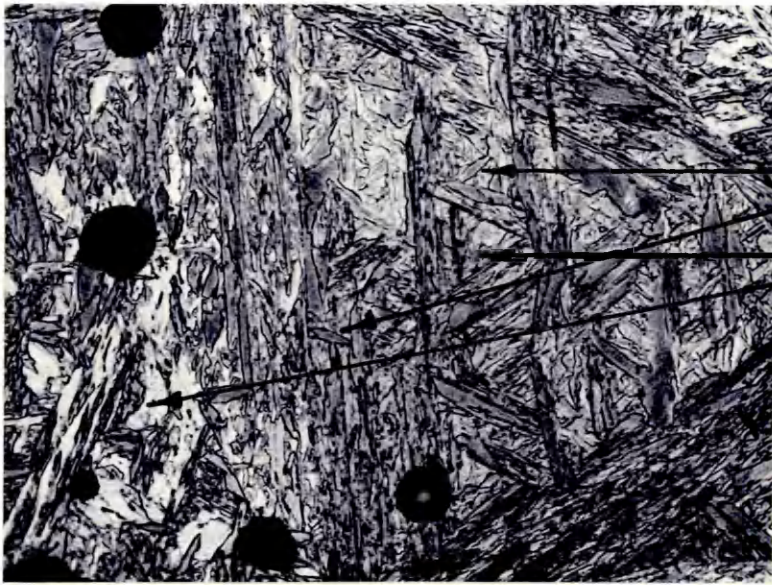
1000 X

FIG. 44.

3% Nickel Blended compact. Sintered for 8 hours at 1300°C.

XP = convex shaped porosity

160 X



A

L

X P



FIG. 45.

3% Nickel Plated compact. Sintered for 15 minutes at 1150°C.

NP = nickel particle agglomerates
N = nickel-rich network

160 X

FIG. 46.

3% Nickel Plated compact. Sintered for 15 minutes at 1150°C. Tempered for 1 hour at 600°C.

IP = interconnected porosity

160 X

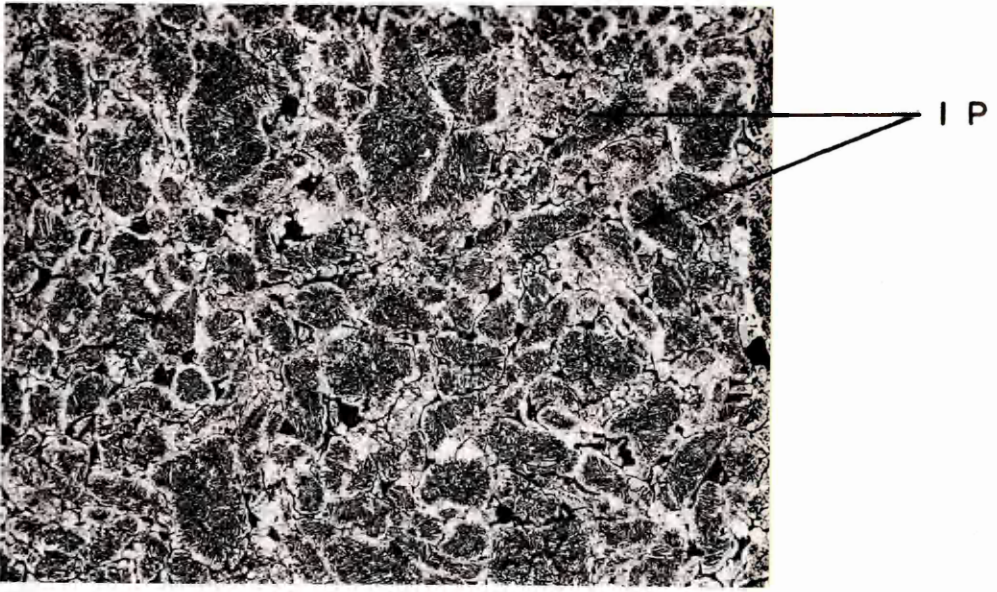
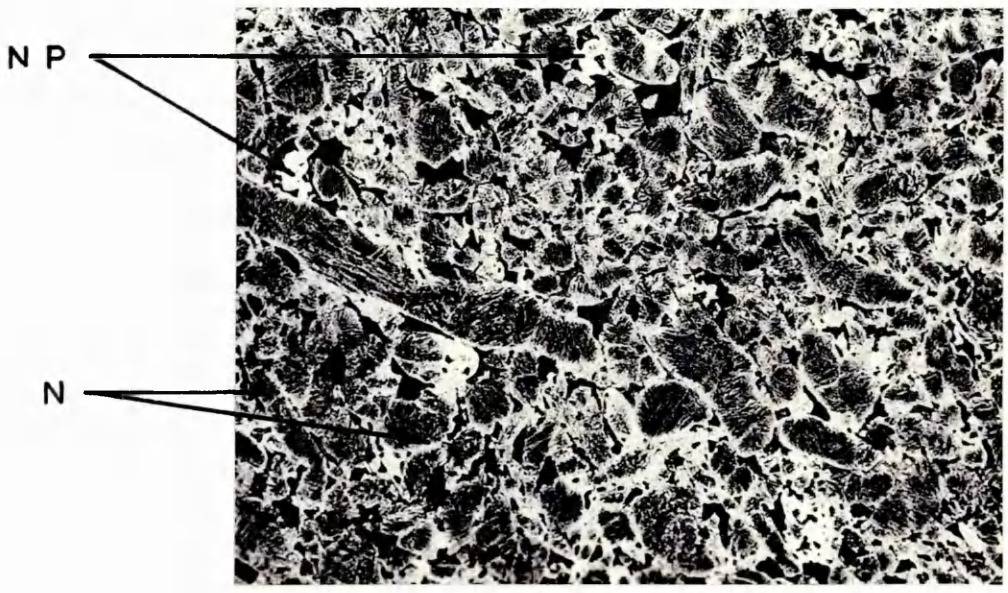


FIG. 47.

3% Nickel Plated compact. Sintered for 15 minutes at 1150°C.

UB = upper bainite

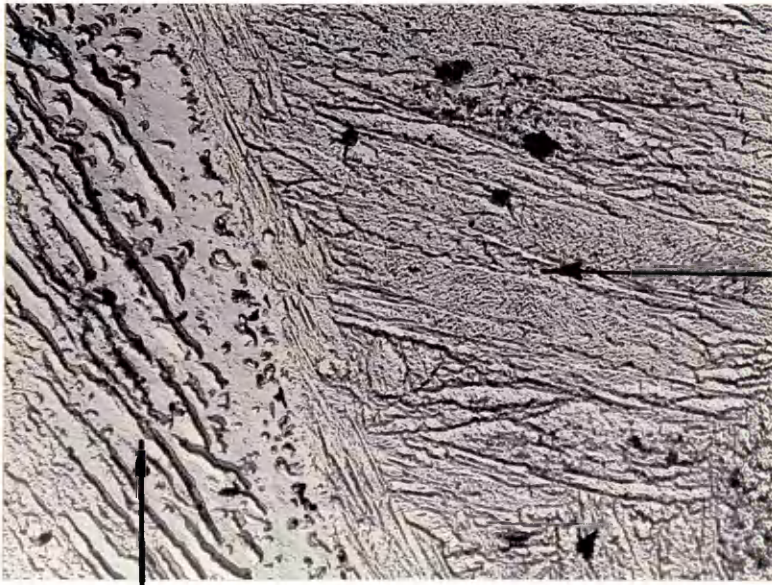
LB/M = lower bainite-martensite aggregate

10 000 X

FIG. 48.

3% Nickel Plated compact. Sintered for 15 minutes at 1150°C.

10 000 X



U B

L B/ M

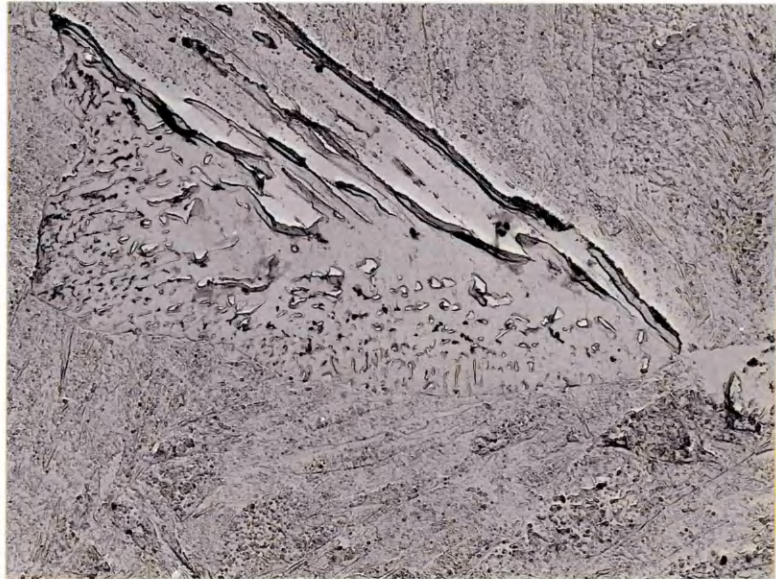


FIG. 49.

3% Nickel Plated compact. Sintered for 1 hour at
1150°C.

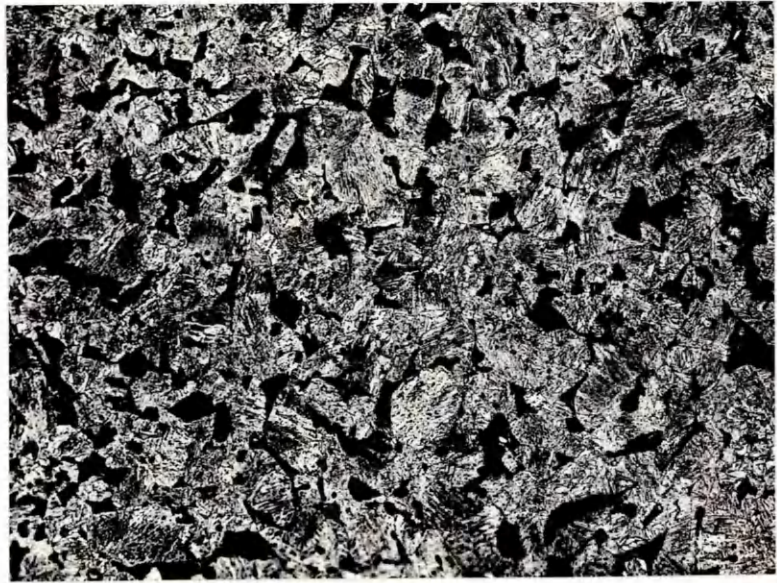
160 X

FIG. 50.

3% Nickel Plated compact. Sintered for 1 hour at
1150°C.

IP = interconnected porosity
L = lath martensite

1000 X



L

IP

FIG. 51.

3% Nickel Plated compact. Sintered for 8 hours at
1150°C.

1000 X

FIG. 52.

3% Nickel Plated compact. Sintered for 15 minutes at
1300°C.

160 X

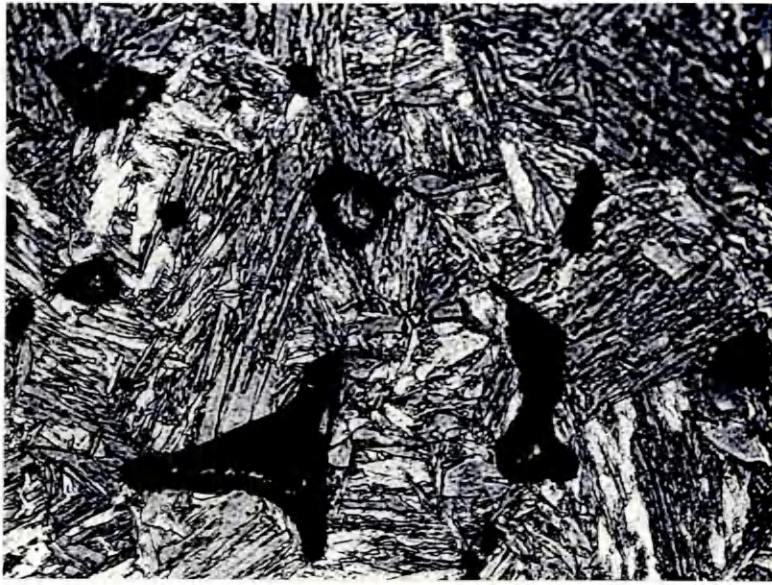


FIG. 53.

3% Nickel Plated compact. Sintered for 15 minutes at
1300°C.

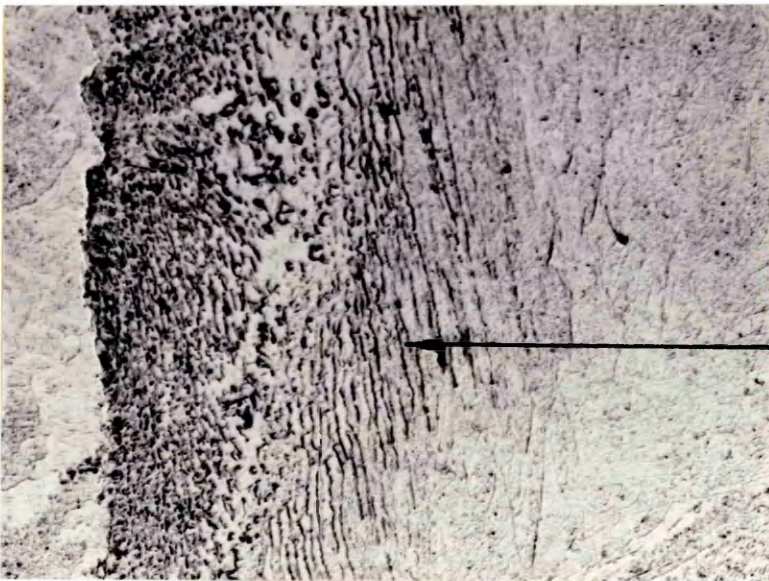
1000 X

FIG. 54.

3% Nickel Plated compact. Sintered for 15 minutes at
1300°C.

UB = upper bainite

10 000 X



UB

FIG. 55.

3% Nickel Plated compact. Sintered for 15 minutes at 1300°C.

LB = lower bainite

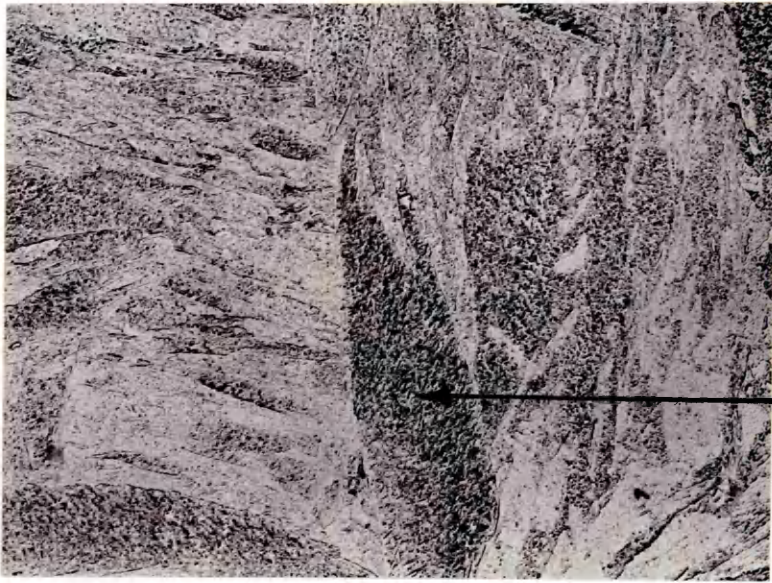
10 000 X

FIG. 56.

3% Nickel Plated compact. Sintered for 15 minutes at 1300°C.

F = ferrite

10 000 X



LB



F

FIG. 57.

3% Nickel Plated compact. Sintered for 8 hours at
1300°C.

XP = convex shaped porosity

160 X

FIG. 58.

3% Nickel Plated compact. Sintered for 4 hours at
1300°C.

10 000 X

X P

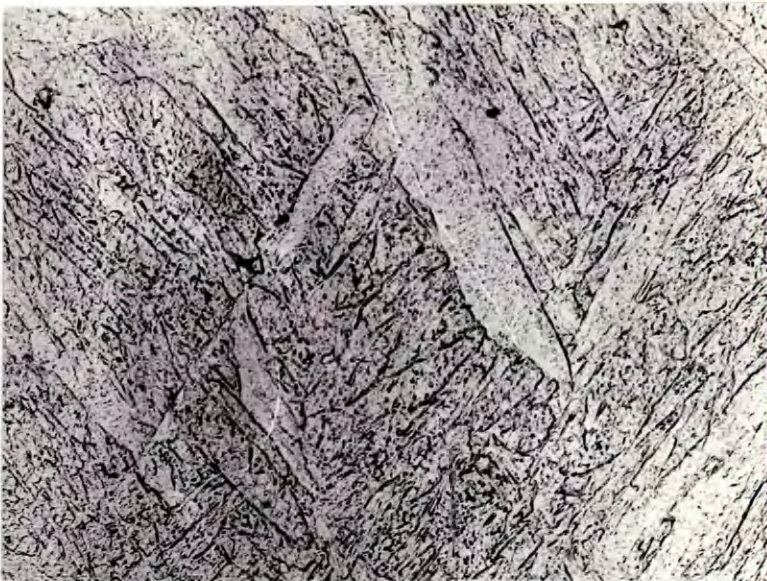
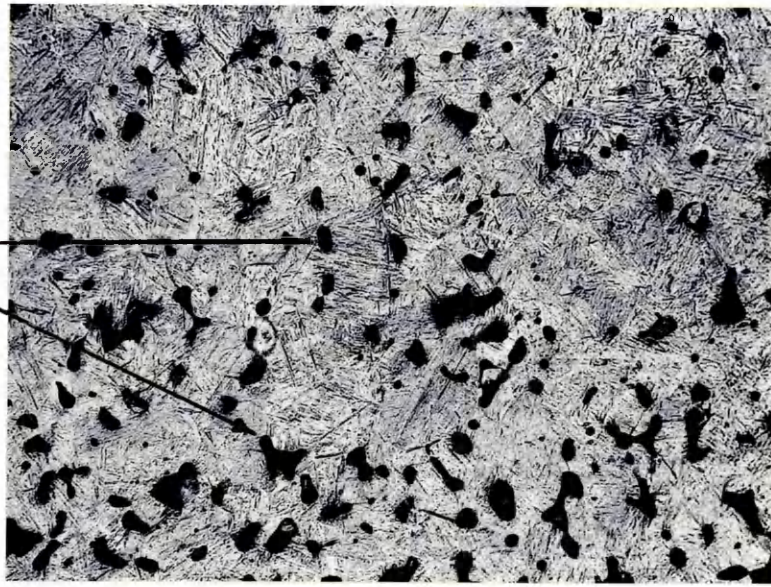


FIG. 59.

3% Nickel Pre-alloyed compact. Sintered for 15 minutes
at 1150°C.

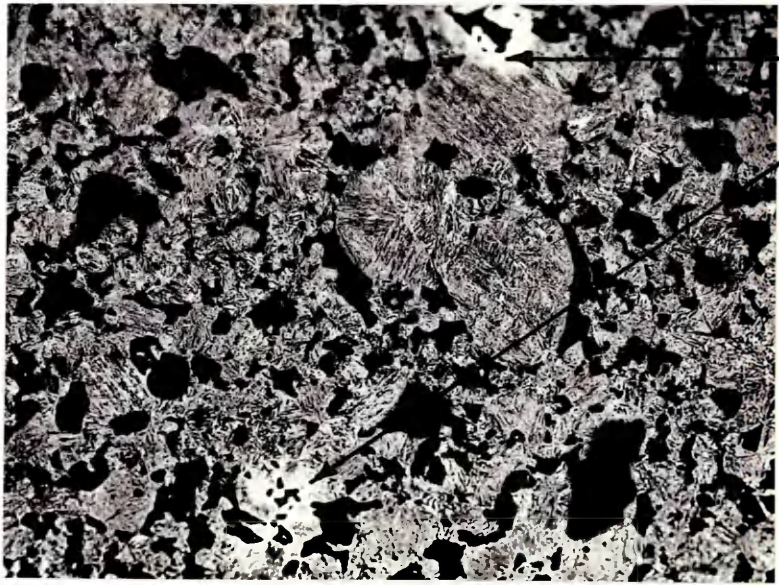
LE = light-etching areas.

160 X

FIG. 60.

3% Nickel Pre-alloyed compact. Sintered for 30 minutes
at 1150°C.

160 X



LE

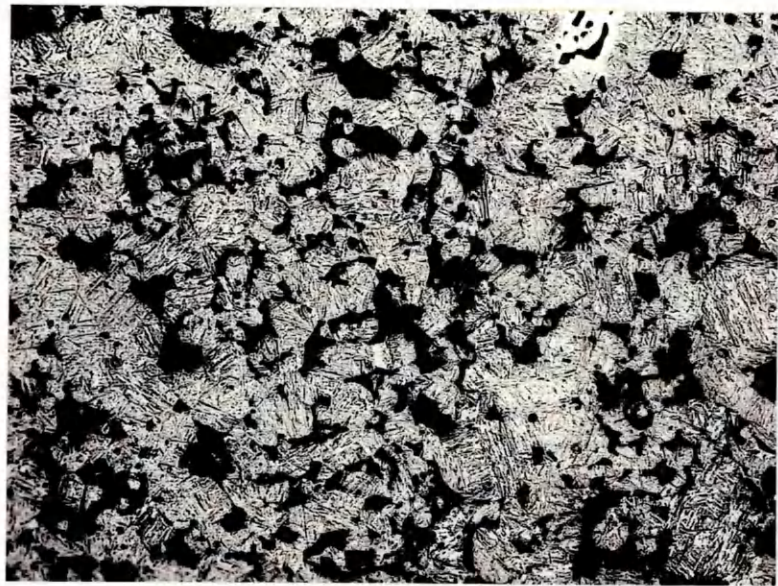


FIG. 61.

3% Nickel Pre-alloyed compact. Sintered for 1 hour
at 1150°C.

160 X

FIG. 62.

3% Nickel Pre-alloyed compact. Sintered for 2 hours
at 1150°C.

160 X

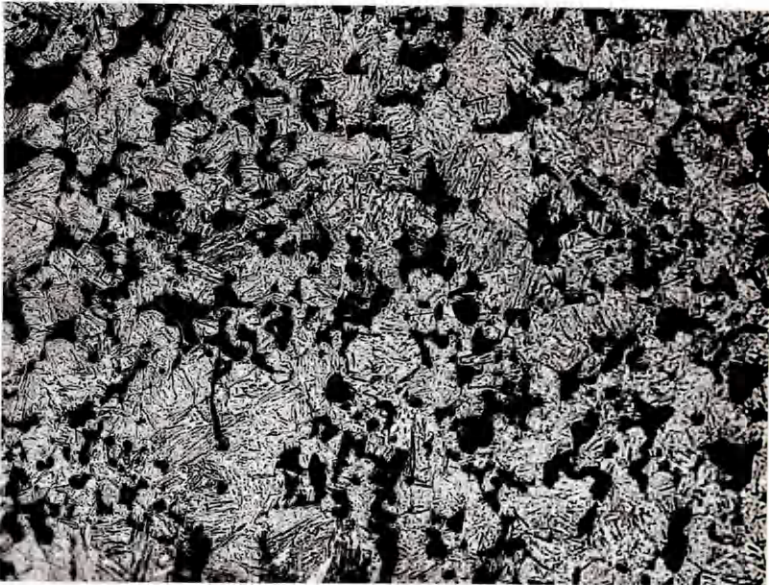
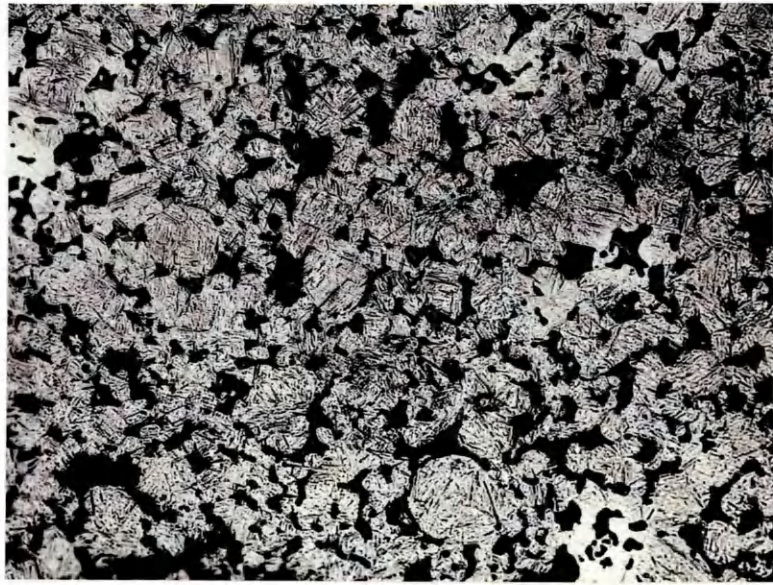


FIG. 63 (a).

Analysis of light-etching areas in FIG. 59.

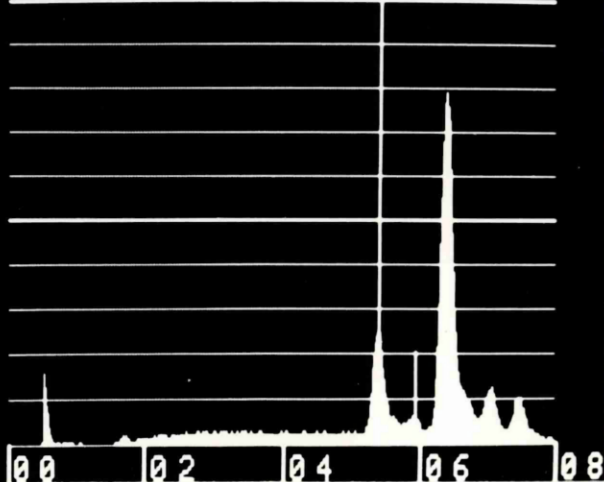
The peaks shown from left to right are $\text{Cr } \alpha$, $\text{Cr } \beta$,
 $\text{Fe } \alpha$, $\text{Fe } \beta$ and $\text{Ni } \alpha$.

FIG. 63 (b).

Analysis of martensite areas in FIG. 59.

The peaks shown from left to right are $\text{Fe } \alpha$, $\text{Fe } \beta$ and
 $\text{Ni } \alpha$.

79 5410EV K Z24 CR
VS:2500 HS: 20EV/CH



79 6400EV K Z26 FE
VS:2500 HS: 20EV/CH

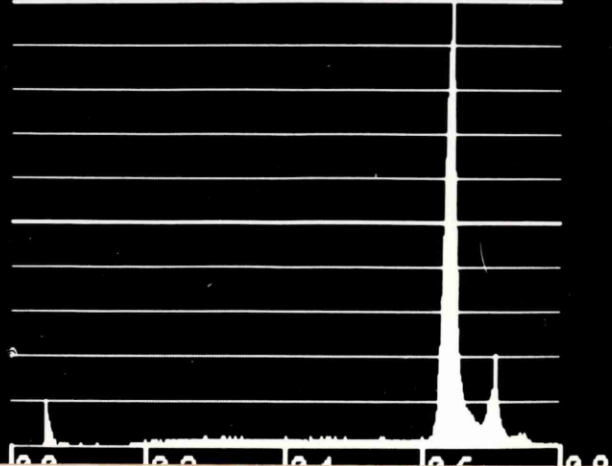


FIG. 64.

3% Nickel Pre-alloyed compact. Sintered for 15 minutes
at 1150°C.

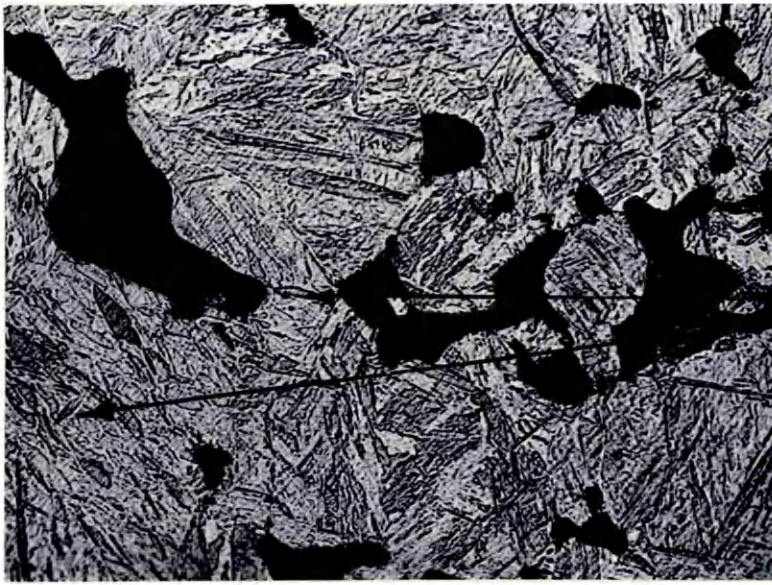
A = acicular martensite.

1000 X

FIG. 65.

3% Nickel Pre-alloyed compact. Sintered for 2 hours
at 1150°C.

1000 X



A

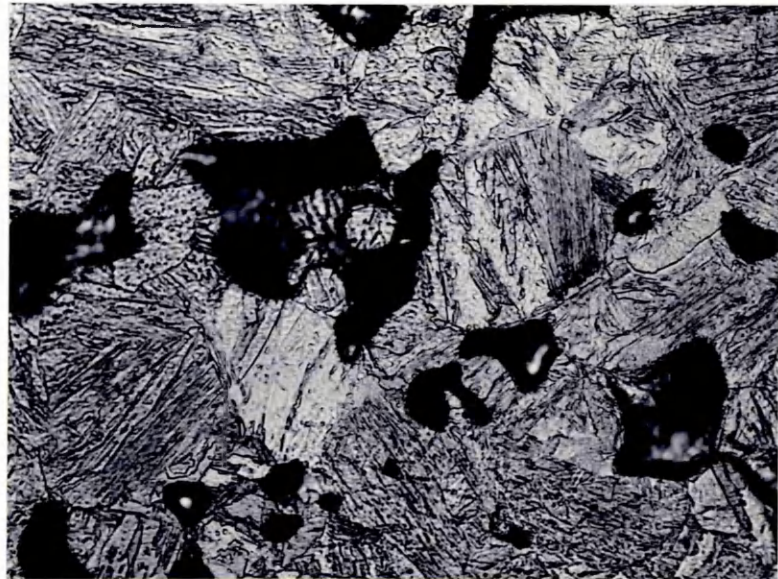


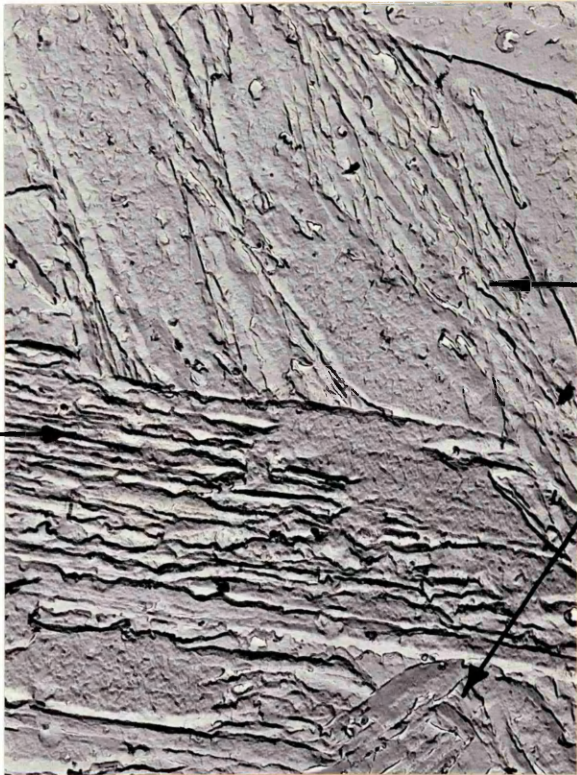
FIG. 66.

3% Nickel Pre-alloyed compact. Sintered for 8 hours
at 1150°C.

L = lath martensite

A = acicular martensite

10 000 X



L

A

FIG. 67.

3% Nickel Pre-alloyed compact. Sintered for 15 minutes
at 1150°C.

IN = new interparticle necks about to form

160 X

FIG. 68.

3% Nickel Pre-alloyed compact. Sintered for
1 hour at 1150°C.

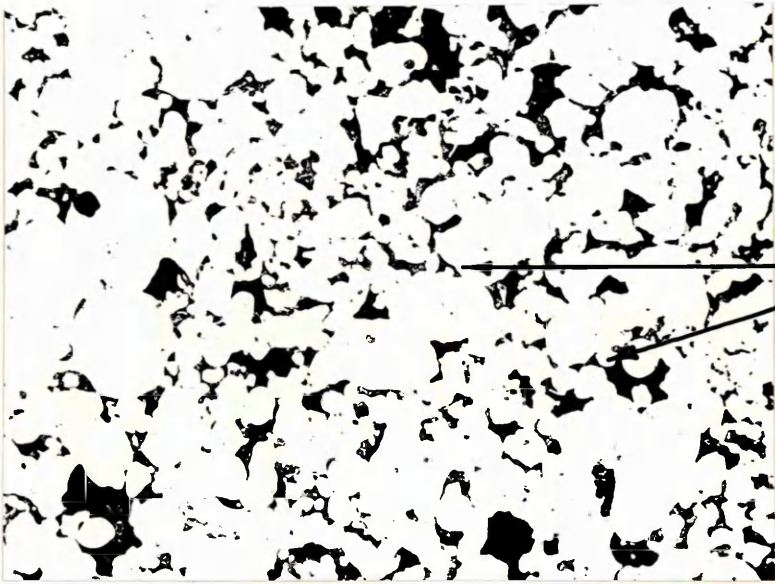
160 X

FIG. 69.

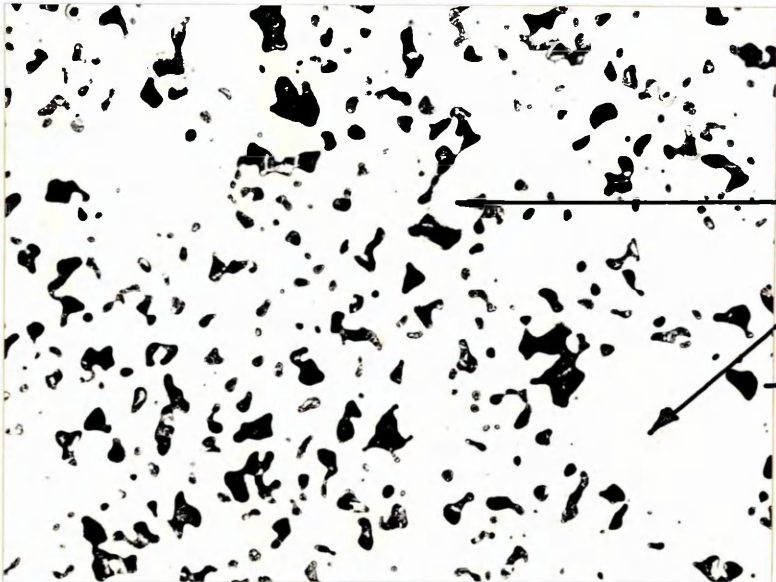
3% Nickel Pre-alloyed compact. Sintered for 8 hours
at 1150°C.

CP = coarse isolated porosity
O = original powder particles

160 X



I N



O

C P

FIG. 70.

3% Nickel Pre-alloyed compact. Sintered for 15 minutes
at 1300°C.

160 X

FIG. 71.

3% Nickel Pre-alloyed compact. Sintered for 15 minutes
at 1300°C.

1000 X

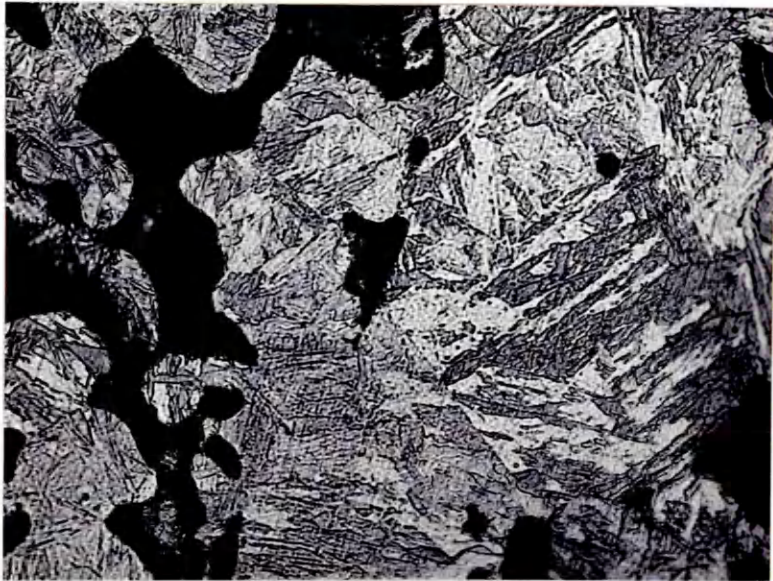


FIG. 72.

3% Nickel Pre-alloyed compact. Sintered for 15 minutes
at 1300°C.

160 X

FIG. 73.

3% Nickel Pre-alloyed compact. Sintered for
1 hour at 1300°C.

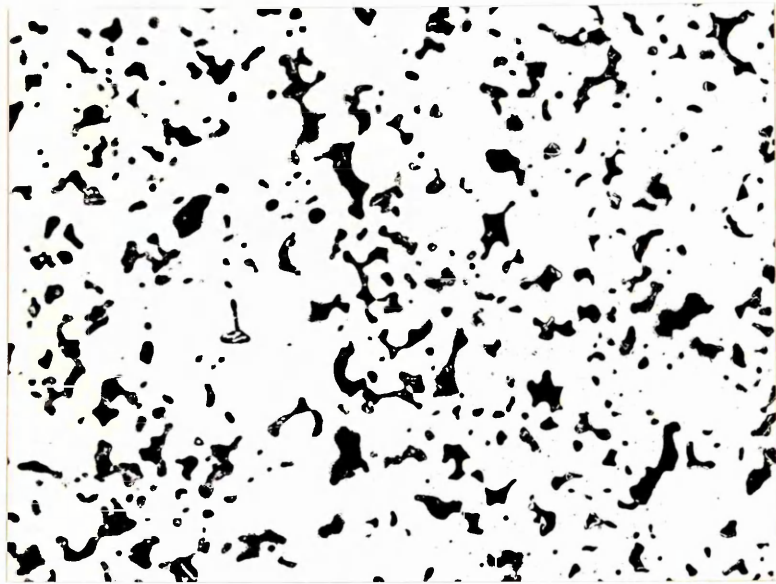
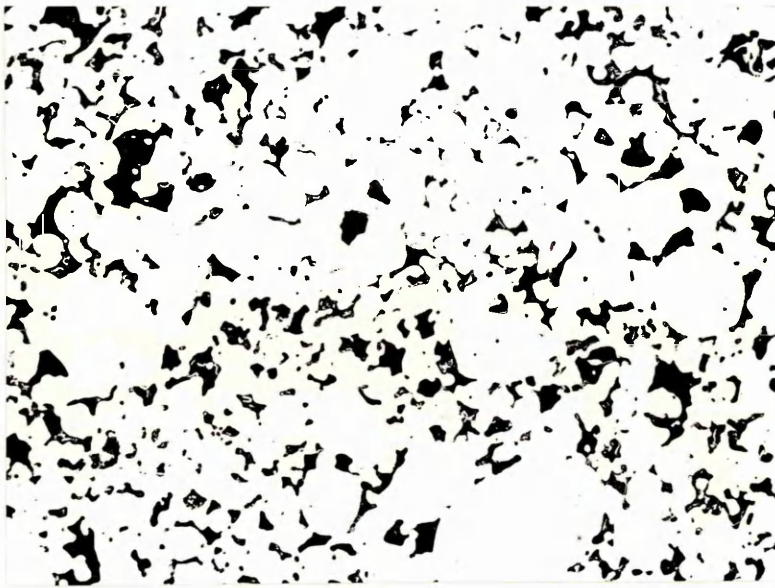
160 X

FIG. 74.

3% Nickel Pre-alloyed compact. Sintered for 8 hours
at 1300°C.

CP = coarse isolated porosity

160 X



C P

FIG. 75.

3% Nickel Blended compact. Sintered for 15 minutes
at 1150°C.

Fracture Face.

480 X

FIG. 76.

3% Nickel Blended compact. Sintered for 15 minutes
at 1150°C.

Fracture Face.

IP = interconnected porosity
IN = interparticle neck
NP = nickel-rich particle
DF = ductile fracture
SS = smooth unsintered surface

1920 X

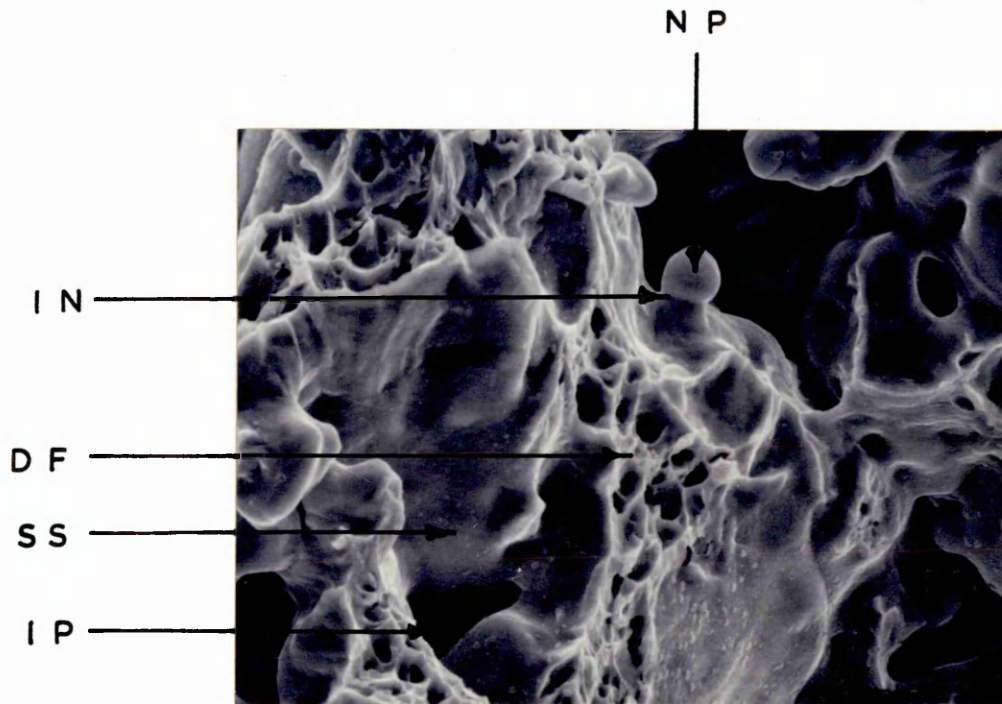
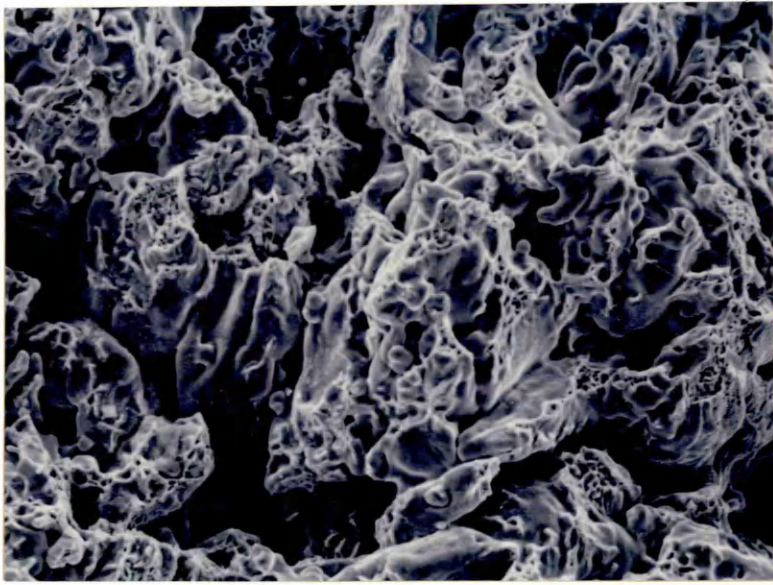


FIG. 77.

3% Nickel Plated compact. Sintered for 15 minutes
at 1150°C.

Fracture Face.

440 X

FIG. 78.

3% Nickel Plated compact. Sintered for 15 minutes
at 1150°C.

Fracture Face.

1600 X

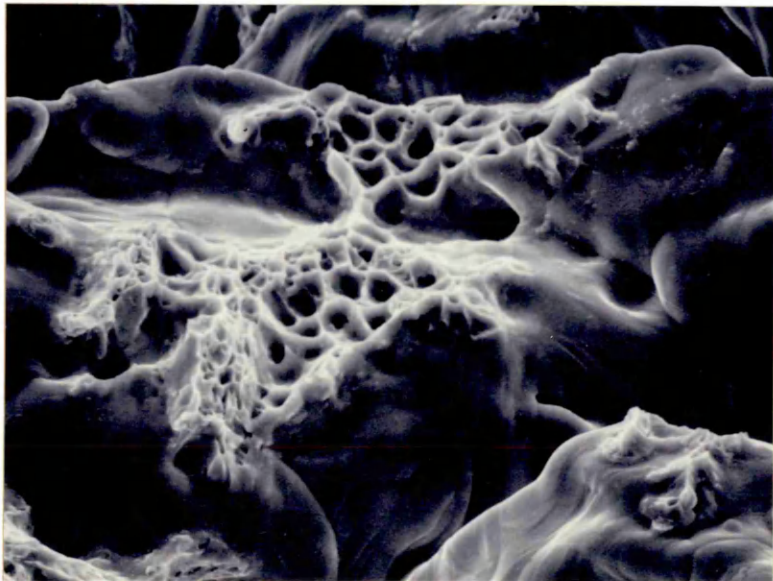
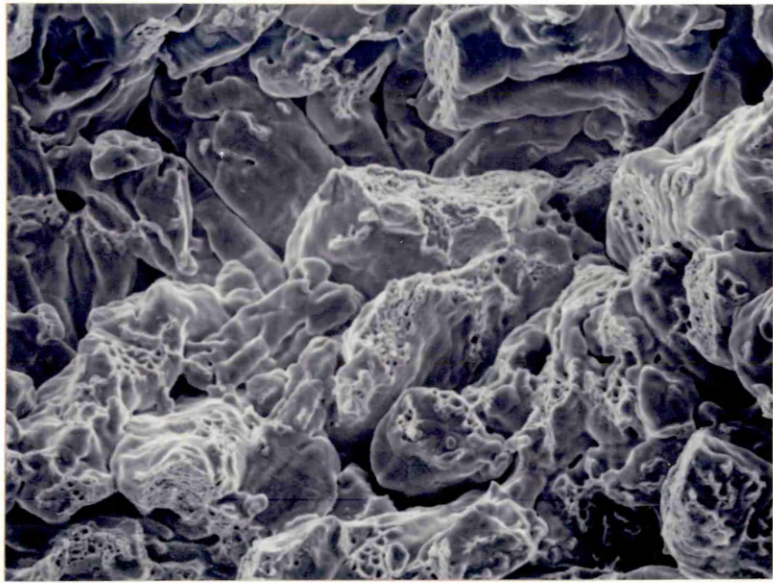


FIG. 79.

3% Nickel Pre-alloyed compact. Sintered for 15 minutes
at 1150°C.

Fracture Face.

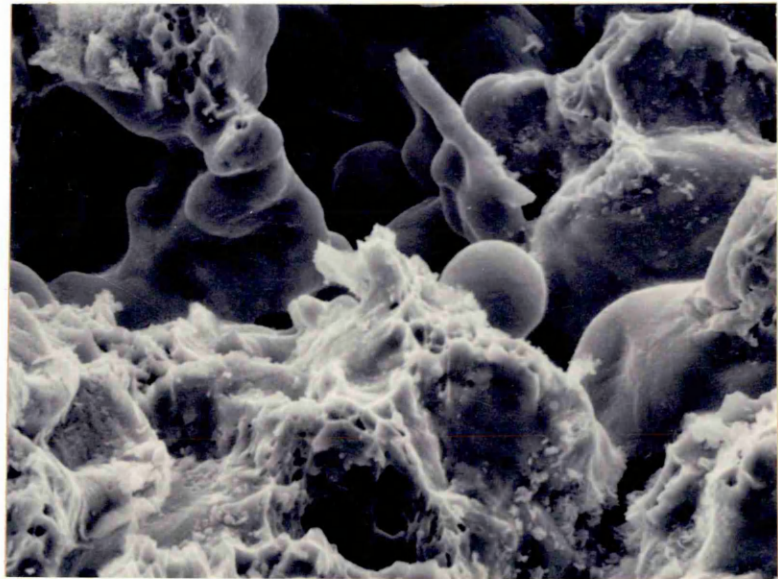
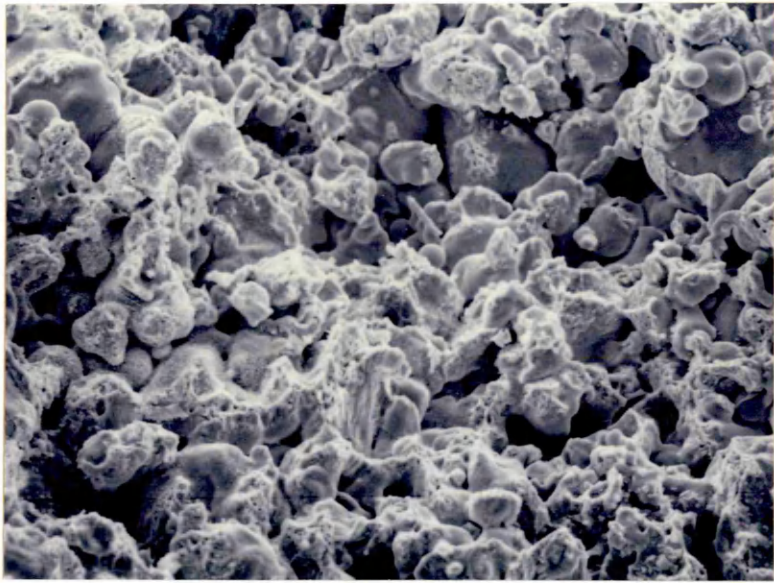
480 X

FIG. 80.

3% Nickel Pre-alloyed compact. Sintered for 15 minutes
at 1150°C.

Fracture Face.

1760 X



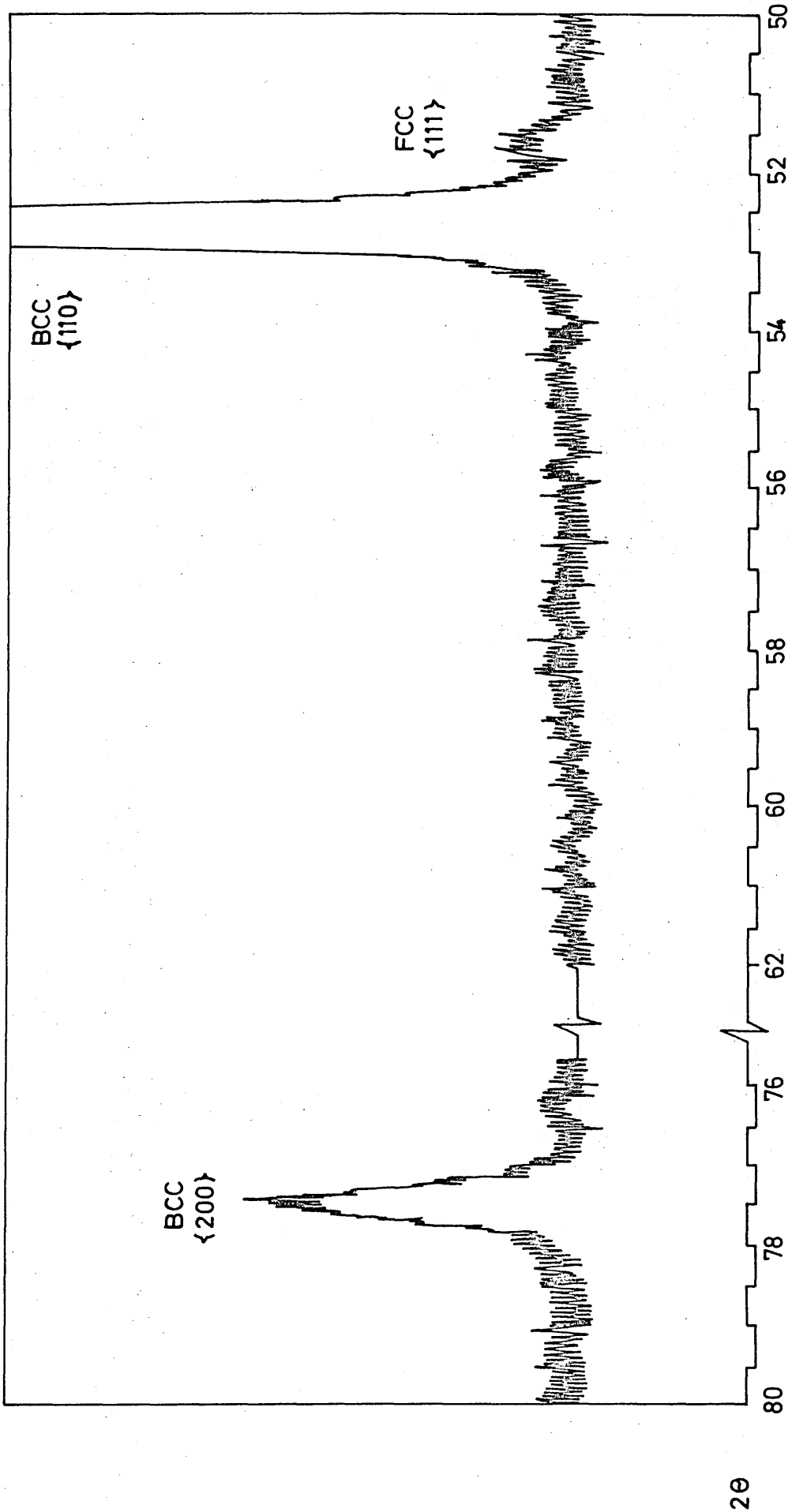


FIG. 81 X-RAY DIFFRACTOMETER CHART RECORD FOR PLATED 3% NICKEL ALLOY (ISOSTATICALLY PRESSED) SINTERED FOR 15 MINUTES AT 1150°C

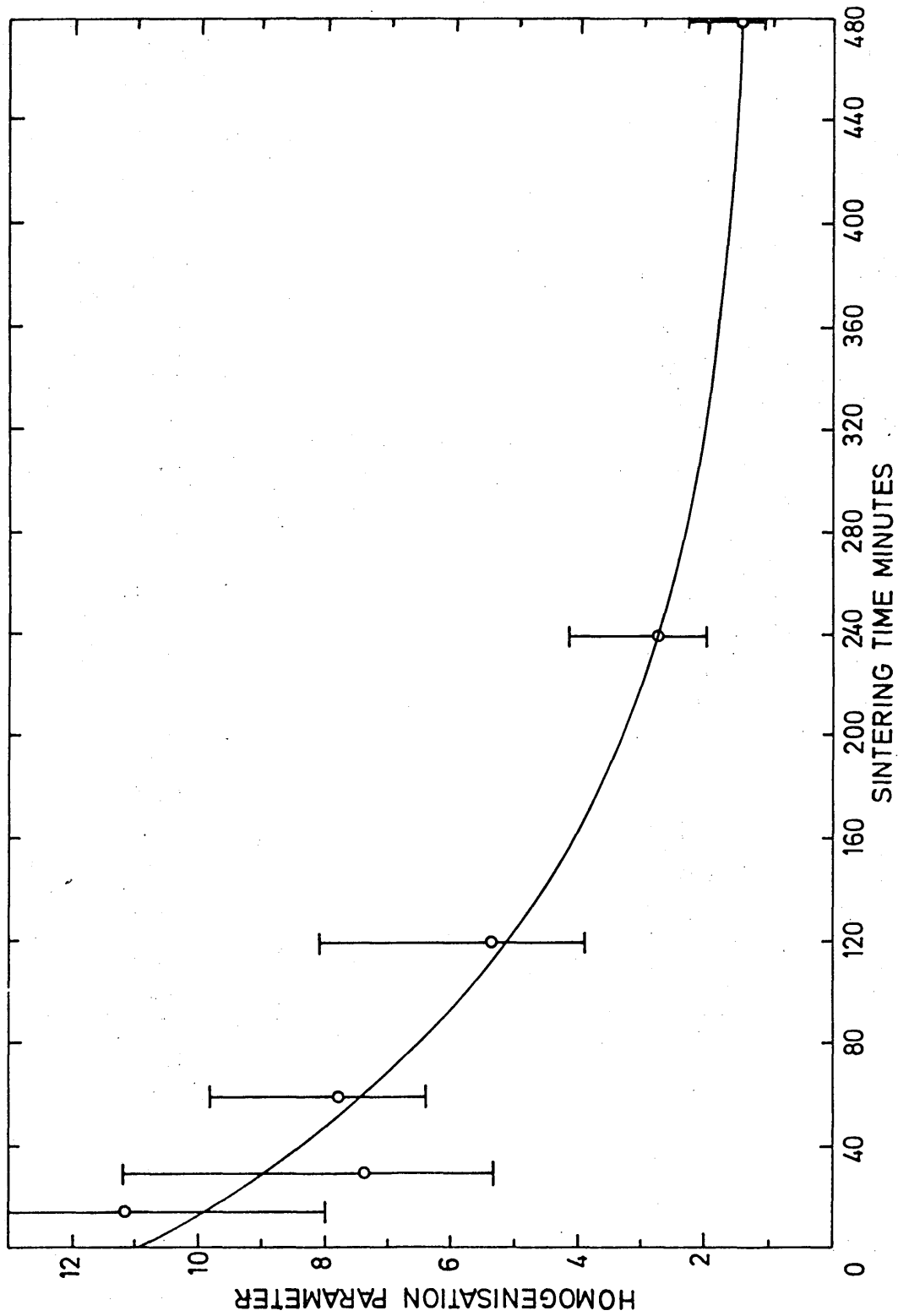


FIG. 82 AREAL ANALYSIS OF IRON: 3% NICKEL ALLOYS (BLENDED) SINTERED AT 1150°C
 PROBE MAGNIFICATION 4800x

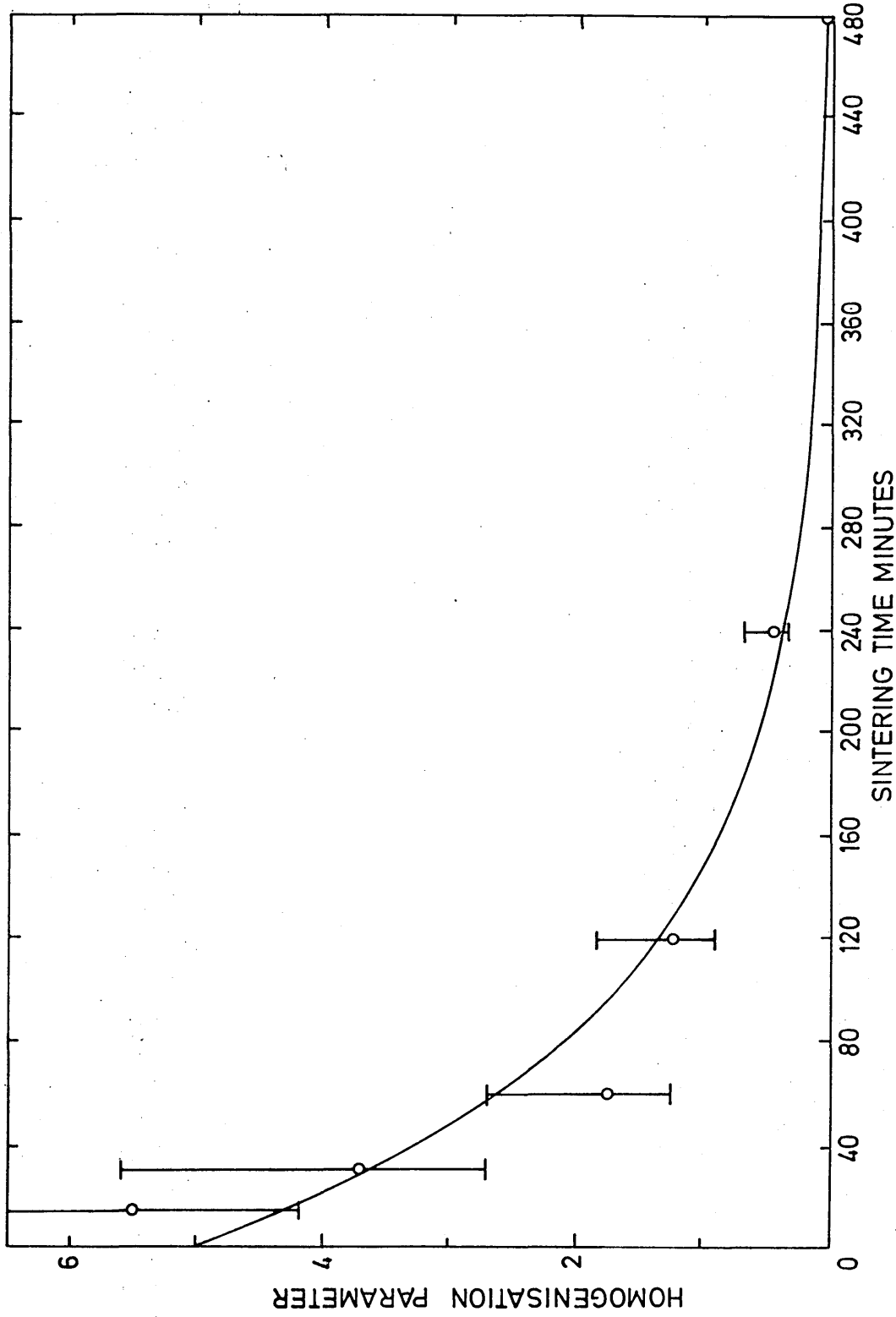


FIG. 83 AREAL ANALYSIS OF IRON: 3% NICKEL ALLOYS (BLENDED) SINTERED AT 1300°C
 PROBE MAGNIFICATION 4800x

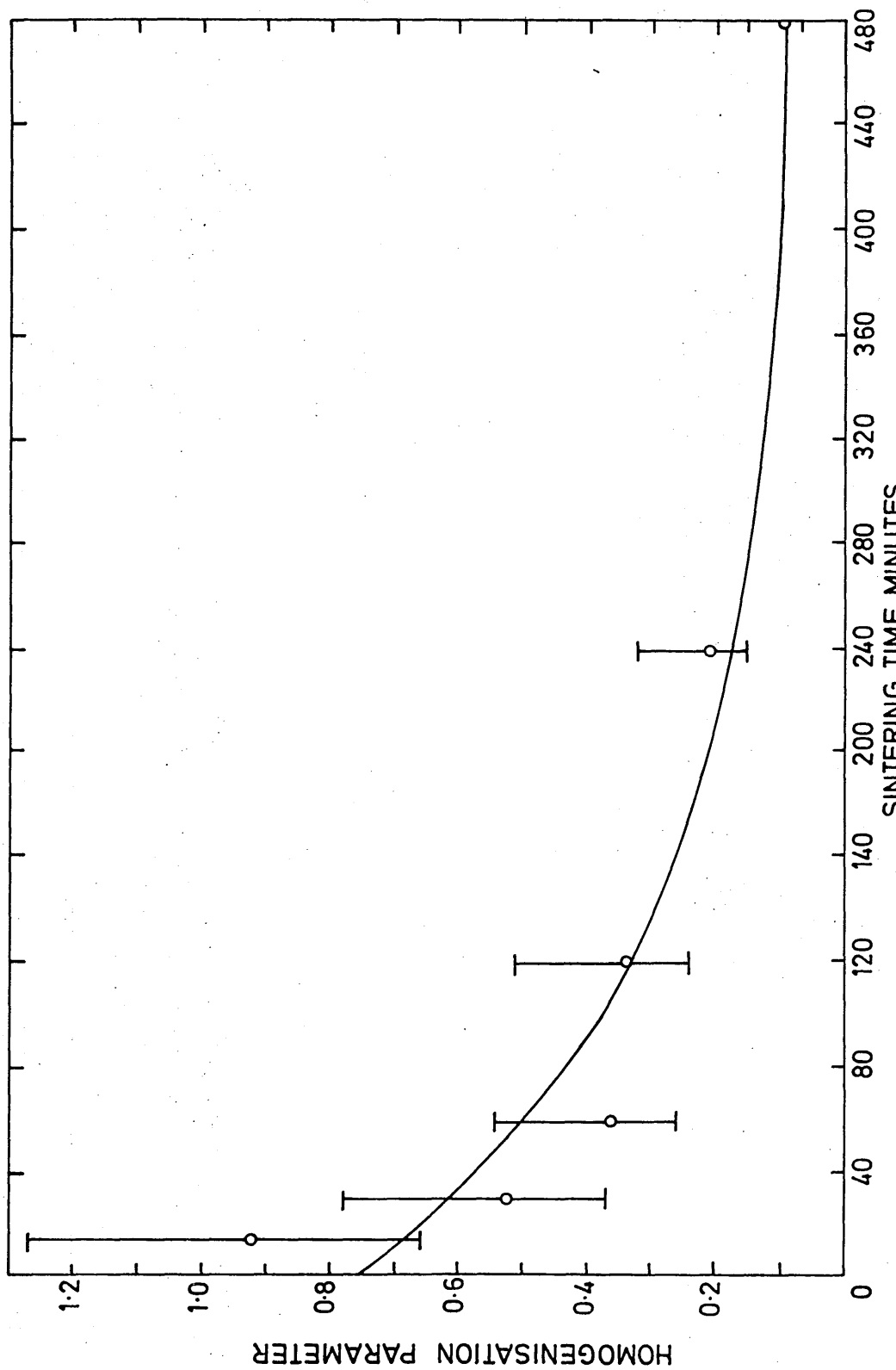


FIG. 84 AREAL ANALYSIS OF IRON 3% NICKEL ALLOYS (PLATED) SINTERED AT 1150°C
PROBE MAGNIFICATION 4800 x

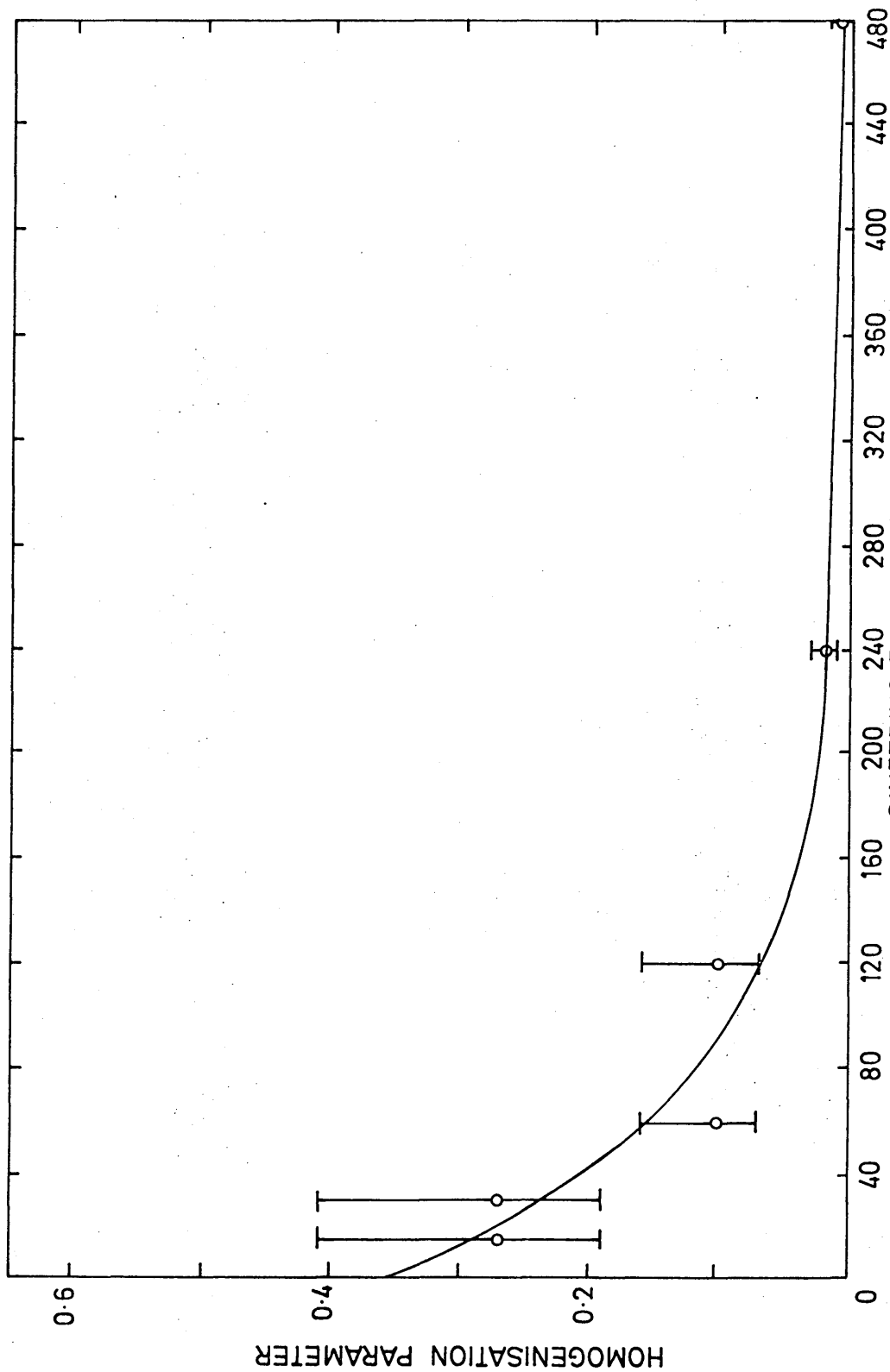


FIG. 85 AREAL ANALYSIS OF IRON: 3% NICKEL ALLOYS (PLATED) SINTERED AT 1300°C
PROBE MAGNIFICATION 4800x

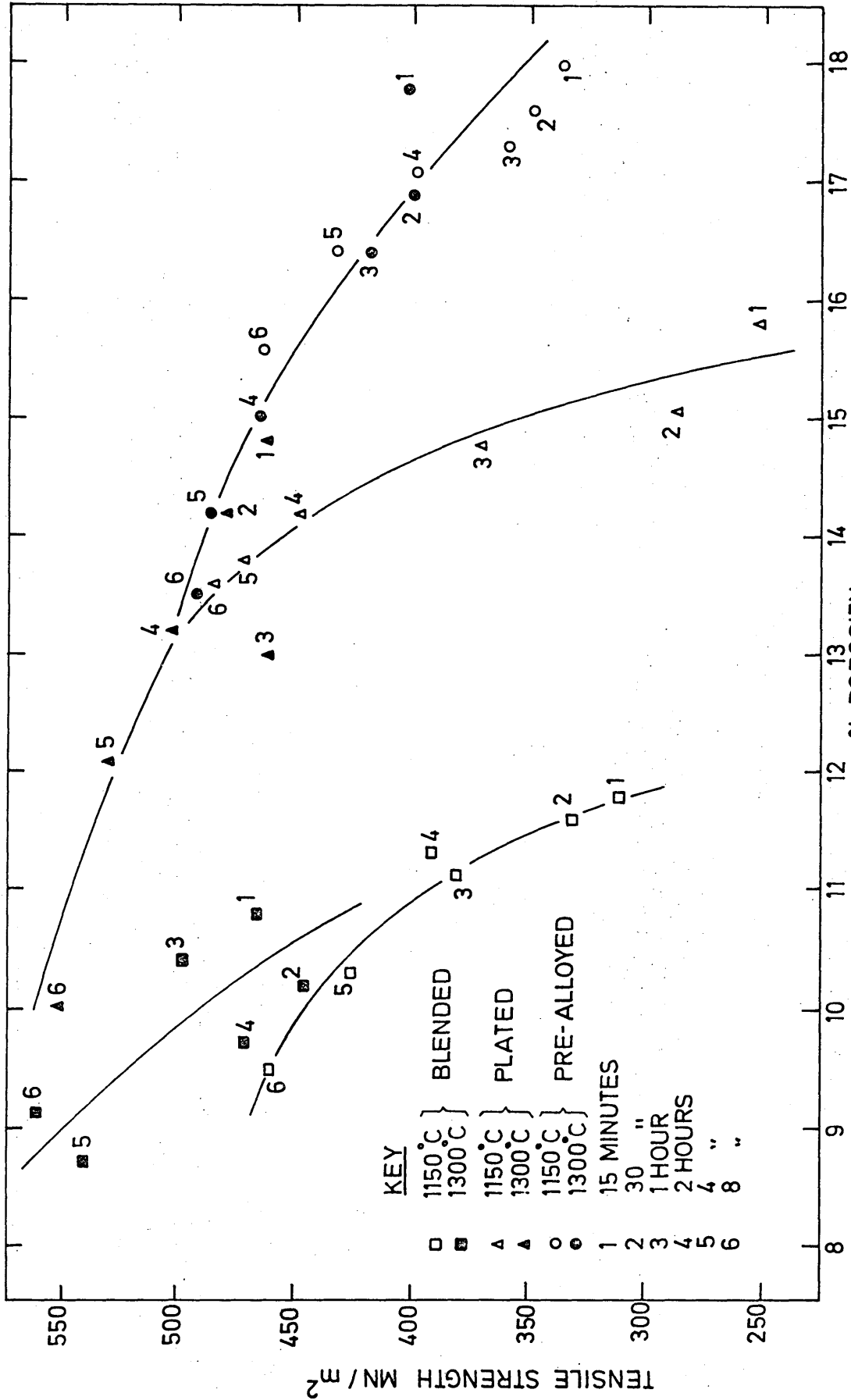
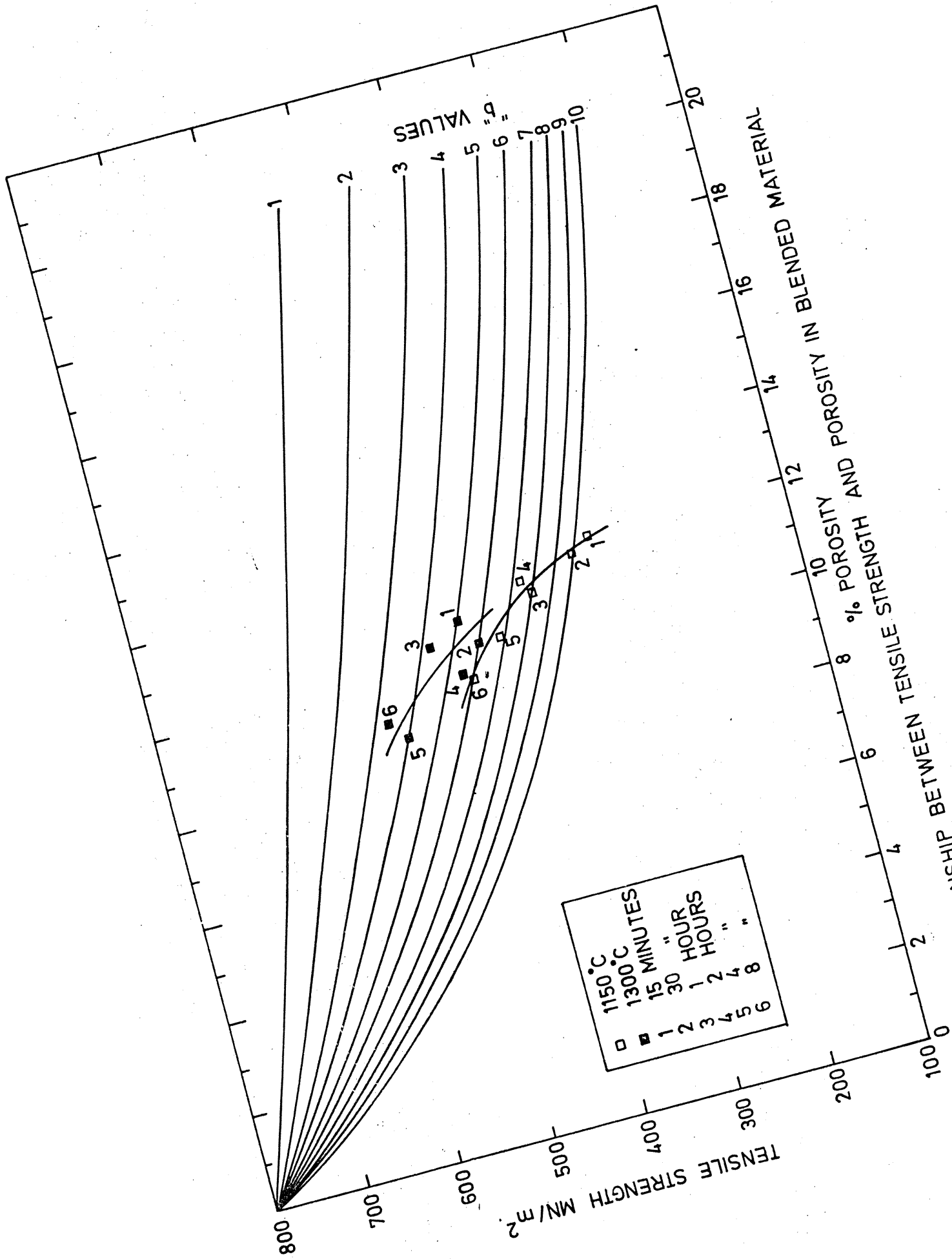
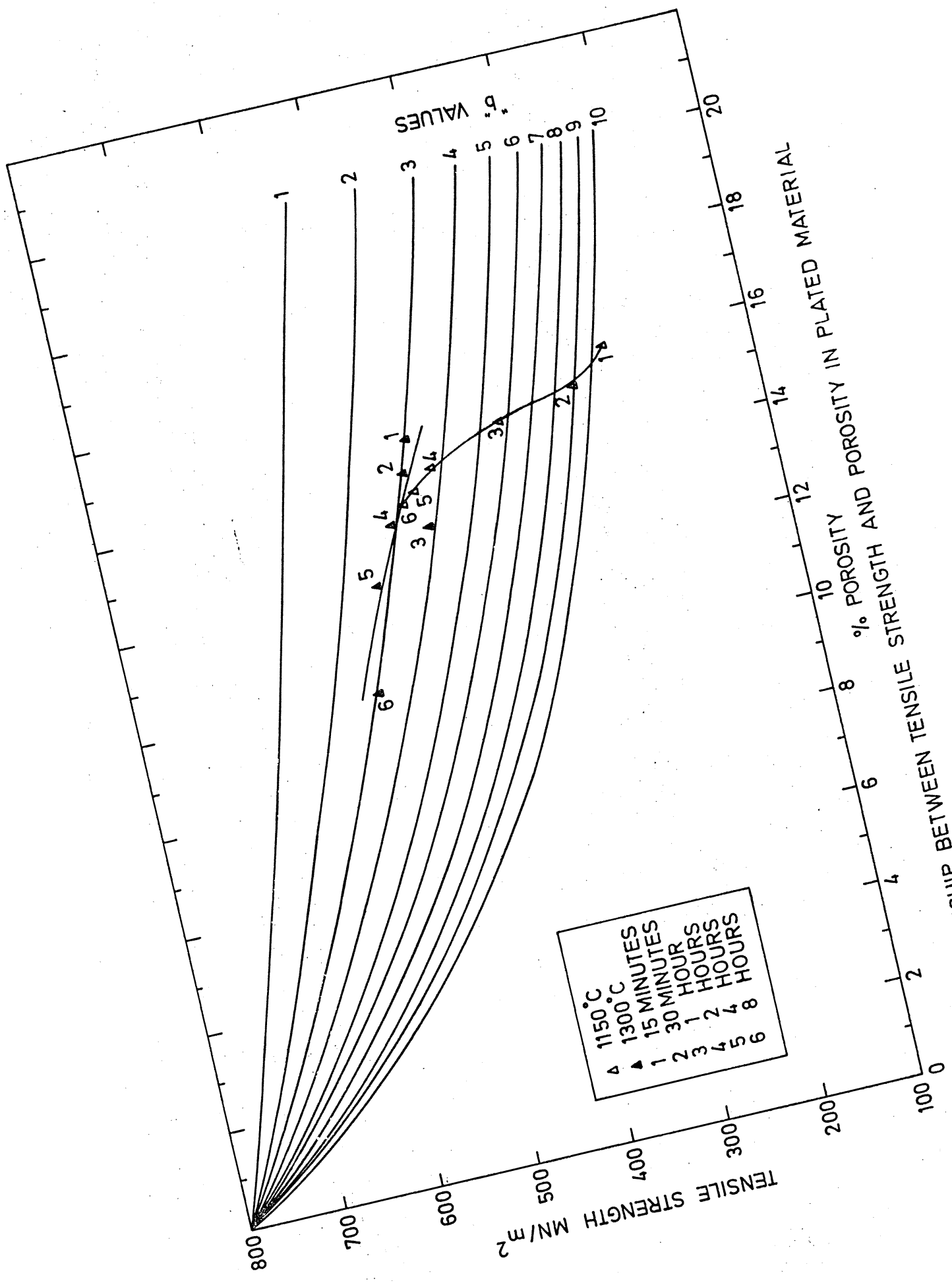


FIG 86 RELATIONSHIP BETWEEN TENSILE STRENGTH AND POROSITY IN BLENDED, PLATED AND PRE-ALLOYED MATERIALS.



RELATIONSHIP BETWEEN TENSILE STRENGTH AND POROSITY IN BLENDED MATERIAL

FIG. 87



RELATIONSHIP BETWEEN TENSILE STRENGTH AND POROSITY IN PLATED MATERIAL

FIG. 88

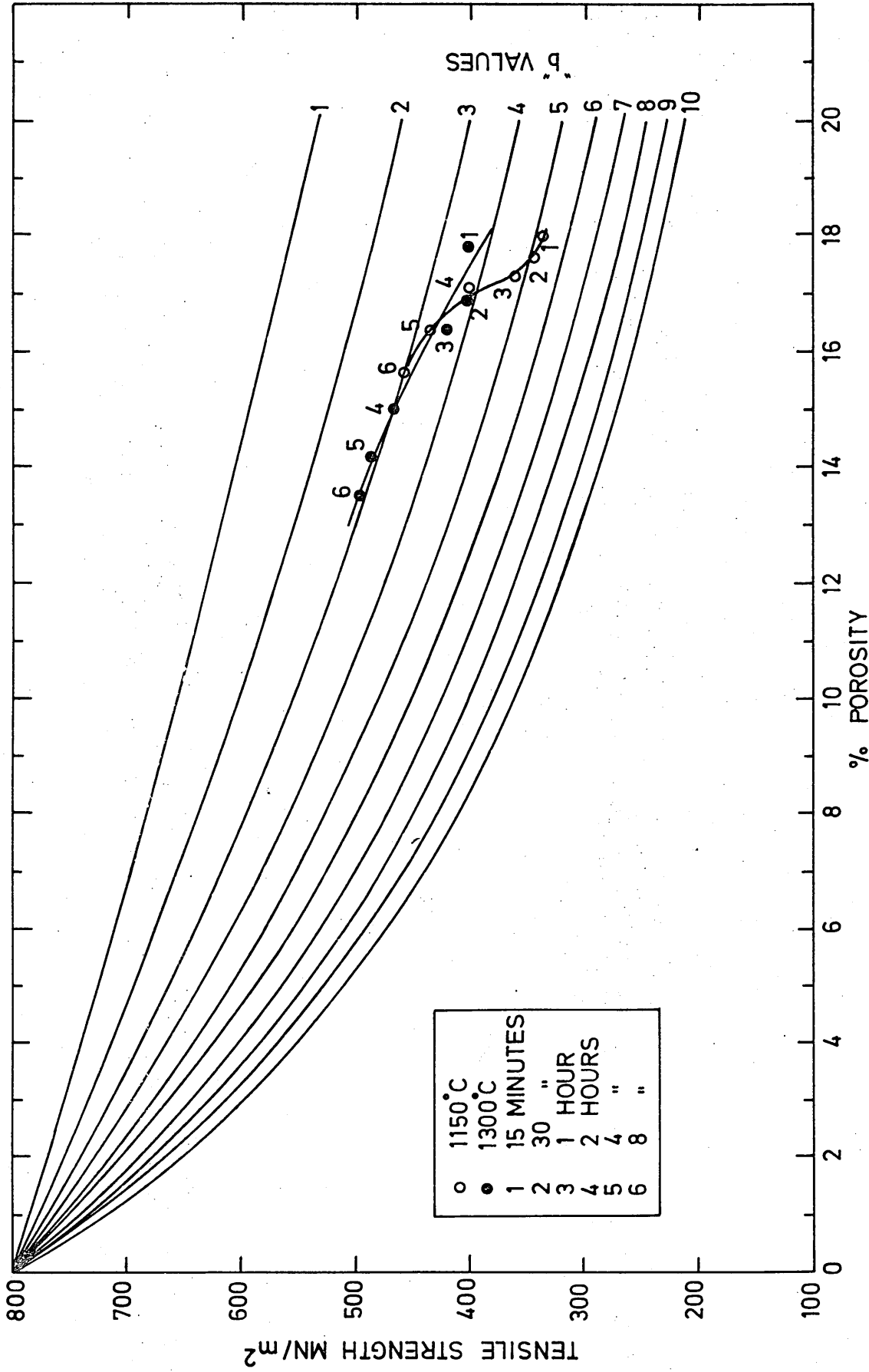


FIG. 89 RELATIONSHIP BETWEEN TENSILE STRENGTH AND POROSITY IN PRE-ALLOYED MATERIAL

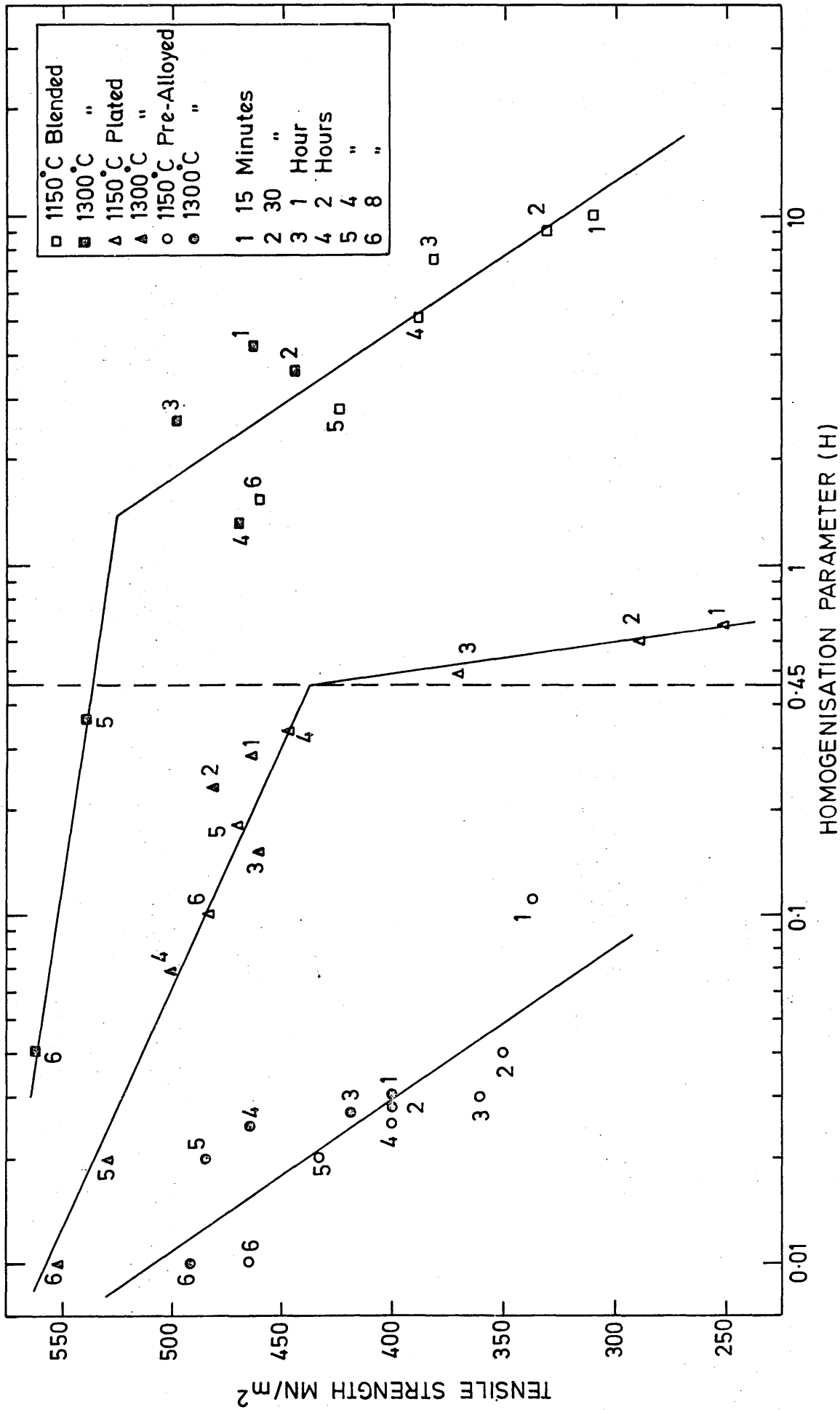


FIG. 90 RELATIONSHIP BETWEEN TENSILE STRENGTH AND HOMOGENISATION PARAMETER IN BLENDED, PLATED AND PRE-ALLOYED MATERIALS.

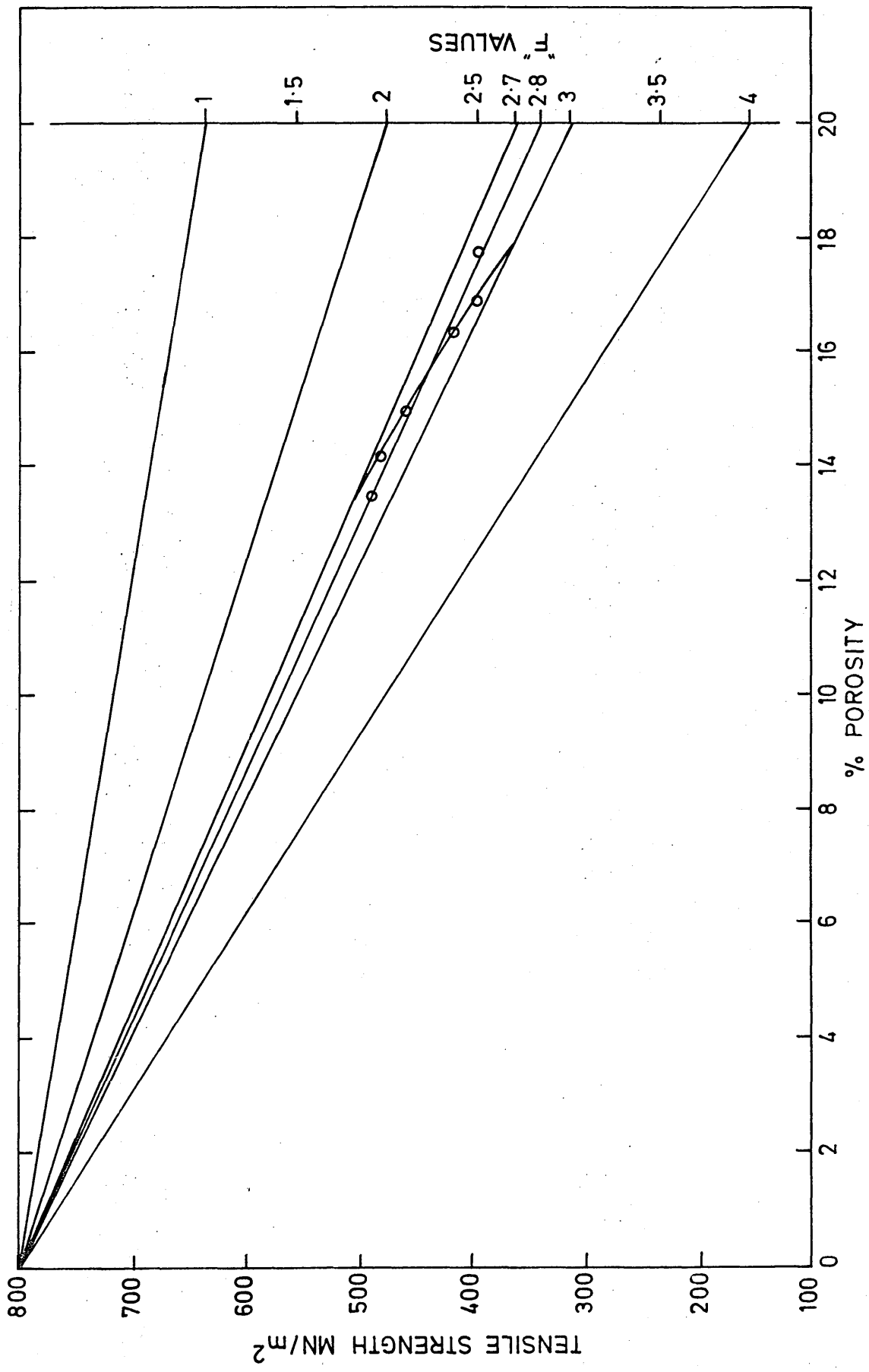
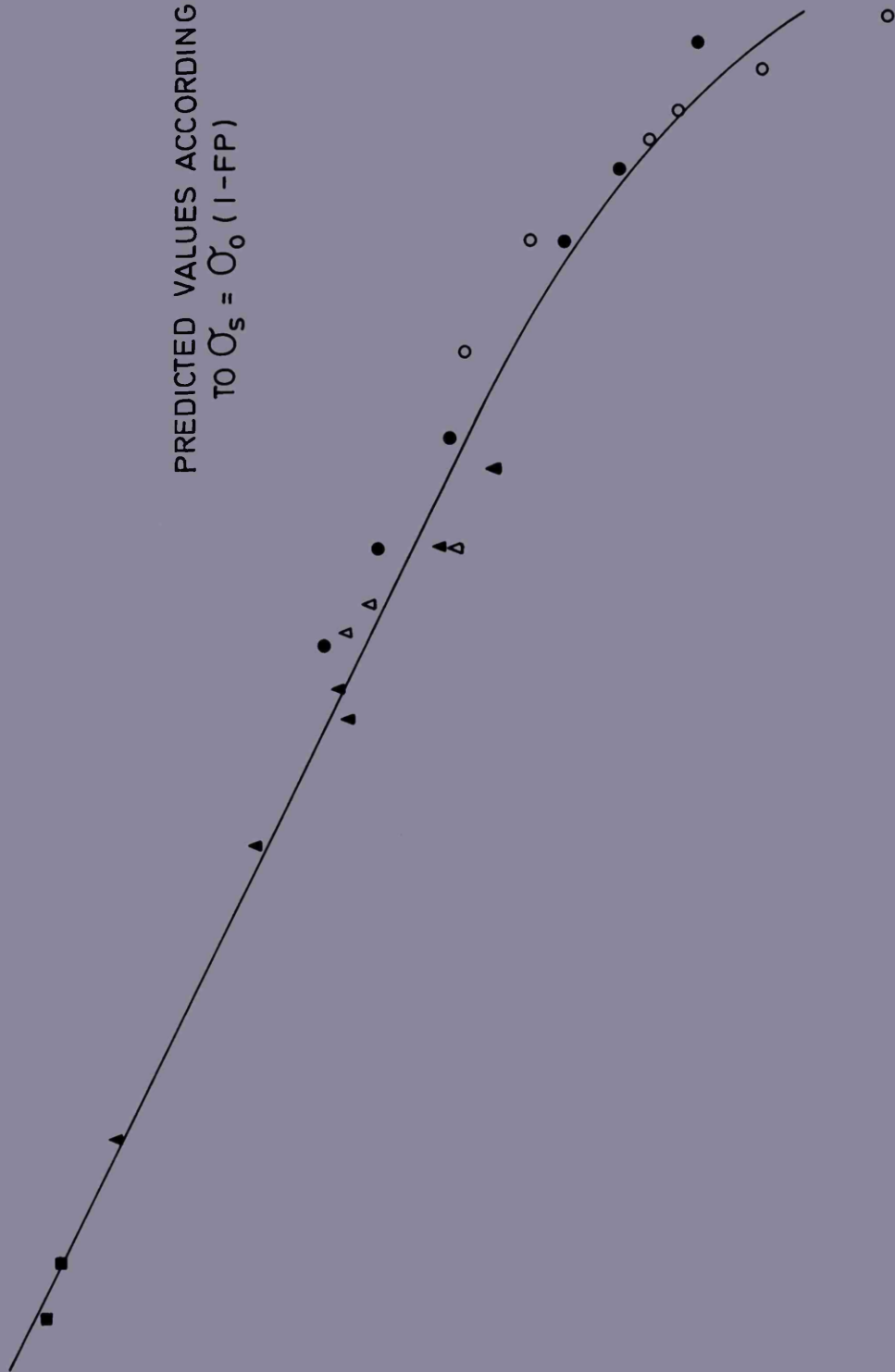
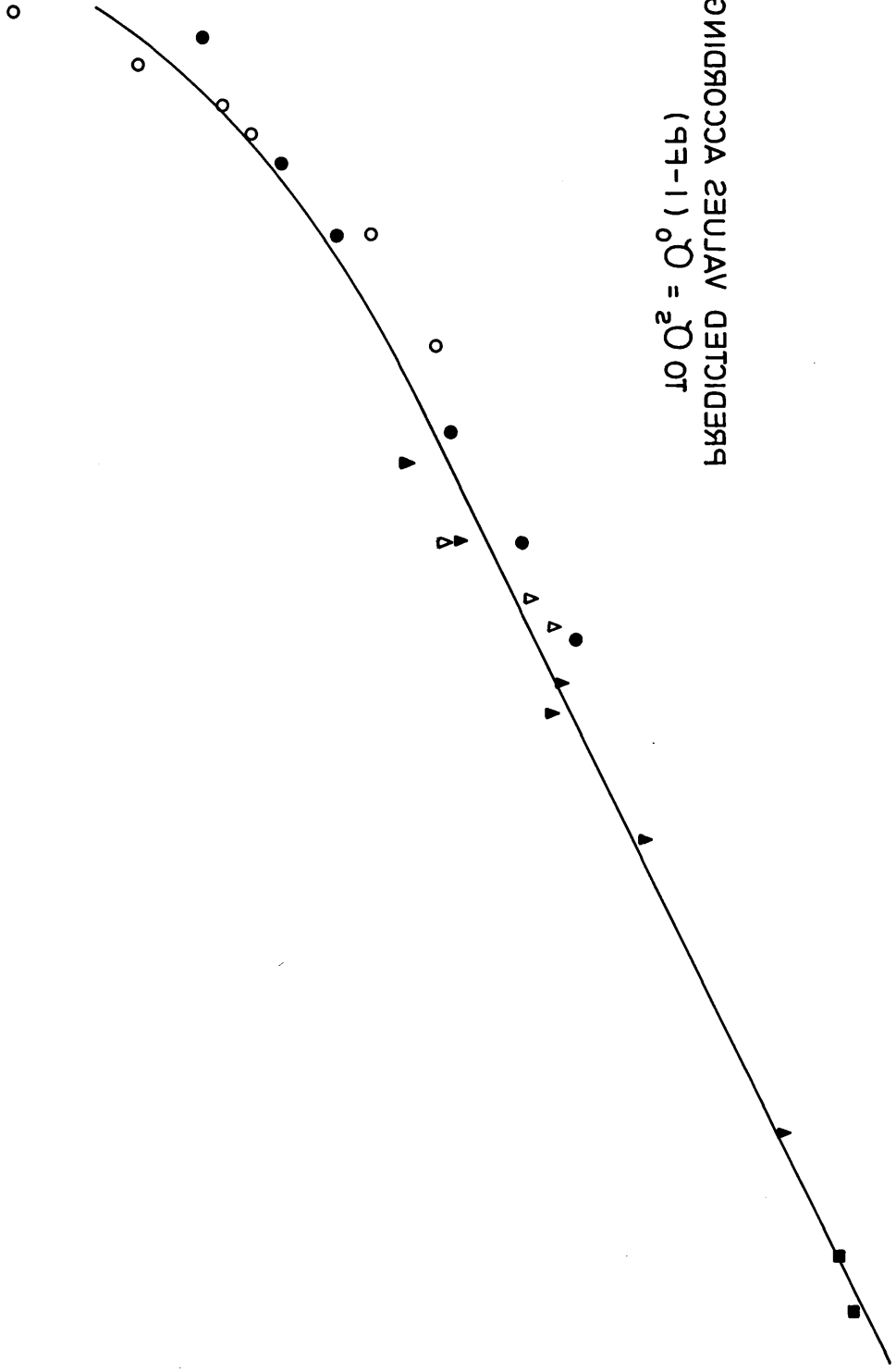


FIG. 91 DETERMINATION OF STRESS CONCENTRATION FACTORS (F)

PREDICTED VALUES ACCORDING
TO $\bar{\sigma}_s = \bar{\sigma}_0 (1 - FP)$



ПРЕДИСЛАВЪТЪ СЪГЛАВЪТЪ
(1-1) $\sigma^2 = \sigma^2$ ОТ



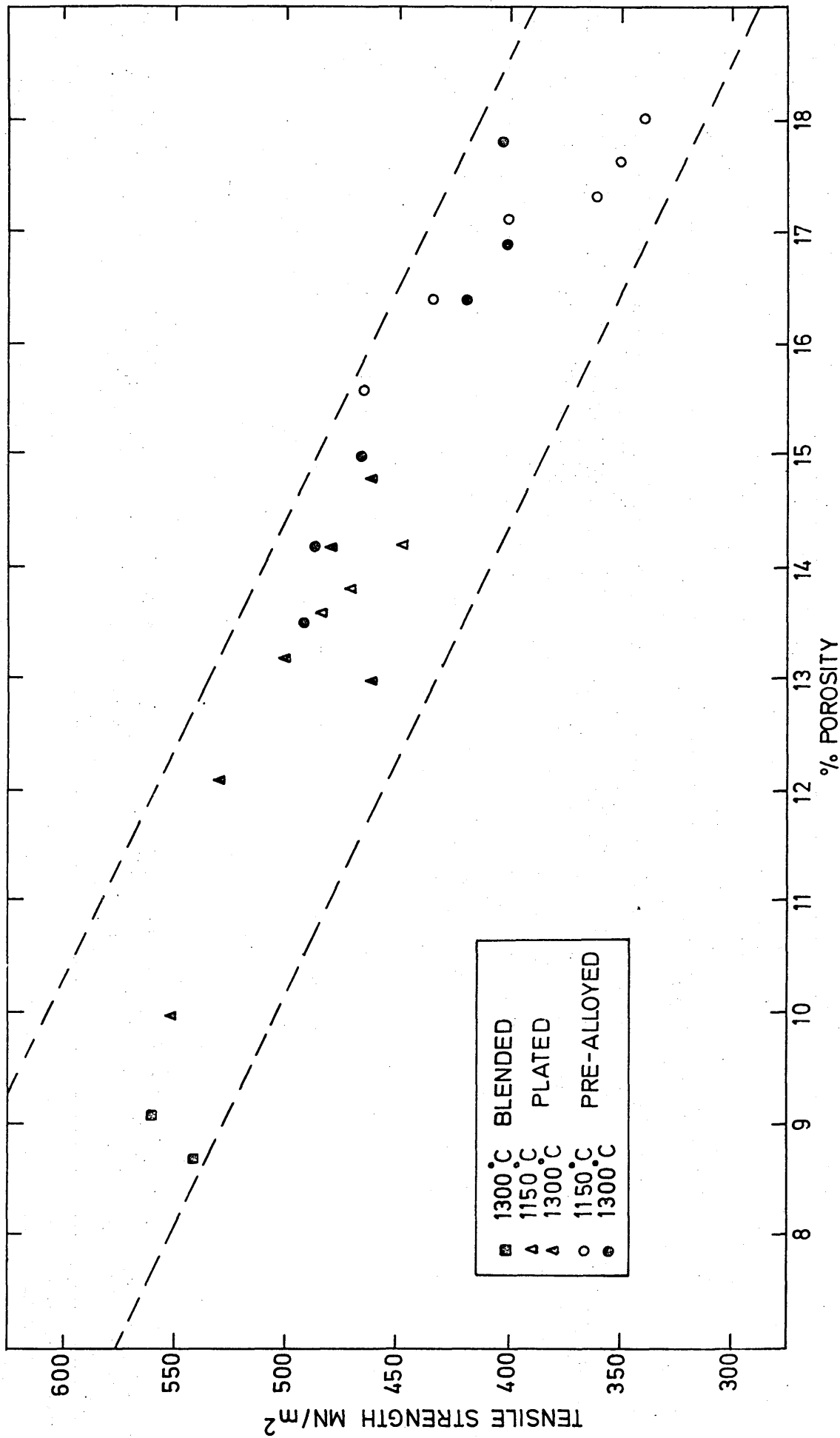


FIG. 92 RELATIONSHIP BETWEEN TENSILE STRENGTH AND POROSITY IN ALLOYS OF HIGH HOMOGENEITY

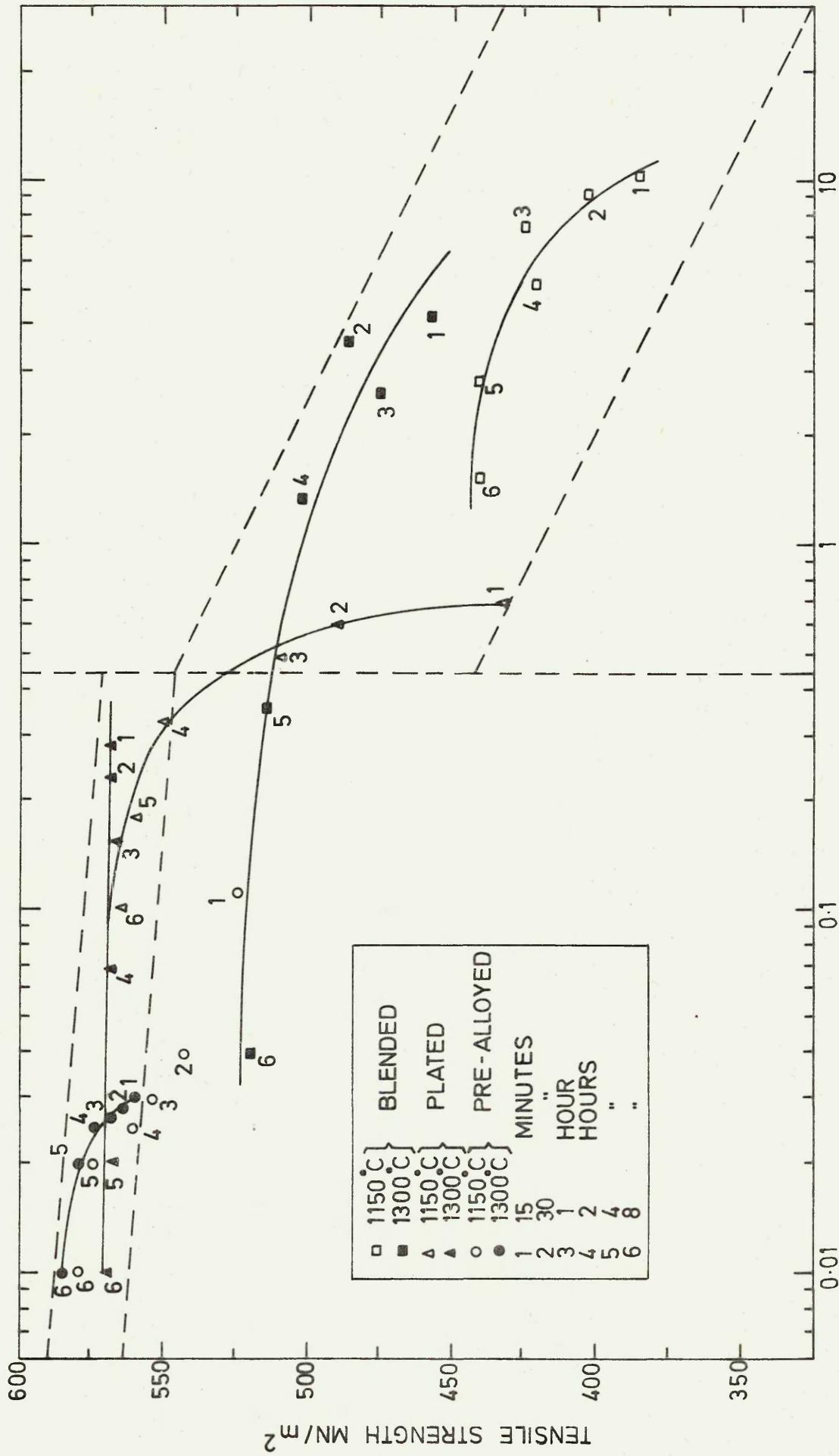


FIG. 93 RELATIONSHIP BETWEEN TENSILE STRENGTH AND HOMOGENISATION PARAMETER IN ALLOYS OF 10% POROSITY.

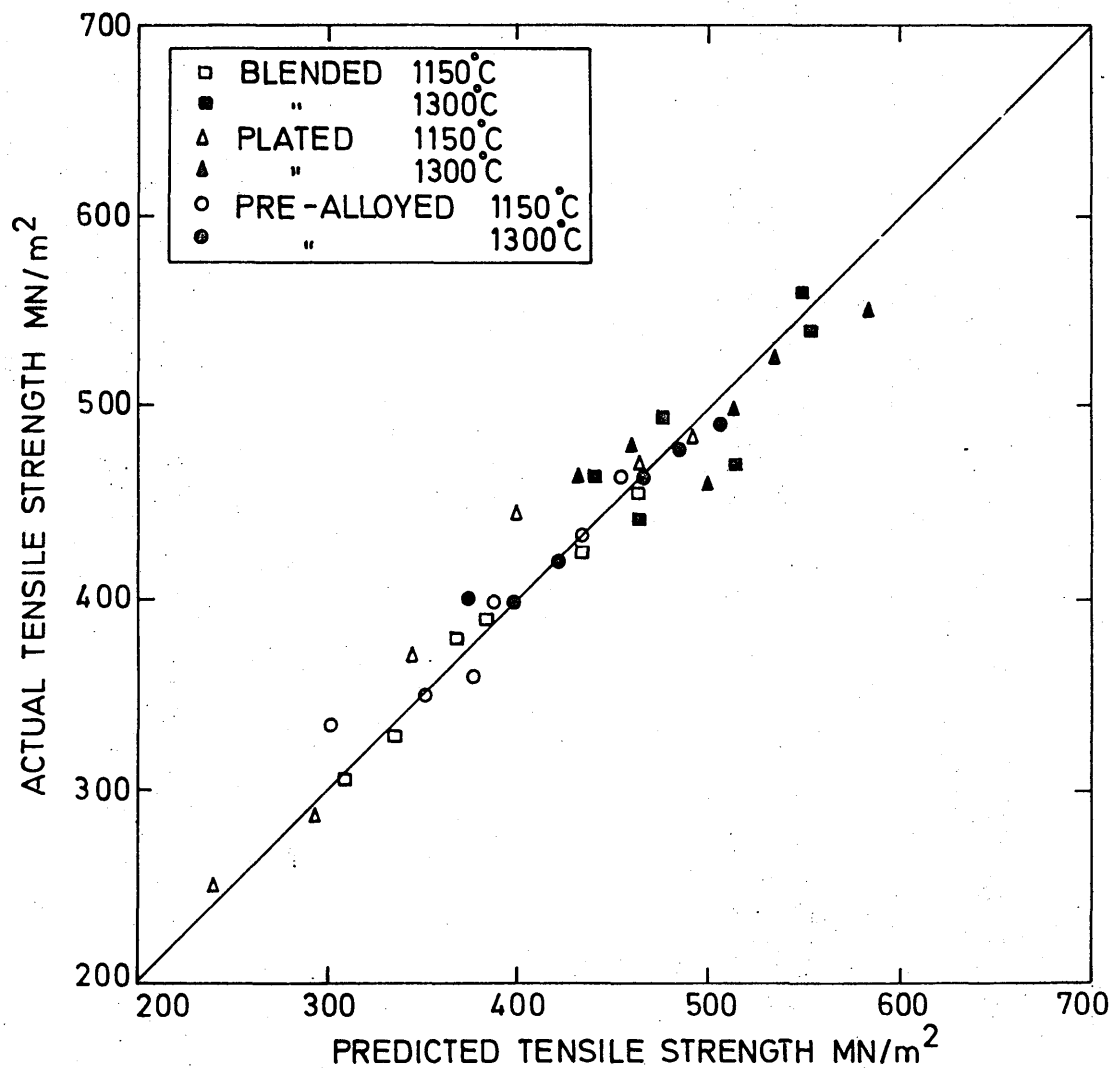


FIG. 94

RELATIONSHIP BETWEEN ACTUAL AND PREDICTED TENSILE STRENGTHS IN ALL ALLOYS SINTERED AT 1150°C AND 1300°C

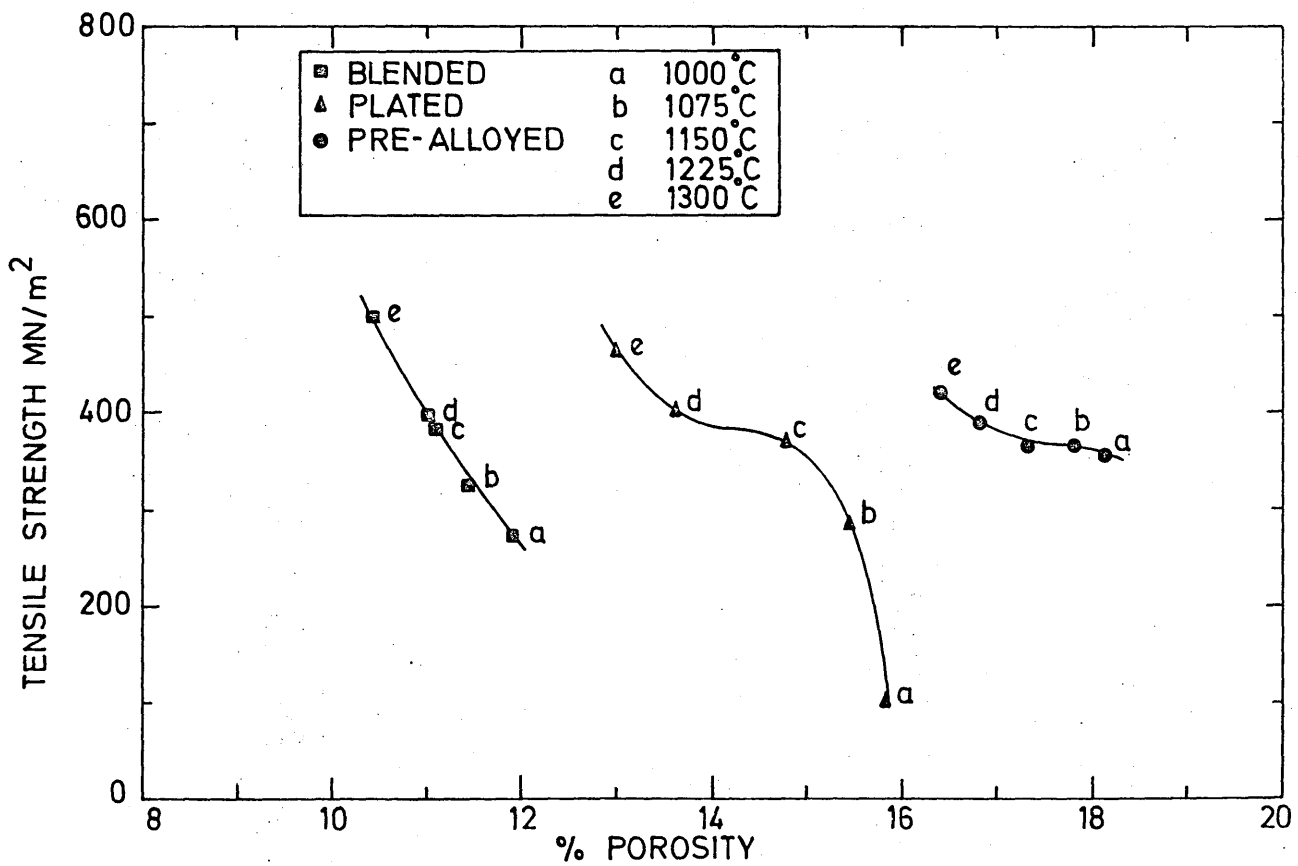


FIG. 95 RELATIONSHIP BETWEEN TENSILE STRENGTH AND POROSITY IN ALLOYS SINTERED FOR ONE HOUR.

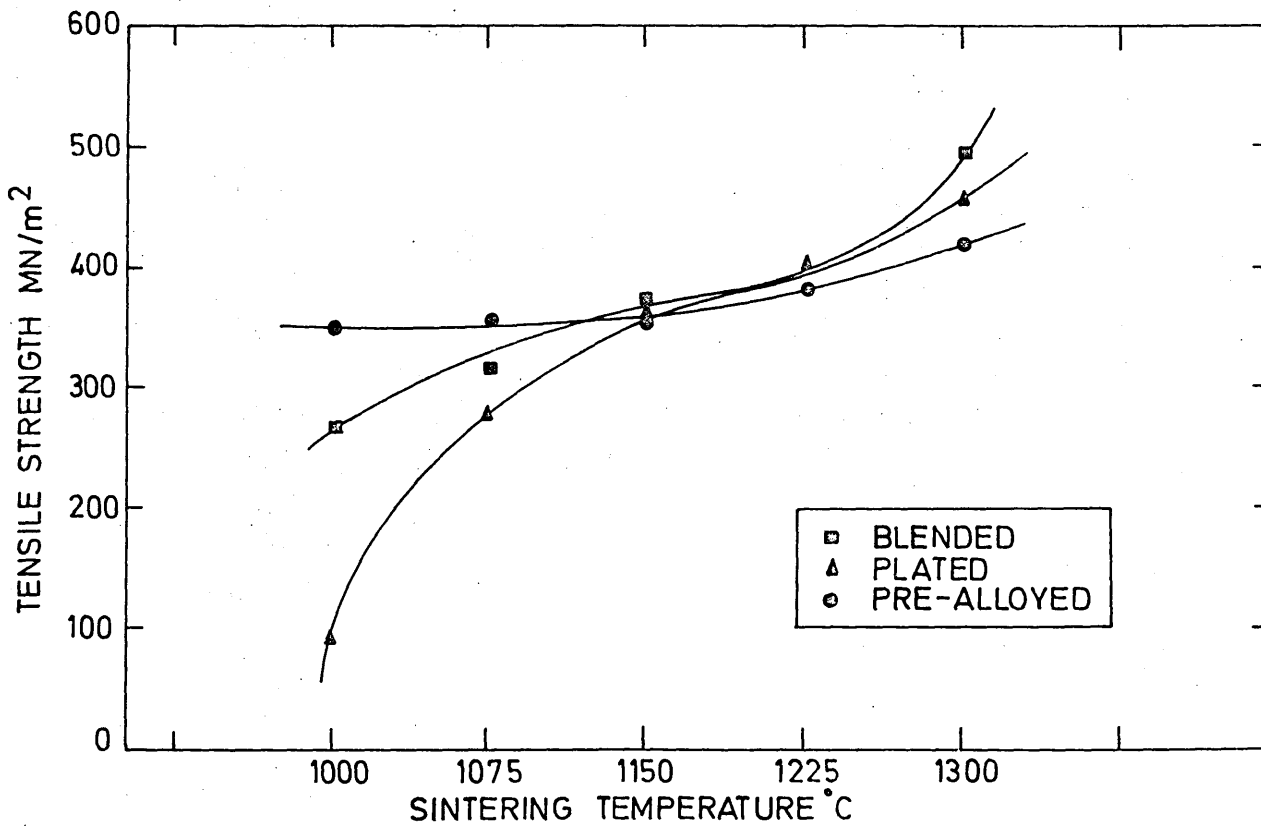


FIG. 96 RELATIONSHIP BETWEEN TENSILE STRENGTH AND SINTERING TEMPERATURE IN ALLOYS SINTERED FOR ONE HOUR.

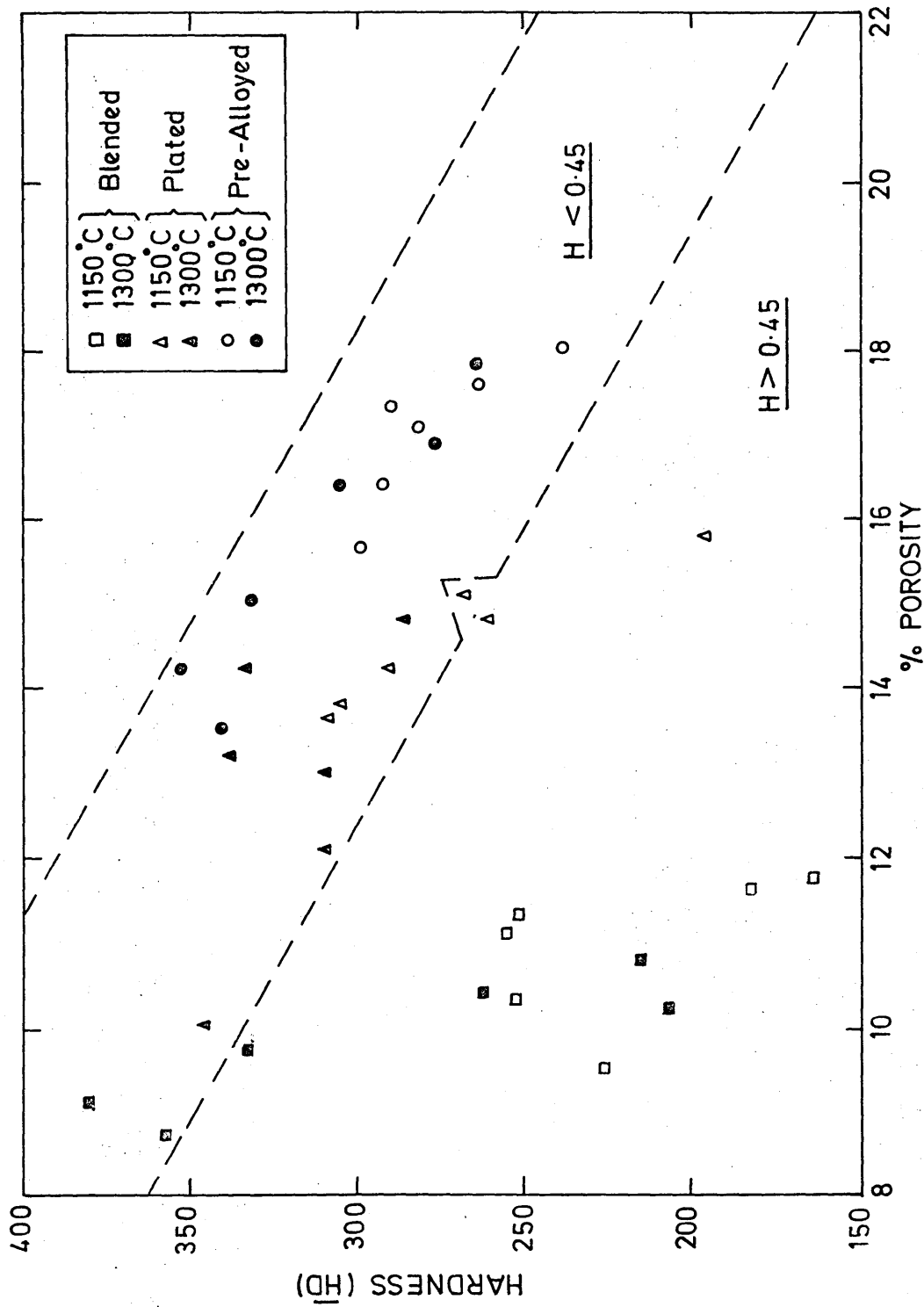


FIG. 97 RELATIONSHIP BETWEEN HARDNESS AND POROSITY IN SINTERED AND QUENCHED MATERIALS

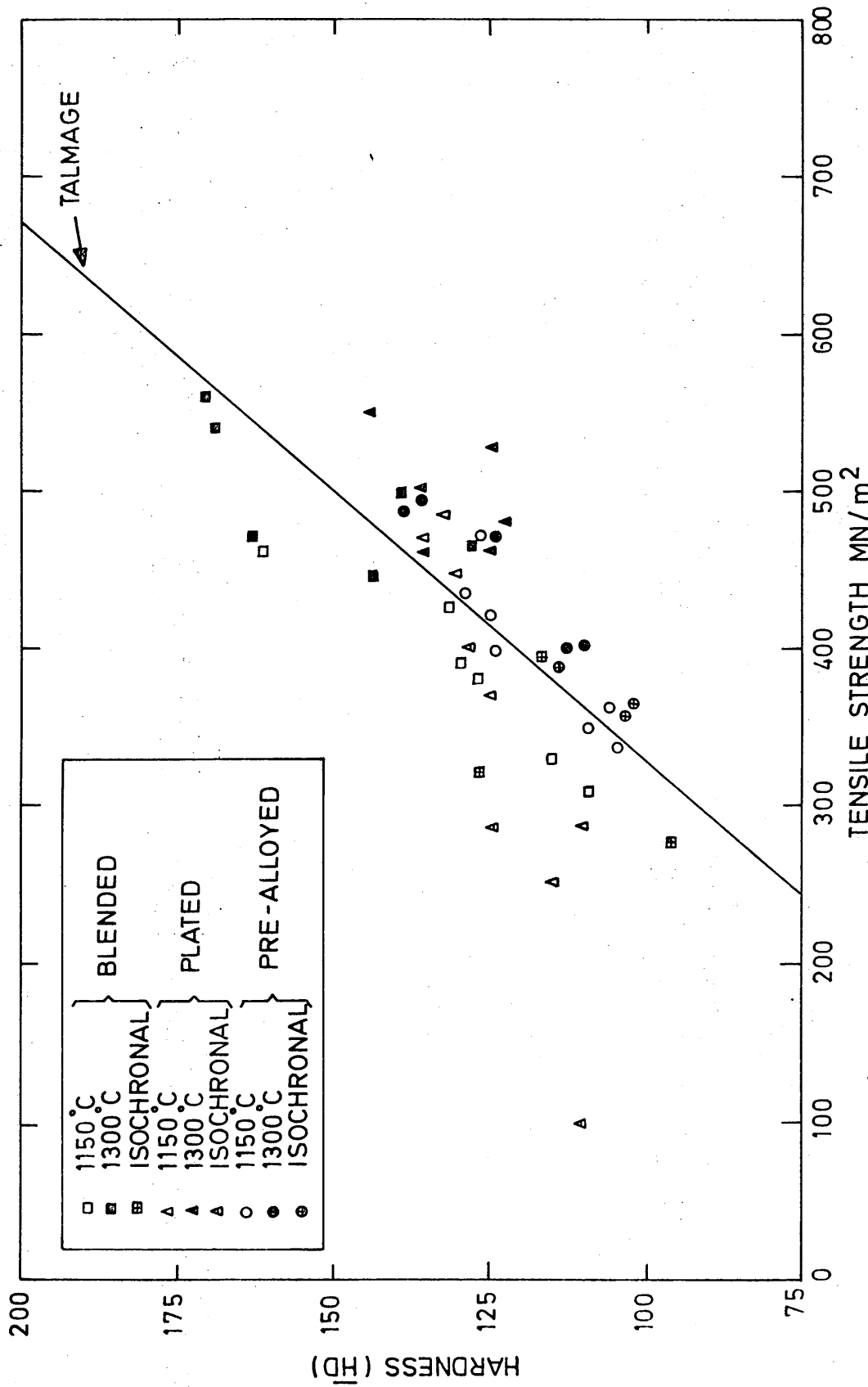


FIG. 98 RELATIONSHIP BETWEEN HARDNESS AND TENSILE STRENGTH IN QUENCHED AND TEMPERED MATERIALS.

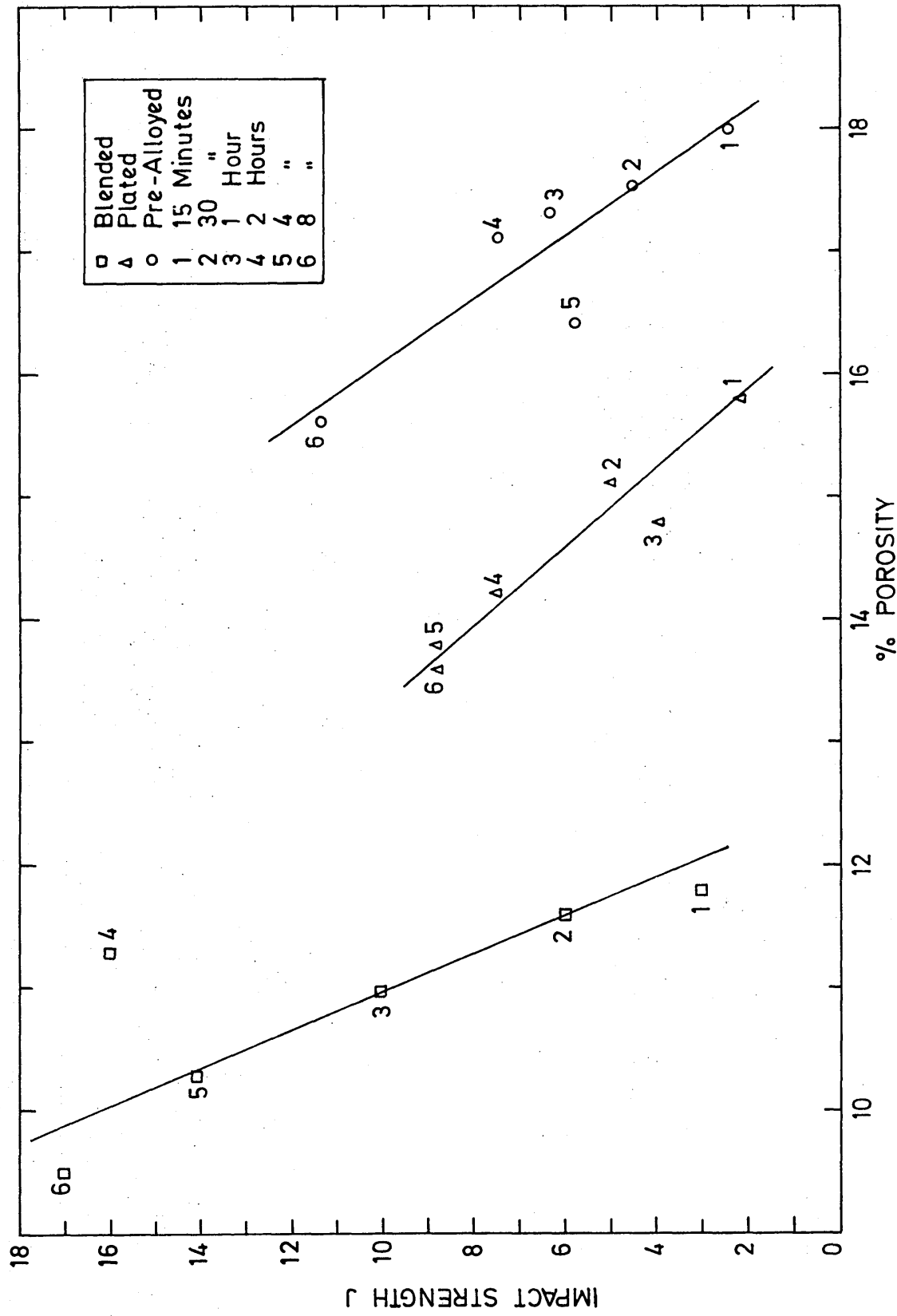


FIG. 99 RELATIONSHIP BETWEEN IMPACT STRENGTH AND POROSITY IN QUENCHED AND TEMPERED ALLOYS SINTERED AT 1150°C

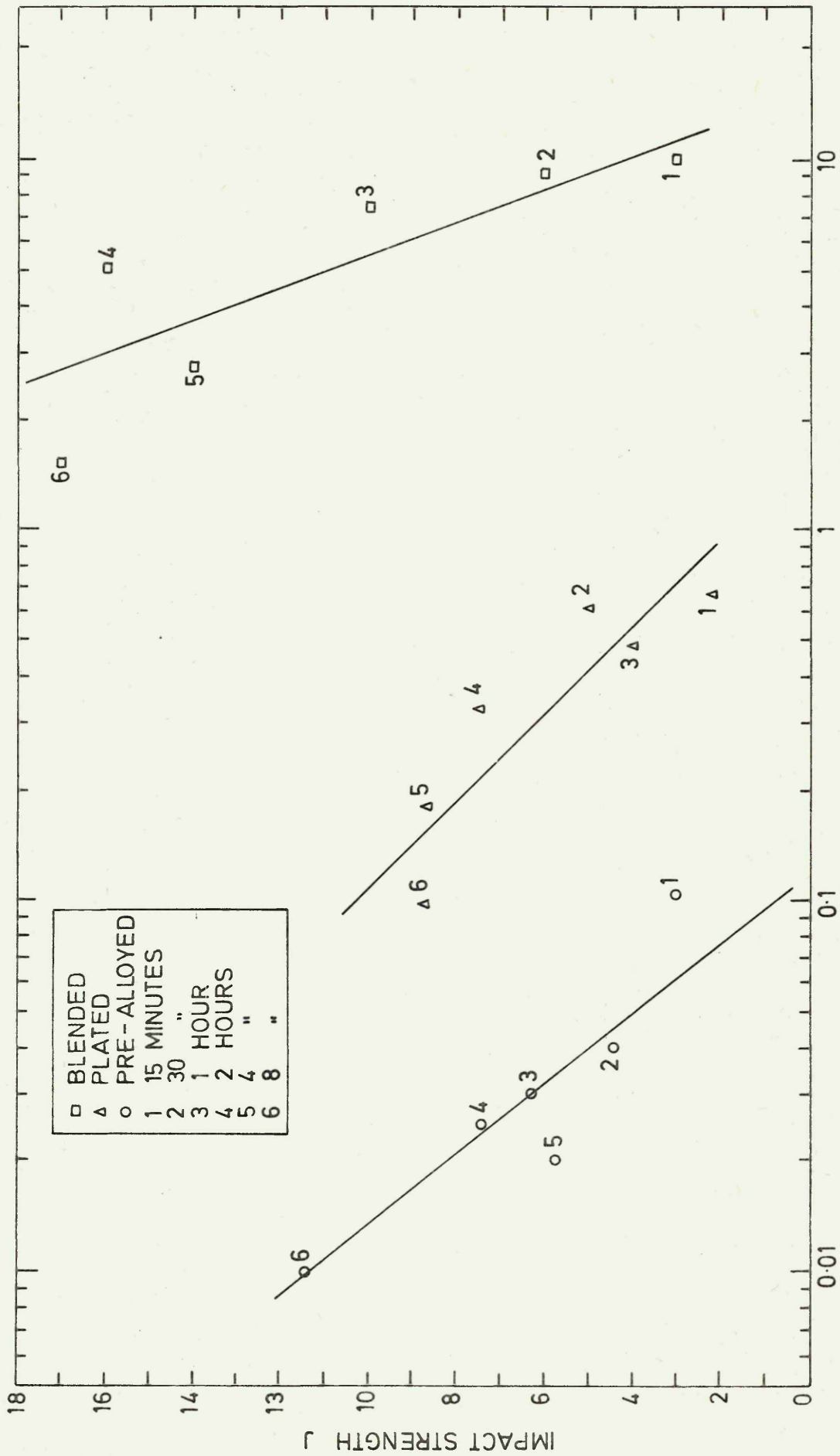


FIG 100 RELATIONSHIP BETWEEN IMPACT STRENGTH AND HOMOGENISATION PARAMETER IN QUENCHED AND TEMPERED ALLOYS SINTERED AT 1150°C

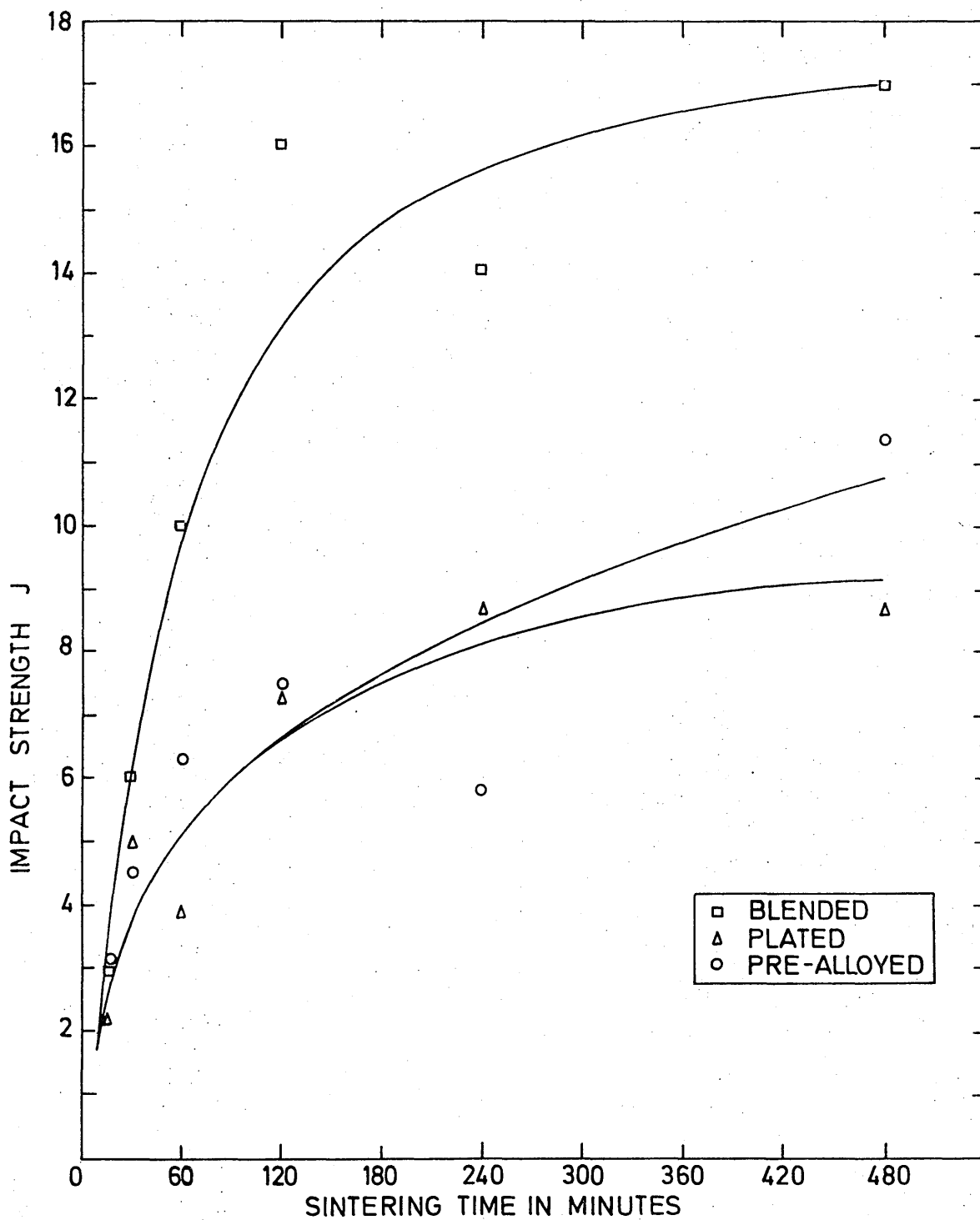


FIG. 101 RELATIONSHIP BETWEEN IMPACT STRENGTH AND SINTERING TIME IN QUENCHED AND TEMPERED ALLOYS SINTERED AT 1150°C.